

GEMS & GEMOLOGY

VOLUME XXXVI

FALL 2000



THE QUARTERLY JOURNAL OF THE GEMOLOGICAL INSTITUTE OF AMERICA



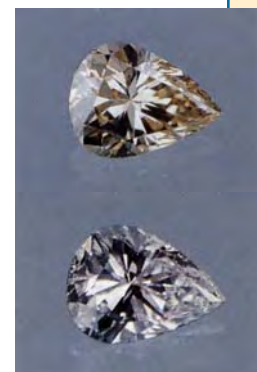
pg. 217



pg. 237



pg. 247



EDITORIAL

189 New Diamond Treatments: What Do They Mean for the Gemological Laboratory?

William E. Boyajian

191 LETTERS

FEATURE ARTICLES

192 GE POL Diamonds: Before and After

Christopher P. Smith, George Bosshart, Johann Ponahlo, Vera M. F. Hammer, Helmut Klapper, and Karl Schmetzer

The first study of GE POL diamonds before and after HPHT processing reveals important clues to their identification.

216 Sapphires from Antsiranana Province, Northern Madagascar

Dietmar Schwarz, Jan Kanis, and Karl Schmetzer

Learn the distinctive features of blue-green-yellow sapphires from the important basaltic deposits near Ambondromifehy.

234 Pre-Columbian Gems and Ornamental Materials from Antigua, West Indies



A. Reg Murphy, David J. Hozjan, Christy N. de Mille, and Alfred A. Levinson

Nondestructive gemological techniques are used to identify ancient jewelry materials of the Saladoid culture and suggest early trade patterns in the eastern Caribbean islands.

NOTES AND NEW TECHNIQUES

246 Gem-Quality Häüyne from the Eifel District, Germany

Lore Kiefert and H. A. Hänni

Explore the properties of this rare bright blue gem.

REGULAR FEATURES

254 Gem Trade Lab Notes

• Cat's-eye chrysoberyl • HPHT-annealed blue and pink diamonds • Diamonds with flower-like inclusions
• Historical diamond report • Black synthetic moissanite • Fracture fillers in ruby • Paraíba tourmaline

260 Gem News

• APEC 2000 report • De Beers's new direction • Mosaic ammonite • Iranian anhydrite • Indian aquamarine
• Hawaiian "precious" coral • Fresnoite • International Geological Congress report • Malagasy lapidary facility
• Ruby and sapphire from Colombia • Lavender sugilite with green spots • Paraíba tourmaline update • "Wine-bottle" tourmaline • Magnetic hematite imitation • Boulder opal imitations • Concave faceting of sapphires

275 2000 Challenge Winners

277 Book Reviews

280 Gemological Abstracts

New Diamond Treatments: What Do They Mean for the Gemological Laboratory?

In each of the last five issues of *Gems & Gemology*, we have published articles on the high pressure/high temperature (HPHT) annealing of diamonds to modify their color. This is arguably one of the most serious challenges the diamond industry has ever faced. Most of these articles have dealt with the decolorization of diamonds as represented by the GE POL process. The paper by Christopher Smith and his colleagues in the present issue is the most recent contribution. It provides some important new data on the characteristics of GE POL diamonds before and after processing.

What, though, does all this mean for the jeweler and gemologist? In particular, what do all these developments mean for a laboratory that is entrusted with the responsibility of identifying these and other treated or synthetic diamonds?

The role of the gemological laboratory has changed in many ways over the past decade. Not only have the techniques and instrumentation for gem identification become more advanced, but the methods and steps in diamond grading have become much more extensive and sophisticated. The new developments in treatments to diamonds and the further advancement of synthetic diamond growth methods have made it necessary for a gemological laboratory to become well equipped and to continually modify the screening methods used to detect such diamonds.

While I cannot speak for all laboratories, there have always been processes incorporated into the servicing procedures of the GIA Gem Trade Laboratory to meet such challenges as synthetics, coatings, fillers, laser drilling, and irradiation. More than a dozen additional detection techniques and instruments have been added to this process in the last five years alone.

Overall, the GIA system has been designed to ensure accuracy, efficiency, and client anonymity throughout the grading process. There are meticulous electronic routing techniques that guide a diamond through the laboratory, which include numerous steps that capture well over 400 separate and distinct pieces of gemological and scientific information.

After careful weighing and measuring, each diamond is processed through a series of instruments designed to differentiate natural from treated and synthetic diamonds, as well as to detect and distinguish diamond

types. These include, but are not limited to, the De Beers DiamondSure, short-wave ultraviolet fluorescence transparency devices, and proprietary spectroscopic instruments designed to measure the presence and level of trace elements, such as nitrogen, in each diamond.

All diamonds that are determined to be type II are then further screened by GIA's most experienced gemologists and research scientists. Some of the techniques and instruments employed include UV-Vis-NIR spectroscopy, high-resolution infrared spectroscopy, and (low temperature) Raman analysis to determine key photoluminescence features. Results from these analyses are then compared with our extensive database on known HPHT-annealed diamonds and untreated type IIa's.

Based on our careful examination of well over 2,000 GE POL diamonds to date, we believe that the vast majority of diamonds that have been decolorized by HPHT annealing can be identified through their properties, the laboratory's grading and research experience,

and the data archived in the laboratory's Horizon operations and management information system.

The proliferation of diamond treatments also raises questions about the fair and accurate representation of these products to tradespeople and consumers alike. There are legitimate markets for enhanced diamonds and an important need for consumers to know exactly what they are purchasing. As a result, we are currently reviewing our reporting policy for some enhanced diamonds and the scope of services we offer.

Yes, there are challenges to the way laboratories must now operate. We must gather more information, using more sophisticated instrumentation, in a process that often requires more time and a tremendous investment in equipment and personnel. Because many of these new treatments cannot be detected with standard gemological equipment, we are all serving a much broader constituency. Nevertheless, we believe that with solid research, with continued cooperation from the trade, and with flexibility and ingenuity, we and other well-equipped gemological laboratories will be able to continue to meet the needs of both the trade and the public.



Robert Shipley Jr. demonstrates GIA's state-of-the-art laboratory equipment in 1938.

*William E. Boyajian, President
Gemological Institute of America*

LETTERS

Pearl Nucleation Misquote?

It is difficult to correlate the statements in the Editor's Summer 2000 editorial about the value of peer review with the errors I found in the article by K. Scarratt et al. on nuclei in Chinese freshwater cultured pearls (FWCPs), which appeared in that same issue [pp. 98–109].

I have been misquoted twice in that article. First, in referencing my article in the April 2000 issue of *Lapidary Journal*, the authors state (p. 98), "Most recently, articles in the trade press (see, e.g., Matlins, 1999–2000a and b, 2000; Ward, 2000) have claimed that the vast majority of large FWCPs currently being described as "non-nucleated" are bead nucleated, with the largest sizes obtained by multiple insertions and reinsertions of nuclei formed from . . . freshwater cultured pearls." I did not say that "the vast majority" of the large round FWCPs are pearl-bead nucleated, because I know that statement is untrue.

This error is repeated on page 107, with the statement: "The recent reports in the trade literature that tissue-nucleated freshwater cultured pearls are being used as 'nuclei' to produce most of the recent large round Chinese FWCPs appear to be based on growth structures observed in pearls that have been cut in half (see, e.g., Matlins, 1999–2000a, 2000; Roskin, 2000; Ward, 2000)." Again, I have never said—or written—that "most" of the large Chinese FWCPs are pearl-bead nucleated because I know that statement is untrue.

On page 29 of my referenced *Lapidary Journal* article I state very clearly, "I came to believe that at least some of the new pearls were being nucleated with old freshwater pearls that may have been tumbled or ground to round." At no time does that sentence say or suggest that I think "the vast majority" or "most" of FWCPs are bead-nucleated.

Just the opposite is true. I wrote that I believe "at least some of the new pearls" are bead nucleated.

Fred Ward
Gem Book Publishers

In reply

The authors and I appreciate this opportunity to clarify the use of Mr. Ward's article as a reference for the two sentences cited above. Indeed, Mr. Ward does state in his article only that he believes "some" of the large Chinese FWCPs are bead nucleated. However, the citation of his article in conjunction with these two statements was not intended to indicate that they were quotations from Mr. Ward. Rather, as is stated in our Guidelines for Authors, "References should be used . . . to refer the reader to other sources for additional information on a particular subject." In his *Lapidary Journal* article, Mr. Ward provides a number of quotes from others that were interpreted to be in support of the argument that bead-nucleated FWCPs are primarily responsible for the large Chinese FWCPs that have recently entered the market. For example, he quotes one pearl dealer (Fuji Voll, p. 29) to the effect that "I agree with you that nucleation with other pearls is the most likely explanation for today's big rounds" and the late John Latendresse (p. 30) "Like you, I have no doubt they are nucleating with other pearls to get the big rounds."

We apologize if our intent was misconstrued, as the desire was not to put words in Mr. Ward's mouth but rather to lead the reader to the extensive information he had gathered from trade representatives, some of which appeared to support the statements indicated. Certainly, Mr. Ward's article provided useful commentary on this topic.

Alice S. Keller
Editor, Gems & Gemology

IN MEMORIAM John Latendresse (1925–2000)

John Robert Latendresse, one of the world's leading authorities on pearls and the creator of the cultured pearl industry in the United States, died on July 23 at his home in Camden, Tennessee, following a battle with lung cancer. He would have been 75 years of age on July 26.

Born in Beresford, South Dakota, Mr. Latendresse settled in Tennessee in the 1950s. In 1954, he founded Tennessee Shell Company, which soon became the world's primary supplier of the shell used to create the mother-of-pearl beads for cultured pearls. Convinced that local mollusks could be used to produce cultured pearls, he founded American Pearl Company, the first pearling company in the United States, in 1961. Over the next 20 years, he painstakingly tested over 300 bodies of water

before determining that the Tennessee River was ideal for culturing freshwater pearls. Today American Pearl Company produces freshwater cultured pearls in distinctive shapes and colors.

Mr. Latendresse was always eager to share his vast knowledge of pearls, and he actively supported research and education efforts. With James L. Sweaney he co-authored "Freshwater Pearls of North America," which appeared in the Fall 1984 issue of *Gems & Gemology* and won the *G&G* Most Valuable Article Award for that year.

John Latendresse is survived by his wife, Chessy, five children, seven grandchildren, and seven great-grandchildren. Always the consummate gentleman and an enthusiastic advocate for strong standards in the pearl industry, he will be greatly missed. Fortunately, the pearl industry will benefit from his legacy for many years to come.



GE POL DIAMONDS: BEFORE AND AFTER

By Christopher P. Smith, George Bosshart, Johann Ponahlo, Vera M. F. Hammer,
Helmut Klapper, and Karl Schmetzer

This study of type IIa GE POL diamonds before and after HPHT annealing by GE significantly expands on their characterization. The color change was dramatic: from the N-O range through Fancy Light brown before, to D-H after. However, there was little change to the inclusions, graining, and strain as a result of HPHT exposure. Photoluminescence (PL) studies—conducted at liquid helium, liquid nitrogen, and room temperatures in the 245–700 nm range—identified a significant reconfiguration of the lattice involving substitutional impurities, vacancies, and interstitials. Key regions of PL activity included the areas of the N3, H3, and N-V centers. X-ray topography identified the extent of lattice distortion. Cathodoluminescence may help establish that a diamond is not HPHT annealed. A distinction between non-enhanced and color-enhanced type IIa diamonds can be made through a combination of observations and features.

ABOUT THE AUTHORS

Mr. Smith is director, and Mr. Bosshart is chief gemologist, at the Gübelin Gem Lab, Lucerne, Switzerland. Dr. Ponahlo is senior research scientist, and Dr. Hammer is research scientist, in the mineralogy and petrography department at the Museum of Natural History, Vienna, Austria. Prof. Klapper is the head of the crystal growth research group at the Mineralogisch-Petrographisches Institut, University of Bonn, Germany. Dr. Schmetzer is a research scientist residing in Petershausen, near Munich, Germany.

Please see acknowledgments at the end of the article.

Gems & Gemology, Vol. 36, No. 3, pp. 192–215
© 2000 Gemological Institute of America

March 1, 1999 is a watershed date in the gem and jewelry trade. This is when General Electric (GE) and Lazare Kaplan International (LKI) unveiled their latest contribution to the diamond and jewelry industry: diamonds that had undergone a new GE process “designed to improve their color, brilliance, and brightness” (Rapnet, 1999). Colloquially, these diamonds became known as “GE POL” or “Pegasus” diamonds, because they were being marketed through LKI subsidiary Pegasus Overseas Ltd. (POL). At the July 2000 Jewelers of America trade show in New York, however, the brand name Bellataire was officially launched.

The first gemological description of GE POL diamonds appeared in fall 1999, when GIA published an overview of the macroscopic and microscopic features observed in 858 GE POL diamonds they had examined up to August 1999 (Moses et al., 1999). Subsequent articles by the SSEF Swiss Gemmological Institute and De Beers provided more analytical details on GE POL diamonds and suggested spectroscopic methods of identification (Chalain et al., 1999, 2000; Fisher and Spits, 2000). The Gübelin Gem Lab (GGL) has had an ongoing cooperation with GE, LKI, and POCL (Pegasus Overseas Company Ltd.) to investigate the gemological and analytical characteristics of GE POL diamonds, in order to help develop identification criteria. Because of this collaboration, staff members at GGL were given the opportunity to document a selection of diamonds taken from current GE production, both prior and subsequent to high pressure/high temperature (HPHT) processing (figure 1).

This study represents the first independent investigation of actual GE POL diamonds both before and after processing by General Electric. Such an investigation is crucial to understanding the mechanisms behind the color alteration and thus to providing greater insight into potential methods of identification. The present report not only addresses the alterations in color, inclusions, graining, and strain produced by the GE process, but it also considerably expands the

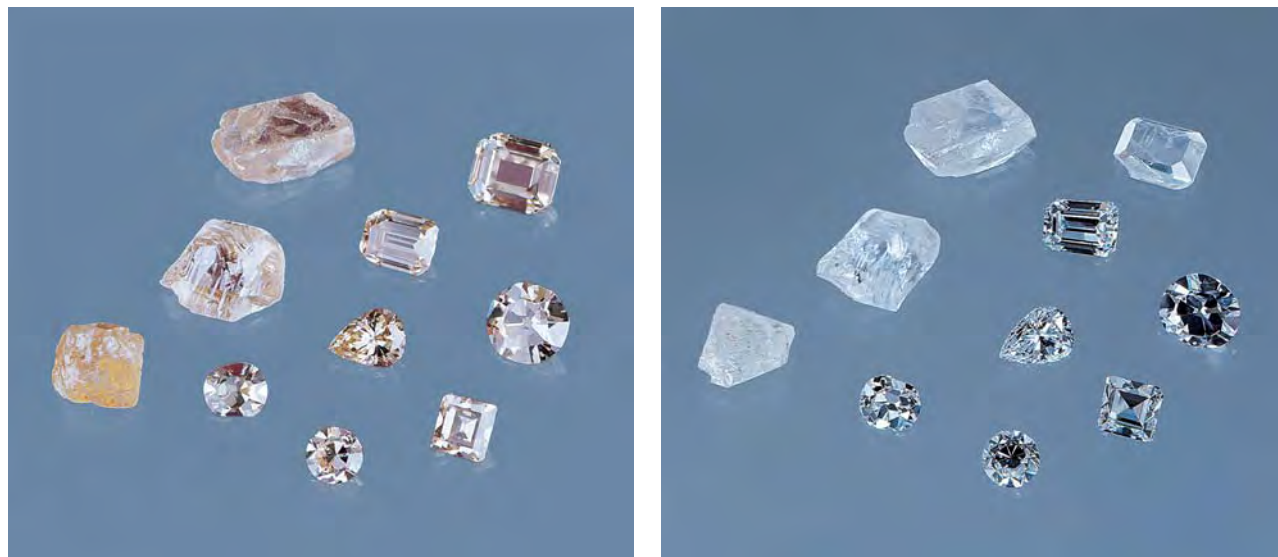


Figure 1. These two illustrations show 10 of the study samples before and after HPHT processing. The brown type IIa diamonds on the left received color grades from the N–O range to Fancy Light brown (C3–C5 on the Argyle scale). Following processing by GE, the color improved dramatically, with the diamonds on the right grading from D to H. The seven faceted samples weigh 0.48 to 2.72 ct, and the three pieces of rough weigh 2.32 to 3.71 ct. Photos by Phillip Hitz.

analytical characterization of GE POL diamonds using photoluminescence data acquired with laser-Raman systems, cathodoluminescence, and X-ray topography. Since brown coloration in type IIa diamonds is associated with plastic deformation of the crystal lattice (Wilks and Wilks, 1991), these advanced analytical techniques were selected to pay particular attention to defect centers, trace impurities, and structural distortion, in order to document the changes that may be taking place in the lattice. For more information on these atomic-level diamond features, the reader is referred to box A.

MATERIALS AND METHODS

Samples. We studied seven faceted stones and three crystals that were selected at random from POCL's stock of brown type IIa diamonds (see, e.g., figure 1). The faceted diamonds ranged from 0.48 to 2.72 ct. The three crystals weighed 2.32 to 3.71 ct; we had windows polished on two of them to permit viewing of their interiors. GE, LKI, and POCL independently confirmed that no pre-processing of the diamonds had taken place. As a "control" sample, a 0.61 ct type IIa brown pear shape was selected from the Gübelin Gem Lab's reference collection and submitted to GE for HPHT processing. All 11 samples were subjected to the tests described below both before and after HPHT processing by General Electric. The precise conditions used by GE are proprietary, and were not revealed to the authors. Of

these 11 samples, six (including the one GGL sample) were selected as representative to show the range of properties and characteristics exhibited by the larger group (table 1).

In the course of grading at GGL, and as part of ongoing research, we have had the opportunity to test many natural, nonprocessed, near-colorless type IIa diamonds and GE POL diamonds by the methods listed below. Our preliminary results for these diamonds are incorporated into the Discussion and Applications sections below.

The Risk Factor. When diamonds (and other gems) are exposed to elevated temperatures and pressures, there is always the risk of thermal shock extending existing fractures or creating new ones. As a graphic reminder of this, two of the 11 samples inexplicably broke in the course of HPHT processing. The 1.92 ct octagonal step cut cleaved along an octahedral plane (111), shearing the stone in two parallel to the table facet; a secondary fracturing took away one corner (refer to the *after* photo of GE4 in table 1). The 1.22 ct round (GE3) had to be considerably reformed because a small section chipped. This damage occurred in both diamonds even though there were no fractures or other inclusions, significant slip traces, or twinning present prior to enhancement. It is interesting that none of the three diamonds that had fractures experienced any damage during HPHT processing.

BOX A: UNDERSTANDING VACANCIES, INTERSTITIALS, AND COLOR CENTERS

Many of the features discussed in this article are related to point defects (e.g., vacancies, interstitials, and substitutional impurities) present at the atomic level in the lattice of a diamond. Figures A-1 to A-3 offer a simplified, two-dimensional illustration of the major defect centers discussed in this article, which relate to HPHT processing of type IIa diamonds.

These three figures are drawn after diagrams provided by the De Beers Diamond Trading Center.

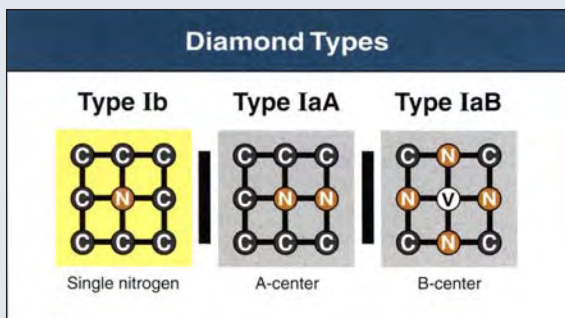


Figure A-1. These schematic diagrams illustrate the occurrence of substitutional impurities in different diamond types; each produces distinctive spectral features in the infrared region and is detectable with IR spectroscopy. In type Ib diamonds, a carbon atom is substituted by a single nitrogen atom. In type Ia diamonds, substitutional nitrogen atoms are aggregated. The most common diamond types are IaA (which have a pair of nitrogen atoms, the A aggregate) and IaB (in which four nitrogen atoms surround a common vacancy, the B aggregate). Those rare diamonds that are classified as type IIa do not show nitrogen (or boron) impurities in their IR spectra.

Gemological Examination and UV-Vis-NIR and IR Testing. Color observations were made in the neutral environment of a MacBeth Judge II light box. Colorimetric measurements were carried out with a Zeiss multichannel color spectrometer (MCS 311). Clarity assessments and the study of internal characteristics such as inclusions and graining were carried out with a binocular microscope and various lighting techniques. We used crossed polarizing filters to observe the internal strain patterns and interference colors.

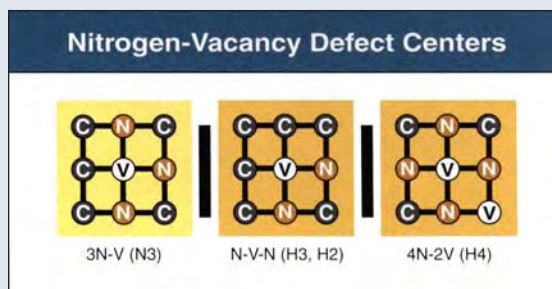


Figure A-2. Diamonds may also contain additional defect centers, which involve the combination of substitutional nitrogen impurities and vacancies. These include the N3 system (three nitrogen atoms surrounding a vacancy), the H3 and H2 systems (an A-aggregate associated with a vacancy[uncharged and negatively charged, respectively]), and the H4 system (a B-aggregate bound to an additional vacancy).

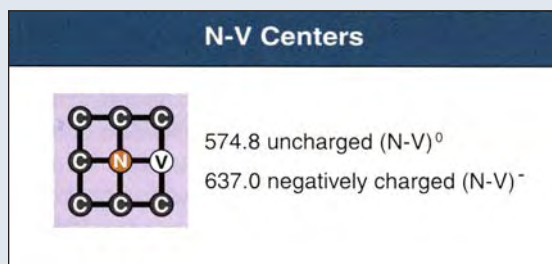


Figure A-3. Illustrated here are the two types of nitrogen-vacancy (N-V) centers (uncharged and negatively charged), where a single nitrogen atom is attached to a single vacancy.

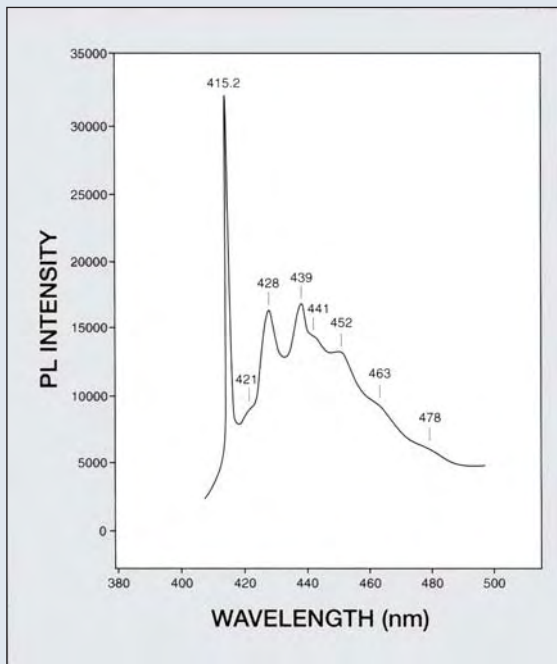
We performed absorption spectroscopy in the ultraviolet (UV), visible (Vis), and near-infrared (NIR) regions of the spectrum (200–2500 nm) with a Perkin-Elmer Lambda 19 spectrometer. We recorded the spectra with the diamonds at both room and liquid nitrogen temperatures; the slit width provided a spectral resolution of 0.2 nm, and the data interval was 0.2 nm.

Mid- and near-infrared absorption spectra were taken at room temperature with a Philips 9624 Fourier-transform infrared (FTIR) spectrometer in the

When a type IIa diamond is exposed to HPHT conditions, the lattice of the diamond goes through a process of reconfiguration. That is, within the lattice, some of the point defects present prior to HPHT processing—such as N-V, H4, and H3 centers and nitrogen aggregates—are broken up. In addition, vacancies and nitrogen impurities will mobilize; vacancies and interstitials may mutually annihilate; and N3 centers are created, as is single substitutional nitrogen.

Definition of Frequently Used Terms

Vacancy—An unoccupied carbon site within the crystal lattice of a diamond.



Interstitial—Any carbon or impurity atom (nitrogen, hydrogen, or boron) that does not occupy a carbon site in the lattice of the diamond, but is situated in a space between regular carbon sites.

Color center—Any point defect (also generally referred to as a defect center) inside the lattice that absorbs visible light and thereby imparts color to the diamond. Examples are vacancies and substitutional impurities (e.g., nitrogen occupying a carbon site). Note that A and B aggregates of nitrogen absorb infrared light only; because they do not absorb in the visible region of the spectrum, they are not color centers.

Photoluminescence Systems. Some point defects luminesce when excited by UV radiation or visible light. This photoluminescence (PL) appears as peaks or bands, some of which represent PL systems, such as N3 or H3. All PL systems behave in a similar fashion, with a zero-phonon line generated by an electronic transition and side bands (also referred to as *phonon replicas*) caused by acoustic transitions in the form of lattice vibrations (i.e., characteristic vibrations of molecules and crystals), as illustrated in figure A-4. Such PL systems may be likened to a stone dropped in water, where the zero-phonon line is the point at which the stone enters the water and the side bands are the ripples that emanate from this point.









Figure A-4. In a PL system such as the N3 illustrated here), H3, or (N-V)⁻, the zero-phonon line (here, the 415.2) is accompanied by a number of side bands. These phonon replicas make up a series of progressively weaker and broader bands at higher wavelengths, which combine to form a structured band with an underlying emission maximum at a characteristic wavelength, such as at approximately 440 nm (N3), 520 nm (H3), and 680 nm (N-V)⁻.

range of 7000 to 400 wavenumbers (cm⁻¹), with a standard 4 cm⁻¹ resolution; we used a SpectraTech diffuse reflectance collector for the faceted samples and a Specac 5× beam condenser for the rough specimens.

Other Advanced Testing. Photoluminescence, cathodoluminescence, and X-ray topography are not standard analytical techniques in most gemological laboratories. However, researchers have applied these techniques to the study of diamonds in order to characterize various types of lattice defects (see, e.g., Wild

and Evans, 1967; Woods and Lang, 1975; Lang and Moore, 1991; Collins, 1992, 1996; Davies, 1999). Photoluminescence (PL) was well described in basic terms by Fisher and Spits (2000, p. 44). Note that a laser is used to study PL features because of its efficient excitation of impurities and defect centers, even when they are present in very low concentrations. Because the photoluminescence of diamonds is a fluorescence behavior, stones may react differently when exposed to various wavelengths. Therefore, the use of lasers with different excitations (i.e., 244 and

TABLE 1. Gemological and other properties before and after HPHT processing for five GE diamonds and one Gübelin Gem Lab reference sample.^a

Property	GE1 0.73 ct		GE2 0.97 ct		GE3 1.22 ct		GE4 1.92 ct	
	Before	After	Before	After	Before	After	Before	After
Appearance								
Approximate color grade ^b	P to Q (C3)	G	Fancy Light brown (C5)	F	Q to R (C4)	F	P to Q (C3)	D
Clarity ^c	Clean (IF to VVS)		Clean (IF to VVS)		Clean (IF to VVS)	Clean, small breakage	Clean (IF to VVS)	Broken into 3 pieces
Fluorescence ^d								
Long-wave	Very faint chalky blue	None	Very faint chalky blue	Very faint chalky blue	Very faint chalky yellow	Very faint blue	Weak greenish yellow	Weak blue
Short-wave	Faint chalky yellow	None	Very faint chalky blue	None	Faint chalky yellow	None	Faint greenish yellow	Faint blue
Graining	None	Very weak	Prominent		None	Faint	Moderate	
Strain pattern ^e	Weak tatami extinction		Weak to moderate banded and tatami extinction		Weak banded and tatami extinction		Weak banded and tatami extinction	
UV-Vis absorption (at liquid nitrogen temperature)	Faint band at 680 nm Slope < 630 nm —	Faint band at 270 nm —	Faint band at 680 nm Slope < 630 nm —	Faint band at 270 nm —	Faint band at 680 nm Slope < 620 nm Faint lines at 229.6 and 236.0 nm	Weak band at 270 nm — Faint lines at 229.6 and 236.0 nm	Faint band at 680 nm Slope < 610 nm Weak lines at 229.6 and 236.0 nm	Faint band at 270 nm — Weak lines at 229.6 and 236.0 nm
Diamond type ^f	IIa with minor H		IIa		IIa with minor IaB		IIa with minor IaB+H	
CL color	Moderate yellow-white	Strong bluish white	Medium blue-white	Strong blue	Moderate yellow-white	Strong blue-white	Strong blue-white	Strong chalky blue
CL spectrum ^g	Two CL bands	Single "blue" band plus shoulder	Two CL bands	Single "blue" band	Two CL bands	Single "blue" band plus weak shoulder	Two CL bands	Single "blue" band
X-ray topography	Moderately perturbed		Weakly perturbed		Strongly perturbed		Faintly perturbed	

^a Includes all critical properties for these representative stones before and after HPHT processing, with the exception of photoluminescence features, which are given in tables 2 and 3.

^b Value in parentheses after terminology developed by Argyle Diamond Co.

^c The Gübelin Gem Lab reference stone was the only fully faceted diamond, thus permitting an exact clarity grade determination. The GE samples were not fully faceted, therefore the exact clarity grade was not pinpointed.

^d Fluorescence was recorded with a long-wave (365 nm) and short-wave (254 nm) unit. We do not believe the change in fluorescence behavior offers a useful identification criterion.

^e Although the extinction pattern may have remained the same after HPHT processing, the overall appearance became slightly more prominent.

^f The H (hydrogen) band is located at 3107 cm⁻¹; the B aggregate band is centered at 1174 cm⁻¹.





^g The two independent CL bands were situated at 430 nm ("blue" band) and at 520 nm ("green" band). After HPHT processing, the band centered at 520 nm was either completely removed or became a faint to weak shoulder at the base of the "blue" band.

325 nm in the UV, 488 nm in the blue, and 514 or 532 in the green regions of the spectrum) may show varying results. For example, the 637 nm system is not excited by the 325 nm "UV" laser and is excited less efficiently by the 488 nm "blue" laser, as compared to the 514 or 532 nm "green" lasers.

Low-temperature conditions are necessary to properly resolve all of the PL features that may be present (Fisher and Spits, 2000). However, we have also included the results of our analyses at room temperature, because these spectra may help confirm that a high-color type IIa diamond

has not been enhanced by HPHT processing.

Photoluminescence spectra were recorded with laser Raman microspectrometers over the range 245–700 nm. For the UV region from 245 to 700 nm, we used a Renishaw System 1000 equipped with a frequency-doubled Argon-ion laser (excitation wavelength at 244 nm). To cover the 325–700 nm range, we used a Dilor LabRam Infinity and a Renishaw System 1000, each equipped with a helium/cadmium (He/Cd) laser (excitation at 324.98 nm). To focus on the region between 550 and 700 nm, we used a Dilor LabRam Infinity equipped with a frequency-

GE5 2.72 ct		GGL1 0.61 ct	
Before	After	Before	After
			
P to Q Range (C3)	H	Fancy Light brown (C5)	D
Clean (IF to VVS)		SI ₁	
Very faint chalky yellow	Weak blue	None	None
Faint chalky yellow	Very faint chalky blue	None	None
Prominent Moderate banded and tatami extinction		Weak	Weak to moderate
Faint band at 680 nm Slope < 620 nm	Weak band at 270 nm —	Faint band at 680 nm Slope < 610 nm	Faint band at 270 nm —
Weak lines at 229.6 and 236.0 nm	Weak lines at 229.6 and 236.0 nm	—	—
IIa with minor IaB + H		IIa	
Moderate chalky yellowish white	Moderate chalky blue-white	Moderate yellowish white	Strong blue
Two CL bands	Single "blue" band plus faint shoulder	Two CL bands	Single "blue" band
Very strongly perturbed		Moderately perturbed	

doubled Nd/YAG laser (excitation at 531.78 nm), as well as a Renishaw System 1000 equipped with an Argon-ion laser providing excitation at 514.5 nm. We used both the Dilor and Renishaw Raman systems to rule out instrumental artifacts. Both systems produced equivalent results of very high spectral resolution. The diamonds were analyzed at temperatures near those of liquid helium ($-263^{\circ}\text{C}/10\text{K}$) and liquid nitrogen ($-196^{\circ}\text{C}/77\text{K}$) and at room temperature (approximately $25^{\circ}\text{C}/298\text{K}$) using a THMS 600 heating and cooling stage manufactured by Linkam Scientific Industries Ltd.

We also performed cathodoluminescence (CL) analyses over the range 380–700 nm using flood gun optical CL microscopy ("cold CL"; see Box B). For this technique, we used a Zeiss microscope and a Luminoscope with a large sample compartment, which also permitted visual observation of the CL colors and phosphorescence effects. For the spectral analyses, we used a monochromator slit width that

provided a resolution of 5 nm. The monochromator sits on top of the microscope and is coupled by optical lenses. The image is then focused on the entrance of the slit of the monochromator to obtain optimal intensity. The acceleration voltage of the electron beam was 4.5 kV with a current of 0.5 mA. Beam energy was kept constant throughout all the tests by pressure regulation of the current, which carried ionized gas (air). Scanning CL microscopy ("hot CL") in the region 200–700 nm was carried out with an Oxford Instruments MonoCL system, with a step-scan of 1 nm, attached to a JEOL JSM 6400 SEM-EDS instrument, operating at an accelerating voltage of 15 kV and a beam current of approximately 1 mA.

X-ray topography was performed with a Seifert ISO-Debyelex 1001 generator using a molybdenum fine focus W2000 Philips X-ray tube. Operation conditions were 50 kV and 25 mA, with a slit beam (white-beam section topography in Laue forward-reflection arrangement). The fine-grained AGFA-Gevaert Structurix D4 film used required exposure times of approximately 12 hours per sample. Using the Laue technique with white X-ray light, no special orientation of the samples was necessary.

RESULTS: GEMOLOGICAL OBSERVATIONS AND UV-VIS-NIR AND INFRARED SPECTROSCOPY

The properties for all of the samples before and after HPHT processing are discussed below. The specific results for five of the GE stones and the one GGL sample are listed in table 1. For the most part, these six samples encompassed all of the features seen in the larger group.

Color Appearance

Before: All 11 samples in this study were originally light to medium brown (figure 1, left; table 1). The GIA color grade equivalents extended from approximately the N to O range through Fancy Light brown. Applying the common diamond trade terminology developed by the Argyle Diamond Co. for their "champagne" diamonds, we estimated their colors to range from C3 to C5 (on a C1 to C10 scale, ranging from pale to extremely dark brown). It is important to note that this group may not represent the full range of colors that are processed by GE.

Colorimetric measurements showed that the original hues (i.e., dominant wavelengths) were located in a narrow range between 578.8 and 580.4 nm. These wavelengths correspond to the yellow to orange-yellow region of the visible spectrum. The measured color saturation ranged from 15.8% to

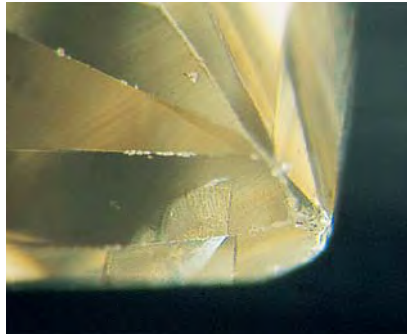


Figure 2. Before processing (left), this fracture in the 0.61 ct GGL sample was bright and reflective. After HPHT processing (right), the area of the original fracture had acquired a coarse (frosted) texture and we noticed the addition of a bright transparent extension, or “fringe.” No graphitization was observed. Photomicrographs by Christopher P. Smith; magnified 55 \times .

25.4% (on a 0 to 100% scale). The tones varied between 2.7 and 4.1 (on a 0 to 10 scale). The ratios of tone and saturation extended from 0.14 to 0.21 (for objective color evaluation, GGL uses a T/S ratio to standardize the description of brown and gray in colored diamonds), corresponding to low or moderate saturations and light to medium tones. The data obtained for this color study are influenced by geometry and surface conditions and therefore may show some variation from one sample to the next.

After: All samples were dramatically enhanced by HPHT processing (figure 1, right). Most were in the colorless range of D to F. One sample retained a slight brownish color and was graded as H on the GIA color-grading scale.

We measured a substantial decrease in saturation and tone, as well as a slight shift in hue, in the processed diamonds. The modified colors varied from 570.6 to 576.4 nm in hue, from 0.8% to 5.2% in saturation, and from 0.5 to 3.0 in tone. These data correspond to an average shift of -5.4 nm in hue, -18% in saturation, and -1.5 in tone from the original, light brown colors. With these data, we can

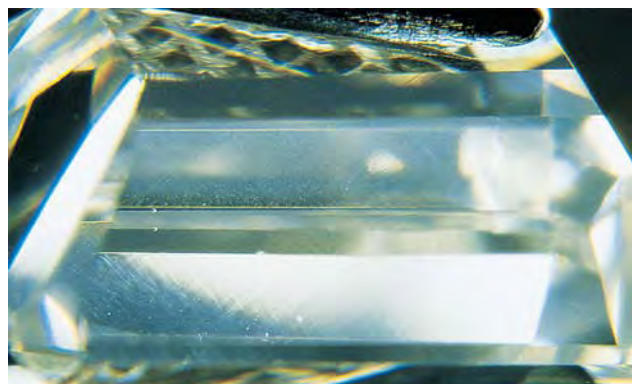
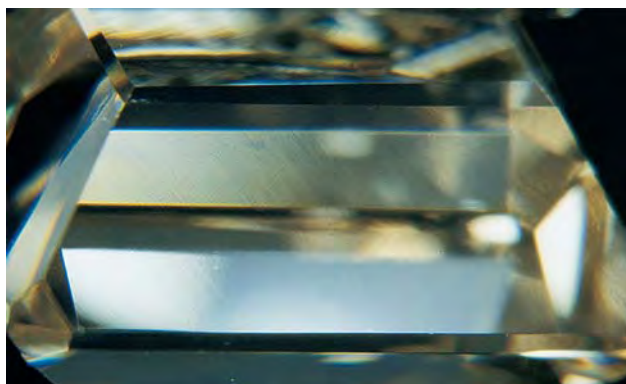
better understand why GE POL diamonds appear yellow, rather than brown, at colors lower than H on the GIA grading scale (refer to diamonds described in Moses et al., 1999; Fisher and Spits, 2000). For the human eye, this is a very sensitive region of the visible spectrum; even a shift of only a few nanometers and a decrease in tone can make the previously brown diamonds appear yellow.

Clarity and Inclusions

Before: Few of the samples contained observable mineral inclusions or fractures. LKI informed us that in their experience, brown type IIa diamond rough is commonly very clean (P. Kaplan, pers. comm., 2000). Two of the POCL samples did contain small fractures. The GGL sample had a tiny crystal with a small, brightly reflective stress halo, as well as two small fractures (see, e.g., figure 2, left) and a natural. Although we did not clarity grade the GE POL diamonds, because only the GGL sample was fully faceted, we determined that the clarity grades would be VVS or better.

After: Re-examination of these diamond inclusions

Figure 3. One sample (2.72 ct) showed significant whitish graining with a “cottony” texture before HPHT processing (left). After processing (right), the fundamental character of the graining had not changed, although it appeared to be slightly more prominent. Such prominent graining imparted an overall haziness to the diamond both before and after enhancement. This diamond also showed the greatest degree of lattice distortion on the X-ray topographs. Photomicrographs by Christopher P. Smith; magnified 14 \times .



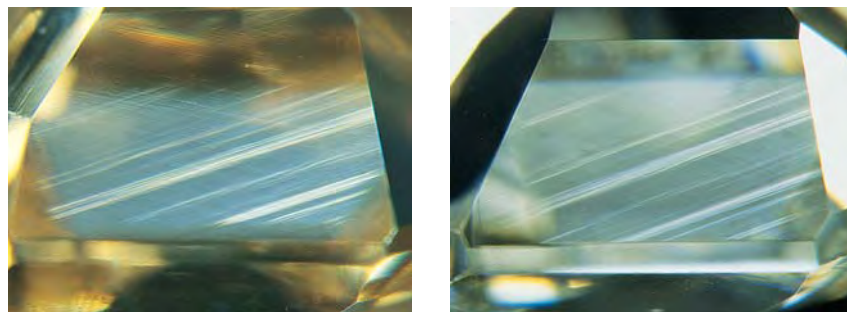


Figure 4. Sample GE 2 (0.97 ct) displayed prominent slip bands (also referred to as whitish or silvery graining). There was no apparent alteration in these bands as a result of HPHT processing (left, before; right, after). Photomicrographs by Christopher P. Smith; magnified 30 \times .

after processing revealed little change as a result of exposure to HPHT conditions. The appearance of the open fractures had altered slightly in some cases, where the fracture walls became textured or frosted as a result of partial dissolution; in other cases, some degree of extension was evident in the creation of an outer “fringe” (see, e.g., figure 2, right). The bright stress fracture in the GGL sample healed in the region immediately surrounding the crystal; yet we observed no healing along the further extension of the stress fracture. The changes observed did not have a significant effect on the clarity grades.

Graining

Before: We did not observe any internal graining in four of the eight faceted samples. The other samples displayed internal graining that ranged from very weak to prominent. In one specimen, the very fine texture of the graining generated a faint overall “sheen” in the stone when it was viewed with dark-field illumination. One sample with prominent (i.e., whitish) graining displayed a distinctly “cottony” texture (figure 3, left). Another sample had significant graining in a linear formation along slip traces (figure 4, left).

After: Although the texture of the graining remained unchanged (figure 4, right) in all samples, the graining itself did appear just slightly more prominent in most (figure 3, right). Overall, however, we did not observe a dramatic alteration (figure 4, right).

Strain Patterns

Before: Anomalous birefringence (caused by strain in the crystal lattice) was noted in all the specimens when they were viewed between crossed polarizers. As is typical of type IIa diamonds, the samples revealed weak to moderate banded and cross-hatched (tatami) extinction patterns, with first-order interference colors of gray and violet to blue, which extended to yellow and orange within patches in two samples (figure 5). In a direction parallel to octahedral crystal faces in one sample, we saw a

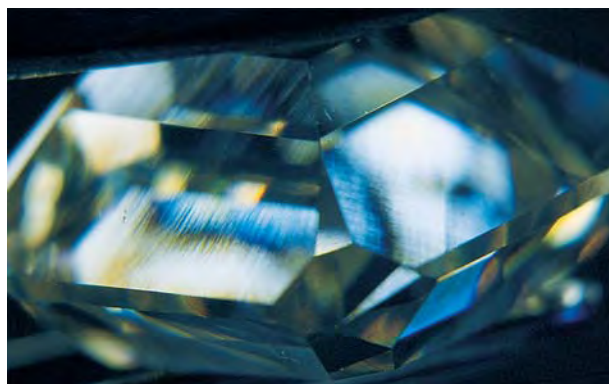
moderate banded strain pattern with weak first-order interference colors (figure 6, left).

After: Overall we did not observe dramatic modifications to the strain patterns after HPHT processing. However, with close inspection we were able to note some subtle changes: Although the actual patterns (i.e., banded and tatami) remained the same, they were very slightly more prominent after processing; the first-order interference colors were also slightly augmented (figure 6, right).

UV-Vis-NIR Absorption Spectroscopy

Before: The spectra of all the samples were remarkably uniform throughout the UV-Vis-NIR range. No absorption bands were observed in the near-infrared (700–2500 nm) region. Only faint bands were detected below 700 nm: N9 lines at 229.6 and 236.0 nm in the UV region of three samples (figure 7 and table 1). Wide, yet faint bands were also detected around 480, 560, and 680 nm in the visible region (the first two discernable only in the MCS spectra), but they were too weak to have any obvious

Figure 5. As is typical for type IIa diamonds, all of the samples studied showed tatami and banded extinction patterns with first-order interference colors when viewed between crossed polarizers. Photomicrograph by Christopher P. Smith; magnified 14 \times .



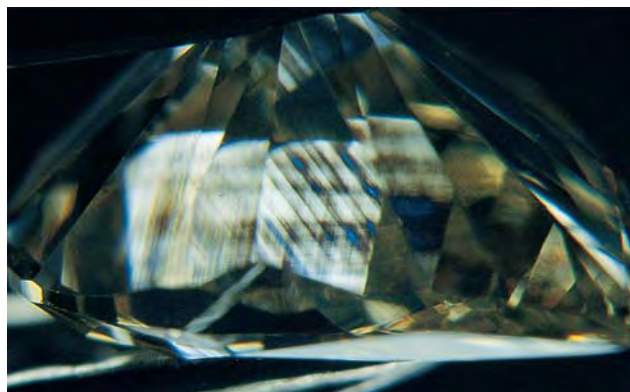


Figure 6. Prior to HPHT processing (left), we observed a banded strain pattern parallel to octahedral growth planes that showed primarily weak (gray) interference colors when viewed between crossed polarizers. After processing (right), the overall pattern remained the same, but the first-order interference colors were slightly stronger (bluer). Note that such strain patterns and interference colors may also be seen in non-enhanced colorless type IIa diamonds. Photomicrographs by Christopher P. Smith; magnified 20 \times .

influence on the bodycolor. In all specimens, the gradual absorption slope (or “continuum”) started at approximately 620 nm and became steeper toward 400 nm, causing the light brown color. The absorption curve continued to climb in the UV region toward the fundamental absorption edge of diamond at 225 nm.

After: There was a significant decrease in the absorption continuum, as well as an overall reduction in the general absorption level. In particular, the slope became very subtle in the visible region and the bands that were barely detectable disappeared. This explains the nearly or completely colorless appearance of the specimens after exposure to HPHT conditions.

However, we also noted that a new, broad, faint-to-weak absorption band had developed in all samples, centered at approximately 270 nm. In the three samples with a trace of B aggregates, this band was accompanied by faint-to-weak absorption lines at the base of the absorption edge—at 229.6, 236.0, and (in one sample only) at 227.4, 243.1, and 249.6 nm—which were unchanged by HPHT processing.

Infrared Spectroscopy

The mid-infrared spectrum of a chemically pure diamond is characterized by the two-phonon and three-phonon absorption bands (2650–1500 and 4000–2650 cm^{-1} , respectively). These features are intrinsic to diamond. The infrared classification of diamond types is based on absorption bands related to nitrogen (N) in the one-phonon region, between 1500 and 1000 cm^{-1} (see, e.g., Fritsch and Scarratt, 1992). It also has been long understood that this was a qualitative as opposed to a quantitative clas-

sification, so that nitrogen and other impurities may still be detected in type IIa diamonds with high-resolution and/or high-sensitivity techniques.

Before: All 11 samples were classified as type IIa, based on the relative absence of IR features in the one-phonon region under typical testing conditions (figure 8 and table 1). By expanding this region however, we noted that some of the samples displayed a weak, broad band at approximately 1174 cm^{-1} , which corresponds to nitrogen in the form of B aggregates. In addition, we recorded a small sharp peak at 3107 cm^{-1} , which identifies traces of hydrogen impurities. Only two of the samples did not show any detectable traces of chemical impurities (nitrogen, hydrogen, or boron).

After: It is interesting that none of the samples revealed any apparent increase or decrease in the nitrogen aggregate or hydrogen contents. Furthermore, as observed with our testing conditions, it appears that no IR absorption bands were either annihilated or generated by the GE process.

RESULTS: PHOTOLUMINESCENCE SPECTROSCOPY

Tables 2 and 3 list all the PL features recorded under room- and low-temperature conditions, respectively, before and after HPHT processing. When evaluating more than one spectrum from a single sample or from multiple samples, it is possible to normalize the spectra by comparing the intensity of the diamond’s Raman signal. Note that as part of their own independent research, GE has used photoluminescence to characterize synthetic diamonds both before and after HPHT

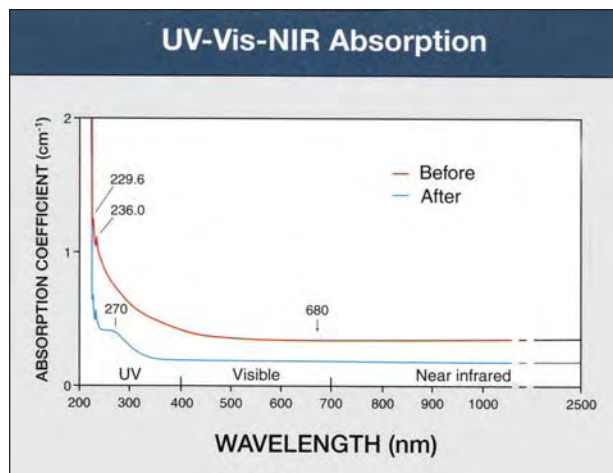


Figure 7. These UV/Vis/NIR absorption spectra of the 2.72 ct sample (GE5), recorded at liquid nitrogen temperature and high resolution, illustrate the absorption characteristics of a GE POL diamond before and after HPHT processing. The light brown (P to Q range) type IIa specimen initially exhibited a faint 680 nm band, an increase in general absorption starting at approximately 620 nm, and the N9 absorption lines at 229.6 and 236.0 nm. In contrast, following HPHT processing, the general absorption of the same sample in the visible region was almost entirely annihilated, which improved the color to an H grade (faint brown). Notably, a broad band centered at about 270 nm also developed (due to the formation of a small amount of single nitrogen). However, the two N9 lines at the base of the fundamental absorption edge (225 nm), appear to be unaffected. The absorption coefficient indicated is approximate.

application (e.g., Jackson and Webb, 1995; Webb and Jackson, 1995; McCormick et al., 1997).

We listed all the PL features recorded, because the presence of some of these peaks and bands in natural, non-HPHT processed type IIa diamonds may be just as important to the identification procedure as features that suggest HPHT processing. Again, see box A for an illustration of the various nitrogen-impurity forms and point defects that will be discussed.

In all cases, liquid nitrogen temperatures were sufficient to resolve all of the PL features recorded. Liquid helium conditions produced no further refinement of the PL bands present, nor any additional PL bands.

Throughout the text, the authors provide designations for the various PL features that were recorded. There are countless scientific publications which describe these features; however, for ease of

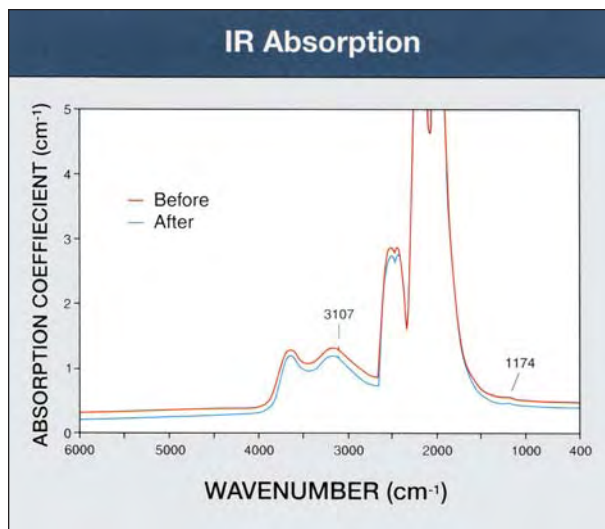


Figure 8. The IR absorption spectra of the GE POL diamond referred to in figure 7 are virtually identical before and after HPHT processing. In particular, the faint hydrogen peak at 3107 cm^{-1} and the faint band at 1174 cm^{-1} (attributed to a trace of B-aggregates) appear unaltered. The absorption coefficient indicated is approximate.

reference, the authors have used extensively the thorough treatises provided by Davies (1977), Walker (1979), Collins (1982), Woods and Collins (1986), Field (1992), Zaitsev et al. (1996 and 1998), and Iakoubovskii (2000).

[Authors' note: In spectroscopy, the terms peak and band are used synonymously. In this article, however, peak is generally used to represent sharp PL features and band to indicate broader PL features. In addition, all room-temperature PL features are indicated only to the full nanometer (e.g., 503 nm), whereas for the low-temperature PL spectra, the sharp peaks are indicated to the tenth of a nanometer (e.g., 503.1 nm) and the bands are indicated to the full nanometer (e.g., 680 nm). A PL system describes a sharp peak (zero phonon line) that is associated with a series of side bands, all of which relate to a single point defect (e.g., N3 or H3; also refer to box A.)

Frequency-Doubled Ar-Ion Laser (244 nm)

Room Temperature

Before: The dominant features were moderate to weak PL bands at 415 (N3), 256, 257, and 267 nm (figure 9A). Weak, broad bands were recorded occasionally at approximately 264, 277, 286, and 291 nm. One sample also revealed a faint, sharp peak at 404 nm.

TABLE 2. Raman photoluminescence features of the diamonds recorded at room temperature, before and after HPHT processing.^a

Laser excitation (nm)	PL feature (nm)	System assignment	Before	After
244	256		x	x
244	257		x	x
244	264		x	
244	267		x	
244	277		x	
244	286		x	
244	291		x	
244	404		x	x
325	406		x	
244, 325	415	N3	x	x
325	421		x	x
325	428		x	x
325	439		x	x
325	441		x	x
325	452		x	x
325	463		x	x
325	478		x	x
325	496	H4	x	
325	503	H3	x	
325	512		x	
325	520		x	
325	528		x	
325, 514	537 ^b		x	
514	567		x	
325, 514/532	576 ^c	(N-V) ⁰	x	x
325, 532	579–580		x	
532	587		x	
532	596		x	
514	613–617		x	
514/532	637	(N-V) ⁻	x	x
514/532	659		x	x
514/532	680		x	x

^a Important note: Not all of the PL features noted in this qualitative listing may be present in every diamond. The system designation—e.g., N3, H3, and (N-V)—is indicated on the zero phonon line. All features in the same system are indicated by the same color.

^b The 537 nm band was resolved into two adjacent peaks at liquid nitrogen temperature (see table 3).

^c The 576 nm band resolved into two adjacent but unrelated peaks at liquid nitrogen temperature.

After: Only the 415 (N3), 256, and 257 nm peaks remained after processing. Under these conditions, all but one sample revealed a general increase in 415 nm emission. The intensity of the 256 and 257 nm peaks appeared unchanged.

Low Temperature

Before: When the samples were cooled, a number of other PL features became evident. The 415.2 (N3) nm peak was dominant, but a number of smaller peaks also were resolved—at 256.2, 257.3, 263.9, 267.3, 277.4, 404.8, 406.0, 412.3, and 417.2 nm (figure 10A).

TABLE 3. Raman photoluminescence features of the diamonds recorded at liquid nitrogen temperature, before and after HPHT processing.^a

Laser excitation (nm)	PL feature (nm)	System assignment	Before	After
244	251.1		x	
244	254.2		x	
244	256.2		x	x
244	257.3		x	x
244	263.9		x	
244	265.1		x	
244	267.3		x	
244	277.4		x	
244	286.0		x	
244	291.6		x	
244, 325	404.8		x	x
244, 325	406.0		x	
325	409.6		x	x
325	412.3		x	x
244, 325	415.2 ^b	N3	x	x
244, 325	417.2		x	x
325	421		x	x
325	423.0		x	
325	428		x	x
325	430.9			x
325	439		x	x
325	441		x	x
325	452		x	x
325	463		x	x
325	478		x	x
325	490.7		x	
325	496.1	H4	x	
325	498.3		x	
325	503.1	H3	x	x
325	504.9		x	
325	512		x	
325	520		x	
325	528		x	
325, 514	535.9		x	
325, 514	537.4		x	
514	558.8		x	
514	566.8		x	
514	569		x	
325, 514/532	574.8 ^c	(N-V) ⁰	x	x
325, 514/532	575.8	Adjacent unrelated peak	x	x
325, 514/532	578.8		x	
532	587		x	
532	596		x	
514	600		x	
514	613–617		x	
514	620		x	
514/532	637.0 ^{c,d}	(N-V) ⁻	x	x
514/532	659		x	x
514/532	680		x	x

^a Important note: Not all of the PL features noted in this qualitative listing may be present in every diamond. The system designation—e.g., N3, H3, and (N-V)—is indicated on the zero phonon line. All features in the same system are indicated by the same color.

^b 415.2 nm peak FWHM = 0.38–0.45 nm (before) and 0.30–0.40 nm (after)

^c 574.8/637.0 ratio = 1.7–7.7 (before) and 0.3–0.7 (after)

^d 637.0 nm peak FWHM = 0.47–0.80 nm (before) and 0.64–1.00 nm (after)

A couple of samples also revealed peaks at 251.1, 254.2, 265.1, 286.0, 291.6, 407.8, and 409.6 nm.

After: In general, the PL features between 400 and 415 nm were removed by HPHT processing, except that in two samples the 412.3 nm peak was reduced to a faint band. Typically, the 415.2 (N3) and 417.2 nm peaks increased in intensity. All of the PL features below 300 nm were either less intense or absent altogether.

He/Cd Laser (325 nm)

Room Temperature

Before: The samples revealed two major PL systems, as well as a series of smaller peaks (figure 9B). The primary system is the N3, with its zero-phonon line (ZPL) at 415 nm (N3) and its associated phonon replicas with peaks at approximately 421, 428, 439, 441, 452, 463, and 478 nm (see box A). The second is the H3 system, which has its ZPL at 503 nm (H3), with the phonon replicas at approximately 512, 520, and 528 nm. As a result of the broadening of these replicas that occurs at room-temperature conditions, a wide, underlying PL emission was readily visible, with its apex at approximately 520–525 nm. Other PL bands were recorded at 404, 496 (H4), 537, 576 (N-V)⁰, and 580 nm.

After: N3 was the only dominant PL system after processing. There was a general increase in the emission of the N3 system and its ZPL at 415 nm. In two samples, the faint, broad band at 404 nm was still present. No other PL bands were visible, including the entire H3 system.

Low Temperature

Before: At low temperature, the N3 and H3 systems were sharper and a number of other PL features appeared (figure 10B). In the area of the N3 system, we recorded additional peaks at 406.0, 409.6, 412.3, 417.2, and 423.0 nm. The width of the 415.2 nm (N3) line measured at the position of half the peak's height (known as "full width at half maximum" or FWHM) was determined to range from 0.38 to 0.45 nm (see Fish and Comins, 1997; Fish et al., 1999).

In the area of the H3 system, all but one of the samples exhibited a 490.7 nm peak (attributed to defects decorating slip planes; Collins and Woods, 1982). Most also showed a 496.1 nm (H4) peak, as well as associated peaks at 498.3 and 504.9 nm, which were equal in intensity.

All but one of the samples revealed two adjacent

(but unrelated) peaks at 575.8 and 574.8 nm (N-V)⁰, ranging from very weak to moderate, with a relative intensity of 575.8 \geq 574.8. (At room temperature, these two peaks merged to form the 576 nm peak.) The variations in relative intensity and band widths recorded during our study are consistent with the findings of Fisher and Spits (2000), which indicate that the 574.8 nm (N-V)⁰ is an independent transition from the 575.8 nm peak. These PL bands were not present in the GGL sample. The 537 nm peak recorded at room temperature also resolved into a pair of independent transitions (535.9/537.4 nm); in two of the samples, however, only the 537.4 nm peak was present. We also recorded a 578.8 nm peak in all samples.

After: We identified a number of significant changes. Several peaks were removed completely, including the 406.0, 423.0, 490.7, 496.1 (H4) and its related peaks at 498.3 and 504.9 nm; the two at 535.9/537.4 nm; the two at 574.8 (N-V)⁰ and 575.8 nm; and the 580 nm peak. In addition, the H3 system was either completely removed, or so drastically reduced that only a very small trace of the 503.1 nm (H3) ZPL was present. The N3 system, however, increased in emission. A small peak at 430.9 nm was increased or introduced in several samples. There was no apparent modification to the remaining peaks.

The FWHM of the 415.2 nm (N3) ZPL was 0.30 to 0.40 nm. A slight narrowing of this ZPL was recorded in all samples.

Ar-ion Laser (514 nm) and Frequency-Doubled Nd/YAG Laser (532 nm)

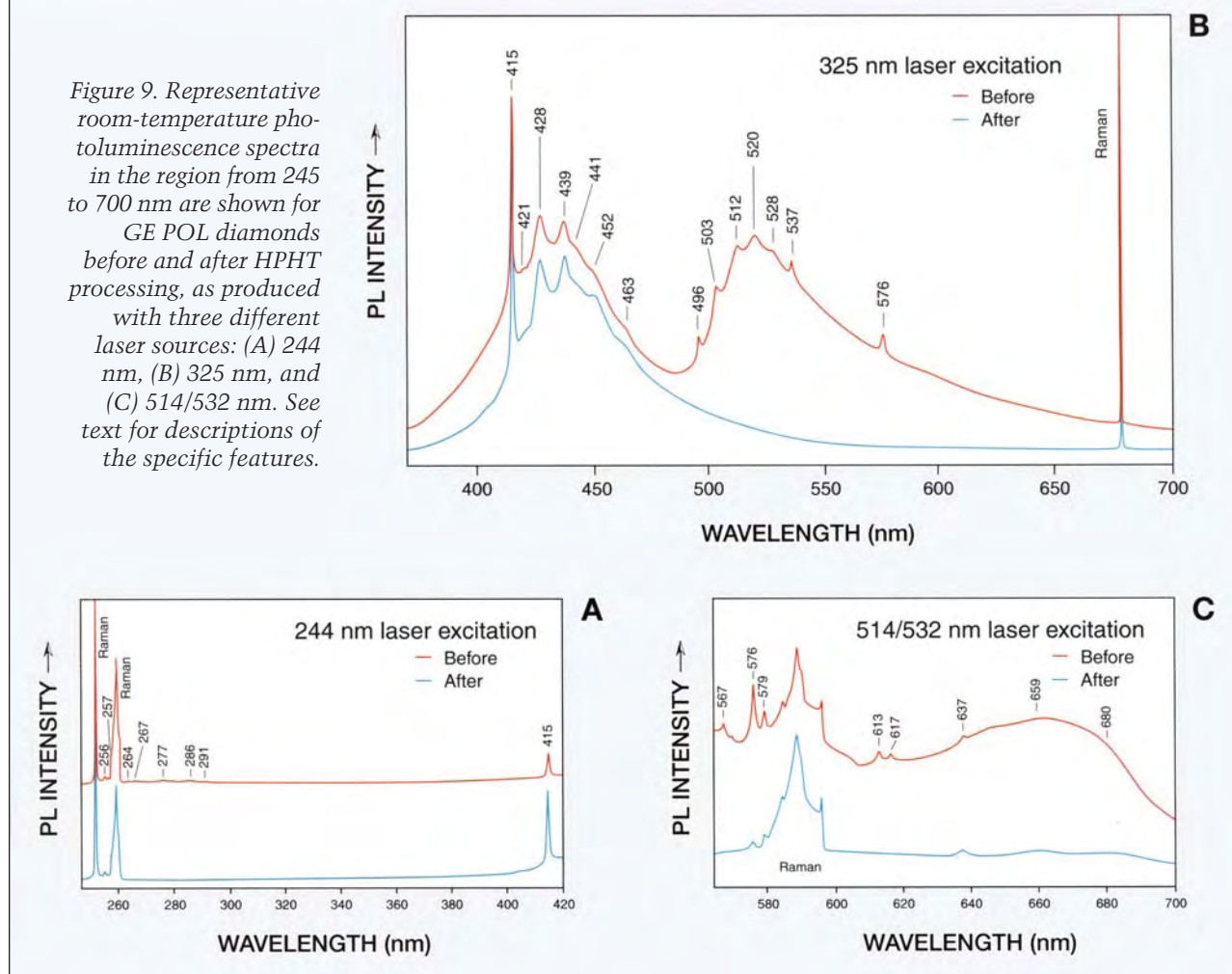
Room Temperature

Before: We recorded a faint to distinct 576 nm peak in all but one of the samples, and a weak peak at 579 nm in all samples (figure 9C). Faint, broad bands were also recorded at 587 nm, 596 nm, and approximately 613–617 nm. Another PL feature in this region was the 637 nm (N-V)⁻ system. In only four of the samples was the ZPL at 637 nm present, ranging from faint to moderate. This PL system was accompanied by broad side bands with maxima at approximately 659 and 680 nm.

After: The 576 nm peak was dramatically reduced in all samples, leaving only traces. In addition, the peaks at 567 and 579 nm, as well as those between 596 and 630 nm, were no longer present. The 637 nm (N-V)⁻ system was generally reduced overall. The GGL sample did not have either the (N-V)⁰ or the (N-V)⁻ centers.

Room-Temperature Photoluminescence

Figure 9. Representative room-temperature photoluminescence spectra in the region from 245 to 700 nm are shown for GE POL diamonds before and after HPHT processing, as produced with three different laser sources: (A) 244 nm, (B) 325 nm, and (C) 514/532 nm. See text for descriptions of the specific features.



Low Temperature

Before: Again, upon cooling, improved resolution yielded additional PL features, as well as more precise peak locations (figure 10C). A series of small peaks were present at 558.8, 566.8, and 569 nm. The two peaks at 574.8 and 575.8 (N-V)⁰ nm were clearly resolved; however, with this excitation, we typically recorded 574.8 > 575.8. One sample showed only the 575.8 nm peak, while another did not show either peak. We observed a faint to weak peak at 578.8 nm in all samples. There were faint, broad bands at approximately 600 and 620 nm in most of the samples analyzed, as well as a sharp 612.3 nm peak in two of them.

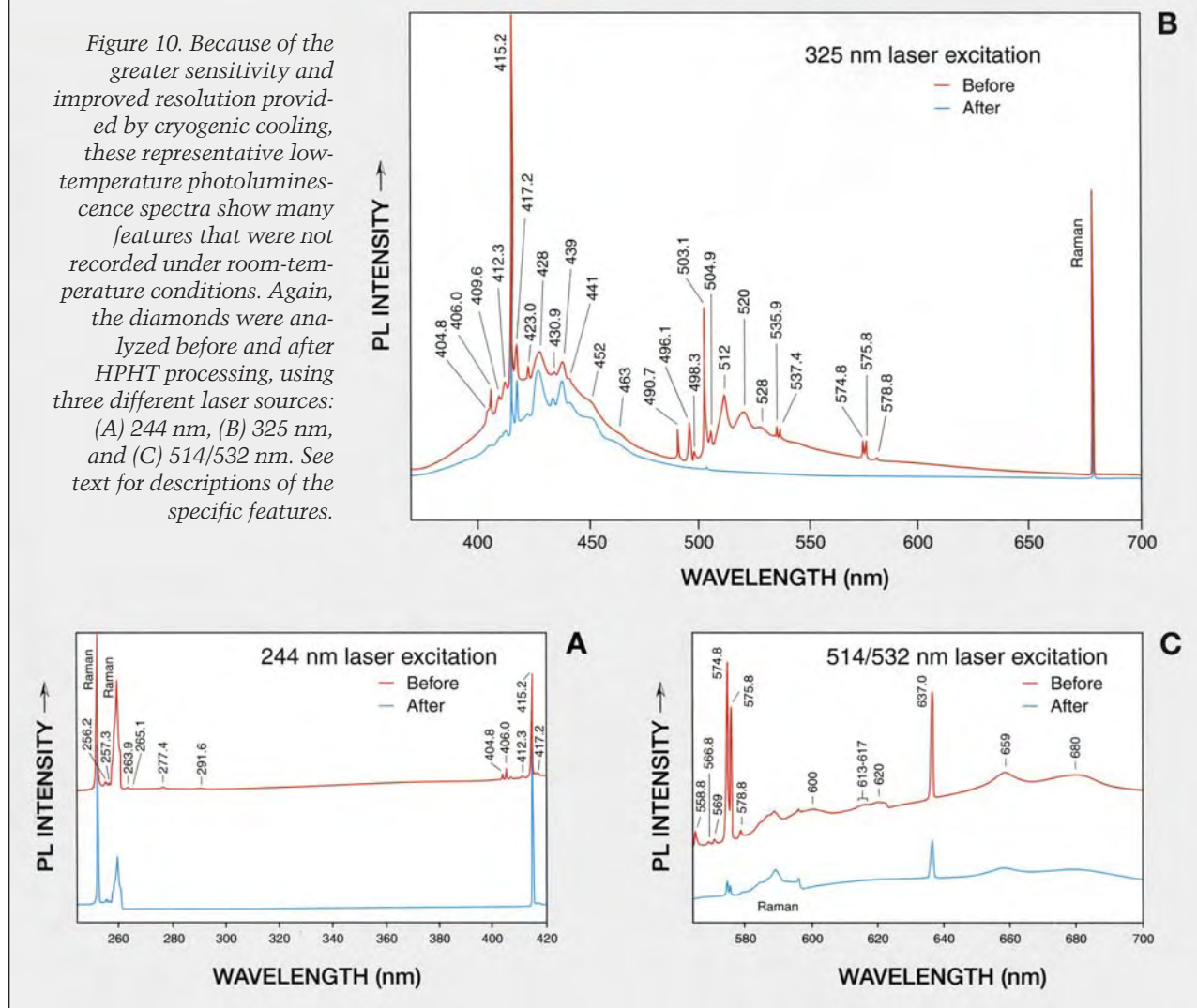
The 637.0 nm (N-V)⁻ system was further refined to reveal sharper, more distinct bands at 637.0 (ZPL), 659, and 680 nm. However, even at low temperature, the 637.0 nm (N-V)⁻ was not present in the

GGL sample. The FWHM of the 637.0 nm ZPL ranged from 0.47 to 0.80 nm, and the ratio of the 574.8/637.0 N-V peaks ranged from 1.7 to 7.7.

After: HPHT processing resulted in significant modification to this region. Again, many PL features were removed, including those at 558.8, 566.8, 569, and 578.8 nm, and between 596 and 630 nm. With this laser and under these conditions, the two at 574.8 (N-V)⁰ and 575.8 nm were dramatically reduced, but still present. The relative intensity of these peaks remained approximately the same, although in a couple of samples the 575.8 nm peak did seem slightly more reduced. In one sample, where there was a strong 574.8 nm (N-V)⁰ peak and only a weak 575.8 nm peak prior to HPHT processing, the 575.8 nm peak was no longer evident. The 637.0 nm (N-V)⁻ system was typically reduced over-

Low-Temperature Photoluminescence

Figure 10. Because of the greater sensitivity and improved resolution provided by cryogenic cooling, these representative low-temperature photoluminescence spectra show many features that were not recorded under room-temperature conditions. Again, the diamonds were analyzed before and after HPHT processing, using three different laser sources: (A) 244 nm, (B) 325 nm, and (C) 514/532 nm. See text for descriptions of the specific features.



all. Even under these conditions, the GGL sample still did not show either of the N-V centers (574.8 or 637.0 nm).

We recorded a distinct reversal in the ratio between the 574.8 and 637.0 nm peaks, as described by Fisher and Spits (2000). In our samples under these conditions, they ranged from 0.3 to 0.7. The FWHM of the 637.0 nm peak also increased slightly to approximately 0.64 to 1.00 nm. The slight broadening of this ZPL also occurred in all samples.

RESULTS: CATHODOLUMINESCENCE AND X-RAY TOPOGRAPHY (See Box B)

Cathodoluminescence Colors

Before: We observed CL colors ranging from a chalky yellow-white of moderate intensity, to a

strong blue-white. Most of the samples displayed an even texture, with no structure to the luminescence visible. However, one did reveal a slightly irregular or “cottony” overall texture, as well as a narrow “vein” that was slightly less luminescent.

After: All samples revealed a general shift in the CL colors toward blue. The strongest shift occurred with samples that changed from a moderate yellow-white to a strong blue-white after processing (figure 11). We noted no change in the distribution of the CL texture.

Cathodoluminescence Phosphorescence

All the samples revealed a rapid and steadily declining phosphorescence, which lasted approximately 1–1.5 seconds, both before and after HPHT processing.

BOX B: CATHODOLUMINESCENCE AND X-RAY TOPOGRAPHY AS NONDESTRUCTIVE TOOLS IN GEMOLOGY

Cathodoluminescence (CL) spectroscopy and X-ray topography can provide a great deal of information about the structure of a diamond. Because HPHT procedures may heal the dislocations and lattice defects that produce certain luminescence centers, these two methods are useful in reconstructing the processes by which the lattice is changed. Although neither method is broadly applied in gemology, CL has been used extensively in technical studies of diamonds (Panczer et al., 1996).

CATHODOLUMINESCENCE

CL is the emission of light from a solid surface when excited by an electron beam. Depending on the accelerating voltage (usually between 1 and 30 kV), the electrons penetrate about 1–3 μm . Some fundamental properties of minerals—such as lattice defects, impurities, and other disturbances in the crystal lattice—are represented by luminescence centers. The energy of the electron beam is transferred within a diamond by these optical centers and can give rise to distinctive CL colors and other patterns. Today, two types of CL equipment are used for gemstones to detect these optical signals.

“Cold CL”: Using flood gun optical microscopy, the luminoscope is mounted on a microscope stage. The electrons are generated in a cold cathode device. This small glass tube contains discharge gas (e.g., air, nitrogen, or helium) as well as the cathode and the anode. As soon as high tension is applied between the cathode and the anode, electrons are created. The electrons pass through the hollow anode and enter the low-evacuated (10^{-2} Torr) sample chamber. A lead-glass window in the sample compartment allows visual observation of the luminescence behavior, so the CL color, zonation, and phosphorescence can be observed. Color photomicrographs of these features can be taken at magnifications up to 125 \times . The light emitted by the diamond is focused via the microscope objective onto a monochromator. Luminescence spectra can be recorded within a range of 380 to 1000 nm (compare to Ponahlo, 1996).

“Hot CL”: Hot-cathode luminescence microscopy is relatively new (Götze, 1996). The CL spectrometer is attached to a scanning electron microscope (SEM), and the electrons are generated by a hot filament. The typical acceleration voltage is 15 kV, and the beam current is about 1 nA. The sample must be mounted on a special holder because of the high vacuum (about 10^{-6} Torr) within the sample compartment. In addition, the diamond must be coated by graphite, both so the SEM can focus on the surface of the sample (at magnifications up to about 100,000 \times) and to

avoid charge clouds generated by the electron beam. This equipment can combine the optical and chemical analytical capabilities of the SEM-EDS system.

Because the electron beam of the SEM is focused, very small areas (<10 μm in diameter) can be analyzed. The main disadvantage is that there is no mechanism for capturing images. Luminescence spectra can be recorded between 200 and 800 nm.

X-RAY DIFFRACTION TOPOGRAPHY

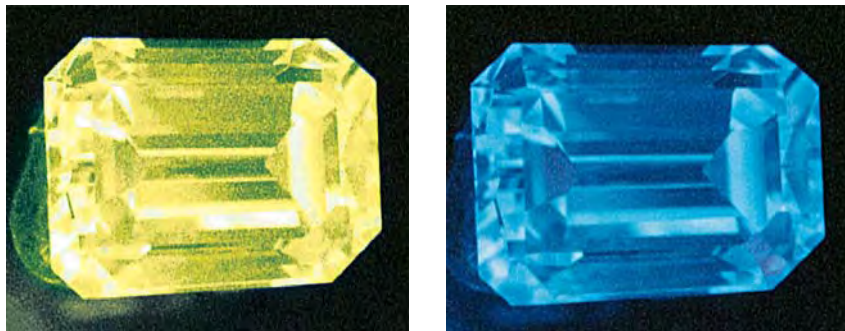
This imaging method allows visualization of defects associated with lattice distortions in a single-crystal material. It can record the spatial distribution of dislocations, growth striations, stacking faults, and even defects detectable by visual inspection, such as inclusions and mechanical damage (e.g., scratches, cracks). Although it is a nonmagnifying method with rather poor spatial resolution, it is highly sensitive to lattice strain. Because of X-ray absorption, it is usually restricted to relatively small crystals or crystal slices of limited thickness. However, diamond has a low absorption of X-rays, so samples with diameters up to 10 mm can be analyzed by using X-rays of appropriate wavelengths.

X-ray topography is based on the diffraction of X-rays by the atomic structure of the crystal. This diffraction is described by the reflection of X-rays by a set of “lattice planes” at discrete angles, according to the Bragg equation. Since there are many sets of lattice planes in a crystal (e.g., corresponding to the faces of the octahedron {111}, the cube {100}, or the rhombododecahedron {110}), X-ray topographs can be recorded with different reflections: 111, 220, etc. For methods using monochromatic X-rays, such as the Lang technique, the orientation of the crystal structure with respect to the morphology of the sample must be known; only one reflection is used, providing a single topograph, and the crystal must be carefully adjusted with respect to the incident beam. See Sunagawa et al. (1998) for a short description of the Lang technique and its application to the study of faceted diamonds.

An alternative method is the old Laue technique, which uses the continuous (“white”) spectrum of a conventional X-ray tube or synchrotron radiation source. This technique does not require a laborious adjustment of the crystal with respect to the incident beam; the X-ray film is simply placed behind the faceted diamond, with no pre-orientation needed. Many topographs (representing different reflections and generated by different wavelengths) are recorded on the film with a single exposure.

For more information on X-ray topography, see the reviews by Lang (1978) and Klapper (1996).

Figure 11. The CL color of the GE POL diamonds prior to processing ranged from chalky yellow-white (left) to blue-white. After processing, all of the samples shifted in CL color to blue (right), with an increase in intensity. Photos by Johann Ponahlo.



Cathodoluminescence Spectroscopy

Before: The CL spectrum of each sample was characterized by two dominant emission bands (figure 12): One band was centered at approximately 430 nm (in the blue region of the spectrum), and the other at about 520 nm (in the green region). Although much remains unknown about the mechanisms that produce these CL bands, the one centered at 430 nm is called the “blue” A band and has been attributed to donor-acceptor pair recombination or to dislocations (Pagel et al., 2000). In addition, it appears that this “blue” A band has been superimposed by the N3 system in the samples included in this study. The band in the green region has been attributed to H3 centers (Sumida et al., 1981; Jorge et al., 1983; Van Enkevort and Visser, 1990; Graham and Buseck, 1994).

It is important to mention that the “green” band revealed significantly less emission with the hot cathode as compared to the flood gun technique, because of polarizing effects of the monochromatic grid in the hot CL spectrometer. With the hot cathode apparatus, the “green” band was always significantly weaker than the “blue” band; in two samples, it was present only as a shoulder to the “blue” band. No other CL bands were observed.

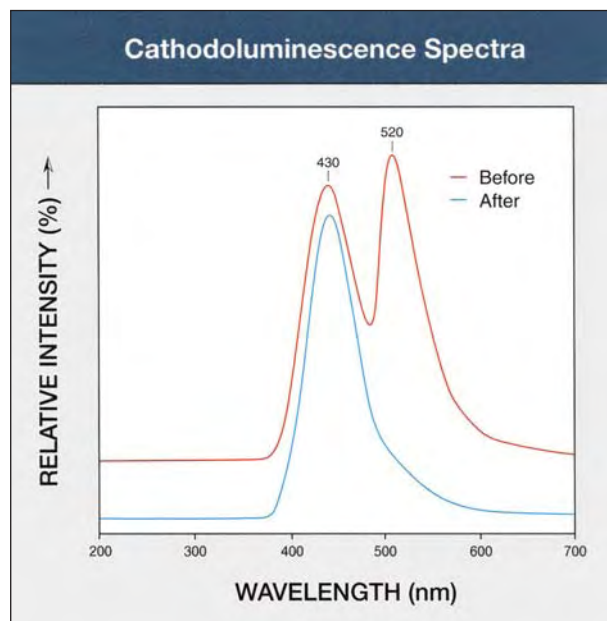
After: The CL spectra were dramatically changed in all diamonds on exposure to HPHT. With the flood gun technique, it was most clearly shown that the “green” band was either dramatically reduced or completely eliminated. A similar decrease of this CL band was reported by Yang et al. (1995). This resulted in a single dominant “blue” band in the spectra for all of the samples after processing. In some diamonds, there also was a general decrease in the emission intensity of the 430 nm band; in others, however, there was a dramatic increase.

X-Ray Topography

Before: X-ray topographs provide a clear picture of the condition of the diamond crystal’s lattice. Using the Laue technique, we identified a wide range of

lattice distortion in the brown type IIa diamonds prior to HPHT enhancement (figure 13). Some samples were relatively “perfect,” in that they displayed only very slight lattice imperfections, which faintly distorted the outline of the topograph, and few or no striations or changes in intensity within it. One sample, however, was heavily distorted: It revealed extreme bending of the lattice planes, as well as highly variable concentrations of lattice strain and defects. All of the other samples were intermediate between these two extremes, with the lattice planes bent to various degrees and concentrations of lattice strain and defects that ranged from homogeneous to highly irregular.

Figure 12. Before processing of the diamonds, cathodoluminescence spectra in the region from 200 to 700 nm revealed a pair of CL bands with maxima at approximately 430 and 520 nm. After HPHT processing, the CL band at 520 nm was typically removed, although a weak shoulder remained for a couple of samples.



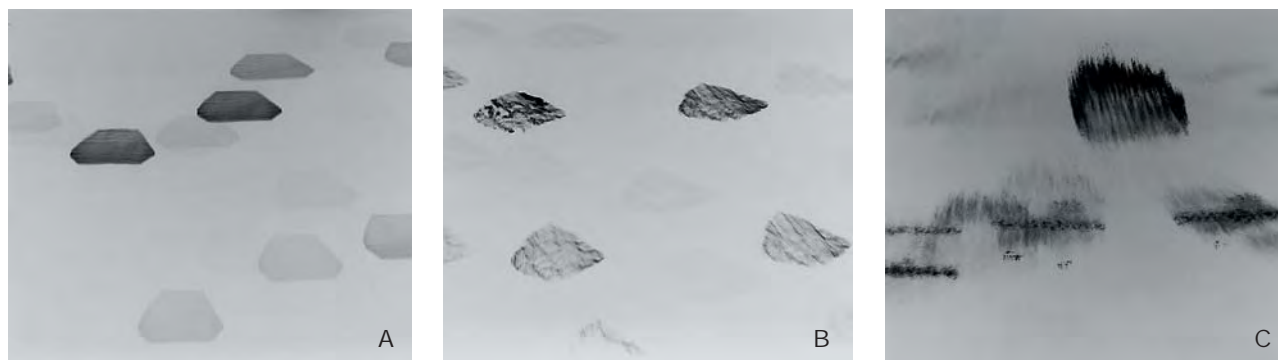


Figure 13. X-ray topography identified a broad range of crystal distortion in the diamonds prior to HPHT processing. Topograph A is of a stone with very little lattice distortion, as may be seen by the geometric outline of the individual topographs and the mostly homogeneous blackening of the X-ray film. The presence of subtle striations indicates that there was also a degree of inhomogeneity in defect centers in certain regions of the crystal lattice. The diamond in topograph B exhibits an intermediate stage of lattice distortion and more prominent inhomogeneity of lattice defects, as can be seen by the uneven blackening of the X-ray film. Topograph C illustrates a diamond with more extreme lattice distortion, with lattice planes that are severely bent and dramatic fluctuations in the concentration of lattice strain and defects, which is evidenced by the amorphous outlines of the topographs and the highly irregular blackening of the X-ray film.

After: We were surprised to see no fundamental modification of the X-ray topographs after the diamonds were exposed to HPHT conditions. The relative perturbation of the crystal lattice was maintained, as was the inhomogeneity of lattice strain. Although we did detect very subtle localized changes in the intensity contrasts of lattice strain and defect concentrations in a couple of the diamonds, this was not consistently the case across the sample population.

DISCUSSION

Visual Appearance and Microscopy. We observed a number of significant changes as a result of GE's exposure of these diamonds to HPHT conditions. The most dramatic change was in color, in one case from Fancy Light brown to D (although not all stones will achieve such results).

We also gained a better understanding of what happens to various inclusions (crystals and fractures) during exposure to HPHT conditions. In the course of our ongoing research, we at GGL—like other researchers (see, e.g., Moses et al., 1999; Chalain et al., 2000)—have noted unusual-appearing inclusions in GE POL diamonds. One persistent question was whether or not the healed fractures observed in GE POL diamonds were previously “open” fractures that actually “healed” under HPHT conditions. In our sample stones, the open fractures clearly did not heal, although they did change slightly in appearance and in some cases were extended, creating an outer fringe. However, we did identify a slight degree of healing immediately surrounding an included crystal.

We did not see any fundamental changes in graining and strain before and after processing. We believe that the subtle increase in intensity of these two properties after HPHT annealing is mainly an optical effect resulting from the removal of the original brown coloration. Therefore, it appears that many of the unusual characteristics noted in other GE POL diamonds are representative of the “starting material” used rather than by-products of the HPHT process itself.

UV-Vis-NIR and IR Spectroscopy. The removal of color was a result of the reduction of the absorption continuum and of the general absorption level in the visible to ultraviolet region of the spectrum. In addition, we witnessed the development of a broad 270 nm band in all of the samples. The 270 nm band is attributed to isolated nitrogen (Dyer et al., 1965). With efficient recording techniques, this band was detectable in the samples color graded as high as D.

We did not record any changes in the IR spectra of our samples before and after treatment. Although all of the samples are type IIa, three of the GE POL diamonds showed at least faint nitrogen absorption at 1174 cm^{-1} caused by the B aggregate. Given sufficient IR sensitivity, evidence for the production of isolated nitrogen in the IR spectra might have been expected in at least some of the diamonds after processing. With our measuring routine, however, we did not detect the 1344 cm^{-1} band or even the weak, broad 1130 cm^{-1} band, both of which are related to isolated nitrogen atoms generated under HPHT con-

ditions, as described by Fisher and Spits (2000). In our experience, the IR spectra of brown diamonds are occasionally accompanied by a very weak hydrogen peak at 3107 cm^{-1} . This line is not introduced during HPHT processing.

Cathodoluminescence. In general, the CL color shifted from yellow to blue as a result of HPHT enhancement. Prior to processing, all of the diamonds had the two CL bands. After processing, only the “blue” band remained, and it was typically of higher intensity. The severe reduction or complete removal of the “green” band was most clearly witnessed with the use of the “cold” flood gun CL method. It appears to correlate with the removal of H3 photoluminescence as detected at room temperature with He/Cd laser excitation.

X-Ray Topography. Most natural diamonds undergo some degree of plastic deformation subsequent to crystal growth. It has been proposed that plastic deformation of natural diamonds takes place after crystallization during cataclysm of mantle rocks (Orlov, 1977) or during eruption of the host magma to the surface (Collins et al., 2000). It is associated with birefringence along more or less parallel and even intersecting lamellar glide systems (Lang, 1967). Brown coloration in natural diamonds is generally believed to be related to such circumstances, although the exact color mechanism is still unknown (Harlow, 1998; Collins et al., 2000). If natural brown type IIa diamonds are exposed to HPHT conditions that permit plastic flow and atomic diffusion within the lattice of the diamond, it is assumed that the lattice distortion and defects are annealed and, consequently, the brown coloration is removed. For a discussion of the methods used to accomplish plastic flow and atomic diffusion in diamond, the reader is referred to Schmetzer (1999).

X-ray topography revealed several important details relating to the distortion present in the crystal lattice and its impact on the brown coloration, strain, and graining of the diamonds we studied. The extremes we recorded in the X-ray topographs of our diamonds (ranging from relatively “perfect” to heavily distorted) were surprising because of the uniformity of color present in the individual diamonds, as well as across the sample population. “Long-range” lattice distortion (i.e., the bending of the lattice over distances of up to several millimeters), which results from plastic deformation and is recorded by this technique, may also be manifest by

such visible dislocation features as graining and strain birefringence. From this work, it is evident that annealing of such long-range lattice distortion is not taking place and thus cannot be responsible for the dramatic removal of the brown coloration. Rather, our results suggest that the brown coloration is linked to submicroscopic structures on or near dislocations, which also occur as a result of plastic deformation. These may consist of vacancies and interstitials attached to a dislocation.

Consequently, we saw that HPHT processing has little if any effect on the macroscopic or long-range lattice distortion indicators (e.g., graining and strain), but it clearly has an impact on submicroscopic structures, as witnessed with PL. Although all of the isolated vacancy-related point defects discussed in this article are well understood in relation to their production of color centers, such point defects attached to a dislocation would produce optical properties very different from those produced in isolation (D. Fisher, pers. comm., 2000).

Photoluminescence. The PL studies revealed some reconfiguration in the lattice of the diamonds, by the reduction, elimination, generation, and/or movement of vacancies and interstitials, as well as of impurity elements. On the basis of this research, it is possible to propose a model for some of the events that were recorded. In particular, this very sensitive method clearly illustrated that minute amounts of nitrogen impurities are present in all of these type IIa samples, even though IR spectroscopy could not always detect them, and revealed the presence of a considerable number of point defects dispersed throughout the crystal lattice.

Our research and that of others (e.g., Collins et al., 2000; Fisher and Spits, 2000) suggests that HPHT processing releases vacancies and interstitials as the dislocations heal. The elimination of the 490.7 nm PL band confirms that changes are taking place at the slip traces (Collins and Woods, 1982; Collins et al., 2000). In a type IIa diamond, there is a mutual annihilation of vacancies and interstitials within the lattice. The overall effect of these changes is to reduce the brown color. In addition, HPHT processing leads to the elimination of N-V centers (through the breakup of N-V or the diffusion of interstitial carbon into the vacancy), as witnessed by the reduction of the 574.8 nm $(\text{N-V})^0$ and 637.0 nm $(\text{N-V})^-$ systems, as well as by the dramatic reduction of the 503.1 nm N-V-N (H3—a vacancy associated with an A aggregate) luminescence and

removal of the 496.1 nm 4N-2V (H4—a vacancy associated with a B aggregate) system. Furthermore, it is believed that the presence of vacancies and mobile nitrogen leads to the production of additional N3 centers (three nitrogen atoms surrounding a common vacancy). This was evidenced by the increase recorded in N3 emission after processing.

Although we did not record the sharp 1344 cm^{-1} or the broad 1130 cm^{-1} IR bands related to single substitutional nitrogen, we did detect the creation of single nitrogen by the development of the 270 nm broad band in the UV region of the spectrum. In their article, Fisher and Spits attributed the production of single nitrogen to the break-up of A-centers. However, from the results of our study, we attribute this to the break-up and mobilization of a vacancy associated with a single nitrogen (i.e., N-V centers; 574.8/637.0) or the diffusion of interstitial carbon into the vacancy. The reduction in the neutrally charged N-V center (574.8 nm) was more dramatic than that of the negatively charged N-V center (637.0 nm), which resulted in a reversal of the relative intensity of $(\text{N-V})^0/(\text{N-V})^-$. This is consistent with the information reported by Fisher and Spits (2000). In addition, although we did not record a statistical modification of the relative intensities of the 574.8/575.8 nm peaks overall, we did note a slightly greater reduction of the 575.8 nm peak in some samples.

The defects responsible for several of the PL bands we recorded are not known. These include the peaks located at 406.0 and 423.0; the 498.3 and 504.9 nm peaks, which seemed to be related to the 496.1 (H4); the 535.9/537.4 pair; and the peaks at 558.8, 566.8, 569, and 578.8 nm. Therefore, we are unable at this time to discuss or explain the mechanics behind their removal during HPHT processing.

In some respects, the GGL sample did not reveal the same PL behavior as the samples from GE. We have attributed this to the fact that, based on the PL emission of the N3 system, this diamond was chemically much more “pure” than the other samples. It was not pre-selected for this condition.

The data recorded from these samples both before and after HPHT processing by GE are consistent with comparable data taken from natural-color brown type IIa diamonds and GE POL diamonds that have been part of a larger ongoing study being conducted by the Gübelin Gem Lab.

[Authors' note: The reconfiguration taking place within the lattice of HPHT-processed type Ia diamonds is somewhat different from that described above for type IIa diamonds, in that typically N-V-

N (H3 and H2) centers are being created. For a discussion of HPHT-processed type Ia diamonds, see Collins et al. (2000) and Reinitz et al. (2000).]

APPLICATIONS: POTENTIAL AND LIMITATIONS

This discussion draws from information gathered in the course of a much larger GGL research project that involves the characterization of HPHT color-enhanced type IIa diamonds and non-enhanced type IIa diamonds (the results of which will be presented in a future paper). On the basis of those data and the results obtained from this before-and-after study, we believe that we can draw several preliminary conclusions with regard to the separation of natural-color type IIa diamonds and GE POL stones.

First, it is important to state that thus far no single property or characteristic has been identified that will unequivocally distinguish between natural high-color type IIa diamonds and GE POL's Bellataire high-color type IIa diamonds. Rather, any such separation must rely on a combination of features and observations. A short-wave UV transparency test (see, e.g., Liddicoat, 1993) is a good method with which to begin the process, that is, to indicate that a diamond is type IIa. However, it must be kept in mind that low-nitrogen-content type Ia diamonds (in particular, type IaB's) are also short-wave UV transparent. Therefore, to firmly identify a type IIa diamond, infrared spectroscopy is necessary.

Second, although the number of high-color HPHT-processed type IIa diamonds in the marketplace may increase in the years to come, at this point there are relatively very few. Therefore, indicators that clearly establish that a diamond has *not* been exposed to HPHT processing are just as crucial to the separation process as characteristics that identify that a diamond *has* been HPHT processed.

Inclusions. The wide diversity of inclusions in diamonds is a hallmark of nature (see, e.g., Gübelin and Koivula, 1986; Roskin, 1994; Koivula, 2000). Since virtually all GE POL stones are the rare type IIa diamonds, which typically are very clean, the vast majority of inclusion features that may be seen in the broad population of diamonds are not observed in GE POL stones.

In fact, only a rather limited variety of inclusions have been noted in GE POL diamonds. These include graphitized inclusions (some with expansion halos), fractures, crystals with stress fractures, and “partially healed” fractures (see also Moses et

al., 1999). As described above, most of these relate to the starting material, and are not a by-product of the HPHT process itself. However, although such internal features may be encountered in nonprocessed diamonds (in particular brown diamonds), they are *not* commonly encountered in nonprocessed high-color type IIa diamonds. Consequently, the observation of such inclusions is not proof of HPHT enhancement, but it should alert the observer that more analytical testing is necessary to confirm the origin of color.

[*Authors' note: According to GE's Dr. John Casey (pers. comm., 2000), the vast majority of GE POL diamonds now being produced are in the clarity range of IF to VVS. Therefore, the inclusion features described above relate more to GE POL diamonds from earlier productions.*]

Graining. A very high percentage of GE POL diamonds reveal weak to moderate internal graining, which is characteristic of the brown starting material used. Such graining has also been encountered in nonprocessed high-color type IIa diamonds, but with much less frequency.

Some types of graining that may be encountered in natural-color diamonds have not been seen in GE POL diamonds thus far. These include reflective graining planes and extensions of surface grain lines. To date, we have observed a very short surface grain line in only one GE POL diamond. It is expected that diamonds with reflective graining or extensive surface grain lines would break along that plane of structural weakness on exposure to HPHT conditions.

Strain Patterns. The anomalous birefringence exhibited by both nonprocessed high-color type IIa diamonds and GE POL diamonds is typified by weak to prominent banded and tatami extinction patterns. Therefore, these patterns are of no use in this separation. Earlier GE POL diamonds occasionally exhibited stronger, mottled strain patterns, with high-order interference colors (see, e.g., Moses et al., 1999; figure 17, left) that were unlike those seen in nonprocessed high-color type IIa diamonds. If such a strain pattern is observed in a high-color type IIa diamond, it is a good indication that the stone may have been HPHT enhanced. [*Authors' note: GE's Dr. Thomas Anthony (pers. comm., 2000) reports that GE POL diamonds with high-order mottled strain were encountered only rarely in early material and are no longer produced.*]

UV-Vis-NIR Absorption Spectroscopy. With the use of high-sensitivity techniques, all of the GE POL diamonds we investigated revealed absorption bands at 236 nm (strongest line of the N9 absorption system, related to B aggregates) and 270 nm (related to single substitutional nitrogen), even in the D-color stones. Although research by GGL and De Beers (D. Fisher, pers. comm., 2000) has shown that the 270 nm band may also occur in nonprocessed type IIa diamonds, it is apparently rare. If this band is recorded in a high-color type IIa diamond, testing should be conducted to confirm the origin of color.

Infrared Spectroscopy. In our experience, high-color diamonds that are short-wave transparent, yet prove to have a small but obvious type Ia component in the IR, are not HPHT enhanced. High-resolution techniques (Fisher and Spits, 2000) have revealed minute traces of absorption characteristic of type Ib diamond (1344 and 1130 cm^{-1}) in HPHT-processed diamonds. Although we did not record these bands in the GE POL diamonds we examined, if present they are a good indication of HPHT enhancement. Observation of hydrogen in a high-color type IIa diamond is not an indication of HPHT color enhancement.

If a diamond of yellow hue (H color or lower) is identified as type IIa by infrared spectroscopy, this is a very strong indication that it has been HPHT processed. [*Authors' note: According to Dr. John Casey (pers. comm., 2000), GE produced diamonds with such low colors only during the early stages of HPHT product development. Presently, the vast majority of GE POL diamonds are in the D through G range, with the highest percentage being D or E.*]

If none of the above-mentioned features is present, IR spectroscopy is not a useful indicator.

Photoluminescence. The most consistent and significant means of distinguishing nonprocessed high-color type IIa diamonds and GE POL diamonds is through a detailed analysis of photoluminescence. Note in this section that it is very important to relate the information to the particular laser excitation used, because certain PL bands behaved slightly differently depending on the excitation. In addition, low-temperature analyses with liquid nitrogen provide the best means to resolve and evaluate the PL spectra, although room-temperature analyses with the 325 nm He/Cd laser may prove useful in some cases.

244 nm Excitation. Our initial results indicate that the presence of 404.8, 406.0, 409.6, and 412.3 nm

PL peaks at low temperature can provide a good indication that a high-color diamond has *not* been HPHT enhanced. The mechanisms responsible for the weak-to-faint PL features noted below 300 nm have not been identified to date, so their relevance to the distinction of GE POL diamonds is currently not clear.

325 nm Excitation. A number of key features can be observed with this laser. In the region surrounding the N3 system, the presence of the 406.0 or 423.0 nm peaks at low temperature provides evidence that the diamond is *not* HPHT enhanced, whereas the 430.9 nm peak is a good indication of HPHT processing. Our initial results suggest that the increased intensity and narrowing of the N3 ZPL do not provide a means of separation.

In the region surrounding the H3 system, again the presence of a number of peaks detected at low temperature can confirm when a type IIa diamond has *not* been HPHT color enhanced. These include the 490.7, the 496.1 (H4) and two associated peaks at 498.3 and 504.9 nm, the 535.0/537.4 pair, and the 574.8 (N-V)⁰ and 575.8 nm peaks, as well as the 578.8 nm PL peak. (It is important to note that some of these peaks may be recorded with the "green" Ar-ion laser after HPHT processing, so this statement relates strongly to the use of the He/Cd laser.) A faint 503.1 nm (H3) ZPL may still be detected after HPHT processing; however, this N-V-N is in such low concentrations post-processing that the phonon replicas, between 510 and 530 nm, are no longer observable.

Room-temperature PL analysis with this laser also may identify a *nonprocessed* high-color diamond, when PL bands are recorded at wavelengths greater than 480 nm. These could include the 496 nm (H4), the H3 phonon replicas, and the 537, 576, and 580 nm PL bands, none of which was visible after HPHT processing. Note that the overall emission of the side-band structure of the H3 system is easier to detect when the stone is at room temperature than at low temperature.

514/532 nm Excitation. At low temperature, the presence of the 558.8, 566.8, and 569 nm peaks, as well as the series of PL bands between 600 and 620 nm, is a good indication that the diamond has not received HPHT processing. The 637.0 nm (N-V)⁻ ZPL has been seen in both nonprocessed and processed high-color type IIa diamonds, and so appears to be of no diagnostic value. Our research confirms the findings of De Beers (Fisher and Spits, 2000), in that we

also witnessed a reversal of the ratio between the 574.8 and 637.0 peaks. A ratio of $574.8 < 637.0$ remains a very good, though not conclusive, indication of HPHT enhancement. The FWHM of the 637.0 nm line was generally greater in processed type IIa diamonds than in nonprocessed specimens that exhibited a 637.0 nm ZPL, but we did record some degree of overlap between the two distributions (as compared to, for example, Hänni et al., 2000).

Cathodoluminescence. With CL spectroscopy, we found it easier to establish that certain diamonds had *not* been color enhanced through HPHT processing than to identify that a diamond *had* been HPHT processed. In our experience, all GE POL diamonds show the single, dominant blue CL band. A small percentage of GE POL diamonds also have a very weak green CL band, which typically is present only as a shoulder to the blue CL band. Many nonprocessed high-color diamonds reveal the same type of CL spectrum; however, others have a more prominent green CL band, which has not been encountered in GE POL diamonds.

In addition, many nonprocessed high-color type IIa diamonds and all the GE POL diamonds we have examined to date display a blue CL luminescence and do not phosphoresce. Still many other nonprocessed high-color type IIa diamonds reveal yellow, pink, or white CL colors or a distinct phosphorescence; none of these reactions has been observed in GE POL diamonds.

X-ray Topography. X-ray topography revealed significant insight into the effects of plastic deformation and its role in the generation of brown color. However, our initial results indicate that it does not provide a means to distinguish GE POL diamonds. De Beers is conducting similar research with transmission electron microscopy (TEM), which is taking this type of work to an atomic level to investigate HPHT-induced modifications to dislocations and the associated changes in electronic states thought to be responsible for the observed brown absorption.

CONCLUSIONS

General Electric was the first to announce the successful HPHT synthesis of diamond in 1955. For the past two decades, GE's Superabrasives division has been exploring methods to improve the optical and mechanical properties of HPHT- and chemical vapor deposition-grown synthetic diamond, both of which have a wide variety of industrial applications. GE's

BOX C: RUSSIAN HPHT-PROCESSED DIAMONDS

General Electric is not the only company with the ability and equipment to apply HPHT techniques to remove the brown coloration in natural type IIa diamonds. De Beers has shown that they can achieve similar results in experiments aimed at establishing identification criteria (see, e.g., Fisher and Spits, 2000), and facilities in Russia and the U.S., as well as elsewhere, certainly have the apparatus and technical expertise to perform HPHT processing (see, e.g., Reinitz et al., 2000). Although the fundamental parameters of HPHT techniques will be similar from one organization to the next, the details of the individual methods will undoubtedly differ.

De Beers was aware of the potential of HPHT color enhancement 20 years ago, and as long as 10 years ago Russian colleagues had told the present authors (CPS and GB) that they were successfully lightening the color of brown diamonds (although the diamond type was not discussed). Unfortunately, we were not able to obtain actual samples at that time. Within the past year, however, we have acquired samples of HPHT-processed diamonds from sources in Russia—both type IIa colorless diamonds (figure C-1) and type Ia yellow-green diamonds.

As part of our research, we performed the same gemological and advanced analytical tests on the Russian samples as are reported in this article. Both types of samples—yellow-green and colorless—were brown before treatment, but we were only able to examine the diamonds after processing. The properties we recorded for the type Ia yellow-green samples are consistent with those described by Reinitz et al. (2000) for HPHT-enhanced yellow-green diamonds.

Although some features noted in the colorless Russian HPHT-processed diamonds do suggest that differences exist in the details of their operating conditions as compared to those used by GE, overall the properties (including photoluminescence and cathodoluminescence spectra) of the Russian stones are consistent with those of the GE POL diamonds

described in this article. The senior author (CPS) examined a pink diamond that reportedly was a type IIa that had been HPHT enhanced in Russia; however, he was not given the opportunity to analyze it.

General Electric, Lazare Kaplan, and Pegasus Overseas Ltd. have been criticized since they first introduced GE POL color-enhanced diamonds. However, they must be commended for announcing this new product before they began to market it and for properly disclosing the diamonds they are processing and selling. HPHT color-enhanced diamonds coming out of Russia (and potentially elsewhere) are not being sold with the same level of conscientiousness toward the diamond trade. We know that some of these diamonds are entering the international trade through various channels without any form of proper disclosure.



Figure C-1. These type IIa diamonds (1.53 and 0.27 ct) were processed in Russia using an HPHT technique similar to that used by GE. They have a frosted surface because they had not yet been repolished after processing. Photo by Phillip Hitz.

research activities in this area primarily have involved the use of a high pressure/high temperature apparatus to achieve plastic flow and atomic diffusion within such materials, whereby "slippage" occurs along crystallographic directions, to remove voids and other defects. It was in the course of this research that GE happened on a means to remove the brown coloration in natural brown type IIa diamonds (J. Casey, pers. com., 2000; see, e.g., Anthony et al., 1995).

It is important to note that General Electric is

not the only firm that has access to such technology. Similar experiments are being made elsewhere (see box C), and HPHT-processed diamonds from other sources may be entering the international trade without disclosure.

This study represents the first detailed analysis of actual GE POL diamonds both before and after HPHT processing by GE. Previous research on this topic was restricted to comparing the analytical details of post-processed diamonds to those of

unrelated natural brown to colorless type IIa diamonds—in effect relying on “reverse engineering” to investigate what changes and effects were taking place as a result of the HPHT processing. Fisher and Spits (2000) described type IIa diamonds that had been HPHT-annealed as part of De Beers’s research into identification techniques; however, there are undoubtedly subtle differences in the processes used by GE and De Beers. Therefore, the study of known GE-processed HPHT diamonds before and after treatment is crucial to the understanding and identification of HPHT-enhanced diamonds in general, and GE POL diamonds in particular.

Although there is still no single feature by which a GE POL diamond can be identified, on the basis of this study and our ongoing research into unprocessed high-color type IIa and GE POL diamonds, we have determined a number of features that we believe will conclusively establish that a diamond is *not* HPHT treated. These include a wide variety of inclusions, some types of graining, and IR spectra, as well as various photoluminescence and cathodoluminescence activities. Indicators that a diamond has been HPHT processed are provided by inclusion features and photoluminescence spectra.

In particular, this study has identified three significant regions of activity in the photoluminescence and cathodoluminescence behavior of these diamonds, between 400 and 700 nm. These are in the spectral regions surrounding the N3 system (around 400 nm), the H3 system (around 500 nm), and the N-V centers (from 550 to 650 nm). To cover this spectral range, we recommend a Raman system that has been optimized for high-spectral resolution analyses at liquid nitrogen temperatures, using an He/Cd laser (324.98 nm excitation) in the UV and an Ar-ion laser (514.5 nm excitation) in the “green” region of the spectrum. (Room-temperature conditions did reveal some usefulness with regard to the H3 emission; however, liquid nitro-

gen temperatures are best suited for this type of analysis.) Not all of the features and mechanisms behind the observed changes are fully understood. As research continues at the Gübelin Gem Lab and elsewhere, we may find that some of these details have greater significance than is presently known.

The separation of HPHT color-enhanced type IIa diamonds is more demanding than the identification of most other forms of color alteration applied to gem-quality diamonds. It is important for the trade to understand that the application of this very sophisticated technology is progressing rapidly. Other colors that may be produced via HPHT processing of natural diamonds include yellow to yellowish green, pink, and blue (J. Casey and T. Anthony, pers. comm., 2000). Those parties involved with HPHT color enhancement will also continue to refine the techniques and conditions that they apply. Therefore, continued research is essential to guarantee that such HPHT-enhanced diamonds are fully characterized and that a means of detection is available.

Acknowledgments: The authors thank General Electric, Lazare Kaplan, and POCL for their support and cooperation, as well as for permitting documentation of the diamonds before and after HPHT enhancement. Drs. Hans-Jürgen Reich and Myriam Moreau performed Dilor LabRam Infinity Raman spectral analyses in Lille, France. Drs. Riccardo Tagliapietra, Ken Williams, and Annette Zimmerman from Renishaw PLC performed Renishaw System 1000 Raman spectral analyses. Geraint Evans, H.H. Wills Physics Laboratory, University of Bristol, U.K., assisted with the 325 nm Raman spectra. Prof. W. Mican and Dr. F. Brandstätter, Museum of Natural History, Vienna, Austria, are thanked for their assistance with scanning CL microscopy. The team at De Beers Diamond Trading Center, Maidenhead, provided valuable discussions and suggestions. Thomas Gübelin, president of Gübelin AG, sponsored this project.

REFERENCES

- Anthony T.R., Banholzer W.F., Spiro C.L., Webb S.W., Williams B.W. (1995) *Toughened Chemically Vapor Deposited Diamond*. European Patent Application, open-laid No. 0 671 482 A1, published September 13, 1995.
- Chalain J.-P., Fritsch E., Hänni H.A. (1999) Detection of GE POL diamonds: A first stage. *Revue de Gemnologie a.f.g.*, No. 138/139, pp. 30–33.
- Chalain J.-P., Fritsch E., Hänni H.A. (2000) Detection of GE POL diamonds: A second step. *Journal of Gemmology*, Vol. 27, No. 2, pp. 73–78.
- Collins A.T. (1982) Colour centres in diamond. *Journal of Gemmology*, Vol. 18, No. 1, pp. 37–75.
- Collins A.T., Woods G.S. (1982) Cathodoluminescence from “giant” platelets, and of the 2.526eV vibronic system, in type Ia diamonds. *Philosophical Magazine B*, Vol. 45, No. 4, pp. 385–397.
- Collins A.T. (1992) The characterisation of point defects in diamond by luminescence spectroscopy. *Diamond and Related Materials*, Vol. 1, No. 5-6, pp. 457–469.
- Collins A.T. (1996) Characterisation of CVD and HPHT diamond. *Conference Proceedings, Italian Physical Society*, Vol. 52, pp. 43–57.

- Collins A.T., Kanda H., Kitawaki H. (2000) Colour changes produced in natural brown diamonds by high-pressure, high-temperature treatment. *Diamond and Related Materials*, Vol. 9, No. 2, pp. 113–122.
- Davies G. (1977) The optical properties of diamond. In P.L. Walker, Jr. and P.A. Throver, Eds., *Chemistry and Physics of Carbon*, Vol. 13, Marcel Dekker, New York, pp. 2–143.
- Davies G. (1999) Current problems in diamond: Towards a quantitative understanding. *Physica B*, Vol. 273–274, pp. 15–23.
- Dyer H.B., Raal F.A., Du Preez L., Loubser J.H.N. (1965) Optical absorption features associated with paramagnetic nitrogen in diamond. *Philosophical Magazine*, Vol. 11, No. 112, pp. 763–773.
- Field J.E. (1992) *The Properties of Natural and Synthetic Diamond*. Academic Press, London, 710 pp.
- Fish M.L., Comins J.D. (1997) Photoluminescence spectroscopy of synthetic diamond. *Materials Science Forum*, Vol. 239–241, pp. 103–106.
- Fish M.L., Massler O., Reid J.A., MacGregor R., Comins J.D. (1999) The application of photoluminescence and Raman spectroscopy of synthetic diamond. *Diamond and Related Materials*, Vol. 8, No. 8–9, pp. 1511–1514.
- Fisher D., Spits R.A. (2000) Spectroscopic evidence of GE POL HPHT-treated natural type IIa diamonds. *Gems & Gemology*, Vol. 36, No. 1, pp. 42–49.
- Fritsch E., Scarratt K. (1992) Natural-color nonconductive gray-to-blue diamonds. *Gems & Gemology*, Vol. 28, No. 1, pp. 35–42.
- Götze J. (1996) Cathodoluminescence in applied geosciences: Investigation of industrial products and use of combined CL and image analysis. *Abstracts of the International Conference on Cathodoluminescence and Related Techniques in Geosciences and Geomaterials*, Nancy, France, pp. 61–62.
- Graham R.J., Buseck P.R. (1994) Cathodoluminescence of brown diamonds as observed by transmission electron microscopy. *Philosophical Magazine B*, Vol. 70, No. 6, pp. 1177–1185.
- Gübelin E.J., Koivula J.I. (1986) *Photoatlas of Inclusions in Gemstones*. ABC Edition, Zurich.
- Hänni H.A., Chalaïn J.-P., Fritsch E. (2000) Letters: New spectral evidence for GE POL diamond detection. *Gems & Gemology*, Vol. 36, No. 2, pp. 96–97.
- Harlow G.E. (1998) *The Nature of Diamonds*. Cambridge University Press, 278 pp.
- Iakaubovskii K., Adriaenssens G.J., Nesladek M. (2000) Photochromism of vacancy-related centres in diamond. *Journal of Physics—Condensed Matter*, Vol. 12, No. 2, pp. 189–199.
- Jackson W.E., Webb S.W. (1995) Synthetic diamond strength enhancement through high pressure/high temperature annealing. *Materials Research Society Symposium Proceedings*, Vol. 383, pp. 267–272.
- Jorge M.I.B., Pereira M.E., Thomaz M.F., Davies G., Collins A.T. (1983) Decay times of luminescence from brown diamonds. *Portugaliae Physica*, Vol. 14, No. 3–4, pp. 195–210.
- Klapper H. (1996) X-ray diffraction topography: Principles and techniques. In A. Authier, Ed., *X-ray and Neutron Dynamical Diffraction Theory and Applications*. Plenum Press, New York, pp. 137–146.
- Koivula J.I. (2000) *The Microworld of Diamonds*. Gemworld International, Northbrook, Illinois.
- Lang A.R. (1967) Causes of birefringence in diamond. *Nature*, Vol. 213, No. 5073, pp. 248–251.
- Lang A.R. (1978) Techniques and interpretations in X-ray topography. In S. Amelinckx, R. Gevers, and J. van Landuyt, Eds., *Diffraction and Imaging Techniques in Materials Science*, North Holland, Amsterdam, p. 623.
- Lang A.R., Moore M. (1991) Cathodoluminescence and X-ray topography of HPHT diamonds. *New Diamond Science and Technology, Proceedings of the 2nd International Conference*, 1990, pp. 683–694.
- Liddicoat R.T. Jr. (1993) *Handbook of Gem Identification*, 12th ed. Gemological Institute of America, Santa Monica, CA, 364 pp.
- McCormick T.L., Jackson W.E., Nemanich R.J. (1997) The characterization of strain, impurity content, and crush strength of synthetic diamond crystals. *Journal of Materials Research*, Vol. 12, No. 1, pp. 253–263.
- Moses T.M., Shigley J.E., McClure S.F., Koivula J.I., Van Daele M. (1999) Observations on GE-processed diamonds: A photographic record. *Gems & Gemology*, Vol. 35, No. 3, pp. 14–22.
- Orlov Y.L. (1977) *The Mineralogy of the Diamond*. John Wiley & Sons, New York.
- Pagel M., Barbin V., Blanc P., Ohnenstetter D. (2000) *Cathodoluminescence in Geosciences*. Springer, Berlin.
- Panczer G., Garg M., Marfunin A.S. (1996) Systems of the interacting luminescence centres in natural diamonds: Laser-induced time-resolved and CL spectroscopy. *Abstracts of the International Conference on Cathodoluminescence and Related Techniques in Geosciences and Geomaterials*, Nancy, France, pp. 109–110.
- Ponahlo J. (1996) Cathodoluminescence: A fast, non-destructive method to distinguish between natural jadeite, dyed jadeite and dyed quartz simulants. *JewelSiam*, Vol. 7, No. 2, pp. 60–65.
- Rapnet (1999) Pegasus Overseas Limited, a subsidiary of Lazare Kaplan International Inc. to offer diamonds with new General Electric Company process—Press Release, March 1.
- Reintz I.M., Buerki P.R., Shigley J.E., McClure S.M., Moses T.M. (2000) Identification of HPHT-treated yellow to green diamonds. *Gems & Gemology*, Vol. 36, No. 2, pp. 128–137.
- Roskin G.A. (1994) *Photo Masters for Diamond Grading*. Gemworld International Inc., Northbrook, IL.
- Schmetzer K. (1999) Clues to the process used by General Electric to enhance the GE POL diamonds. *Gems & Gemology*, Vol. 35, No. 4, pp. 186–190.
- Sumida N., Lang A.R., Wills H.H. (1981) Cathodoluminescence and TEM studies of dislocation-rich natural diamonds. *Institute of Physics Conference Series*, No. 60, Section 6, pp. 319–324.
- Sunagawa I., Yasuda T., Fukushima H. (1998) Fingerprinting of two diamonds cut from the same rough. *Gems & Gemology*, Vol. 34, No. 4, pp. 270–280.
- Van Enckevort W.J.P., Visser E.P. (1990) Photoluminescence microtomography of diamond. *Philosophical Magazine B*, Vol. 62, No. 6, pp. 597–614.
- Walker J. (1979) Optical absorption and luminescence in diamond. *Reports on Progress in Physics*, Vol. 42, pp. 1605–1659.
- Webb S.W., Jackson W.E. (1995) Synthetic diamond crystal strength enhancement through annealing at 50 kbar and 1500°C. *Journal of Materials Research*, Vol. 10, No. 7, pp. 1700–1709.
- Wild R.K., Evans T. (1967) Birefringence, X-ray topography and electron microscope examination of the plastic deformation of diamond. *Philosophical Magazine*, Vol. 15, pp. 267–279.
- Wilks E.M., Wilks J. (1991) *Properties and Applications of Diamond*. Butterworth-Heinemann, Oxford.
- Woods G.S., Collins A.T. (1986) New developments in spectroscopic methods for detecting artificially coloured diamonds. *Journal of Gemmology*, Vol. 20, No. 2, pp. 75–82.
- Woods G.S., Lang A.R. (1975) Cathodoluminescence, optical absorption and X-ray topography studies of synthetic diamonds. *Journal of Crystal Growth*, Vol. 28, pp. 215–226.
- Yang X.X., Barnes A.V., Albert M.M., Albridge R.G., McKinley J.T., Tolk N.H. (1995) Cathodoluminescence and photoluminescence from chemical-vapor-deposited diamond. *Journal of Applied Physics*, Vol. 77, No. 4, pp. 1758–1761.
- Zaitsev A.M., Melnikov A.A., Denisenko A.V., Varichenko V.S., Job R., Fahrner W.R. (1996) Luminescence characterization and application of diamond. *Materials Research Society Symposium Proceedings*, Vol. 416, pp. 113–124.
- Zaitsev A.M. (1998) Optical properties. In M.A. Prelas, G. Popovici, and L.K. Bigelow, Eds., *Handbook of Industrial Diamonds and Diamond Films*. Marcel Dekker Inc., New York, pp. 227–376.

SAPPHIRES FROM ANTSIRANANA PROVINCE, NORTHERN MADAGASCAR

By Dietmar Schwarz, Jan Kanis, and Karl Schmetzer

Since 1996, large quantities of yellow to blue sapphires have been recovered from alluvial deposits derived from basaltic rocks in northern Madagascar. The crystal morphology, internal growth patterns, mineral inclusions, absorption spectra, and trace-element contents of these northern Madagascar sapphires are typical of “basaltic-magmatic” sapphires. Comparison of the properties of these sapphires to those of sapphires from different basaltic sources reveals no significant differences. The northern Madagascar sapphires are distinct from those from Andranondambo, a skarn-related deposit in southeastern Madagascar.

Madagascar was first visited by Europeans in 1500, when the Portuguese navigator Diego Diaz landed at a beautiful and well-protected bay on the northern tip of the island. Another Portuguese seafarer, Hernán Suarez, was sent to Madagascar by the Viceroy of India and also landed at this bay, in 1506. Thereafter, the name *Diego Suarez* was adopted for both the bay and the nearby town. Although the town has recently reverted to its Malagasy name, Antsiranana, many in the gem trade continue to use the old name when referring to sapphires from northern Madagascar (figure 1), which have been mined there since the mid-1990s.

The principal deposits are actually situated about 70 km south of Antsiranana, in the Ambondromifehy region in and near the Ankarana Special Reserve (figure 2), in Antsiranana Province. Elsewhere in northern Madagascar, sapphires have been found near Ambilobe and Milanoa (Superchi et al., 1997), which are located about 40 km and 100 km, respectively, south of Ambondromifehy. The properties of all of the samples from these areas are consistent with those of “basaltic-magmatic” sapphires that are known from eastern Australia, Nigeria, Thailand, Laos, and Cambodia. These sapphires are generally blue-violet, blue, greenish blue, greenish yellow, or yellow, and thus were designated “BGY [blue-green-yellow] sapphires” by Sutherland et al. (1998a).

So far, only limited gemological data on the sapphires from northern Madagascar have been published (see, e.g., Superchi et al., 1997; Schwarz and Kanis, 1998). This article presents a more complete gemological and mineralogical description of this material.

HISTORY

Until fairly recently, sapphire occurrences in Madagascar were mentioned only occasionally in the literature. A few years ago, however, attractive blue sapphires were discovered at Andranondambo, in the southeastern part of the

ABOUT THE AUTHORS

Dr. Schwarz (Gubelinlab@compuserve.com) is research manager at the Gubelin Gem Lab, Lucerne, Switzerland. Dr. Kanis, a consulting geologist and gemologist specialized in gemstone occurrences, lives in Veitsrodt, near Idar-Oberstein, Germany. Dr. Schmetzer is a research scientist residing in Petershausen, near Munich, Germany.

Please see acknowledgments at the end of the article.

Gems & Gemology, Vol. 36, No. 3, pp. 216–233
© 2000 Gemological Institute of America



Figure 1. Basalt-associated sapphire deposits were discovered in the Antsiranana Province of northern Madagascar in 1996. The blue-violet, blue, and greenish blue to greenish yellow colors shown here (1.04–2.98 ct) are typical of these sapphires; some exhibit distinct color zoning (see inset, 8.25 and 3.26 ct). Courtesy of Menavi International Ltd.; photo by Maha Tannous.

island, approximately 90 km northeast of Tolanaro/Fort Dauphin (Schwarz et al., 1996; Kiefert et al., 1996; Milisenda and Henn, 1996; Gübelin and Peretti, 1997; figure 2, inset). During the years following the Andranondambo “rush,” other deposits were discovered in the same region.

In 1996, blue-violet, blue, greenish blue, greenish yellow, and yellow (BGY) sapphires were discovered near Ambondromifehy (Bank et al., 1996; Lurie, 1998). A parcel of sapphires from this new area was first examined by one of us (KS) in June of that year. Later, numerous parcels became available for testing, and several brief articles were published (Bank et al., 1997; Superchi et al., 1997; Gonthier, 1997; Schwarz and Kanis, 1998).

The Ambondromifehy deposit soon became one of the most productive sources of commercial-quality sapphire in the world (“Sapphire mining halted. . .,” 1998). When the potential of the region became known, several thousand miners abandoned the Andranondambo area and migrated north to Ambondromifehy. During a brief visit there in July 1997, one of us (JK) saw thousands of miners digging sapphires west of the main road, No. 6, approximately 2.5 km southwest of Ambondromifehy village. By early 1998, about 10,000 diggers were active in the area (Lurie, 1998; “Sapphire mining halted. . .,” 1998). Nigerian and Thai buyers purchased much of the daily sapphire production.

Unfortunately, much of the digging occurred within the borders of the 18,225 hectare Ankarana Special Reserve (figure 2), a nature reserve well known for its magnificent karst topography. The

World Wildlife Fund for Nature (WWF), which had been involved in managing the reserve since 1985, pressured the Malagasy government to stop the illegal mining. The government’s solution was to prohibit all mining and commerce in sapphires from northern Madagascar, beginning in mid-April 1998. This comprehensive ban was applied to activities both within and outside the reserve (Lea, 1998; Lurie, 1998; “Sapphire mining halted. . .,” 1998). However, because the government lacked the means to enforce this decision, the illegal mining and buying continued. Recognizing its failure to halt these activities, the government officially lifted the ban on August 17, 1998 (Holewa, 1998; Banker, 1998).

With the October 1998 discovery of attractive sapphire, ruby, and other gems west and south of the Isalo National Park (i.e., near Ilakaka, Sakaraha, and Ranohira; see, e.g., Johnson et al., 1999; Schmetzer, 1999a; figure 2, inset), many miners moved from the Ambondromifehy region to these extensive new alluvial deposits. By spring 1999, almost no mining activity was observed in Antsiranana Province (Schmetzer, 1999a), although some of the miners subsequently returned to the area when they could not obtain productive claims in the Ilakaka region (Laurs, 2000).

LOCATION AND ACCESS

The Ambondromifehy sapphire deposits are located at 12°54’S, 49°12’E (Carte topographique Ambilobe, 1:100,000, feuille U 32). The main road (RN6) from Antsiranana to Ambondromifehy is an all-weather

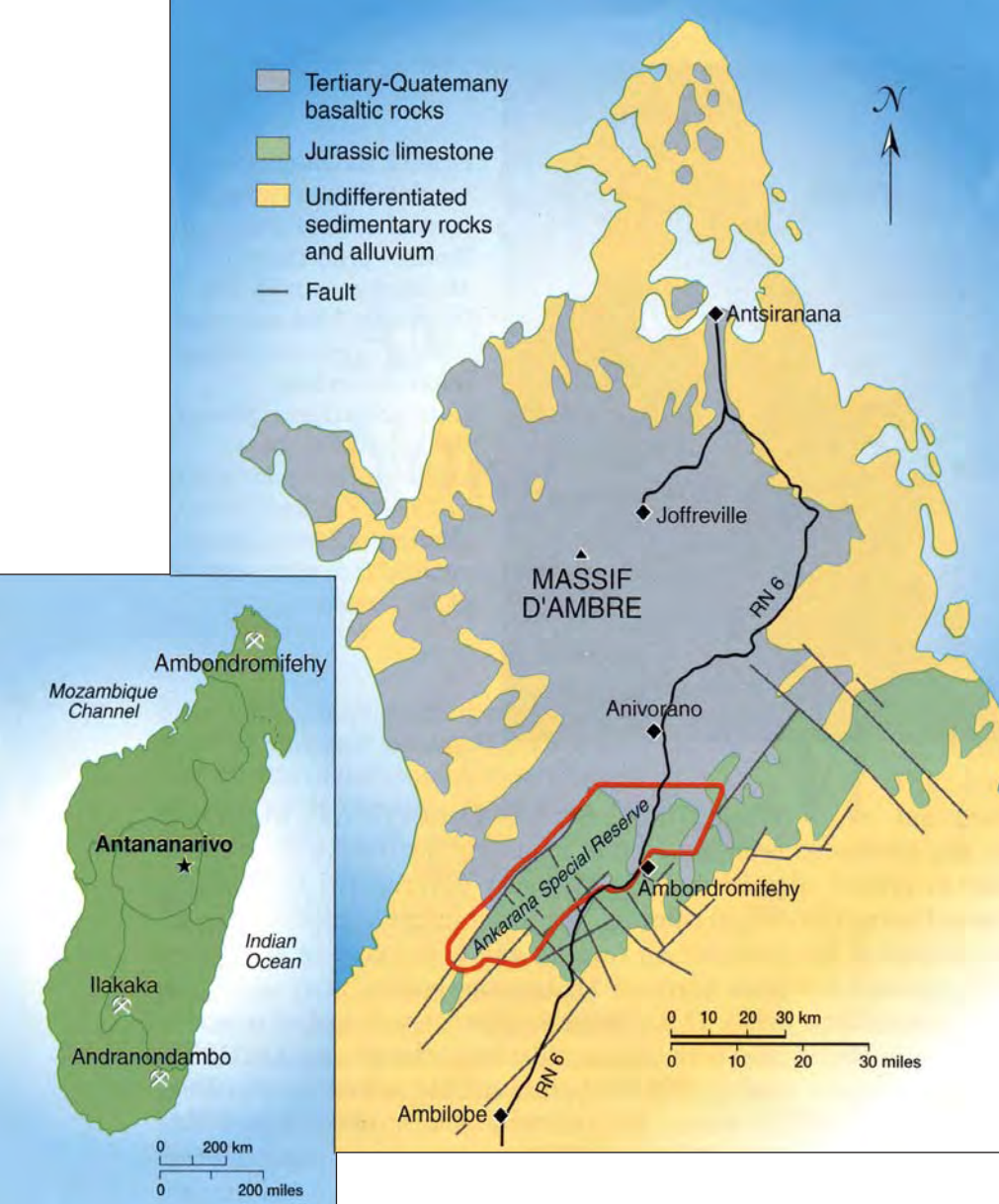


Figure 2. The most important sapphire deposits in Antsiranana Province, at the northern tip of Madagascar, are located in the Ambondromifehy region in and near the Ankarana Special Reserve. These deposits are associated with basalts of the Massif d'Ambre volcano. Erosion of the basalts deposited sapphire-bearing sediments on nearby limestones, particularly in the Ambondromifehy region. Other basalt-related sapphire deposits are located up to 100 km further south, near Ambilobe and Milanoa (not shown on the map). Geology after Saint-Ours and Rerat (1963), Saint-Ours et al. (1963), and Besairie (1969). The inset shows the location of the three major sapphire deposits in Madagascar: Ambondromifehy, Andranondambo, and Ilakaka.

paved road. It is not difficult to reach the various deposits from the main road on foot, although for safety reasons visitors should always be escorted by a reliable guide. One author (JK) noticed that the sapphire dealers are particularly unwelcoming to unescorted foreigners for fear of competition.

Diggers use local names to indicate the various sites where they work. For example, the occurrence visited by JK in 1997 is called Antokotaminbato, which is located approximately 2.5 km southwest of Ambondromifehy on the main road.

GEOLOGY AND OCCURRENCE

Corundum deposits related to alkali basalts are common in many regions—especially eastern Australia and Southeast Asia, but also Nigeria (Kanis and Harding, 1990). The origin of these rubies and sapphires has been widely debated among geologists and mineralogists (for a summary, see, e.g., Levinson and Cook, 1994; Sutherland et

al., 1998a). The alkali basalts are thought to carry the corundum crystals to the surface from the earth's interior, where they formed. Note, however, that different sources of gem corundum may be entrained by the basaltic magmas. New studies have shown that some basaltic fields (e.g., in Australia, Cambodia, Laos, and Thailand) yield two types of corundum: the "basaltic-magmatic" (hereafter, *magmatic*)—or BGY—sapphires are found together with "basaltic-metamorphic" (hereafter, *metamorphic*) pastel-colored sapphires and rubies. The latter gems are thought to be derived from metamorphic or metasomatic source rocks in the earth's interior. The two types of basalt-hosted sapphires can be identified by trace-element chemistry and/or absorption spectroscopy (Sutherland et al., 1998a and b).

Northern Madagascar is mostly covered by a 3,500 km² area of volcanic origin (again, see figure 2) that dates from the early Tertiary period to the

Quaternary. The 35-km-wide stratovolcano, the Massif d'Ambre, is constructed of alternating layers of lava and pyroclastic deposits along with abundant dikes and sills. Beneath the summit (which reaches 1,475 m above sea level), the mountain slopes gently from 800 m to 500 m into the surrounding flat plains. The sources of all major rivers in the region are found on the slopes of the Massif d'Ambre, and they have undoubtedly affected the formation of placer sapphire deposits.

Sapphire-bearing alluvial material derived from the eroded alkali basalts was deposited in voids and crevices of the weathered Jurassic Ankarana limestone that lies south of the Massif d'Ambre. Occasionally, these sediments are cemented by secondary carbonates (figure 3). Recent prospecting has failed to locate any sapphire-bearing basalt flows, perhaps because they lie buried beneath subsequent barren lava flows or were fully eroded in the area ("An initial appraisal . . .," 1997).

MINING AND PRODUCTION

The local miners dig pits up to 8 m deep to reach the sapphires, which are concentrated in the lower levels of the alluvium. The areas around the roots of the trees (mainly bamboo in this region) are also favorable sites, because the greater decomposition of the soil makes digging easier (figure 4). Mechanized mining has been conducted by only two companies, which set up operations outside the Ankarana reserve (see, e.g., figure 5). Significant quantities of commercial-grade sapphire were pro-

Figure 3. Sapphire crystals from northern Madagascar are occasionally found embedded in carbonate-cemented sediments. The dark blue sapphire shown here measures 14 mm long. Photo by M. Glas.



Figure 4. Miners at Ambondromifehy have found that digging around the roots of trees is the easiest way to recover sapphires. Photo by J. Kanis.

duced by these operations (see, e.g., figure 6). One of these, IMA Group/Suzannah, produced over 350 kilograms of corundum during the years 1996-1998, of which generally 12%–16% was facetable (Issac Mehditash, pers. comm., 2000).

An indication of the amount and quality of sapphires produced from one of these mines (ABFG) is given in box A. Heating is required for all but a very small percentage (usually <5%) of the rough gem sapphires from Ambondromifehy. Typically, heat treatment is applied to remove milky areas and to develop a blue to blue-violet color in unattractive white, yellowish green, or greenish yellow samples. The temperature, time, and gas atmosphere must be strictly controlled to prevent the sapphires from becoming too dark.

MATERIALS AND METHODS

The total sample set consisted of more than 1,000 BGY sapphire crystals, about 250 faceted sapphires, and 80 star (cabochon-cut) sapphires. From this large group, we selected the samples that were tested by the various methods described below.

All the sapphires were purchased in Madagascar by several gem dealers or by one of the authors (JK). No samples from trade centers outside Madagascar (e.g., Bangkok) were included in the study. The samples reportedly came from the Ambondromifehy region, which is the center of sapphire mining activity in northern Madagascar. However, the parcels also may have included magmatic sapphires from other sources within Antsiranana Province, as dealers



Figure 5. At this mechanized operation in the Anivorano area (the “M4” pit), a track-hoe dumps sapphire-bearing alluvium into a trommel (right). The gem-bearing gravel is then pumped from the small pit on the left to a nearby washing plant (see inset). Photos courtesy of Mega Gem s.a.r.l.

typically mix sapphires from different producers in a single parcel.

The fashioned samples were cut in Madagascar. The authors polished one or two windows on about 100 of the rough crystals to facilitate testing. The faceted stones reportedly had not been subjected to heat treatment before examination. However, one of us (KS) treated about 500 of the crystals to study

Figure 6. The rough sapphires are hand-sorted on light tables into separate quality and size categories. These parcels, totaling approximately 50 kg, were produced from the “M4” pit. Photo courtesy of Mega Gem s.a.r.l.



the effects of heating. These crystals were originally milky white, greenish yellow, and greenish blue. Details of the heat treatment process used are proprietary.

About 30 faceted samples and crystals with polished windows (which represented the full range of colors available) were tested by standard gemological methods for optical properties, fluorescence, and density (hydrostatically). Morphological and crystallographic features of about 100 crystals were determined with a standard goniometer. The inclusion features and internal growth structures (i.e., color zoning and growth planes) of about 70 faceted and 30 rough sapphires were examined with a horizontal microscope using an immersion cell. Solid inclusions were identified by laser Raman microspectrometry with a Renishaw Raman microprobe or a Philips XL 30 scanning electron microscope equipped with an energy-dispersive spectrometer (SEM-EDS).

Polarized ultraviolet-visible-near infrared (UV-Vis-NIR, 280 to 880 nm range) absorption spectra were recorded for 15 rough and 15 faceted natural-color sapphires (again, all colors; selected from the 100 examined microscopically above)—and approximately 30 heat-treated rough sapphires before and after treatment—with Leitz-Unicam SP 800 and Perkin Elmer Lambda 9 spectrophotometers. The orientation of the rough samples was determined in accordance with their external morphology. For the faceted sapphires, we selected only those samples with table facets that were oriented perpendicular to the c-axis, which produce the most accurate polarized spectra. For 10 samples selected on the

BOX A: SAPPHIRE PRODUCTION FROM THE ABFG MINE, AMBONDROMIFEHY AREA

Compiled by M. Sevdermish, MENAVI International, Ramat Gan, Israel

At the time of this contributor's visit in mid-1999, the ABFG mine was a small mechanized operation located about 16 km south of Anivorano, close to the border of the Ankarana Special Reserve. An excavator and a water cannon were used to transport the gem-bearing soil into jigs, where the heavy components were separated and collected. Final sorting of the concentrate was done by hand.

The operation typically extracted 3-5 kg of sapphires in a 10-hour shift. Only about 17% of the rough produced was usable for heat treatment and cutting (table A-1). The color distribution of the original, untreated rough was reminiscent of Australian rough:

- 35% very milky bluish green (very few pieces are facetable after heating; most are low quality to cabochon, too dark)
- 30% very milky, almost opaque very dark blue (too dark after treatment)
- 23% transparent very dark blue, some with green or yellow zoning (nearly black after treatment)
- 5% pale gray or greenish blue and transparent (pale-colored crystals with small patches or zones of blue or green sometimes resulted in fine blue gems after treatment)
- 5% pale blue, milky (produced medium- to fine-quality gems after treatment, usually less than 1 ct after faceting)
- 2% other colors: yellow, "oily" green, and bicolored (most do not react to heating, but some "oily" green stones became almost black)

After the rough was sorted and cleaned, all samples of sufficient clarity and with a potentially suitable color were heat-treated. Virtually none of the rough produced from the ABFG mine was suitable for cutting before heat treatment. After each careful-

TABLE A-1. Characteristics of rough sapphires from the ABFG mine, before heat treatment.

Average weight (grams)	% of production	% cuttable	Cuttable as a % of total
>1	11	5-10	1
0.5-1.0	16	10-15	1.6
0.2-0.5	30	15-20	5
0.1-0.2	40	20-25	8
<0.1	3	25-30	1
Total	100		16.6

ly performed heating run (all treatment was conducted outside Madagascar), the sapphires were again sorted and some were removed for further heating. Up to 10 heat treatments at different atmospheric and temperature conditions may be necessary to achieve cuttable rough. The color distribution of the sapphires from the ABFG mine after heat treatment was as follows:

- 5% fine blue
- 30% medium blue
- 30% medium blue with greenish overtone
- 15% dark blue-violet, similar to dark Australian sapphires
- 5% greenish yellow
- 15% not usable (heavily included and/or uneven color distribution)

The weight and yield distribution of stones faceted from the treated rough are shown in table A-2.

In summary, about 5 kg of rough sapphire from this mine would be expected to yield 900 carats of faceted stones; this corresponds to a total yield from the rough of 3.6%. As of mid-2000, mechanized mining at ABFG had been halted.

TABLE A-2. Weight and yield distribution of heat-treated sapphires from the ABFG mine.

Weight category (grams)	Usable rough from total production (%)	Yield of faceted material from usable rough (%)	Average ct weight of faceted stones	Yield from 5 kg of rough (ct)
>0.5	2.6	16	1.0	100
0.2-0.5	5	18	0.3	350
<0.2	9	20	0.1	450

basis of their visible-range absorption spectrum, we also measured polarized spectra in the IR region up to 1800 nm using the Perkin Elmer Lambda 9 spectrophotometer.

The chemical composition of 137 rough (with at least one polished window) and fashioned samples, representing all color groups and the asteriated stones, was analyzed by energy-dispersive X-ray fluorescence (EDXRF) spectroscopy. These analyses were performed with a Tracor Northern Spectrace 5000 system, using a program specifically developed for trace-element geochemistry of corundum by Prof. W. B. Stern, Institute of Mineralogy and Petrography, University of Basel. These data were compared to EDXRF results of Schwarz et al. (1996) for sapphires from Andranondambo, Madagascar.

RESULTS

The results are summarized in table 1 and discussed below.

Visual Appearance. The natural-color Ambondromifehy sapphires (as they will be referred to in this section, although some may be from other deposits in Antsiranana Province) spanned a wide range of hues: blue-violet and various shades of blue, greenish blue, greenish yellow, and yellow (figures 7 and 8). One lot of 50 greenish yellow sapphires subjected to heat treatment showed almost no reaction, but the remaining 450 samples became a significantly more attractive blue-violet to blue. The greatest difficulty encountered during heat treatment was in making the crystals more trans-

TABLE 1. Gemological characteristics of sapphires from Antsiranana Province, Northern Madagascar.

Property ^a	No. samples	Description
Color	ca. 1,300	Homogeneous coloration (i.e., blue-violet, blue, greenish blue, greenish yellow, or yellow) is rare. More common is distinct color zoning with blue-violet, greenish blue to greenish yellow, and yellow domains. Also bi- and tri-colored stones ^b .
Clarity	ca. 1,300	Very clean to fairly included. Many natural-color stones show translucent milky white or blue areas; some stones are completely translucent. Heating usually improves transparency.
Refractive indices	30	$n_g = 1.761\text{--}1.765$ $n_o = 1.769\text{--}1.773$
Birefringence	30	0.008
Optic character	30	Uniaxial negative
Specific gravity	30	3.99–4.02
Pleochroism	ca. 100	<i>Yellow:</i> Light yellow c-axis, slightly more intense yellow ⊥ c-axis (i.e., almost no pleochroism) <i>Greenish blue:</i> Yellow c-axis, blue to blue-violet ⊥ c-axis <i>Intense blue to blue-violet:</i> Blue c-axis, blue-violet ⊥ c-axis <i>Greenish yellow to yellowish green:</i> Greenish yellow to yellow-green c-axis, blue to blue-violet ⊥ c-axis
Fluorescence	30	Inert to long- and short-wave UV radiation
UV-Vis absorption spectra	60	Intense bands at 376, 388, and 450 nm in <i>yellow</i> sapphires. <i>Blue</i> and <i>greenish blue</i> sapphires also show intense bands with maxima at about 560 nm (⊥c > c), and at about 870–880 nm (⊥c > c). <i>Greenish yellow to yellowish green</i> sapphires have an additional weak absorption band at 542 nm (c > ⊥c).
Internal features Growth characteristics	100	<ul style="list-style-type: none"> • Often strong color zoning. • Growth patterns <ol style="list-style-type: none"> (1) Looking ⊥ c-axis: Either ω or z with n and c; combination of c with r; occasionally, oscillatory zoning between hexagonal dipyramids (e.g., ω and z) (2) At an inclination of 5°–10° to c: Characteristic pattern of ω or z faces (3) At about 30° to c-axis: Characteristic structure of two n faces and one r face. • Occasionally, lamellar twinning parallel to r.
Inclusions		<ul style="list-style-type: none"> • Mineral inclusions: Most common in unheated samples are mineral grains surrounded by a discoid fissure with flattened two-phase (liquid-gas) inclusions in a rosette-like pattern oriented parallel to the basal pinacoid c. • Feldspar (as “rosette mineral” or in grains), zircon (some with unoriented tension cracks), columbite (needle-like crystals with Nb>Ta), spinel (hercynite), uraninite, and unidentified mineral grains (some with “comet tails”). • Unhealed or partially healed fissures; two-phase (liquid-gas) inclusions.

^a In general, the properties of the heat-treated sapphires duplicate those of the natural-color samples. Any differences are specifically noted in the text.

^b Heat treatment under strictly controlled conditions is necessary for most Antsiranana sapphires to remove milky areas and to develop a blue to blue-violet color in unattractive white, yellowish green, or greenish yellow samples.

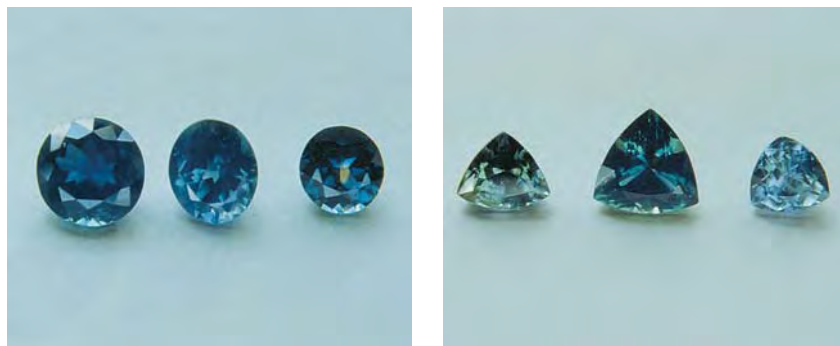


Figure 7. The Ambondromifehy area produces sapphires in a broad range of colors. These include the natural-color blue-violet and blue (left) and greenish blue (right) sapphires illustrated here. The blue-violet stone on the far left measures 8 × 10 mm; the largest greenish blue sapphire is 10 mm in longest dimension. Photos by M. Glas.

parent without causing them to become too dark.

Most of the sapphires—both natural color and heat treated—showed distinct color zoning, with blue-violet, greenish blue to greenish yellow, and yellow domains within a single crystal. A small number revealed homogeneous coloration in these hues. Bicolored and tricolored stones also have been cut (figure 9).

A large number of the natural-color stones had translucent milky white or blue areas; some stones were completely translucent. This “milky” was typically removed with heat treatment. The remainder of the material was more transparent.

The milky white, grayish white, blue, or blue-violet cabochons we examined (figure 10) showed a sharp six-rayed star. In some of these star sapphires, and at least one faceted stone, we observed a colorless to gray core that was surrounded by a milky white to blue-violet rim (figure 10, inset). With the exception of a few stones cut as a novelty for collectors, the core is typically removed during cutting. Twelve-rayed star sapphires from northern Madagascar are extremely rare (see Schmetzer, 1999b).

Figure 8. These unheated samples show the appearance of yellow sapphires from Ambondromifehy. Note the sharp blue color zones in the 5 × 7 mm stone on the lower left. Photo by M. Glas.

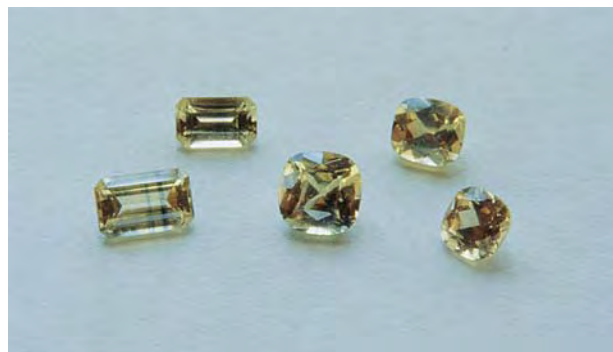


Figure 9. Prominent color zoning is shown by these particolored (yellow, greenish blue, and blue) Ambondromifehy sapphires. The stone on the far right measures about 4 × 8 mm. Photo by M. Glas.

Crystal Morphology. The sapphire crystals typically showed an elongated, barrel-shaped habit, although all were somewhat rounded and corroded. Most of the crystals were broken at both ends and revealed portions of only one hexagonal dipyrmaid as the dominant external form. A few samples were broken only at one end, and less than 5% of all the crystals examined were complete (i.e., with all faces intact).

In general, one of the hexagonal dipyrmaids ω $\{14\ 14\ \bar{2}8\ 3\}^*$ or z $\{22\bar{4}1\}$ was combined with the basal pinacoid c $\{0001\}$. Frequently, smaller faces of the rhombohedron r $\{10\bar{1}1\}$ and of an additional hexagonal dipyrmaid n $\{22\bar{4}3\}$ also were identified. Six combinations of these forms were observed (figure 11): $(c\ \omega)$, $(c\ z)$, $(c\ \omega\ r)$, $(c\ z\ r)$, $(c\ \omega\ r\ n)$, and $(c\ z\ r\ n)$.

Gemological Properties. For the most part, the properties of the heat-treated sapphires duplicated those of the natural-color samples. Any differences are specifically noted in the following discussion.

*Limitations in our measurement techniques did not allow us to distinguish between the two hexagonal dipyrmaids ω $\{14\ 14\ \bar{2}8\ 3\}$ and ν $\{44\bar{8}1\}$.



Figure 10. Star sapphires from Ambondromifehy are commonly gray to blue. The largest cabochon here measures 9×10 mm. The sapphires in the inset have been cut to show the unusual cores seen in some of the samples; the faceted stone is 10×11 mm. Photos by M. Glas.

The densities and R.I.'s of the Andromifehy sapphires match those from other magmatic deposits. Measured densities vary between 3.99 and 4.02 g/cm^3 . R.I.'s range from 1.761 to 1.765 for n_e and from 1.769 to 1.773 for n_o , with a birefringence of 0.008 .

Figure 11. The morphology of Ambondromifehy sapphires is dominated by hexagonal dipyrramids ω or z combined with the basal pinacoid c . Additional hexagonal dipyrramids n as well as rhombohedra r are also occasionally observed.



We observed four major types of pleochroic colors:

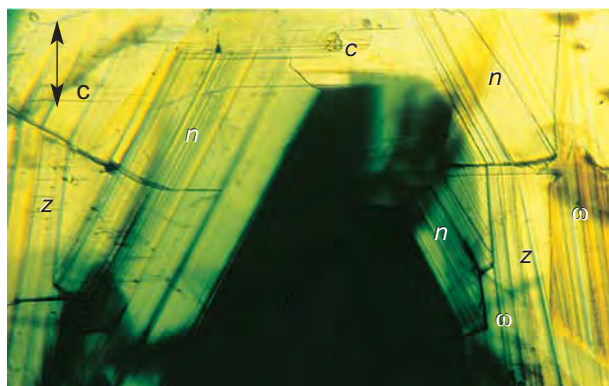
1. \parallel c-axis light yellow, \perp c-axis somewhat more intense yellow, for yellow sapphires (i.e., samples with almost no pleochroism)
2. \parallel c-axis yellow, \perp c-axis blue to blue-violet, for greenish blue sapphires
3. \parallel c-axis blue, \perp c-axis blue-violet, for intense blue to blue-violet sapphires
4. \parallel c-axis greenish yellow to yellow-green, \perp c-axis blue to blue-violet, for greenish yellow to yellowish green sapphires

The distinct color zoning shown by most of the sapphires (see, e.g., figure 9) usually consisted of a combination of two of the four pleochroic types mentioned above. In rare cases, we saw areas with three different types of pleochroism in a single color-zoned crystal.

The sapphires were inert to both long- and short-wave UV radiation.

Microscopic Characteristics. Most of the samples examined showed some fractures and two-phase (liquid-gas) inclusions, but these were not distinctive. Although many of the untreated stones showed some milkiness, no "silk" or other oriented mineral inclusions were visible in our samples at the magnification used for gemological microscopy (up to

Figure 12. This sample, viewed perpendicular to the c-axis, shows the typical growth patterns found in Ambondromifehy sapphires. Two hexagonal dipyrramids ω and n are present in combination with the basal pinacoid c . Oscillatory zoning of ω with a third hexagonal dipyrramid z is present in the lower right. Photomicrograph by K. Schmetzer; immersion, magnified $40\times$.



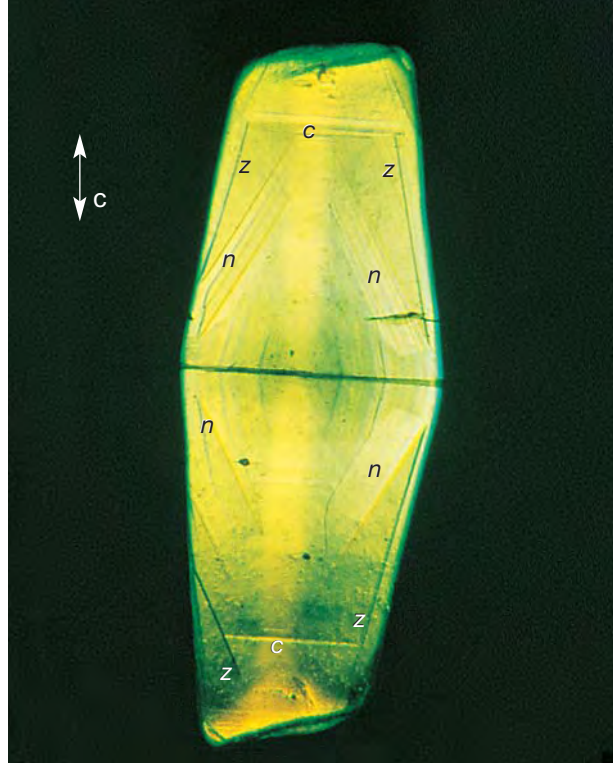


Figure 13. When viewed perpendicular to the *c*-axis, this Ambondromifehy sapphire crystal shows a first hexagonal dipyramid *n* that is overgrown by a second hexagonal dipyramid *z*; the basal pinacoid *c* is also developed. Photomicrograph by K. Schmetzer; immersion, crossed polarizers, magnified 20 \times .

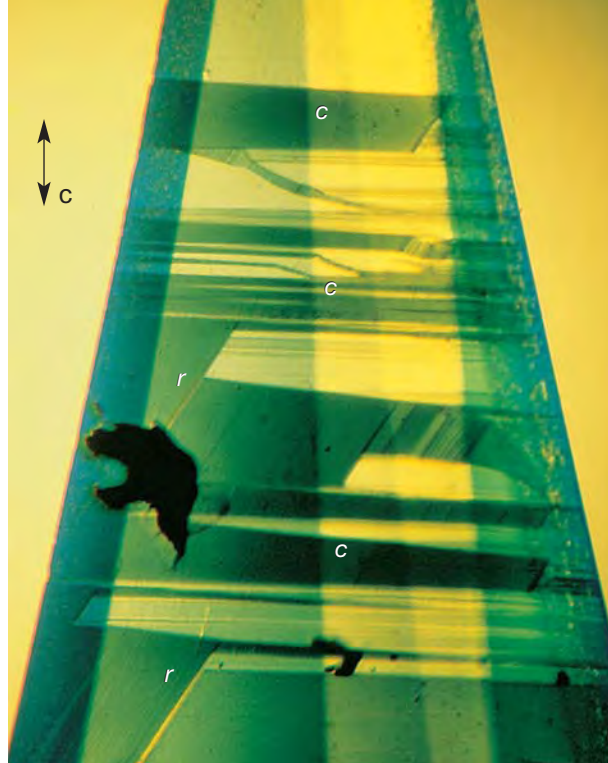


Figure 14. In this view perpendicular to the *c*-axis of a sapphire crystal from Ambondromifehy, intense color zoning is associated with the growth patterns. The positive rhombohedron *r* and basal pinacoid *c* are evident. Photomicrograph by K. Schmetzer; immersion, magnified 30 \times .

100 \times). We observed distinct mineral inclusions in only about 10%–20% of the samples examined. However, structural properties, notably specific growth features that can be used to indicate a natural origin, were found in most samples.

Growth Features. The internal growth patterns seen with immersion clearly reflect the external morphology of the samples. When the sample was observed perpendicular to the *c*-axis, two different types of morphology usually were evident (see also figure 11), that is, one of the two hexagonal dipyramids ω or *z* (which were dominant in the external

morphology) in combination with a third dipyramid *n* and the basal pinacoid *c* (figures 12 and 13). When viewed from another direction also perpendicular to the *c*-axis, a combination of the basal pinacoid *c* with the positive rhombohedron *r* was observed (figure 14). Occasionally, an oscillatory zoning between different hexagonal dipyramids (e.g., ω and *z*) is observed (again, see figure 12). Rotation of a sample through an angle of 30 $^\circ$, with *c* as the rotation axis, generally reveals a characteristic variation between these two frequently observed patterns (*c* ω *n*) or (*c* *z* *n*) in one orientation, and (*c* *r*) in the other (figure 15). Color zoning associated with growth zoning is

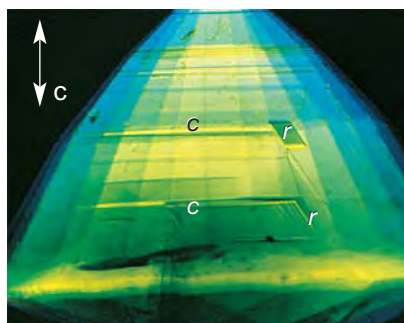
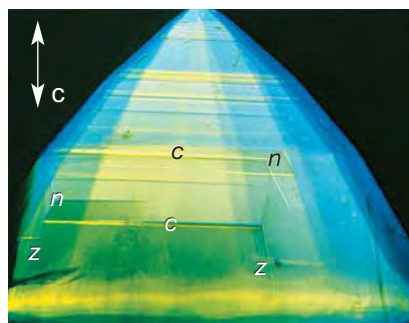


Figure 15. In these two views, a faceted Ambondromifehy sapphire has been rotated 30 $^\circ$ around the *c*-axis. On the left, a combination of two hexagonal dipyramids *n* and *z* are present with the basal pinacoid *c*. On the right, a combination of the rhombohedron *r* with *c* is seen. Photomicrographs by K. Schmetzer; immersion, crossed polarizers, magnified 25 \times (left) and 30 \times (right).

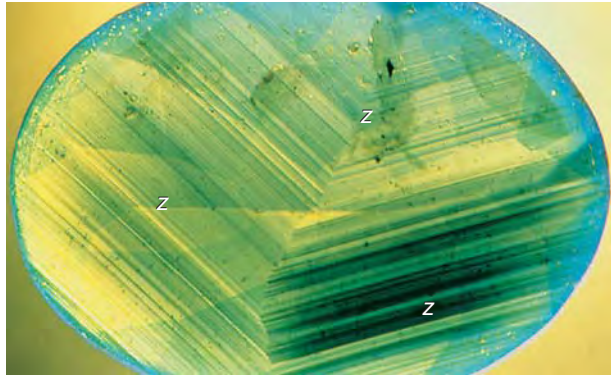


Figure 16. When inclined about 10° to the c-axis, a growth pattern consisting of several hexagonal dipyramids is normally seen in Ambondromifehy sapphires. In this case, two z faces are observed. Photomicrograph by K. Schmetzer; immersion, magnified 25x.

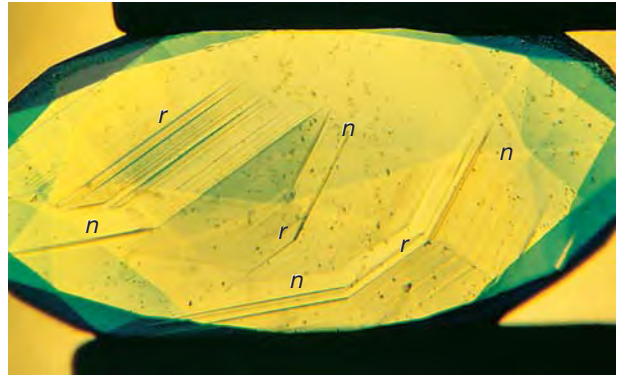


Figure 17. At an inclination of about 30° to the c-axis, the typical growth patterns seen in Ambondromifehy sapphires consist of n and/or r faces. In this orientation, a characteristic pattern (n r n) is seen. Photomicrograph by K. Schmetzer; immersion, magnified 30x.

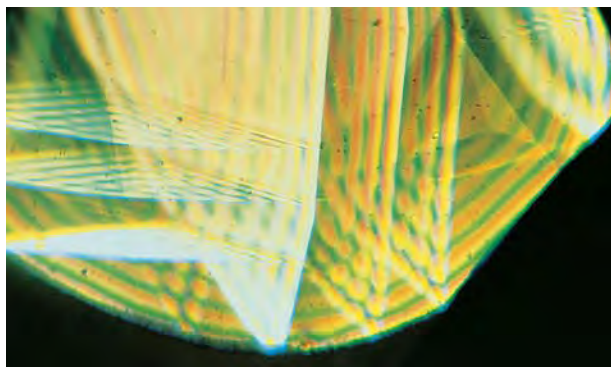
present frequently, but not in all samples.

At an inclination of 5° or 10° to the c-axis, a characteristic pattern consisting of the two hexagonal dipyramids ω or z was observed (figure 16). When the stone was inclined about 30° to the c-axis, a characteristic structure consisting of two n faces and one r face is seen (figure 17).

The hexagonal dipyramids ω or z were also dominant in the samples with asterism.

Twinning. Lamellar twinning parallel to the positive rhombohedron r occasionally was observed, usually as one or two isolated twin lamellae and less frequently as one or two sets of parallel twin lamellae (figure 18).

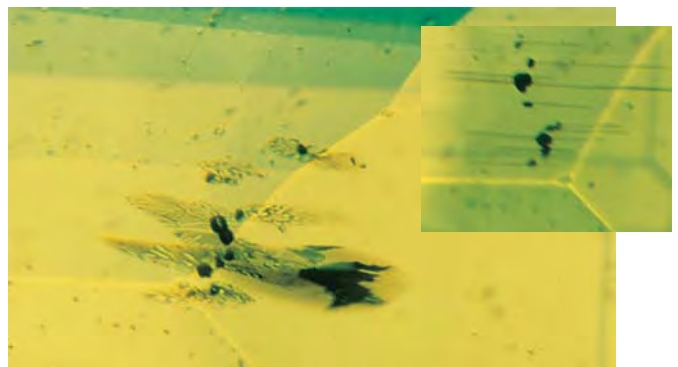
Figure 18. Two sets of intersecting twin lamellae are visible in this Ambondromifehy sapphire. Photomicrograph by K. Schmetzer; crossed polarizers, magnified 40x.



Mineral Inclusions. With Raman analysis and/or SEM-EDS, we confirmed inclusions of feldspar, zircon, columbite (with Nb>Ta), spinel (hercynite), and uraninite.

The most common inclusion in the unheated samples was a mineral grain surrounded by a discoid fissure with flattened two-phase (liquid-gas) inclusions in a rosette-like pattern. These rosettes show a consistent orientation parallel to the basal pinacoid c and, consequently, are seen best when viewed perpendicular to the c-axis (figures 19 and 20). We identified some of the mineral grains in the rosettes as feldspar.

Figure 19. The most frequently observed mineral inclusions in Ambondromifehy sapphires are feldspar crystals that are surrounded by rosettes of two-phase (liquid-gas) inclusions. The inset (view perpendicular to c) reveals the specific orientation of these flattened rosettes parallel to the basal pinacoid c. Photomicrographs by K. Schmetzer; immersion, magnified 50x and 60x (inset).



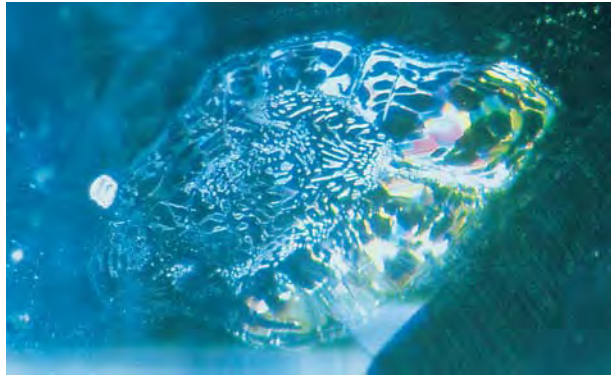


Figure 20. In a view almost parallel to the *c*-axis of this sapphire, the fine structure of a two-phase rosette surrounding a tiny feldspar crystal becomes visible. Photomicrograph by E. Gübelin; magnified 65 \times .

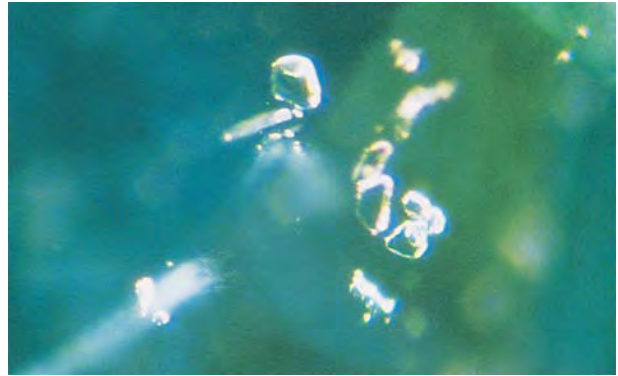


Figure 21. Groups of mineral inclusions, which have not yet been identified, were occasionally seen in the Ambondromifehy sapphires. Photomicrograph by E. Gübelin; magnified 65 \times .

The rosettes are distinct from typical mineral inclusions with tension cracks (i.e., zircon in our samples), which are not oriented in a specific direction to the host sapphire crystal. Tension cracks surrounding mineral inclusions without a specific orientation were also observed occasionally in the heat-treated Ambondromifehy samples.

Another type of feldspar inclusion consisted of grains that lacked the rosette-like two-phase inclusions. Spinel and uraninite inclusions also occurred as grains, but they were seen only rarely in our samples. Columbite occurred as needles, which were found to contain only small amounts of tantalum (i.e., the analyses showed Nb>Ta).

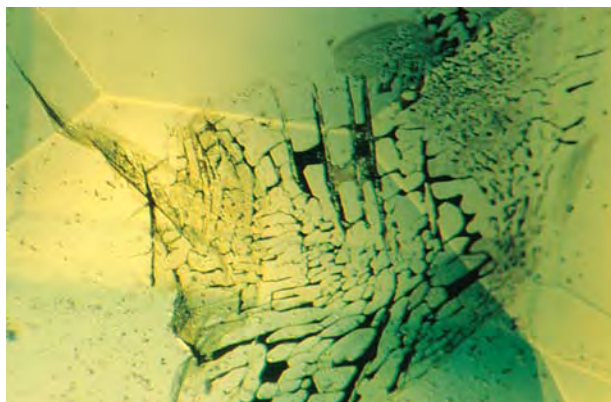
In a few samples, we observed groups of uniden-

tified mineral grains (figure 21) or other unidentified minerals accompanied by a "comet tail." Partially healed fissures also were present in some of the sapphires (figure 22).

Superchi et al. (1997) mentioned two additional minerals—pyrochlore and calcite—as inclusions in Ambondromifehy sapphires, but we did not identify these minerals in any of our samples.

Spectroscopic Properties and Color. The absorption spectra of the Ambondromifehy sapphires (see, e.g., figure 23) are typical of those recorded in BGY magmatic sapphires from other localities (see, e.g., Schmetzer and Bank, 1980, 1981; Schmetzer, 1987; Kiefert and Schmetzer, 1987; Smith et al., 1995). We recorded a continuous series of absorption spectra covering the entire range of colors, including yellow, greenish blue, and intense blue to blue-violet (figure 24A–C). All of these spectra had intense Fe³⁺ absorption bands at 376, 388, and 450 nm with weak polarization dependency, as generally is recorded for yellow sapphires (figure 24A). In the blue and greenish blue sapphires, the basic absorption spectrum found in yellow sapphires was superimposed by intense absorption bands assigned to Fe²⁺/Ti⁴⁺ charge transfer (maximum at about 560 nm with polarization $\perp c > \parallel c$), as well as to an Fe²⁺/Fe³⁺ pair absorption (maximum at about 870–880 nm with polarization $\perp c > \parallel c$)^{*}. Due to the high intensity of

Figure 22. Partially healed fissures were present in some of the Ambondromifehy sapphires. Photomicrograph by K. Schmetzer; immersion, magnified 45 \times .



^{*}Because of technical inconsistencies, the polarized absorption spectra of magmatic sapphires published by Schwarz et al. (1996) and Sutherland et al. (1998b) are partly incorrect in the range above 800 nm. In particular, an absorption maximum at about 800 nm in the spectra $\perp c$ is not realistic.

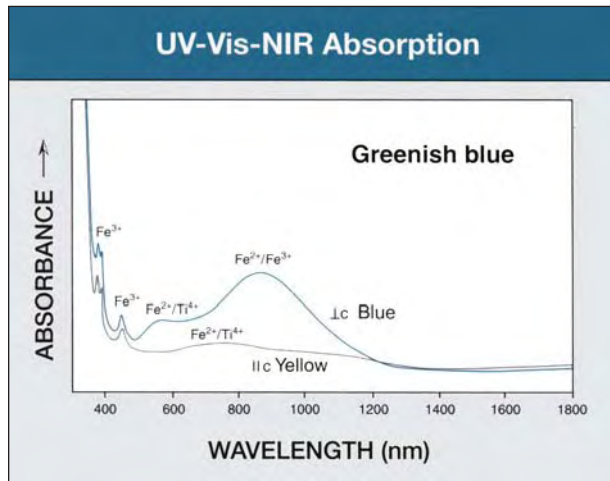


Figure 23. This absorption spectrum of a greenish blue *Ambondromifehy* sapphire (pleochroism llc yellow, lc blue) in the 280 to 1800 nm range consists of a strong Fe^{2+}/Fe^{3+} band with a maximum in the infrared region, strong Fe^{2+}/Ti^{4+} pair absorption bands in the visible region, and Fe^{3+} bands in the blue-violet and UV regions.

the Fe^{2+}/Fe^{3+} pair absorption, a second Fe^{2+}/Ti^{4+} maximum at about 700 nm with polarization llc \perp lc (see figure 24E) is generally not resolvable. The spectra of the heat-treated intense blue-violet samples were identical to those of untreated sapphires of similar color.

In greenish yellow to yellowish green samples, the intermediate spectrum of greenish blue sapphire was superimposed by an additional weak absorption band in the 500–550 nm range (polarization llc $>$ lc; figure 24D). This absorption band causes a shift of the pleochroic color parallel to the c-axis from yellow to yellow-green or green; consequently, it shifts the overall color of the sapphire from greenish blue to greenish yellow or yellowish green. An absorption at 542 nm with identical polarization has also been documented in Verneuil titanium-doped synthetic sapphires, where it was assigned to Ti^{3+} (McClure, 1962). Although we do not know the exact mechanism by which Ti^{3+} stabilizes in iron-

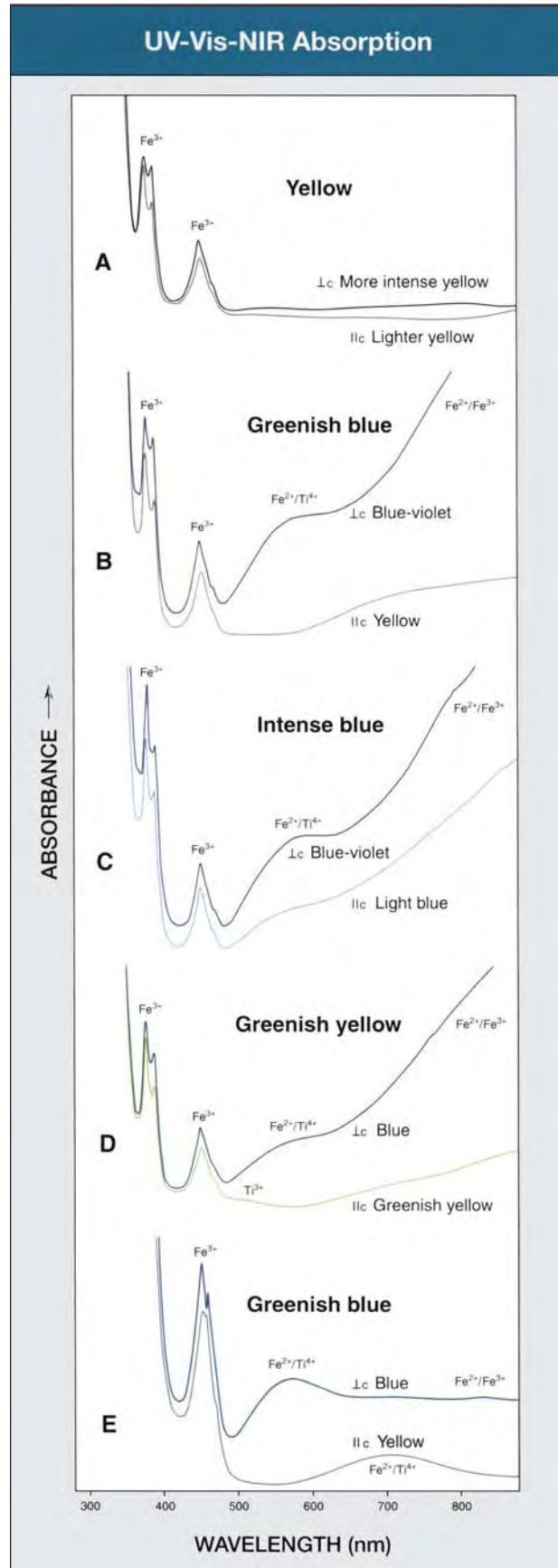


Figure 24. These absorption spectra in the 280–880 nm range cover the entire range of colors seen in *Ambondromifehy* sapphires. The spectra consist of superimposed Fe^{2+}/Fe^{3+} and Fe^{2+}/Ti^{4+} pair absorption bands, as well as intense Fe^{3+} and weak Ti^{3+} bands. Variations in the color/pleochroism of the sapphires is determined by the relative intensities of these absorption bands.

bearing natural sapphires, there has been no other assignment of this weak absorption maximum. It is worth mentioning that another example for the coexistence of Ti^{3+} and Fe^{2+} was found in Czochralski-pulled synthetic pink sapphire by spectroscopic examination (Johnson et al., 1995).

In magmatic sapphires, Fe^{2+}/Fe^{3+} pair absorption in the 870–880 nm range is, in general, much stronger than the Fe^{2+}/Ti^{4+} absorption bands at 560 and 700 nm (see, e.g., figures 23 and 24B–D). Only one of the Ambondromifehy samples, which had extremely pronounced and complex color zoning, revealed an absorption spectrum in which the Fe^{2+}/Ti^{4+} pair absorption bands were stronger than the Fe^{2+}/Fe^{3+} band in the infrared region (figure 24E).

Chemical Composition. Trace-element analysis has proved valuable in the identification of gem corundums formed in different geologic environments, as well as in the laboratory (see, e.g., Sutherland et al., 1998b; Muhlmeister et al., 1998;

Schwarz and Stern, 2000). The trace-element contents of 137 sapphires from northern Madagascar are presented in table 2.

Vanadium and chromium, in general, were below the detection limit of the analytical method used (about 0.005 wt.% V_2O_3 or Cr_2O_3). Only a few samples revealed traces of vanadium or chromium that were slightly above the detection limit. All samples revealed concentrations of iron and gallium that were typical of magmatic sapphires (see, e.g., Sutherland et al., 1998b).

The titanium content of the pure yellow samples was always below the detection limit (about 0.005 wt.% TiO_2). All of the samples with higher titanium values had blue color zones or a blue color component. Transparent, facet-quality samples (i.e., those that usually do not need heat treatment) other than yellow consistently revealed a low, but distinct, titanium content—averaging about 0.02 wt.% TiO_2 . Those samples with a milky white component, the typical material subjected to heat treatment, aver-

TABLE 2. EDXRF analyses of sapphires from Antsiranana Province, northern Madagascar, with comparison to Andranondambo.^a

Sample type	No. of samples	Concentration (wt.%)				
		TiO_2	V_2O_3	Cr_2O_3	$Fe_2O_3^b$	Ga_2O_3
Transparent yellow	14	bdl	bdl	bdl	0.73–1.56 (1.24)	0.02–0.06 (0.04)
Transparent yellow and blue (zoned), greenish yellow to yellowish green, greenish blue, blue, and blue-violet	94	0.005–0.11 (0.02)	bdl–0.01 bdl	bdl–0.01 bdl	0.46–1.73 (1.10)	0.02–0.07 (0.03)
Translucent greenish blue, blue, and blue-violet ^c (all milky, no cores)	19	0.02–0.15 (0.08)	bdl–0.01 bdl	bdl	0.66–1.40 (1.18)	0.02–0.08 (0.05)
Translucent gray and light blue star sapphires (all milky or with milky zones)	5	0.06–0.10 (0.08)	bdl–0.01 bdl	bdl	0.33–0.57 (0.44)	0.01–0.04 (0.02)
Zoned star sapphires	5					
Colorless to gray cores		0.02–0.04 (0.03)	bdl–0.01 bdl	bdl	1.24–2.31 (1.74)	0.05–0.11 (0.08)
Medium to intense blue rims ^d (all milky or with milky zones)		0.06–0.23 (0.15)	0.005–0.01 (0.01)	bdl	1.53–1.90 ^e (1.64)	0.06–0.90 ^e (0.09)
Overall Ambondromifehy ^f	137	bdl–0.23 (0.03)	bdl–0.01 bdl	bdl–0.01 bdl	0.33–1.90 ^e (1.00)	0.02–0.10 ^e (0.04)
Andranondambo ^g	80	0.01–0.10 (0.04)	bdl–0.01 bdl	bdl–0.01 bdl	0.12–0.61 (0.27)	0.01–0.04 (0.02)

^aMinimum and maximum values are given, along with the average (in parentheses below each range); bdl = below detection limit.

^bTotal iron as Fe_2O_3 .

^cThese sapphires turn intense blue to blue-violet after heat treatment.

^dSame samples as the ones with the colorless to gray cores.

^eOne sample showed distinctly higher contents of Fe_2O_3 (3.86 wt.%) and Ga_2O_3 (0.15 wt.%).

^fColorless to gray cores of zoned star sapphires not included.

^gFrom Schwarz et al. (1996); for additional microprobe analyses, see Kiefert et al. (1996).

aged about 0.08 wt.% TiO₂, well above the mean value for the transparent sapphires.

In star sapphires and in milky stones, the measured elemental concentrations may be influenced by the presence of tiny inclusions such as rutile or ilmenite that reach the surface of the host corundum, rather than simply by the presence of transition metals within the corundum structure. In all the asteriated cabochons with a sharp six-rayed star, appreciable amounts of titanium were detected. In the milky white and gray to light blue star sapphires, the iron values were distinctly lower than those determined for more intense-blue star stones. Samples of the latter type were found to contain a colorless to gray transparent core (see, e.g., figure 10, inset), which lacks asterism and shows very low titanium contents (see table 2).

When we compared the data for all of the samples using correlation diagrams, we found no geochemical correlation between titanium and either iron or gallium; the concentrations of these elements varied independently. However, with greater iron contents, a trend toward increasing gallium values became evident.

As mentioned earlier, many sapphire fields from eastern Australia (particularly the Barrington basalt province in New South Wales) and Southeast Asia (e.g., West Pailin, Cambodia; Ban Huai Sa, Laos; and Chanthaburi, Thailand) are distinguished by the presence of two distinct corundum suites, which are thought to represent different sources in the earth's interior that were captured by basaltic magmas as they traveled to the surface (Sutherland et al., 1998b). These two corundum suites can be separated by trace-element contents, that is, by diagramming (1) Fe₂O₃/TiO₂ versus Cr₂O₃/Ga₂O₃, and (2) Fe₂O₃/Cr₂O₃ versus TiO₂/Ga₂O₃ (figure 25). In making these comparisons, we assigned a value of 0.005 for concentrations below the detection limit (i.e., for some TiO₂ and most Cr₂O₃ values). All of the sapphires from northern Madagascar that we analyzed by EDXRF belong to the magmatic suite.

DISCUSSION

Comparison to "Basalt-Hosted Magmatic" Sapphires from Other Localities. The sapphires from northern Madagascar showed the typical morphology of magmatic corundum, that is, faces of the basal pinacoid *c*, the positive rhombohedron *r*, as well as different hexagonal dipyrramids. In particular, these sapphires formed as barrel-shaped crystals with dominant ω or *z* hexagonal dipyrramids, and subordi-

nate *c*, *r*, and *n* faces; prismatic forms were not observed. The correlation between external crystal faces and internal growth structures has been shown for corundums from practically all basalt-hosted sources (Kiefert, 1987; Kiefert and Schmetzer, 1987 and 1991), including magmatic Vietnamese sapphires (Smith et al., 1995).

The following have been identified as typical mineral inclusions observed in magmatic sapphires: assemblages of feldspars (albite, calcic plagioclase, Na- and/or K-rich sanidine), zircon, columbite, rutile, hematite (sometimes in solid solution with ilmenite), spinel (hercynite, magnetite, gahnospinel, and/or cobalt-spinel), uranium-pyroxene, pyrrhotite, thorite, and uraninite; low-Si and Fe-rich glassy inclusions have also been identified (see, e.g., Moon and Phillips, 1984, 1986; Coldham, 1985, 1986; Gübelin and Koivula, 1986; Irving, 1986; Kiefert, 1987; Kiefert and Schmetzer, 1987; Coenraads et al., 1990, 1995; Aspen et al., 1990; Guo et al., 1992, 1994, 1996a and b; Sutherland, 1996; Sutherland and Coenraads, 1996; Krzemnicki et al., 1996; Sutherland et al., 1998a and b; Malíková, 1999).

The mineral inclusions identified in Ambondromifehy sapphires (e.g., feldspar, zircon, columbite, hercynite, uraninite, pyroxene) are typical of magmatic sapphires. The most common mineral inclusions in Ambondromifehy sapphires are feldspar crystals surrounded by "rosette-like" fissures. Similar-appearing inclusions have been described for corundums from elsewhere (see, e.g., Kiefert and Schmetzer, 1987; Guo et al., 1996a), with their consistent orientation—parallel to the basal pinacoid *c*—but not with the frequency observed in the northern Madagascar sapphires.

Some Ambondromifehy sapphires contain a colorless to gray central core, with a hexagonal outline, which is surrounded by milky white to blue-violet areas (figure 10, inset). This unusual feature is rarely found elsewhere. Similar colorless core zones, but with a triangular outline, occur in blue magmatic-type sapphires from Vietnam (Smith et al., 1995).

The UV-Vis-NIR absorption spectra of the Ambondromifehy BGY magmatic sapphires have features typical of those seen in basaltic sapphires from other localities (Schmetzer, 1987; Schmetzer and Kiefert, 1990; Kiefert and Schmetzer, 1991; Krzemnicki et al., 1996; Schwarz et al., 1996; Sutherland et al., 1998b). Therefore, absorption spectra cannot be used to distinguish Ambondromifehy sapphires from those of other basaltic fields.

As shown in the correlation diagrams (figure 25), the trace-element contents of Ambondromifehy sapphires overlap with those of magmatic samples from Barrington and Pailin (see Sutherland et al., 1998b). Further overlap has been observed in population fields of magmatic sapphires from Nigeria, Laos, and various other Australian basalt fields (D. Schwarz, unpublished data). Similar trace-element contents were also described for magmatic sapphires from Shandong Province, China (Guo et al., 1992). Consequently, the separation of magmatic sapphires from different basalt fields by their trace elements seems rather unlikely. Nor is there any significant difference in internal features or gemological properties that could be used to separate sapphires formed in this environment.

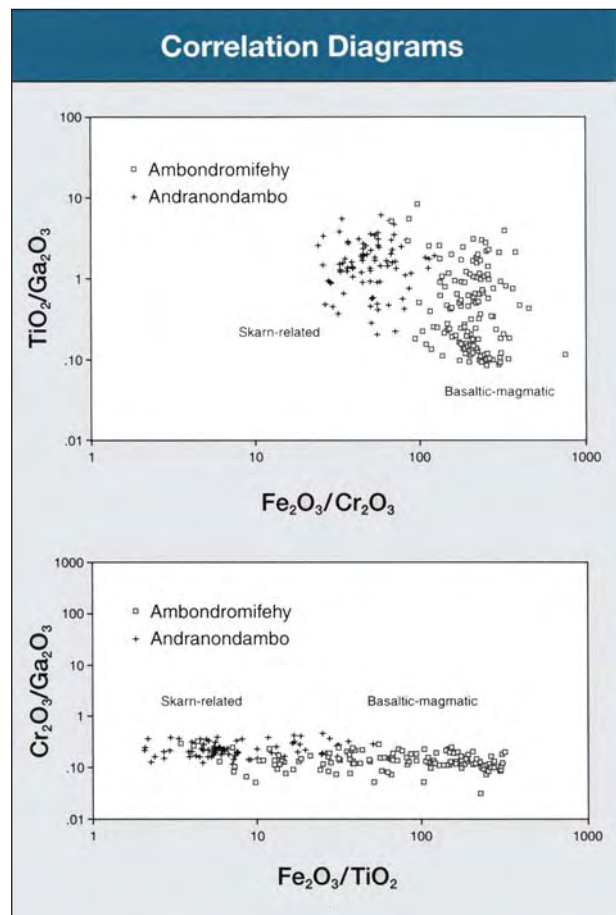
Comparison to Andranondambo Sapphires. The gemological characteristics of sapphires from Andranondambo, southeastern Madagascar, were detailed by Schwarz et al. (1996) and by Kiefert et al. (1996). Subsequent studies of the associated mineral assemblages attributed their formation to metamorphic skarn processes (Gübelin and Peretti, 1997). The magmatic sapphires from northern Madagascar can be separated from the skarn-related Andranondambo sapphires on the basis of diagnostic growth patterns, inclusions, and spectroscopic features (see references cited above). Here, we compare the chemical properties of gem corundum from these two important localities (table 2).

Ambondromifehy sapphires typically show higher iron and gallium concentrations than Andranondambo stones. Individual trace elements show considerable overlap, so are not diagnostic. However, using the previously described correlation diagrams of $\text{Fe}_2\text{O}_3/\text{TiO}_2$ versus $\text{Cr}_2\text{O}_3/\text{Ga}_2\text{O}_3$ and $\text{Fe}_2\text{O}_3/\text{Cr}_2\text{O}_3$ versus $\text{TiO}_2/\text{Ga}_2\text{O}_3$, a clear separation between most samples from these two deposits is possible (figure 25). We found that it is also possible to separate similarly colored blue sapphires from the new metamorphic Ilakaka deposits by trace-element chemistry (D. Schwarz, unpublished data).

Distinction from Synthetic Sapphires. The separation of Ambondromifehy sapphires from synthetic blue or yellow sapphires, regardless of the growth method (e.g., flame-fusion, flux, floating zone, Czochralski-pulled, hydrothermal), is fairly simple. Most of the internal features (e.g., growth patterns and mineral inclusions, when present) seen in the natural stones differ quite markedly from those

observed in laboratory-grown sapphires. Absorption spectra of Ambondromifehy sapphires overlap with those of some synthetic sapphires (e.g., some flux-grown Chatham or hydrothermal Russian synthetic sapphires). However, the trace-element composition of the natural sapphires reveals significant differences from their man-made counterparts. In general, with careful microscopic examination, the experienced gemologist can determine conclusively the natural or synthetic origin of an unknown sapphire in the yellow to blue color range (see, e.g., Liddicoat, 1989; Thomas et al., 1997).

Figure 25. In these trace-element correlation diagrams, the population field of the skarn-related sapphires from Andranondambo shows minor overlap with that of the magmatic samples from Ambondromifehy. Chemical correlation diagrams are one of the techniques used to separate sapphires and rubies from different host rocks.



SUMMARY AND CONCLUSIONS

A large region in northern Madagascar, near the town of Ambondromifehy, has been the source of considerable quantities of sapphires in a variety of colors, but primarily blue, blue-violet, greenish blue, and yellow. Much of the digging for these alluvial deposits has occurred in or near the Ankarana Special Reserve, which has led to significant problems with ecologists. Most of the sapphires in virtually all hues are heat treated to remove milkiness in all or part of the stone and produce a better color. Ninety per cent of the crystals heat treated for this study changed to a more transparent and more attractive blue-violet to blue. Several asteriated stones were examined, a few with unusual colorless to gray cores.

The faceted Ambondromifehy sapphires showed distinctive internal growth patterns. In addition, many contained unusual rosette-like features: mineral grains (some identified as feldspar) surrounded by a discoid fissure with flattened two-phase inclusions. Spinel, uraninite, and columbite were also identified.

The absorption spectra and EDXRF analyses provided results that are typical for basaltic-magmatic sapphires from other localities. However, these same analyses (as well as internal growth patterns

and inclusions) can be used to separate magmatic sapphires from sapphires that formed in a different environment, such as the skarn-related sapphires from the Andranondambo deposit in southeastern Madagascar.

Although mining in Ambondromifehy dropped sharply with the discovery of sapphires in Ilakaka (and the movement of miners to that area), activity in northern Madagascar has increased in recent months. It appears that there is still considerable potential, but most of the mining continues to be small scale, with little or no mechanization.

Acknowledgments: The authors are grateful to E. J. Petsch, Idar-Oberstein, and to several other gem dealers (who wish to remain anonymous) for supplying the sapphire samples used in this study. M. Sevdemish, Menavi International, Ramat Gan, Israel, is thanked for supplying production information and samples for photography. Issac and Ben Mehditash of Mega Gem s.a.r.l. also provided information and photos. QRP Trade Ltd., Bangkok, performed some sample preparation. Dr. H. D. von Scholz and P. Roth, SUVA, Lucerne, performed SEM-EDS analyses of mineral inclusions. Raman analyses were done by W. Atichat and her team at the Department of Mineral Resources, Bangkok. M. Zachovay of Edigem Ltd., Lucerne, helped edit the original manuscript and drew the correlation diagrams.

REFERENCES

- An initial appraisal of sapphire deposits located in the Antsiranana region of Northern Madagascar. (1997) Report prepared by Ransome Consulting, Cape Town, South Africa, for IMA Group s.a.r.l., 3 pp.
- Aspen P., Upton B.G.J., Dicken A.P. (1990) Anorthoclase, sanidine and associated megacrysts in Scottish alkali basalts: High pressure syenitic debris from upper mantle sources? *European Journal of Mineralogy*, Vol. 2, pp. 503-517.
- Bank H., Henn U., Milisenda C.C. (1996) Korunde aus Madagaskar. *Gemmologie. Zeitschrift der Deutschen Gemmologischen Gesellschaft*, Vol. 45, No. 4, p. 155.
- Bank H., Henn U., Milisenda C.C. (1997) Sapphire aus Madagaskar. *Gemmologie. Zeitschrift der Deutschen Gemmologischen Gesellschaft*, Vol. 46, No. 3, pp. 123-124.
- Banker T. (1998) Madagascar mining update. *ICA Gazette*, November/December 1998, p. 6.
- Besairie H. (1969) Geological Map 1:500,000, Antsiranana sheet. Service Geologique Madagasikara, Antananarivo.
- Coenraads R.R., Sutherland F.L., Kinny P.D. (1990) The origin of sapphires: U-Pb dating of zircon inclusions sheds new light. *Mineralogical Magazine*, Vol. 54, pp. 113-122.
- Coenraads R.R., Vichit P., Sutherland F.L. (1995) An unusual sapphire-zircon-magnetite xenolith from the Chanthaburi gem province, Thailand. *Mineralogical Magazine*, Vol. 59, pp. 465-479.
- Coldham T. (1985) Sapphires from Australia. *Gems & Gemology*, Vol. 21, No. 3, pp. 130-146.
- Coldham T. (1986) Inclusions in Australian sapphire before and after heat treatment. *Australian Gemmologist*, Vol. 16, pp. 122-125.
- Gonthier E. (1997) Les saphirs du nord de Madagascar. *Revue de Gemmologie A.F.G.*, No. 132, pp. 14-17.
- Gübelin E.J., Koivula J.I. (1986) *Photoatlas of Inclusions in Gemstones*. ABC Edition, Zürich, 532 pp.
- Gübelin E.J., Peretti A. (1997) Sapphires from the Andranondambo mine in SE Madagascar: Evidence for metasomatic skarn formation. *Journal of Gemmology*, Vol. 25, No. 7, pp. 453-470.
- Guo J.F., Griffin W.L., O'Reilly S.Y. (1994) A cobalt-rich spinel inclusion in a sapphire from Bo Ploi, Thailand. *Mineralogical Magazine*, Vol. 58, pp. 247-258.
- Guo J.F., O'Reilly S.Y., Griffin W.L. (1992) Origin of sapphire in eastern Australian basalts: Inferred from inclusion studies. *Geological Society of Australia, Abstracts*, Ballarat University College, No. 32, pp. 219-220.
- Guo J.F., O'Reilly S.Y., Griffin W.L. (1996a) Corundum from basaltic terrains: A mineral inclusion approach to the enigma. *Contribution to Mineralogy and Petrology*, Vol. 122, No. 4, pp. 368-386.
- Guo J.F., O'Reilly S.Y., Griffin W.L. (1996b) Zircon inclusions in corundum megacrysts: I. Trace element geochemistry and clues to the origin of corundum megacrysts in alkali basalts. *Geochimica et Cosmochimica Acta*, Vol. 60, No. 13, pp. 2347-2363.

- Guo J., Wang F., Yakoumelos G. (1992) Sapphires from Changle in Shandong province, China. *Gems & Gemology*, Vol. 28, No. 4, pp. 255–260.
- Holewa P. (1998) Ban Lifted in Madagascar. *Gemkey*, November–December 1998, p. 13.
- Irving A.J. (1986) Polybaric magma mixing in alkali basalts and kimberlites: Evidence from corundum, zircon and ilmenite megacrysts. *4th International Kimberlite Conference, Perth, Geological Society of Australia Abstracts, Series 16*, pp. 262–264.
- Johnson M.L., Koivula J.I., McClure S.F., DeGhionno D. (1999) Gem news: Blue, pink, and purple sapphires from Ilakaka, Madagascar. *Gems & Gemology*, Vol. 35, No. 2, pp. 149–150.
- Johnson M.L., Mercer M.E., Fritsch E., Maddison P., Shigley J.E. (1995) "Ti-sapphire": Czochralski-pulled synthetic pink sapphire from Union Carbide. *Gems & Gemology*, Vol. 31, No. 3, pp. 188–195.
- Kanis J., Harding R.R. (1990) Gemstone prospects in Central Nigeria. *Journal of Gemmology*, Vol. 22, No. 4, pp. 195–202.
- Kiefert L. (1987) Mineralogische Untersuchungen zur Charakterisierung und Unterscheidung natürlicher und synthetischer Sapphire. Diploma Thesis, University of Heidelberg, 203 pp.
- Kiefert L., Schmetzer K. (1987) Blue and yellow sapphire from Kaduna Province, Nigeria. *Journal of Gemmology*, Vol. 20, No. 7/8, pp. 427–442.
- Kiefert L., Schmetzer K. (1991) The microscopic determination of structural properties for the characterization of optical uniaxial natural and synthetic gemstones. Part 3: Examples for the applicability of structural features for the distinction of natural and synthetic sapphire, ruby, amethyst and citrine. *Journal of Gemmology*, Vol. 22, No. 8, pp. 471–482.
- Kiefert L., Schmetzer K., Krzemnicki M.S., Bernhardt H.-J., Hänni H.A. (1996) Sapphires from the Andranondambo area, Madagascar. *Journal of Gemmology*, Vol. 25, No. 3, pp. 185–209.
- Krzemnicki M.S., Hänni H.A., Guggenheim R., Mathys D. (1996) Investigations on sapphires from an alkali basalt, South West Rwanda. *Journal of Gemmology*, Vol. 25, No. 2, pp. 90–106.
- Laurs B.M. (2000) Gem news: Update on some Madagascar gem localities. *Gems & Gemology*, Vol. 36, No. 2, pp. 165–167.
- Lea R. (1998) Saphir: Exploitation interdite à la réserve spéciale d'Ambondromifehy. *DMD (Dans les Media Demain)*, Vol. 12, No. 574, pp. 13–15.
- Levinson A.A., Cook F.A. (1994) Gem corundum in alkali basalt: Origin and occurrence. *Gems & Gemology*, Vol. 30, No. 4, pp. 253–262.
- Liddicoat R.T. Jr. (1989) *Handbook of Gem Identification*. GIA, Santa Monica, CA.
- Lurie M. (1998) Madagascar ban puts sapphire ventures in limbo. *Colored Stone*, Vol. 11, No. 5, pp. 119, 140, 142, 143.
- Maliková P. (1999) Origin of sapphires from the Jizerska Louka alluvial deposit in North Bohemia, Czech Republic, Europe. *Australian Gemmologist*, Vol. 20, No. 5, pp. 202–206.
- McClure D.S. (1962) Optical spectra of transition-metal ions in corundum. *Journal of Chemical Physics*, Vol. 36, No. 10, pp. 2757–2779.
- Milisenda C.C., Henn U. (1996) Compositional characteristics of sapphires from a new find in Madagascar. *Journal of Gemmology*, Vol. 25, No. 3, pp. 177–184.
- Moon A.R., Phillips M.R. (1984) An electron microscopy study of exsolved phases in natural black Australian sapphire. *Micron and Microscopica Acta*, Vol. 15, No. 3, pp. 143–146.
- Moon A.R., Phillips M.R. (1986) Inclusions in sapphire and heat treatment. *Australian Gemmologist*, Vol. 16, pp. 163–166.
- Muhlmeister S., Fritsch E., Shigley J.E., Devouard B., Laurs B.M. (1998) Separating natural and synthetic rubies on the basis of trace-element chemistry. *Gems & Gemology*, Vol. 34, No. 2, pp. 80–101.
- Saint-Ours J. de, Rerat J.C. (1963) Geological Map 1:100,000, sheet Montagne d'Ambre. Service Géographique à Madagascar.
- Saint-Ours J. de, Dormois R., Rerat J.C. (1963) Geological Map 1:100,000, sheet Ambilobe-Betsiaka. Service Géographique à Madagascar.
- Sapphire mining halted in northern Madagascar (1998) *ICA Gazette*, May/June, pp. 6–7.
- Schmetzer K. (1987) Zur Deutung der Farburgsache blauer Sapphire—eine Diskussion. *Neues Jahrbuch für Mineralogie Monatshefte*, Vol. 1987, No. 8, pp. 337–343.
- Schmetzer K. (1999a) Ruby and variously coloured sapphires from Ilakaka, Madagascar. *Australian Gemmologist*, Vol. 20, No. 7, pp. 282–284.
- Schmetzer K. (1999b) Gem news: Twelve-rayed star sapphire from Madagascar. *Gems & Gemology*, Vol. 35, No. 2, pp. 148–149.
- Schmetzer K., Bank H. (1980) Explanations of the absorption spectra of natural and synthetic Fe- and Ti-containing corundums. *Neues Jahrbuch für Mineralogie Abhandlungen*, Vol. 139, No. 2, pp. 216–225.
- Schmetzer K., Bank H. (1981) The colour of natural corundum. *Neues Jahrbuch für Mineralogie Monatshefte*, Vol. 1981, No. 2, pp. 59–68.
- Schmetzer K., Kiefert L. (1990) Spectroscopic evidence for heat treatment of blue sapphires from Sri Lanka—additional data. *Journal of Gemmology*, Vol. 22, No. 2, pp. 80–82.
- Schwarz D., Kanis J. (1998) Madagascar: Korunde aus Nord und Süd. *extraLapis*, Vol. 15, pp. 60–63.
- Schwarz D., Petsch E.J., Kanis J. (1996) Sapphires from the Andranondambo region, Madagascar. *Gems & Gemology*, Vol. 32, No. 2, pp. 80–99.
- Schwarz D., Stern W.B. (2000) Chemical fingerprinting as a tool for the characterization of gem corundums from different genetic environments. *Abstracts Volume (CD-ROM), 31st International Geological Congress, August 6–17, Rio de Janeiro, Brazil*.
- Smith C.P., Kammerling R.C., Keller A.S., Peretti A., Scarratt K.V., Khoa N.D., Repetto S. (1995) Sapphires from southern Vietnam. *Gems & Gemology*, Vol. 31, No. 3, pp. 168–186.
- Superchi M., Donini A., Muzzioli D., Roman E. (1997) Sapphire occurrences at Ambondromifehy on the Antsiranana Province, North Madagascar. *26th International Gemmological Conference, Idar-Oberstein, Abstract Volume*, pp. 62–63.
- Sutherland F.L. (1996) Alkaline rocks and gemstones, Australia: A review and synthesis. *Australian Journal of Earth Sciences*, Vol. 43, pp. 323–343.
- Sutherland F.L., Coenraads R.R. (1996) An unusual ruby-sapphire-sapphirine-spinel assemblage from the tertiary Barrington volcanic province, New South Wales, Australia. *Mineralogical Magazine*, Vol. 60, No. 4, pp. 623–638.
- Sutherland F.L., Hoskin P.W.O., Fanning C.M., Coenraads R.R. (1998a) Models of corundum origin from alkali basaltic terrains: A reappraisal. *Contributions to Mineralogy and Petrology*, Vol. 133, No. 4, pp. 356–372.
- Sutherland F.L., Schwarz D., Jobbins E.A., Coenraads R.R., Webb G. (1998b) Distinctive gem corundum suites from discrete basalt fields: A comparative study of Barrington, Australia, and West Pailin, Cambodia, gemfields. *Journal of Gemmology*, Vol. 26, No. 2, pp. 65–85.
- Thomas V.G., Mashkovtsev R.I., Smirnov S.Z., Maltsev V.S. (1997) Taurus hydrothermal synthetic sapphires doped with nickel and chromium. *Gems & Gemology*, Vol. 33, No. 3, pp. 188–202.

PRE-COLUMBIAN GEMS AND ORNAMENTAL MATERIALS FROM ANTIGUA, WEST INDIES

By A. Reg Murphy, David J. Hozjan, Christy N. de Mille, and Alfred A. Levinson

Two archeological sites that were discovered recently on the island of Antigua appear to have had flourishing lapidary industries. Excavation of these sites, which date to about 250–500 AD (Saladoid period), has revealed beads, pendants, and “zemis” made from a variety of materials, with shell being the most abundant. All of the unworked materials (e.g., shell, carnelian, and diorite) are of local origin. However, amethyst, nephrite, serpentine, and turquoise were found only as finished gems; these are not local and imply that trade or exchange existed between Antigua and other parts of the Caribbean and possibly the Americas during Saladoid time.

Pre-Columbian gems and ornamental materials (fashioned as beads, pendants, and “zemis” [distinctive pointed religious objects]) from the Caribbean Islands have been known since the 1870s (Watters, 1997a). Although such materials from various islands have been described in anthropological or archeological publications (e.g., Ball, 1941; Cody, 1991a; Watters and Scaglione, 1994), they have not been documented previously from the island of Antigua.

Two archeological sites discovered recently on Antigua—Elliot’s and Royall’s (Murphy, 1999)—clearly were jewelry manufacturing centers, as evidenced by the presence of gem and ornamental materials in all stages of manufacture, from the raw material to the finished product (e.g., Watters, 1997b). Previously, only a few other isolated prehistoric gem items composed of minerals or rocks (carnelian and diorite) were discovered on Antigua, although shell beads are fairly common (Murphy, 1999). In this article, we report the results of our research on the ancient jewelry industry of Antigua by cataloguing the lapidary objects and identifying the minerals and rocks from which they are fashioned (see, e.g., figure 1), as well as suggesting whether they are of local or nonlocal geographic origin. We then compare these results to those for three other lapidary-containing archeological sites in the eastern Caribbean Islands.

DESCRIPTION OF THE SITES

The site at Elliot’s was discovered in early 1996 while the land was being prepared for agriculture. It covers an area of about 5,550 m². The Royall’s site, discovered in January 1998 during land clearing for a housing development, covers an area of about 39,000 m²; it is the largest of at least 120 known prehistoric archeological sites on Antigua



ABOUT THE AUTHORS

Dr. Murphy (museum@candw.ag) is an archeologist at the Museum of Antigua and Barbuda, St. John’s, Antigua. Mr. Hozjan is a geologist with Overburden Drilling Management Ltd., Ottawa, Canada; and Ms. de Mille is a doctoral student in the Department of Archeology, University of Calgary, Alberta, Canada. Dr. Levinson (levinson@geo.ucalgary.ca) is professor emeritus in the Department of Geology and Geophysics, University of Calgary.

Please see acknowledgments at the end of the article.

*Gems & Gemology, Vol. 36, No. 3, pp. 234–245
© 2000 Gemological Institute of America*



Figure 1. These beads and pendants are representative of the many different lapidary objects that were recovered from the Elliot's site on the Caribbean island of Antigua. From the top left: Column 1 = tuff, nephrite; column 2 = barite, serpentine, diorite; column 3 = nephrite (frog carving), amethyst, chalcedony; carnelian (fragment); column 4 = amethyst, quartz, carnelian. All of these objects are finished except for the barite and chalcedony, which lack drilled holes. Note, for scale, that the nephrite carving in column 1 is 6.5 cm long and 0.7 cm wide.

(Nicholson, 1993). The sites are located approximately 12 km (7 miles) apart (figure 2), amid grassland and scrub vegetation. Their names are derived from nearby historical sugar plantations (on some maps or in other publications, these localities are spelled "Elliot's" and "Royal's" or "Royals").

Within two weeks of the discovery of each site, members of the Museum of Antigua and Barbuda began surface reconnaissance. It was immediately evident that the sites contained a diverse selection of the material culture of the early inhabitants, including lapidary and ceramic items, as well as stone artifacts such as axes. Surface sampling conducted in July 1998 by the University of Calgary Archeology Field School Antigua confirmed the temporal and cultural affiliation of these ancient settlements.

BACKGROUND

Archeology. The human history of Antigua is intimately associated with that of the other islands in the Lesser and Greater Antilles (again, see figure 2), and derives from the migration of ancient Amerindians from mainland regions (Wilson, 1997a, b). The earliest substantiated settlement in Antigua is dated at about 1775 BC (Nicholson, 1993). In approximately 450 BC, Saladoids began to settle in the Antigua region (Rouse, 1976; Murphy, 1999). *Saladoid* is a generic name given to an Arawak-speaking, pre-Columbian, ceramic- and agriculture-oriented people from the lower Orinoco River valley; the type archeological site is at Saladero, Venezuela (Rouse, 1992; Allaire, 1997). Over time, the Saladoids traveled from Trinidad



Figure 2. The Lesser Antilles is a chain of predominantly volcanic islands that stretches about 700 km (435 miles) along the eastern part of the Caribbean Sea, from the Virgin Islands and Sombrero in the north to Trinidad in the south. The Greater Antilles is another group of mainly larger islands to the north and west that includes Cuba, Jamaica, Hispaniola, and Puerto Rico. The West Indies includes the Lesser Antilles, the Greater Antilles, and the Bahamas. The Elliot's and Royall's archeological sites are located in eastern and northern Antigua, respectively, only about 12 km from each other.

northward to the Virgin Islands and Puerto Rico.

The lapidary items described here are associated with the Saladoid culture, specifically during the period 250–500 AD. This is based on carbon-14 age dates of 435 and 440 AD on charcoal at the Royall's site, and on diagnostic pottery at both the Royall's and Elliot's sites (figure 3). These sites are representative of the peak of Saladoid culture and artistry (Murphy, 1999).

Over time, certainly from 800 AD onward, the Saladoid culture evolved into various regional island cultures throughout the Antilles. The Historic Age of the Leeward Islands (the northern half of the Lesser Antilles, which includes Antigua) began in 1493 with their discovery by the Spanish. It appears, however, that the complex artistry and lapidary

skills of the Saladoid culture had been lost by that time (Nicholson, 1993; Murphy, 1999). It is also evident that there was no trade in nonindigenous gem materials, because no such materials have been found in post-Saladoid archeological sites (Rouse, 1992; Crock and Bartone, 1998). The earliest European settlement of Antigua was British colonization in 1632 (Nicholson, 1991).

Geology. A brief review of the geology of Antigua is useful for inferring the local or nonlocal origin of the gems and ornamental materials recovered.

Of the several studies that have been made on the geology of the Lesser Antilles in general, and of Antigua in particular, those by Martin-Kaye (1969), Multer et al. (1986), and Weiss (1994) are particularly

applicable to this report. These islands form an arcuate chain that separates the Caribbean Sea from the Atlantic Ocean (again, see figure 2). The location of the islands, and the great amount of volcanic activity characteristic of this part of the Caribbean, is related to plate tectonics, specifically to the subduction of the Atlantic Plate under the Caribbean Plate.

Essentially, Antigua is made up of volcanic rocks on which limestones were deposited; all the rocks are Oligocene in age (ca. 36–23 million years old). The island is divided into three geologic regions with distinctive physiographic characteristics (figure 4). As summarized from Weiss (1994):

- The Basal Volcanic Suite occupies the southwestern 40% of Antigua. It consists mainly of basalt and andesite flows, and pyroclastic rocks (e.g., tuff). The Suite also contains some minor intrusive plugs (e.g., quartz diorite), dikes, and sills, as well as some sedimentary rocks (e.g., limestones) intercalated with the volcanics. This part of the island is characterized by rugged topography.
- The Central Plain Group occupies the central 20% of the island. It consists predominantly of sedimentary rocks (e.g., limestone, chert), with minor amounts of volcanic rocks (e.g., tuff).

Figure 3. Anthropomorphic (human-like) effigies such as these, which are common on ceramic vessels from the Saladoid period, helped establish the approximate time period when these lapidary sites were active. These figurines were found at the Royall's site, but identical objects have been recovered from Elliot's and many other 250–500 AD Saladoid sites in the Lesser Antilles and Venezuela. The larger effigy is about 7.8 cm in its long direction.



Figure 4. This simplified geologic map of Antigua illustrates the three main rock units (after Weiss, 1994). The Elliot's and Royall's ancient lapidary sites are on the Antigua Formation, which consists mostly of carbonate rocks (limestones and ancient coral reefs).

Topographically, the Group occupies an area of low relief.

- The Antigua Formation, the youngest of the three regions, occupies the northeastern 40% of Antigua, including the smaller offshore islands. It consists predominantly of limestones and ancient coral reefs. The area is moderately rugged, and the highly indented coast is characterized by bays fringed with mangroves and sand beaches. Many living coral reef communities thrive within and offshore the bays and islands. The Elliot's and Royall's lapidary industry sites are found within this geologic formation.

MATERIALS AND METHODS

Preliminary surface (figure 5) and subsurface sampling was conducted at each site to confirm its archeological nature. Subsequently, four pits (each 1 m²) at Royall's (see, e.g., figure 6) and one at Elliot's were excavated by brush and trowel, in 10 cm levels. All soil was passed through 2 mm mesh sieves to facilitate the recovery of minute beads and lithic by-product debris; material smaller than 2 mm was discarded. All cultural material recovered, including beads and raw materials that showed evidence of having been worked, was retained for analysis (see Murphy, 1999, for further details of the field procedures). By mid-1999, less than one percent of the area of each site had been studied.

A total of 642 specimens collected over two field seasons (during the summers of 1997 and 1998) were selected for this research: 149 from Elliot's (see, e.g., figure 1) and 493 from Royall's. They were



Figure 5. Students from the University of Calgary Archeology Field School Antigua are shown here shovel testing (i.e., examining surface samples, to approximately the depth and width of a shovel, to determine the boundaries of the site) at Royall's in July 1998.

sorted into categories based on visual characteristics such as color, composition (e.g., shell or rock), shape, and physical properties such as specific gravity. They were further categorized as finished jewelry, blanks (partially worked material), *zemis*, or raw

Figure 6. This pit at the Royall's site measures 1 m² and 90 cm (about 3 ft.) deep. The black horizon on the bottom is an ancient soil (paleosol) horizon. All Saladoid-period archeological objects (including gem and related materials) recovered from this site have been found only above the paleosol horizon.



(unworked) materials. Excluded from this study were various rock types (basalt, felsic volcanics, and some limestones), ceramic materials, faunal remains (e.g., animal and fish bones), and artifacts such as axes, because they were not used by the Saladoid culture for jewelry or other ornamental purposes. Raw shell materials were not included in this study, as they are extremely common and difficult to distinguish from food-related shell debris or shells used for other purposes.

Representative samples from each category were selected for detailed mineralogical or petrologic identification. Customarily, archeological artifacts are not subjected to destructive analytical techniques. Thus, analysis on most of the study specimens was limited to nondestructive methods: that is, microscopic examination (at least 100 specimens), specific gravity measured by the hydrostatic method (at least 40 specimens), and qualitative chemical composition for sodium and heavier elements (on at least 40 specimens) by energy-dispersive X-ray spectrometry using a Cambridge Model 250 scanning electron microscope (SEM-EDS). Refractive indices could not be obtained with a gemological refractometer for any of the specimens, as received, because of the poor quality of their surface polish; however, a flat surface was polished on one chalcedony sample for R.I. determination. Laser Raman microspectrometry was used to confirm our identification of five finished specimens.

Limited destructive testing was done on broken or partially finished specimens, or on raw materials. These included 25 powder X-ray diffraction (XRD) analyses, 20 hardness (scratch) determinations, and effervescence with dilute hydrochloric acid to test for carbonates (on about 20 samples). Eleven thin sections were made for petrographic study of expendable rough or broken fragments of rocks such as tuff and diorite, and minerals such as chalcedony. After documenting representative samples of the minerals and rocks, we identified most of the remaining specimens by comparison, using microscopic study and one or more of the nondestructive methods discussed above.

The several varieties of quartz (amethyst, carnelian, chalcedony, and jasper) were distinguished following the nomenclature of Hurlbut and Kammerling (1991). Thus, we use *chalcedony* as a general term for microcrystalline to cryptocrystalline fine-grained varieties of quartz that are translucent, commonly light colored with a waxy luster, and have the following properties: an S.G. lower than 2.60, slight porosity (which may be seen

TABLE 1. Saladoid gem and ornamental materials from Antigua identified in this study.^a

Gem and ornamental materials	Elliot's site					Royall's site				
	Raw material	Beads (blank)	Beads (finished)	Pendants (finished)	Zemis	Raw material	Beads (blank)	Beads (finished)	Pendants (finished)	Zemis
Quartz family gems										
Amethyst			3							
Carnelian	1		2			45	7	4		
Chalcedony	7	3				5	2	1		
Chert	1					1		1		
Jasper						3				
Quartz	6		3			13	2	3		
Other gem materials										
Barite	2	1	1			5	2	1		
Calcite	1	3	1			36	5	18		
Malachite		1								
Nephrite				2						1
Serpentine			1					3		
Shell (aragonite/calcite)	— ^b	21	52		9	— ^b	72	181	34	7
Turquoise								1		
Rocks										
Diorite			6		2			11	4	
Limestone		6	1	5		8	6 ^c	6	3	
Tuff				7	1	2				
Total	<u>18</u>	<u>35</u>	<u>70</u>	<u>14</u>	<u>12</u>	<u>118</u>	<u>96</u>	<u>230</u>	<u>42</u>	<u>7</u>

^aAll gem materials and rocks are inferred to be from Antigua except amethyst, nephrite, serpentine, and turquoise.

^bRaw shell material was not included because it is difficult to distinguish food-related shells from those intended for other purposes.

^cIncludes three samples of travertine.

in thin section), and an R.I. of about 1.54 (as determined on the one specimen polished specifically for this study). We use the term *chert* for a microcrystalline siliceous rock of sedimentary origin, which may contain amorphous silica (opal) and the siliceous remains of organisms, in accordance with the definition of Jackson (1997).

RESULTS

Of the 642 specimens from both sites, we categorized 300 finished beads, 131 blank beads, 56 finished pendants (no pendant blanks were recovered), 19 zemis, and 136 raw materials (table 1). We identified 13 gem materials and three rock types. Nine of the gems were identified by X-ray diffraction analysis (augmented by visual discrimination and thin-section study in the case of the quartz family gems): aragonite (shell), barite, calcite (both shell and non-biogenic types), carnelian, chalcedony, chert, malachite, nephrite, and serpentine (see, e.g., figure 1). The remaining four gem materials were determined by their physical properties (e.g., S.G.) and/or chemical components by SEM-EDS: amethyst, jasper, quartz (colorless or near-colorless, transparent or

translucent), and turquoise. Our identifications of five finished specimens were confirmed by Raman analysis: nephrite (2 samples), serpentine (antigorite; 2), and turquoise (1). One finished specimen we identified as nephrite could not be confirmed by Raman analysis because of the poor surface polish. The three rock types were identified as diorite, limestone (including travertine), and tuff by petrographic (thin section) and binocular microscopy, as well as by visual observation.

Various green materials with specific gravities of 2.2–2.6 were common at both sites, and presented special problems in both identification and nomenclature. Figure 7 illustrates six such specimens, which were identified by a combination of X-ray diffraction analysis and thin-section and microscopic studies as: chalcedony (3 samples), tuff (2), and chert (1).

Gem Materials. *Quartz Family Minerals.* The three *amethyst* beads are semi-transparent, pale purple, and grade into colorless quartz (again see figure 1). The *carnelian* samples are semi-transparent to translucent brownish red to orangy red (figures 1



Figure 7. These green specimens, which are similar in both appearance and specific gravity (2.2–2.6), could not be identified conclusively without the use of X-ray diffraction analysis or other advanced techniques. They are (clockwise, from the large specimen on the bottom): tuff (about 3 cm long), malachite-rich tuff bead blank, chert bead, with all of the last three chalcedony.

Figure 8. Carnelian was one of the most common gem varieties observed at the two lapidary sites, as raw material, blanks, and finished beads. These are from the Royall's site; the smallest bead measures approximately 12 mm and the largest piece of rough, 4 cm.



Figure 9. Shown here are a variety of semi-transparent to translucent objects from the Royall's site that have been fashioned from single crystals or masses of calcite (which is distinct from the opaque calcite derived from shells). They represent all stages in the production of small beads. The smallest bead shown here measures approximately 3 mm; the largest piece of rough, 4 cm.

and 8). The *chalcedony* objects (figures 1 and 7) are either white or green.

Two green *chert* specimens from the Royall's site (again, see figure 7) were found to consist of quartz, cristobalite, and mordenite; one also contained analcime. A green radiolarian chert was found at Elliot's. The three specimens of *jasper* raw material are opaque due to admixture with abundant iron oxides. Transparent colorless *quartz* beads and pieces of rough were found at both sites (figure 1).

Figure 10. This 9 × 11 mm bead, from the Royall's site, is the only piece of turquoise identified from the samples studied. Photo by Maha Tannous.



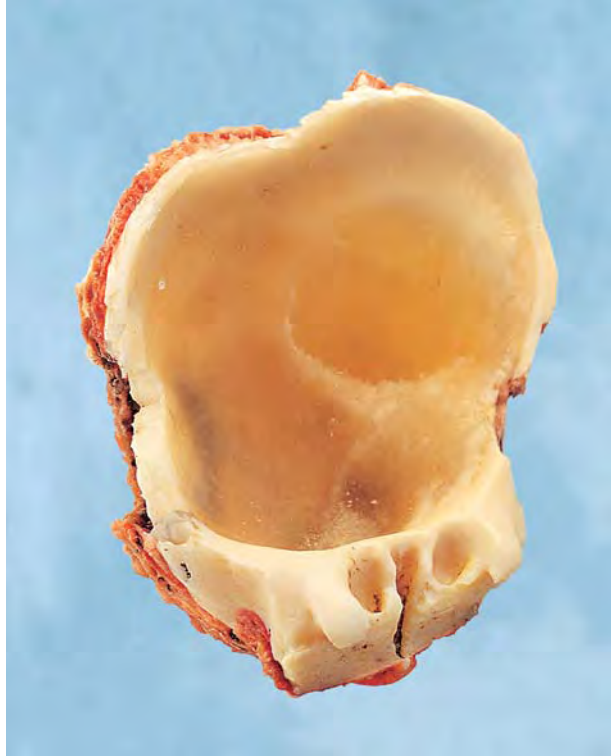


Figure 11. Note that there are two parts to this thorny oyster (*Spondylus americanus*) shell: The inner (white) part is composed of aragonite, while the outer (red) part has been converted to calcite. The specimen is about 9.6 cm long and 7.6 cm wide.

Other Gem Materials. Also as illustrated in figure 1, a small number of white to yellowish white opaque pieces and finished beads of *barite* were found at each site. *Calcite* (white to tan) was particularly abundant at the Royall's site. The semi-transparent to translucent calcite fashioned from crystals (figure 9) is easily separated from the opaque calcite derived from shell, which typically has a reddish component (discussed below).

One specimen of *malachite*-rich tuff (figure 7) was found at the Elliot's site. The three finished pendants identified as *nephrite* (two are shown in figure 1) range from slightly yellowish green to very dark green. The *serpentine* beads (again, see figure 1) range from yellowish green to dark green. One small bluish green *turquoise* bead was found at the Royall's site (figure 10).

Shell was the most abundant locally available ornamental material; it represents 74% of all the worked (i.e., finished and blank) objects in this study. Thirteen species of shellfish have been identified at the Elliot's and and/or Royall's sites (Murphy, 1999). However, the shell jewelry and ornamental objects we examined were made from only two species: (1) predominantly, the queen conch (*Strombus gigas*); and (2) to a lesser extent, the thorny oyster (*Spondylus americanus*).

Many shells are composed of aragonite when initially formed by the living shellfish. However, aragonite is not a stable mineral and, especially in the marine environment, the outer part will rapidly (in a matter of years) convert to calcite (figure 11). Thus, depending on what part of the shell is used for jewelry, the piece could contain aragonite and/or calcite. Most of the specimens in this study are aragonite.

The skill with which Saladoid craftsmen designed and manufactured ornamental shell objects may be gauged from the disc-shaped beads shown in figures 12 and 13, and from the pendants in figure 14. Zoomorphic (e.g., animal heads; see the bird-shaped pendant in figure 14) and anthropomorphic (e.g., human faces; see figure 3) themes are common and also skillfully produced in shell throughout the region inhabited by the Saladoid culture. Figure 15 illustrates *zemis* carved from shell material.

Figure 12. These white beads and a blank from the queen conch (*Strombus gigas*) were found at the Royall's site. All are composed of aragonite. The blank is about 34 mm in its longest dimension, and the smallest bead is about 3 mm in diameter.



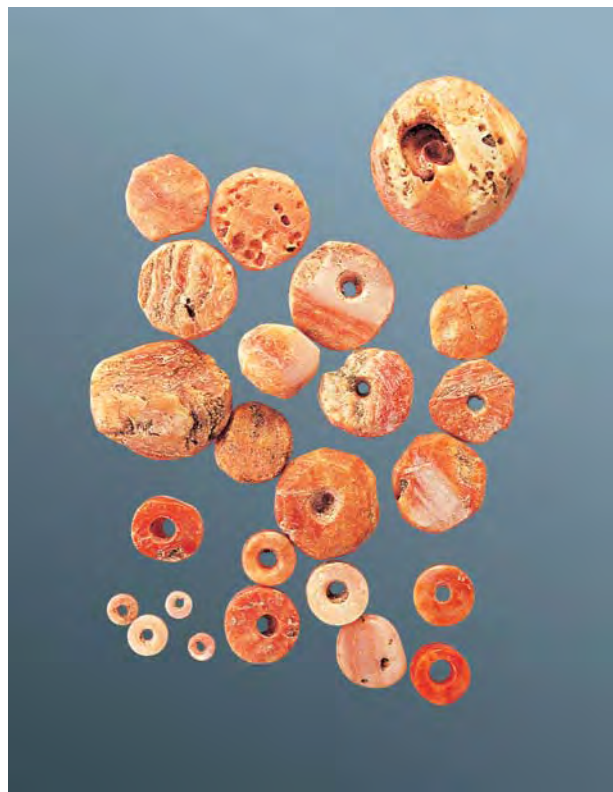


Figure 13. Red beads and blanks from the Royall's site represent all stages of bead production. Composed of calcite, they originate from the outer part of the thorny oyster shell. The largest blank is about 15 mm in its longest dimension, and the smallest bead has an external diameter of about 2.5 mm.

Rocks. The coarse-grained, unaltered *diorites* vary from light to dark, as determined by the relative amounts of white and black minerals (see figures 1 and 16). Thin-section examination revealed that the diorite is composed of variable amounts of plagioclase and amphibole, with minor quartz.

Most of the *limestones* are light colored, but some have dark streaks or zones of organic matter. Three specimens from Royall's are composed of calcite and have the distinctive wavy textures of travertine (see, e.g., figure 17); we have classified them as limestones.

The *tuff* specimens showed the greatest variation in color appearance, texture, and mineral composition of the three rock types studied (again, see figures 1 and 7). They were also the most problematic to classify. In general, the tuff samples are light to medium green, have an altered fine-grained matrix, and have a low specific gravity; these characteristics reflect tuff's origin as consolidated volcanic ash.

DISCUSSION

Sources of the Lapidary Materials. Even though Antigua is a small island, most of the gem materials and rocks listed in table 1 are known to occur there. Barite, carnelian, chalcedony, chert, jasper, and quartz (both transparent and translucent) were mentioned in the geologic literature of the early to mid-19th century (Anonymous, 1818; Nugent, 1818, 1821; Hovey, 1839). Martin-Kaye (1959) described a barite quarry from which this mineral was mined between 1942 and 1945; he also mentions two small occurrences of malachite that are found as accumulations (as pockets or flakes) or stains within tuffs. Shell is abundant in the waters and reefs surrounding Antigua, as well as in certain units of the Antigua Formation. Limestone and tuff are common constituents of the Antigua Formation and Basal Volcanic Suite, respectively. The diorite may have come from an outcrop on the south coast of Antigua that was documented by Multer et al. (1986).

Calcite has not been reported from Antigua as transparent or translucent crystals or masses, although it may be present in solution cavities in limestones of the Antigua Formation. The same observation applies to travertine. Indeed, at the American Museum of Natural History in New York, there are etched "dog tooth" calcite crystals up to 4 cm in length, with clear portions inside, that are reportedly from St. John's, Antigua (G. E. Harlow, pers. comm., 1999). Thus, we believe that the calcite found at both the Elliot's and Royall's sites is probably of local origin.

There are no geologic reports or known occurrences of amethyst, nephrite, serpentine, or turquoise on Antigua. Given the geology of the island, we do not expect them to be present—although we recognize that since carnelian, chalcedony, and quartz exist on the island, the occurrence of amethyst is a possibility, especially in the basalts. We propose that amethyst, nephrite, serpentine, and turquoise are of nonlocal origin. Noteworthy is the fact that there are only 11 such nonlocal specimens (about 2% of the total), and these have been found only as finished objects.

Other Saladoid Lapidary Sites in the Eastern Caribbean. Comparison of our data to those obtained from three well-documented Saladoid lapidary sites of comparable age on three islands in the eastern Caribbean (figure 2) is instructive. The three sites are: Vieques Island, Puerto Rico (Chanlatte



Figure 14. These aragonite pendants were carved from queen conch shell. The artifact on the right (about 4 cm tall) is in the form of a bird.

Baik, 1983; Cody, 1990; Rodríguez, 1991); Pearls, Grenada (Cody, 1990; Cody, 1991a and b); and Trants, Montserrat (Watters and Scaglione, 1994; Crock and Bartone, 1998).

We do not know what role shell jewelry played in these three sites, because those conducting the research on the gems and ornamental stones were concerned primarily with jewelry composed of minerals and rocks. We do know that most of the gem materials and rocks, except for barite and tuff, listed in table 1 also have been found in at least one of these three other Saladoid lapidary sites. However, there are distinct differences in details of the production at the various sites. For example, Grenada probably was a center for the manufacture of amethyst beads (Cody, 1991b), whereas Montserrat specialized in carnelian beads (Watters and Scaglione, 1994). If only the mineral and rock component of the Antigua production is considered (again, see table 1), then carnelian was a major cutting material (second only to calcite) at this location, as it was at Montserrat. Further, raw material and blank beads of carnelian greatly exceeded the number of finished beads at Montserrat (Watters and Scaglione, 1994), which is identical to the situation at Royall's. These similarities between Antigua and Montserrat are not surprising, given the close proximity of these islands to each other (again, see figure 2).

Through the courtesy of Dr. D. R. Watters, we compared about 30 specimens of rough (unworked) carnelian from the Trants site with 12 specimens

of rough carnelian from the Royall's site. The carnelians from both sites are remarkably similar in appearance (e.g., some are mottled with color gradation from orangy red to white chalcedony,

Figure 15. The pre-Columbian (specifically Saladoid) Caribbean spiritual ornaments known as *zemis* always have the same approximate shape, regardless of their particular origin or composition. These *zemis* are carved from queen conch shell; the widest specimen measures 3.5 cm.





Figure 16. The color of diorite varies depending on the proportion of light and dark minerals (predominantly plagioclase and amphibole, respectively) that are present, as shown by these four beads and a zemi from the Elliot's site. The largest bead measures about 4.4 cm, and is broken.

some have dark orangy red rinds surrounding white opaque chalcedony, some have a banded texture with the bands ranging in color from orangy red to white, and some are translucent with only a slight reddish color), which suggests the same geologic source. As carnelian is reportedly nonlocal to Montserrat, it is possible that the supply of this material came from Antigua, which suggests trading between these two islands.

Sources of the Nonlocal Materials. The four nonlocal worked minerals (amethyst, nephrite, serpentine, and turquoise) from Antigua are also found at most of the other eastern Caribbean sites. A challenge for archeologists has been to determine the original source of these minerals. Most favor South America, because of the generally accepted migration path of the Saladoid people (see above). Possible South American sources are hypothesized by Cody (1990, 1991a) for amethyst (Brazil and Guyana), nephrite (Brazil, Guyana, and Venezuela), serpentine (Venezuela), and

turquoise (Brazil and Chile), based solely on their known geologic occurrences. Turquoise from the southwestern U.S. seems unlikely, because significant mining did not start there until about the 5th century AD (Ball, 1941). Several authors (e.g., Rodríguez, 1991) suggest southwestern Puerto Rico as a source of serpentine. Nevertheless, with respect to South American sources for the nonlocal gem materials found in the Caribbean Islands, Watters (1997a, p. 7) pointed out that "empirical evidence of such sources is largely lacking."

CONCLUSION

A flourishing lapidary industry, attributed to people of the Saladoid culture, existed on Antigua during the period 250–500 AD. From excavations at the Elliot's and Royall's archeological sites, 13 gem materials (including shell) and three rock types used for gem and ornamental purposes have been identified. Most of the jewelry artifacts recovered (mainly beads) were made of shell. Calcite, carnelian, quartz, diorite, and limestone were also important lapidary materials. Eleven of the 642 specimens studied are composed of minerals (amethyst, nephrite, serpentine, and turquoise) that do not

Figure 17. These bead blanks from the Royall's site are made of limestone, probably travertine. The larger one measures about 3 cm.



occur on Antigua. These were found only as finished objects, and apparently arrived on Antigua as a result of trade. We can only speculate as to the geographic origins of these nonlocal samples.

The lapidary industry in Antigua appears to have similarities with that at nearby Montserrat, specifically in that carnelian was important among the stone objects at both sites. This article demonstrates how the gemological characterization of ancient gem materials can help archaeologists locate the source of the rough materials used in ancient jewelry and suggest early trade patterns.

Acknowledgments: Dr. Murphy thanks Dr. D. R. Watters of the Carnegie Museum of Natural History in Pittsburgh for supplying the authors with rare literature references, and John Fuller of Antigua for field assistance. The authors also thank the following (all at the University of Calgary): Dr. G. Newlands, who took all specimen photos not acknowledged to others; M. Glatiotis, for assisting with chemical analyses using the scanning electron microscope and for X-ray diffraction analyses; J. Resultay, for preparing thin sections; and Professors L. V. Hills, J. W. Nicholls, and R. J. Spencer, for helpful discussions. J. I. Koivula at GIA in Carlsbad kindly performed the Raman analyses.

REFERENCES

- Allaire L. (1997) The Lesser Antilles before Columbus. In S. M. Wilson, Ed., *The Indigenous People of the Caribbean*, University Press of Florida, Gainesville, FL, pp. 20–28.
- Anonymous (1818) Petrified wood from Antigua. *American Journal of Science*, Vol. 1, pp. 56–57.
- Ball S.H. (1941) The mining of gems and ornamental stones by American Indians. *Smithsonian Institution, Bureau of American Ethnology Bulletin No. 128, Anthropological Papers*, No. 13, pp. 1–77.
- Chanlatte Baik L.A. (1983) *Catálogo Arqueología de Vieques*. Museo de Antropología, Historia y Arte, Universidad de Puerto Rico, Recinto de Río Piedras, 90 pp.
- Cody A.K. (1990) Prehistoric patterns of exchange in the Lesser Antilles: Materials, models, and preliminary observations. M.A. thesis, San Diego State University, 422 pp. [University Microfilms, No. 1344090]
- Cody A. (1991a) Distribution of exotic stone artifacts through the Lesser Antilles: Their implications for prehistoric interaction and exchange. In A. Cummins and P. King, Eds., *Proceedings of the Fourteenth Congress of the International Association for Caribbean Archaeology*, Barbados, 1991, pp. 204–226.
- Cody A.K. (1991b) From the site of Pearls, Grenada: Exotic lithics and radiocarbon dates. In E.N. Ayubi and J.B. Haviser, Eds., *Proceedings of the Thirteenth Congress of the International Association for Caribbean Archaeology, Curaçao, 1990*, Reports of the Archaeological-Anthropological Institute of the Netherlands Antilles, No. 9, Willemstad, Curaçao, pp. 589–604.
- Crock J.G., Bartone R.N. (1998) Archaeology of Trants, Montserrat, Part 4: Flaked stone and stone bead industries. *Annals of Carnegie Museum*, Vol. 67, No. 3, pp. 197–224.
- Hovey S. (1839) Geology of Antigua. *American Journal of Science*, Vol. 35, pp. 75–85.
- Hurlbut C.S., Kammerling R.C. (1991) *Gemology*, 2nd ed. John Wiley, New York.
- Jackson J.A. (1997) *Glossary of Geology*, 4th ed. American Geological Institute, Alexandria, VA.
- Martin-Kaye P.H.A. (1959) *Reports on the Geology of the Leeward and British Virgin Islands*. Voice Publishing Co., St. Lucia, 117 pp.
- Martin-Kaye P.H.A. (1969) A summary of the geology of the Lesser Antilles. *Overseas Geology and Mineral Resources*, Vol. 10, No. 2, pp. 172–206.
- Multer H.G., Weiss M.P., Nicholson D.V. (1986) *Antigua. Reefs, Rocks & Highroads of History*, Contribution No. 1, Leeward Islands Science Associates, St. John's, Antigua.
- Murphy A.R. (1999) The prehistory of Antigua, Ceramic Age: Subsistence, settlement, culture and adaptation within an insular environment. Ph.D. thesis, Department of Archeology, University of Calgary, Calgary, Alberta, Canada, 320 pp.
- Nicholson D.V. (1991) *The Story of English Harbour*. Historical and Archeological Society of Antigua, St. John's, Antigua.
- Nicholson D.V. (1993) *The Archaeology of Antigua and Barbuda*. Museum of Antigua and Barbuda, St. John's, Antigua.
- Nugent N. (1818) Notices of geology in the West-Indies. *American Journal of Science*, Vol. 1, pp. 140–142.
- Nugent N. (1821) A sketch of the geology of the island of Antigua. *Transactions of the Geological Society (London)*, Vol. 5, pp. 459–475.
- Rodríguez M. (1991) Early trade networks in the Caribbean. In A. Cummins and P. King, Eds., *Proceedings of the Fourteenth Congress of the International Association for Caribbean Archaeology*, Barbados, 1991, pp. 306–314.
- Rouse I. (1976) The Saladoid sequence on Antigua and its aftermath. In R. P. Bullen, Ed., *Proceedings of the Sixth International Congress for the Study of Pre-Columbian Cultures of the Lesser Antilles*, Gainesville, FL, pp. 35–41.
- Rouse I. (1992) *The Tainos: Rise and Decline of the People Who Greeted Columbus*. Yale University Press, New Haven, CT.
- Watters D.R. (1997a) Stone beads in the prehistoric Caribbean. *Bead Study Trust Newsletter*, No. 29, Spring, pp. 7–8.
- Watters D.R. (1997b) Maritime trade in the prehistoric eastern Caribbean. In S. M. Wilson, Ed., *The Indigenous People of the Caribbean*, University Press of Florida, Gainesville, FL, pp. 88–99.
- Watters D.R., Scaglione R. (1994) Beads and pendants from Trants, Montserrat: Implications for the prehistoric lapidary industry of the Caribbean. *Annals of Carnegie Museum*, Vol. 63, No. 3, pp. 215–237.
- Weiss M.P. (1994) Oligocene limestones of Antigua, West Indies: Neptune succeeds Vulcan. *Caribbean Journal of Science*, Vol. 30, No. 1–2, pp. 1–29.
- Wilson S.M., Ed. (1997a) *The Indigenous People of the Caribbean*. University Press of Florida, Gainesville, FL.
- Wilson S.M. (1997b) Introduction to the study of the indigenous people of the Caribbean. In S. M. Wilson, Ed., *The Indigenous People of the Caribbean*, University Press of Florida, Gainesville, FL, pp. 1–8.

GEM-QUALITY HAÜYNE FROM THE EIFEL DISTRICT, GERMANY

By Lore Kiefert and H. A. Hänni

Haüyne is a rare mineral and an extremely rare gemstone. Recently, the authors studied a large number of faceted haüynes from the Eifel district of Germany. The R.I. and S.G. data were consistent with those reported in the literature, and the samples' identity was confirmed by Raman spectrometry, with the key maxima at 543 and 988 cm^{-1} . EDXRF analyses revealed potassium and iron, as well as the major and minor elements expected in haüyne. Although mineral inclusions were uncommon, apatite and augite were identified, and negative crystals (often surrounded by healed fractures) were seen in approximately one-third of the stones. Short needles and fine, dust-like particles were present in about half the samples. Paraffin wax was identified in some open fissures.

In the summer of 1999, the authors were surprised to receive 100 faceted haüynes (pronounced "how-eeen") for analysis. The client who submitted these stones subsequently fashioned most of them into a brooch set with diamonds and a pink sapphire (figure 1). This butterfly brooch sold at the Sotheby's November 1999 Geneva auction for 45,000 SFr (approximately US\$30,000).

In spite of its attractive color, however, haüyne is rarely seen in jewelry. Not only is the mineral

itself rare, but it also has a relatively low hardness (5.5–6 on Mohs scale).

Transparent haüyne primarily occurs as small crystals (see also Mertens, 1984) of an unusual bright "apatite" to "sapphire" blue color. Mineralogically, it is a feldspathoid that belongs in the sodalite group (which also includes sodalite, lazurite, and nosean), and is often one of the components of lapis lazuli. The chemical formula for haüyne is ideally $(\text{Na,Ca})_{4-8}\text{Al}_6\text{Si}_6(\text{O,S})_{24}(\text{SO}_4\text{,Cl})_{1-2}$ (Mandarino, 1999). The crystal system for this silicate is cubic, the crystal class is $\bar{4}3m$. Cleavage planes are distinct in the {110} direction, and twinning is common along {111}. Haüyne has been reported as white to gray, green, yellow, and red (Arem, 1987), but only the blue color has been noted thus far as faceted material.

GEOLOGY AND OCCURRENCE

Haüyne is found in association with alkaline volcanic rocks (mainly phonolites, which are composed of alkali feldspar, mafic minerals, and felds-

ABOUT THE AUTHORS

Dr. Kiefert (gemlab@sssf.ch) is a research scientist and assistant director of the SSEF Swiss Gemmological Institute, Basel, Switzerland. Dr. Hänni (H-A.Haenni@uni-bas.ch) is director of SSEF and professor of gemology at Basel University, Switzerland.

Please see acknowledgments at end of article.

Gems & Gemology, Vol. 36, No. 3, pp. 246–253

© 2000 Gemological Institute of America



Figure 1. The authors had an opportunity to examine all of the hâüynes before they were set in this attractive brooch with diamonds and a pink sapphire. The hâüynes range from 0.095 to 0.173 ct. Photo courtesy of Della Valle.

pathoids; figure 2). It has been reported from many countries, including the U.S., Canada, France, Italy, Spain (Tenerife), Morocco, and Germany (Arem, 1987). In Germany, it occurs in relative abundance near Laacher See in the Eifel Mountains as gem-quality crystals of an unusual blue color and transparency. Gem-quality material has not been reported from other sources (Fischer and Bürger, 1976; Arem, 1987).

In the Eifel Mountains, hâüyne formed in a magma chamber approximately 2–4 km below the surface, together with a suite of minerals including sanidine, nosean, nepheline, leucite, plagioclase, amphibole, augite, magnetite, titanite, phlogopite, apatite, and olivine (Matthes, 1983; Wörner and Schmincke, 1984). This phonolitic magma was volatile-rich and chemically zoned, with a strong decrease in sulfur during progressive magmatic differentiation, which is interpreted to be partially caused by crystallization of hâüyne (Harms and Schmincke, 2000). This magma erupted approximately 12,900 years ago, and the resulting volcanic rocks were deposited in three zoned layers. The bottom layer, which corresponds to the top of the magma chamber, is relatively crystal-poor and consists of a nearly aphyric, highly differentiated phonolite. The top layer, which transported the contents of the bottom of the magma chamber with crystal enrichment, consists of a relatively crystal-rich mafic phonolite. Hâüyne is found throughout

all three layers (Schmincke, 2000; Harms and Schmincke, 2000).

We know of no attempts to mine hâüyne commercially. Most of the crystals are found by amateur collectors (see, e.g., Linde, 1998). In the Eifel district,

Figure 2. At Laacher See, hâüyne is found in a phonolitic pumice. This crystal measures 1.5 mm in longest dimension. Photo by Jean-Pierre Chalain.





Figure 3. These 100 faceted round and oval häüynes, which were submitted to SSEF for examination, represent a large portion of the samples examined for this study. They were reportedly from Laacher See, in the Eifel Mountains of Germany. The stones range from 0.095 to 0.173 ct. Photo by Lore Kiefert.

the majority of the stones come from a commercial pumice mine. Whenever a new layer is blasted from the high wall of pumice stone, collectors arrive to search for these rare blue crystals. On the market, even the rough stones are sold by carat weight rather than by grams (C. Wild, pers. comm., 2000).

MATERIALS AND METHODS

The 100 faceted round and oval häüynes that were submitted to our laboratory for examination (figure 3) ranged from 0.095 to 0.173 ct (and from 3.11–3.16 × 2.02 mm to 3.68–3.74 × 2.56 mm for the round stones; 3.50 × 2.81 × 1.66 mm to 4.15 × 3.92 × 2.20 mm for the ovals). Additional häüynes from the Eifel district were supplied by the companies Gebrüder Bank and W. Constantin Wild, both of Idar-Oberstein, Germany: approximately 80 crystal fragments between 0.01 and 0.15 ct, 15 small faceted stones (0.02–0.10 ct), and six larger faceted stones (0.15–0.83 ct). A 1.5 mm (diameter) crystal in pumice matrix (again, see figure 2) and a faceted häüyne of 0.15 ct from the SSEF collection completed the samples. All häüyne in this study was mined in the Eifel district (C. Wild and G. Bank, pers. comm., 2000).

We measured the refractive indices of 10 samples with an Eickhorst GemLED refractometer with an LED monochromatic light source (equivalent to

NaD light, $\lambda = 589$ nm). Specific gravity was determined hydrostatically for 31 faceted samples. For all samples, we observed reaction to long-wave (365 nm) and short-wave (254 nm) ultraviolet radiation in a darkened room. Internal features of all samples were examined using a standard gemological microscope in conjunction with brightfield, darkfield, and oblique fiber-optic illumination. Photomicrographs were taken with a Wild M8/MPS55 stereozoom microscope.

We recorded visible-range spectra for three faceted samples of variable color intensity using a Hitachi U4001 spectrophotometer in the 290–800 nm range. We recorded infrared spectra for three stones in the range 500–6000 cm^{-1} with a Phillips PU 9800 Fourier transform infrared (FTIR) spectrometer to check for any treatment. Qualitative chemical analyses by energy dispersive X-ray fluorescence (EDXRF) of four faceted samples were performed using a Tracor Spectrace 5000 instrument, optimized for the detection of medium-weight (Ca-Ga) elements. We recorded Raman spectra on four samples (three faceted and one crystal), plus the

TABLE 1. Properties of häüyne from the Eifel district, Germany.

Ideal formula	$(\text{Na,Ca})_{4-8}\text{Al}_6\text{Si}_6(\text{O,S})_{24}(\text{SO}_4,\text{Cl})_{1-2}$
Color	Light blue to dark blue
Clarity	Transparent to translucent
Refractive index	1.498–1.507
Birefringence	None, sometimes slight anomalous birefringence
Optical character	Isotropic
Specific gravity	2.46–2.48
Hardness	5.5–6 (reported) ^a
UV fluorescence	
Long-wave (365 nm)	Inert to bright orange
Short-wave (254 nm)	Inert to slightly red
Inclusions	Apatite, augite, unidentified small needles and particles, unidentified dark opaque hexagonal mineral, negative crystals, partially healed fissures, and fissures treated with paraffin wax
UV-Vis absorption	Spectroscope: Broad weak band in the yellow range Spectrophotometer: Broad band at 600 nm, small band at 380 nm, absorption edge at 300 nm
FTIR spectral features	Major absorption bands at 3593 and 3697 cm^{-1}
Raman spectral features	Major peaks at 440, 543, 988, 1089, and 1635 cm^{-1}

^aFrom Arem (1987).



Figure 4. The h a y ne samples examined ranged from a deep “sapphire” blue to a light “apatite” blue. These faceted stones weigh 0.2–0.8 ct. Photo by Lore Kiefert.

inclusions in several stones, with a Renishaw Raman System 1000 spectrometer equipped with a CCD Peltier detector and an argon ion laser (514 nm) with a power of 25 mW.

RESULTS AND DISCUSSION

The properties determined for these samples are summarized in table 1 and discussed below.

Physical Properties. The samples ranged from a light blue similar to that of Para iba tourmaline or apatite, to a dark blue similar to that described for fine Kashmir sapphire (figure 4). Most of the samples, however, were an evenly distributed medium blue (see, e.g., figure 3 and the third and fourth stones from the left in figure 4). We did not observe color zoning in any of our samples.

The samples were very consistent in specific gravity (2.46–2.48), which corresponds to the range of 2.40–2.50 reported in the literature (Arem, 1987; Deer et al., 1992). Refractive index results, between 1.498 and 1.507, also were consistent with the range cited in the literature (1.490–1.508; Bank, 1977, 1978–1979; Arem, 1987; Deer et al., 1992).

Approximately one-third of the 100 samples submitted to our laboratory (and a smaller proportion of the other samples) showed orange fluorescence to long-wave UV radiation; the remaining samples were inert. When fluorescence is observed, it is considered characteristic of h a y ne from the Eifel district (Webster, 1994). The inconsistency in fluorescence reaction that we observed was also mentioned by Bank (1977). Most of the h a y nes showed a very weak reddish fluorescence to short-wave UV.

Microscopic Properties. In approximately half of the samples, we observed short needles and fine dust-like particles arranged in lines, similar to rutile needles or partially dissolved rutile in sapphires (figure 5).

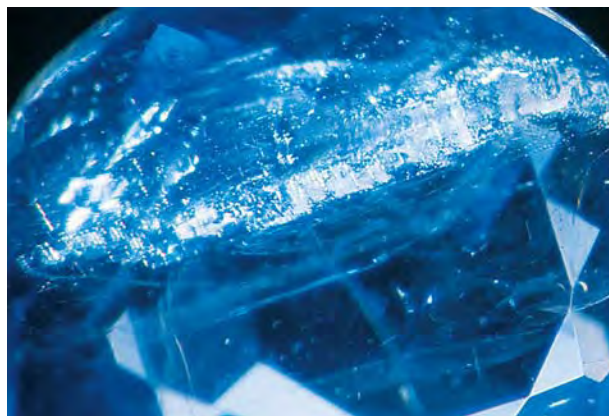


Figure 5. Short needle-like inclusions and fine dust-like particles were observed in about half the h a y nes examined. The needles were generally oriented parallel to growth planes. Photomicrograph by H. A. H anni; magnified 30 .

Elongate, transparent, prismatic crystals (figure 6), identified as apatite by Raman microspectrometry, were seen in two samples. In contrast to our findings, W orner and Schmincke (1984) stated that apatite never occurs in h a y ne from the Eifel district. Another mineral, which was exposed at the surface of one of the samples shown in figure 4, was identified as augite, which is also a common xenocryst in the Eifel district phonolite (W orner and Schmincke, 1984). A dark opaque hexagonal crystal exposed at

Figure 6. Elongate prismatic crystals, identified as apatite by Raman analysis, were seen in two of the h a y ne samples. Note also the piece of host rock evident on the surface of this sample, shown here at the upper left. Photomicrograph by H. A. H anni; magnified 30 .





Figure 7. This hexagonal opaque crystal exposed at the surface of a polished haüyne was not identifiable with Raman analysis, possibly because it was metallic or too decomposed. Photomicrograph by H. A. Hänni; magnified 50 \times .

the surface of another stone could not be identified (figure 7). This inclusion may be metallic or too decomposed to give a useful Raman signal.

Negative crystals were observed in a third of the stones; some were well formed (figure 8), and some were rounded with a frosted surface (figure 9). They were frequently surrounded by healing fissures that resembled those seen around negative crystals in sapphires from Sri Lanka. In some cases, however, the partially healed fissures had an appearance similar to that of glass fillings in rubies (figure 10). Glass inclusions outlining growth zones in haüyne from the Eifel district were described by Harms and

Figure 9. This rounded negative crystal has a frosted surface and, like the smaller negative crystal on the lower right, a rosette-like healing fissure. Photomicrograph by H. A. Hänni; magnified 40 \times .



Figure 8. Commonly seen in the haüynes examined were well-formed negative crystals with rosette-like healing fissures (right, within the bright spot) or partially healed fissures with interference colors and a worm-like "fingerprint" structure (on the left). Photomicrograph by H. A. Hänni; magnified 40 \times .

Schmincke (2000). Five of the samples examined contained remnants of the host rock (see, e.g., figure 6). Where the rough surface of the original crystal face was still visible, corrosion was evident.

Fissures filled with an oily to waxy substance were common in many of the 100 haüynes that were originally submitted to the laboratory for identification. This substance was identified as paraffin wax by FTIR and Raman analyses (see below). Because haüyne has a low refractive index, which is close to that of paraffin wax or oil, the filled frac-

Figure 10. In a number of the haüynes, the partially healed fissures resembled the glass fillings seen in some rubies. Photomicrograph by H. A. Hänni; magnified 30 \leftrightarrow .



tures sometimes showed orange to pinkish flashes; these resembled the orange flashes observed in emeralds with resin-filled fractures (Kiefert et al., 1999; Johnson et al., 1999).

Spectral Features. UV-Vis spectrometry showed a major absorption band centered at approximately 600 nm, maximum transmission at 476 nm (figure 11), a small absorption band centered at 380 nm, and an absorption edge at 300 nm in the three stones tested. This is in agreement with the absorption spectrum reported for haüyne by Henn and Bank (1990). Note in figure 11 that the absorption band at 600 nm increases in intensity with increasing depth of color, while the other spectroscopic features remain the same.

An absorption band at 600 nm, measured with electron paramagnetic resonance (EPR) spectroscopy, also has been described for sodalite and lazurite. This feature was ascribed to a color center associated with S_3^- (Marfunin, 1979), which has been attributed to radiation damage (Vassilikou-Dova and Lehmann, 1990) and may be responsible for the blue color. Henn and Bank (1990) relate the orange fluorescence of this mineral group to the presence of S_2^- , which causes the 380 nm absorption band. Note that only a weak, broad absorption band in the yellow region is visible with a handheld type of spectroscope.

The FTIR spectra in the region between 4000 and 2400 cm^{-1} of two stones in which magnification had revealed evidence of a waxy filler showed two major groups of peaks (figure 12): One is typical for haüyne and lies between 3000 and 3800 cm^{-1} (comparison with a "clean" sample); the other group of peaks (between 2840 and 2960 cm^{-1}) is characteristic of paraffin wax. This latter group is attributable to the artificial filling of fissures with wax.

Chemical Properties. As noted above, the ideal chemical formula of haüyne is $(\text{Na,Ca})_{4-8}\text{Al}_6\text{Si}_6(\text{O,S})_{24}(\text{SO}_4,\text{Cl})_{1-2}$. Qualitative EDXRF chemical analysis of four stones showed, besides the detectable elements given in this formula (i.e., calcium, silicon, aluminum, and sulfur), small but significant amounts of potassium (K) and iron (Fe), as illustrated in figure 13.

According to Wörner and Schmincke (1984), it is difficult to perform microprobe analysis of haüyne because of the large sodium content, the decomposition of the haüyne under the electron beam, and the problem in assigning SO_3 (as analyzed) to SO_3 and S. Therefore, those authors considered their microprobe

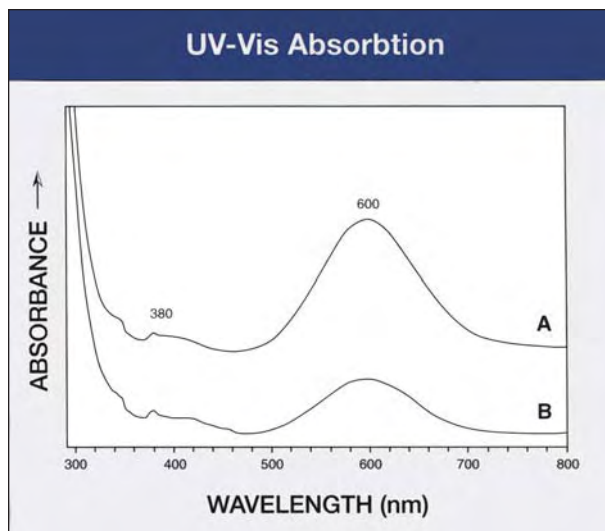
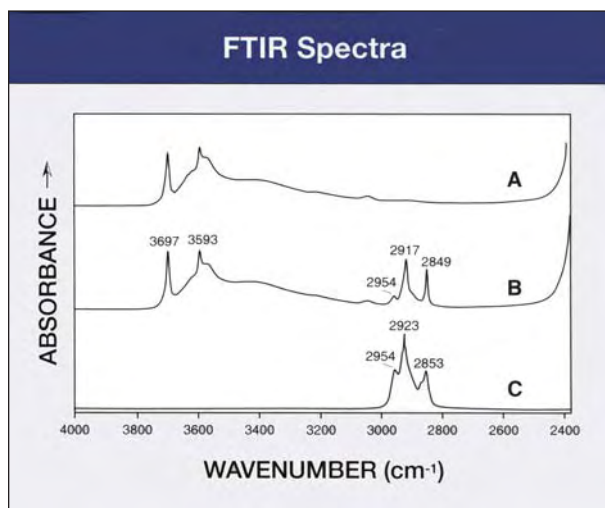


Figure 11. Note the characteristic absorption bands at 380 and 600 nm—and the transmission maximum at 476 nm—in these UV-Vis absorption spectra of a medium blue (A) and a light blue (B) haüyne.

analyses of seven samples to be qualitative at best. The elements measured by our qualitative EDXRF analysis (including the significant amounts of K and Fe) are consistent with the chemical data provided by these and other researchers for haüyne from Laacher See and from Italy (see also Deer et al., 1963; Xu and Veblen, 1995; Sapozhnikov et al., 1997).

Figure 12. Shown here are the FTIR spectra measured between 4000 and 2400 cm^{-1} of (A) haüyne, (B) wax-treated haüyne, and (C) paraffin wax. The peaks at 3697 and 3593 cm^{-1} are characteristic for haüyne.



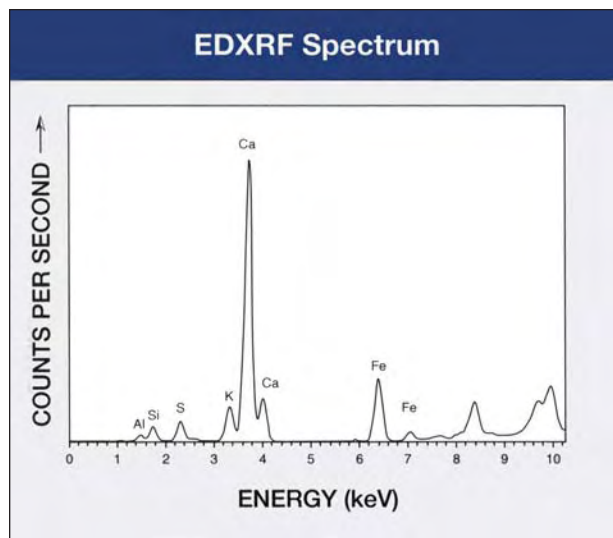
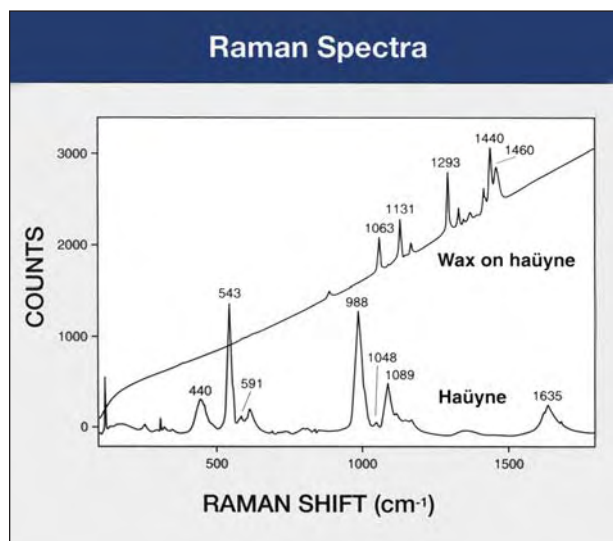


Figure 13. In addition to calcium, silicon, aluminum, and sulfur, EDXRF analyses of the haüyne samples revealed significant potassium and iron. The features above 8 keV are instrumental artifacts related to the tungsten anode.

Raman Spectrometry. Raman analysis was performed on the haüyne itself and on all inclusions that were large enough to analyze. The Raman spectra of the four haüyne samples tested (see, e.g., figure 14) are in agreement with the results given by Maestrati (1989), but they differ significantly

Figure 14. The upper Raman spectrum is of paraffin wax found on the surface of a faceted haüyne, whereas the lower spectrum is of a haüyne reference sample.



from those provided in the Renishaw Raman database.

Raman analysis identified both apatite and augite as inclusions in some of the samples. In addition, in one of the several samples that revealed fissure fillings with magnification, the filler was exposed on the surface of the stone, so we were able to get a particularly good Raman signal. The pattern matched that of paraffin wax (figure 14), which confirmed the results recorded with the FTIR spectrometer (again, see figure 12).

Separation from Possible Imitations. The bright blue color of haüyne might be duplicated by cobalt glass, blue cubic zirconia, or cobalt spinel. Lazurite and blue apatite also may resemble haüyne. Careful determination of the optic character (haüyne is cubic), R.I., S.G., and absorption spectrum will, however, enable a firm identification of haüyne. This mineral is clearly distinguishable from other minerals of the sodalite group by its Raman spectrum.

CONCLUSIONS

Although usually considered a collector's stone because of its rarity, haüyne may be found in expensive jewelry, as was the case with several of the stones tested for this article (again, see figure 1). The use of haüyne in a brooch is appropriate given its low hardness.

The geology and petrology of the deposit at Laacher See (Eifel district) in Germany have been well studied. It is interesting to note that similar volcanic deposits containing haüyne are rare, and we know of no other deposits of the blue gem-quality material. Although the German source has been productive for a long time—haüyne was first described from Germany in 1807 (Clark, 1993)—an accumulation of 100 faceted stones is surprising due to the relative scarcity of the material.

Acknowledgments: The authors thank P. Giese for taking FTIR, EDXRF, and UV-Vis spectra; Dr. M. Krzemnicki and J.-P. Chalain for their critical discussions; the company Della Valle of Geneva for supplying the original samples and the photo of the butterfly brooch; and Dr. J. Arnoth and Dr. K. Schmetzer for helping locate mineralogical literature about haüyne from the Eifel district. The companies Gebrüder Bank and W. Constantin Wild, both of Idar-Oberstein, Germany, kindly supplied a large number of additional samples.

REFERENCES

- Arem J.E. (1987) *Color Encyclopedia of Gemstones*, 2nd ed. Van Nostrand Reinhold, New York, 248 pp.
- Bank H. (1977) Durchsichtiger, schleifwürdiger Hauyn aus der Eifel. *Zeitschrift der Deutschen Gemmologischen Gesellschaft*, Vol. 26, No. 4, p. 207.
- Bank H. (1978–1979) Gemological notes: Blue gem hauyne. *Gems & Gemology*, Vol. 16, No. 4, p. 123.
- Clark A.M. (1993) *Hey's Mineral Index*, 3rd ed. Natural History Museum Publications, Chapman & Hall, London.
- Deer W.A., Howie R.A., Zussman J. (1963) *Rock-Forming Minerals, Vol. 4: Framework Silicates*. Longman, London, 435 pp.
- Deer W.A., Howie R.A., Zussman J. (1992) *An Introduction to the Rock-Forming Minerals*, 2nd ed. Longman Scientific & Technical, Essex, England, 696 pp.
- Fisher K., Bürger H. (1976) Hauyn. *Lapis*, Vol. 1, No. 2, pp. 30–32.
- Harms E., Schmincke H.-U. (2000) Volatile composition of the phonolitic Laacher See magma (12,900 yr BP): Implications for syn-eruptive degassing of S, F, Cl and H₂O. *Contributions to Mineralogy and Petrology*, Vol. 138, pp. 84–98.
- Henn U., Bank H. (1990) Über die Farbe der Sodalith-Mineraie: Sodalith, Lasurit (Lapis lazuli) und Hauyn. *Zeitschrift der Deutschen Gemmologischen Gesellschaft*, Vol. 39, No. 2/3, pp. 159–163.
- Johnson M.L., Elen S., Muhlmeister S. (1999) On the identification of various emerald filling substances. *Gems & Gemology*, Vol. 35, No. 2, pp. 82–107.
- Kiefert L., Hänni H.A., Chalain J.P., Weber W. (1999) Identification of filler substances in emeralds by infrared and Raman spectroscopy. *Journal of Gemmology*, Vol. 26, No. 8, pp. 501–520.
- Linde C. (1998) Hauyn-Kristalle von Teneriffa. *Lapis*, Vol. 23, No. 1, p. 22.
- Maestrati R. (1989) *Contribution à l'édification du catalogue Raman des gemmes*. Unpublished diploma thesis, Diplôme d'Université de Gemmologie, Université de Nantes, France.
- Mandarino J.A. (1999) *Fleischer's Glossary of Mineral Species 1999*. The Mineralogical Record Inc., Tucson, AZ.
- Marfunin A.S. (1979) *Spectroscopy, Luminescence and Radiation Centers in Minerals*. Springer-Verlag, Berlin, p. 282.
- Matthes S. (1983) *Mineralogie. Eine Einführung in die spezielle Mineralogie, Petrologie und Lagerstättenkunde*. Springer-Verlag, Berlin, p. 183.
- Mertens R. (1984) Hauyn, ein seltener Edelstein. *Zeitschrift der Deutschen Gemmologischen Gesellschaft*, Vol. 33, No. 1/2, pp. 65–67.
- Sapozhnikov A.N., Ivanov V.G., Piskunova L.F., Vasil'ev E.K. (1997) X-ray powder diffraction data of hauyne with incommensurate modulated structure from volcanic rocks of Laacher Lake, Germany. *Powder Diffraction*, Vol. 12, No. 1, pp. 3–6.
- Schmincke H.-U. (2000) *Vulkanismus*. Wissenschaftliche Buchgesellschaft, Darmstadt, Germany, 264 pp.
- Vassilikou-Dova A.B., Lehmann G. (1990) Paramagnetic defects in the mineral hauyne. *Crystal Research and Technology*, Vol. 25, No. 5, pp. 525–529.
- Webster R. (1994) *Gems, Their Sources, Descriptions and Identification*, 5th ed. Rev. by P. G. Read, Butterworth-Heinemann Ltd., Oxford, England, p. 342.
- Wörner G., Schmincke H.-U. (1984) Mineralogical and chemical zonation of the Laacher See tephra sequence (East Eifel, W. Germany). *Journal of Petrology*, Vol. 25, Part 4, pp. 805–835.
- Xu H., Veblen D.R. (1995) Transmission electron microscopy study of anisotropic and isotropic hauyne. *American Mineralogist*, Vol. 80, No. 1/2, pp. 87–93.

UP TO A
\$22.00
VALUE!

FREE file case!

(while supplies last)

With any three years of back issues



Round out your reference library
with a leather-like file case embossed with
the **GEMS & GEMOLOGY** logo!

ORDER TODAY!

Call Toll Free 800-421-7250 ext. 7142 or 760-603-4000, ext. 7142

(Please see the ad in this issue for a list of topics covered in specific back issues,
and please mention this ad when ordering)

There's nothing like having
what you need, when you need
it. That's why no gemological
reference library is complete
without GEMS & GEMOLOGY. In
addition to in-depth research
and gem locality articles, every
beautifully illustrated issue fea-
tures unique sections like Lab
Notes and Gem News. Taken
together, they provide a depth
and breadth of gemological
information you simply cannot
find anywhere else. Take advan-
tage of this special offer and
complete your back issues today!

GEMS & GEMOLOGY

A wealth of information
at your fingertips.

LAB NOTES

Editors

Thomas Moses, Ilene Reinitz, and
Shane F. McClure
GIA Gem Trade Laboratory

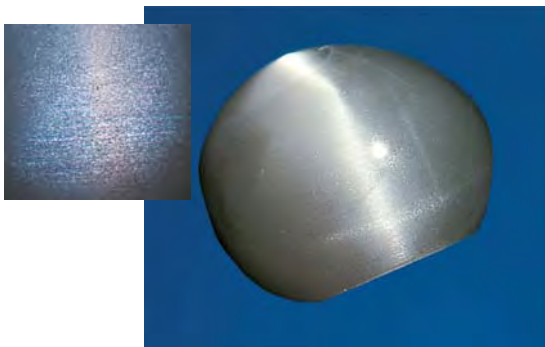
Contributing Editors

G. Robert Crowningshield
GIA Gem Trade Laboratory, East Coast
Karin Hurwit, Mary L. Johnson,
and Cheryl Y. Wentzell
GIA Gem Trade Laboratory, West Coast

An Unusual CAT'S-EYE CHRYSOBERYL

When the West Coast laboratory recently received a translucent gray chatoyant cabochon for identification from K & K International in Falls Church, Virginia (figure 1), the last thing we thought it could be was chrysoberyl, even though that was how it was represented by our client. Nothing about its appearance suggested chrysoberyl, not even the appearance of the inclusions. Gemological testing revealed a spot refractive index of 1.75, a specific gravity of 3.69 (measured hydrostatically), and no visible absorption spectrum or fluorescence. Although these properties could indicate chrysoberyl, they were

Figure 1. Although chatoyancy is common in chrysoberyl, this 7.29 ct cabochon is the first gray cat's-eye chrysoberyl seen in the laboratory. The color in this stone appears to be caused by dense concentrations of gray platelets, which are also the cause of the chatoyancy (inset, magnified 30 \times).



also consistent with several other gems. Nevertheless, the spectrum obtained with the Raman microspectrometer was a perfect match to our reference for chrysoberyl.

This is the first gray cat's-eye chrysoberyl we have seen in the laboratory. Microscopic examination of the 7.29 ct stone indicated that the inclusions were the probable cause of the gray color; they looked gray in transmitted light, while the host material appeared near-colorless. Chrysoberyl is seldom colorless, especially in gem quality. Instead of the long, fine needles or "silk" that are normally present in cat's-eye chrysoberyl, these gray inclusions formed a dense cloud of tiny, oriented reflective platelets. Light reflection from these platelets caused the chatoyancy. Even more unusual was the presence of a weak star oriented off-center toward one end of the stone (not completely visible in the photo). We have seen only a few star chrysoberyls in the lab. The last one we reported on was greenish brown and also had the star oriented off-center (Summer 1989 Lab Notes, p. 102).

SFM

DIAMOND

Blue and Pink, HPHT Annealed

As part of our ongoing research for means to identify HPHT-annealed diamonds, the East Coast laboratory recently analyzed 11 pink and four blue diamonds that had been subjected to this process (see, e.g., figure 2). These diamonds were submitted to the laboratory from Bellataire Diamonds, which is responsible for

marketing GE POL diamonds in the United States.

The diamonds weighed 0.75 to 14.93 ct. The pink diamonds showed a wide range of color saturation, from the equivalent of Faint to Fancy Deep; the blue diamonds ranged from the equivalent of Very Light to Fancy Intense. The clarity grades ranged from IF to VS₂ and from VVS₁ to VVS₂ for the pink and blue diamonds, respectively. The pink diamonds were type IIa, based on their mid-infrared spectra and their transparency to short-wave UV radiation. The blue diamonds were type IIb; that is, they showed both electrical semi-conductivity and characteristic boron features in the mid-infrared. According to Chuck Meyer, managing director of Bellataire Diamonds, the pink and blue diamonds represent a very small fraction of the overall GE POL production. Because of the rarity of the starting material that can generate these colors, he does not expect them to be readily available commercial items.

Gemologically, these HPHT-annealed diamonds show properties that are commonly observed in natural-color type IIa pink and type IIb blue diamonds, particularly the details of color zoning, and reactions to long-wave and short-wave UV. We would expect the same types of alteration of inclusions to occur as were previously reported for HPHT-annealed

Editor's note: The initials at the end of each item identify the editor(s) or contributing editor(s) who provided that item.

*Gems & Gemology, Vol. 36, No. 3, pp. 254-259
©2000 Gemological Institute of America*



Figure 2. The laboratory recently examined several blue and pink diamonds that had been color enhanced by an HPHT process similar to that used to decolorize GE POL diamonds. These diamonds range from 0.75 to 3.59 ct.

near-colorless type IIa diamonds (T. Moses et al., "Observations on GE-processed diamonds," Fall 1999 *Gems & Gemology*, pp. 14–22), but these 15 diamonds did not show any diagnostic inclusions. Using a Raman unit, we obtained photoluminescence (PL) spectra on these HPHT-annealed pink and blue diamonds, which we compared to PL spectra for more than 100 natural-color pink and blue diamonds. It appears that some of the identification criteria proposed by D. Fisher and R. A. Spits ("Spectroscopic evidence of GE POL HPHT-treated natural type IIa diamonds," Spring 2000 *Gems & Gemology*, pp. 42–49) to differentiate D-to-Z range GE POL diamonds from natural type IIa diamonds may be applicable in the identification of the HPHT-annealed pink diamonds. We are using this spectroscopic method and other techniques to investigate possible identification criteria for both the pink and blue diamonds. *Matt Hall and TM*

With Flower-like Inclusions

Two rather different diamonds seen in the East Coast laboratory showed similarly shaped inclusion patterns reminiscent of flowers or stars. One, a 6.23 ct near-colorless partly rounded octahedron with a translucent, etched surface (and sparse brown radiation

stains) revealed the gray clouds shown in figure 3 (left) through two natural cleavage surfaces. The other, a 0.71 ct Fancy Deep brownish orange round brilliant, displayed its inclusions through the table (figure 3, right). The inclusion patterns in both diamonds showed six-fold symmetry, with at least two "rings" around the center part, one distinctly hexagonal.

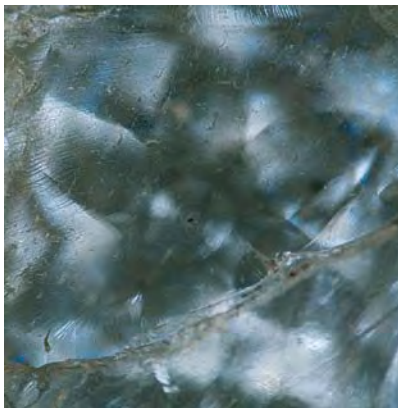
In the 6.23 ct diamond, wide, petal-like gray clouds radiated from the center part of the inclusions; these clouds fluoresced yellow to

both long- and short-wave UV. The sample showed a strong line at 415 nm and a weak one at 563 nm in a desk-model spectroscope, and strong peaks in the mid-infrared at 3105, 3235, 4165, and 4494 cm^{-1} , which are related to hydrogen. These gemological properties and spectroscopic results were first described in 1993 (E. Fritsch and K. Scarratt, "Gemological properties of type Ia diamonds with an unusually high hydrogen content," *Journal of Gemmology*, Vol. 23, No. 8, pp. 451–460).

When the 0.71 ct round brilliant was viewed over diffused light, the saturated bodycolor showed some zoning, with concentrations of darker color around the edges of the star-like inclusions. The clouds themselves appeared to consist of pinpoints, and were rather narrow compared to the clouds in the other diamond. No part of this stone fluoresced to either wavelength of UV. The UV-visible spectrum showed rising absorption from about 500 nm toward the blue region, and the mid-infrared spectrum showed mostly type Ib with a small IaA component, and no absorptions due to hydrogen.

As discussed in a Spring 1999 Lab Note (pp. 42–43), such clouds in diamonds are actually phantoms, in which internal crystal planes of the diamond became outlined by minute

Figure 3. The gray "flower" in this 6.23 ct rough diamond (left, magnified 20 \times) is caused by concentrations of hydrogen. Concentrations of pinpoints produce a "star" shape in the 0.71 ct Fancy Deep brownish orange round brilliant on the right. In both cases, the morphology of the growing diamond crystal controlled the shape of the inclusions.



inclusions trapped during growth. Don't let the hexagonal appearance of the clouds fool you. As suggested in the earlier Lab Note, the clouds that form such a six-rayed star or flower still follow diamond's cubic crystal system: The inclusions are most likely trapped along the edges of a hex-octahedron, a common internal growth stage for diamond.

Wendi Mayerson and IR

An Historical Report

In the archives at GIA's Richard T. Liddicoat Library and Information Center, we found an early lab report (no. 294) that was personally signed by Robert Shipley Jr. on March 13, 1937. The item being tested was noted as a "green transparent brilliant in ladies [sic] 20 irid 80 plat ring." (The fee charged for determining the origin of color was \$10.) The comments on the report, shown in figure 4, note that the hardness is greater than 9 and was determined by using hardness points. The report also notes that the material was "Isotropic; shows strain spots of color localized beneath facet surfaces; breaks through surfaces at each spot." The item was set on an unexposed piece of AGFA film that, when developed, showed evidence of radiation, which resulted in the concluding remark: "Diamond: All tests known to this laboratory indicate color is due to alteration as result of exposure to bombardment by alpha particles, perhaps of radium."

Robert Shipley Sr. began providing laboratory services in Los Angeles under the auspices of the newly formed Gemological Institute of America in 1931. His son, Robert Shipley Jr., was the developer of a number of gemological instruments as well as a key staff member.

Al Gilbertson

SYNTHETIC MOISSANITE: A Black Diamond Substitute

Several black round brilliants, ranging from 0.50 to over 20 ct were recently submitted to the East Coast laboratory

LABORATORY REPORT # 294

SENT BY _____

NATURE OF SPE Green transparent brilliant in ladies 20 irid 80 plat ring

TESTS MADE:

Refractive Index _____ by _____

Specific Gravity 3.52 Wt. in H₂O _____ by _____

Pleochroism _____ by _____

Optic Character None by _____

Inclusions Isotropic; shows strain spots _____

Hardness greater than 9; breaks through surfaces at each spot by _____

Additional Tests 9 _____ by _____

THE RESULTS OF THE ABOVE TESTS INDICATE THE SPECIMEN TO BE:

REMARKS: Diamond
All tests known to this laboratory indicate color is due to alteration as result of exposure to bombardment by alpha particles, perhaps of radium.

RECEIVED _____ TESTS BY _____ RETURNED _____ FEE _____

KEY: D. - Dichroscope; D.B. - Diamond Balance; E. - Endoscope; F. - Fluorescence; H.L. - Heavy Liquid; H.Pl. - Hardness Plates; H.Po. - Hardness Points; J.B. - Jolly Balance; L. - 10X Loupe; M. - Microscope; P. - Pocket Polaroscope; P.I. - Pearl Illuminator; R. - Refractometer; S. - Spectroscope.

Figure 4. This 1937 GIA laboratory report for a treated-color green diamond was signed by Robert Shipley Jr.

by a client who acquired them as synthetic black diamond, allegedly of Russian origin (see, e.g., figure 5). Examination with a fiber-optic light showed that the material was actually very dark bluish green, which is typical of diamonds that have been irradiated to "black." However, microscopic examination revealed strong doubling of numerous stringers and needles (figure 6), which proved that the stones were doubly refractive. These inclusions were reminiscent of those reported in near-colorless synthetic moissanite (see, e.g., K. Nassau et al., "Synthetic moissanite: A new diamond substitute," Winter 1997 *Gems & Gemology*, pp. 260-275). The specific gravity was measured hydrostatically as 3.20, which confirmed the identity

of these pieces as synthetic moissanite. Diamond imitations are frequently subjected to hardness testing in the trade, and one of these samples had several deep, eye-visible scratches on the table.

With the increased popularity of black diamonds in jewelry, this material could pose an identification challenge if small sizes were mounted. Although its homogeneous appearance—even under strong illumination, such as that from a fiber-optic light—is very different from that of natural-color black diamond, this would not rule out natural diamond treated by laboratory irradiation. The stringers and needles seemed to have some color associated with them; their appearance suggested that they



Figure 5. These round brilliants (the unmounted one weighs 10.30 ct) were represented as synthetic black diamond, but they were identified as very dark bluish green synthetic moissanite.

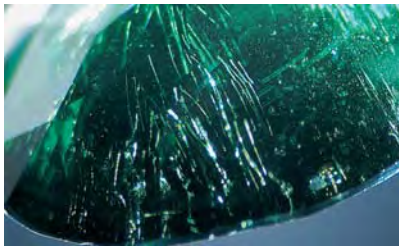


Figure 6. A strong light source showed this synthetic moissanite to be dark bluish green. With magnification, characteristic stringers and needles were visible as double images, proving the anisotropic nature of the material. Magnified 12 \times .

may have resulted from incomplete crystallization. Such inclusions, and the anisotropic nature of the material that they reveal, readily separate synthetic moissanite from diamond.

SFM and TM

RUBY

An Investigation of Fracture Fillers in Mong Hsu Rubies

As a common practice, the heat treatment of rubies and sapphires is at least several decades old. To improve their color and clarity, parcels of gems are heated in oxidizing or reducing environments to temperatures as high as 1,300°C to 1,900°C (T. Themelis, 1992, *The Heat Treatment of Ruby and Sapphire*, Gemlab Inc., Houston TX). Typically, the rough gems are covered with a "firecoat" material such as borax. (With regard to treatment in Thailand, Themelis [*op. cit.*, pp. 109–110] mentioned borax [hydrous sodium borate] as the most common additive to corundum during the heating process, although boric acid, oxidizing and reducing agents, ashes, topsoil or clay, buffalo dung, and banana leaves were also noted; "additive secrets" were carefully guarded by the treaters.) Using such a "firecoat" leads to a notable effect: Fractures and cavities in the heat-treated corundum become filled with a foreign substance.

Such material has been noted

particularly in Mong Hsu rubies (A. Peretti et al., "Rubies from Mong Hsu," Spring 1995 *Gems & Gemology*, pp. 2–26; H. A. Hänni, "Short notes on some gemstone treatments," *Journal of the Gemmological Association of Hong Kong*, Vol. 20, pp. 44–52), and several hypotheses have been advanced as to how this material forms in the fractures. Two gemologists with substantial worldwide ruby-buying experience recently brought us some typical commercial Mong Hsu material from the market in Bangkok to learn more about these fracture-filling materials. We examined five pieces of heated rough, two of unheated rough, and two heated faceted rubies with a scanning electron microscope and an electron microprobe, to explore the composition and textures of the material(s) produced in the fractures.

The nature of the substance in fractures in heat-treated ruby is not well understood. It has been referred to both as a glass (e.g., K. Scarratt et al., "Glass filling in sapphire," *Journal of Gemmology*, Vol. 20, No. 4, 1986, pp. 203–207) and as a flux (e.g., Peretti *op. cit.*; J. L. Emmett, "Fluxes and the heat treatment of ruby and sapphire," Fall 1999 *Gems & Gemology*, pp. 90–92), but these two terms are neither synonyms nor antonyms. *Glass* refers to the state of the material (a

noncrystalline solid); *flux* refers to the ability of one substance to lower the melting point of another substance with which it is mixed.

We collected both back-scattered electron (BSE) images—which show the physical arrangement of the host ruby, the fracture, and the filling material—and EDX chemical information (assisted by Dr. Chi Ma, Caltech, Pasadena). We also analyzed two faceted samples by electron microprobe, to verify the EDX chemical analyses with the more accurate WDX technique and check for the presence of boron with a light-element detector. The presence of boron would be consistent with the reported use of borax in the heat-treatment process.

One unheated sample showed rough surfaces, with stepped crystal edges visible at high magnification. The freshly broken surface of one heated sample (figure 7, left) looked conchoidal under SEM examination at low magnification (figure 7, center); however, with higher magnification the fractured area was seen to consist of sharp-edged planes (figure 7, right). In contrast, exposed surfaces of these heat-treated rubies looked smooth-edged with magnification. This difference in texture shows that the ruby "molecules" have been rearranged at the gem's surface, similar to the etching and redeposition that gem crystals can undergo in pegmatites and hydrothermal environments.

Figure 8 (left) shows two ruby crystals that had been stuck together during heat treatment; in the region where the two rubies are joined together, the surfaces curve smoothly from one to the other (figure 8, center). A fine fringe of 40-micron-long sub-parallel ruby crystallites has grown on the smaller crystal in this sample (figure 8, right), which indicates redistribution of the corundum with the "firecoat" acting as a flux. We believe that these crystallites represent new growth for several reasons: They are too small and delicate to have survived mining in their undamaged state, and they are not quite parallel to one another, which indicates that they

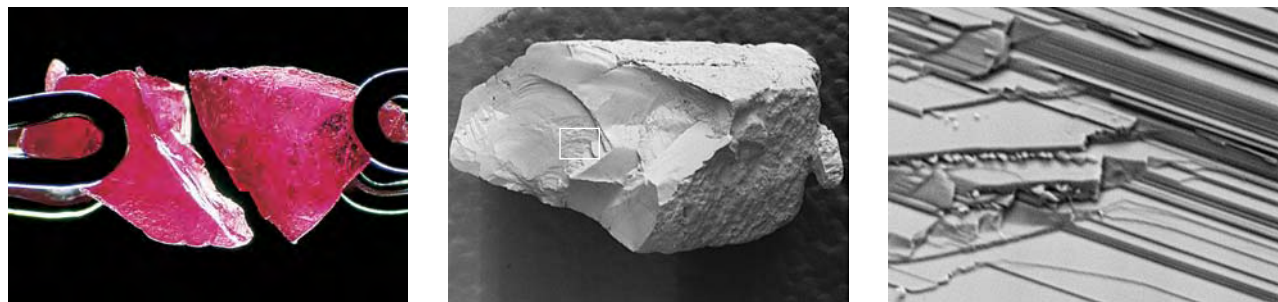


Figure 7. This 0.34 ct heat-treated Mong Hsu ruby was broken in two (left) and the fracture examined by SEM. At 19× magnification (center), the backscattered-electron SEM image showed conchoidal fracturing along the break. At higher magnification (1500×, right), sharp layers are seen along the broken surface.

probably grew fast rather than in equilibrium with their host crystal.

Another sample of heated rough showed that the “firecoat” material may form secondary veinlets branching off a fracture (figure 9) along parallel (parting) planes in the ruby. Where it reached the surface, the vein material appeared brighter in BSE images than the ruby around it, indicating that it had a higher mean atomic weight than the ruby. This brightness was relatively uniform (in all the samples where such material was observed), implying that the material was a homogeneous glass.

In reflected light, one faceted ruby showed broad fissures filled with foreign material (figure 10). These were easily seen with the SEM, as they appeared both brighter in the BSE images and softer than the surrounding corundum (deeper polishing lines are visible in figure 10). Note that the

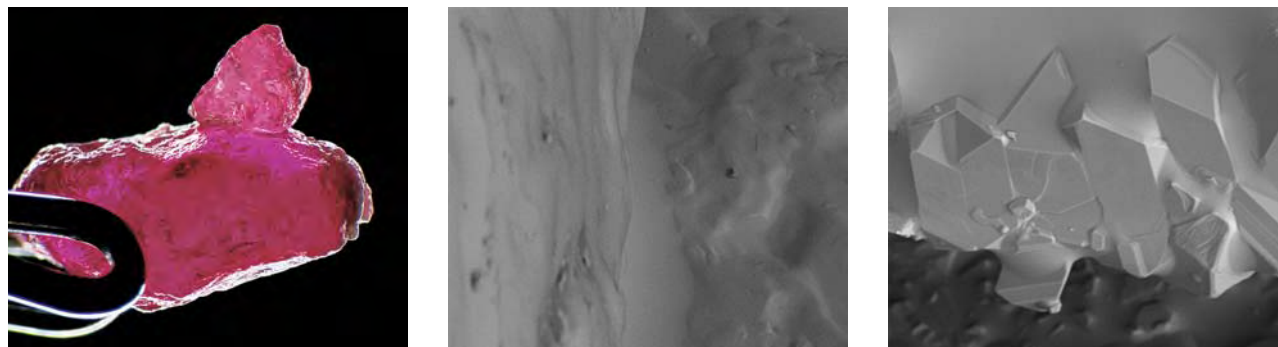
fissure in this ruby was not completely filled by the glass-like substance; a crack was still visible alongside the “glass.” A fissure in the second faceted ruby was quite thin and looked like a line of disconnected dots, even at high magnification, which prevented chemical analysis of fracture material in this sample.

SEM-EDX analysis revealed that the “glass” vein in one rough heated Mong Hsu ruby contained Na, Mg, Al, Si, P, Ca, and Ti, with phosphorus the largest peak after Al. Glass in a fissure in one of our faceted rubies contained the same elements, although with more Si than P. Electron microprobe analyses of five points in the filler in this sample revealed a relatively large amount of boron, up to 4.5 wt. % B_2O_3 , as well as P, Si, Al, and other oxides. This glass has an average composition of

$Na_{0.1}Mg_{0.2}B_{0.1}Al_{0.6}Si_{0.6}P_{0.2}O_3$. In 1995, Juan Cozar (“ICA laboratory alert update no. 56, 24 August 1995: Rubies with fissures and cavities filled with aluminum and sodium phosphate glass,” *South African Gemmologist*, Vol. 9, No. 3, pp. 16–17) provided SEM-EDX analyses of glass in heat-treated rubies that also contained major P, Al, Na, Si, and Ti, as well as minor Ca and Fe.

The “firecoat” used in the heat treatment is strongly indicated in the formation of this filler, as the commonly occurring mineral inclusions in ruby do not contain sufficient boron to produce this composition. However, neither borax nor inclusions of apatite can account for the large amount of phosphorus found here and by Cozar; this chemistry suggests that one or more additional components were added to the “firecoat.” In addition to

Figure 8. These two heated rubies (0.41 ct total) are attached to each other despite different crystallographic orientations (left—transmitted and reflected light; magnified 15×.) Center—This BSE image (magnified 750×) shows the surface curving smoothly where the two rubies are joined, demonstrating surface remobilization. Right—These 40-micron-high ruby crystals were growing on the free surface of the smaller ruby; they indicate recrystallization in the heat-treating environment (magnified 750×).



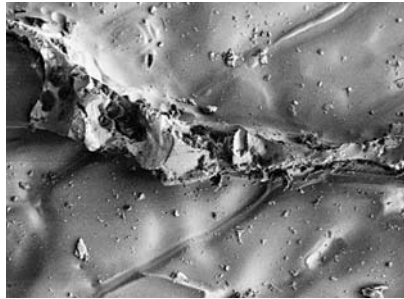
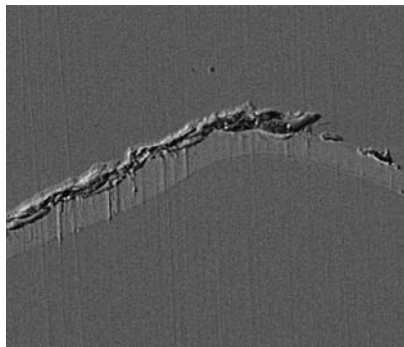


Figure 9. This 2.34 ct heated rough ruby appeared to be held together by a layer of “firecoat.” Additional veinlets spread out from the main vein along parting planes. The relative brightness of this material indicates that it has a higher mean atomic weight than the ruby. BSE magnified 150 \times .

some of the materials Themelis mentioned, high-technology materials such as BPSG (boron phospho-silicate glass), useful to the semi-conductor industry for its low flowing point of 700° to 1000°C, could yield the composition we found.

The texture and chemistry of all the fillers we observed was consistent with glass formed from chemicals

Figure 10. The large glass-filled fissures crossing the table of this 1.09 ct heated Mong Hsu ruby appear brighter than the surrounding ruby in this BSE SEM image. The deeper polishing lines indicate that the filler is softer than the ruby. Notice the gap along one side of the “glass.” Magnified 600 \times .



used to coat the rubies during the heat-treatment process. At this time, if this material is visible with a standard gemological microscope, the GIA Gem Trade Laboratory refers to it with the following comment: “Foreign material is present in some surface reaching fractures.” If large filled cavities are present on the stone, we state instead, “Foreign material is present in some surface cavities.” We plan to continue to investigate heat-treated Mong Hsu rubies to explore additional questions regarding this glassy material.

MLJ and SFM

TOURMALINE Rough from Paraíba

Wilford Schuch of King Prestor John Corp., New York, submitted the bright violet and blue rough stone shown in figure 11 to the East Coast lab this summer. The client was seeking confirmation that this 19.49 ct stone, which he had purchased in Brazil, was tourmaline from Paraíba. Although he was offered smaller pieces of other rough, up to 5 ct, only this piece showed the “electric” colors that took the gem trade by storm 10 years ago.

The refractive indices of 1.630–1.659 (taken on a flat portion of the crystal), along with the uniaxial character and S.G. (measured hydrostatically) of 3.09, identified the rough as tourmaline, although these refractive indices are at the high end of the range. The overall morphology was equant, but there were striations parallel to the c-axis, a common feature in tourmaline. The stone showed pleochroism in deep violet-blue and a lighter blue-green. It was inert to both long- and short-wave UV. Microscopic examination revealed a large fracture, small reflective crystalline inclusions, and two-phase inclusions, some arranged in a “fingerprint.” The hand spectroscope showed broad absorption in the green and red areas of the spectrum.

UV-visible spectroscopy confirmed these broad bands, with strong absorption above 600 nm; a wide, moderately strong peak centered at 500 nm; and



Figure 11. All physical, chemical, and spectroscopic properties pointed to Paraíba, Brazil, as the source of this 19.49 ct bright violet and blue tourmaline.

a weak absorption at 414 nm. EDXRF qualitative chemical analysis, under conditions sensitive for transition metals and heavier elements, revealed Cu, Mn, Ca, Ti, K, Bi, and Ga.

This combination of properties is comparable to those described for tourmaline from Paraíba (E. Fritsch et al., “Gem-quality cuprian-elbaite tourmalines from São José da Batalha, Paraíba, Brazil,” Fall 1990 *Gems & Gemology*, pp. 189–205), especially the violetish blue sample from that study. However, both refractive indices were significantly higher, and the birefringence was slightly higher, than the values reported previously. Our client received an identification report with the conclusion “tourmaline,” and a separate research letter stating that the 19.49 ct rough showed properties consistent with this locality. To the best of our knowledge, the Paraíba region is the only source of gem-quality copper-bearing tourmalines. IR

PHOTO CREDITS

Maha Tannous photographed figures 1, 5, and 11. Elizabeth Schrader took figure 2. Vincent Cracco provided figure 3. Shane McClure photographed the figure 1 inset and figure 6. Mary Johnson provided figures 7 and 8 (center and right for both) 9, and 10. John Koivula was the photographer for figures 7 and 8 (both left).

GEM NEWS

Editors • Mary L. Johnson, John I. Koivula,
Shane F. McClure, and Dino DeGhionno
GIA Gem Trade Laboratory, Carlsbad, California

Contributing Editors
Emmanuel Fritsch, IMN, University of Nantes, France
Henry A. Hänni, SSEF, Basel, Switzerland
Karl Schmetzer, Petershausen, Germany

DIAMONDS

APEC 2000 International Jewellery Conference features diamonds, education, and treatments. This two-day (August 28 and 29) conference was sponsored by the Asia-Pacific Economic Cooperation Forum (APEC), which comprises 21 economies from the Asia-Pacific region, and was held in conjunction with the "JAA Australian Jewellery Fair 2000." The two main themes were economic policy and new technological challenges. As a result, the topics covered were wide ranging, from the role of tariffs in the changing global marketplace to the identification of treatments in diamonds and jadeite. Following are some highlights of the gemological topics discussed.

Martin Rapaport, of the *Rapaport Diamond Report*, gave an impassioned plea for the jewelry industry to support a global solution to the problem of diamonds being sold to finance warfare in volatile African nations such as Angola and Sierra Leone. Because conflict diamonds cannot be separated from nonconflict (or "peace") diamonds scientifically, and it is virtually impossible to trace conflict diamonds from their source into the legitimate market, Mr. Rapaport and other leaders of the diamond industry (in particular, the members of the newly formed World Diamond Council) are working with the United Nations to establish a mechanism to control the flow of *nonconflict* diamonds. For such a plan to work, the diamond industry must change the way it does business, and governments must do their job in maintaining controls at the points of export and import.

David Peters, of Jewelers of America, spoke on identifying training needs in the retail sector and especially the importance of understanding and motivating the adult learner. In a separate session, Mr. Peters examined the benefits of disclosing treatments and synthetics. Not only is this legally and ethically correct, but it also helps the retailer and the industry as a whole win back customer confidence. **Bill Sechos**, of the Gem Studies Laboratory in Sydney, Australia, outlined training needs for the gemologist. He stressed the importance of continuing education (given the sophisticated new treatments and synthetics),

and of identifying resources to solve gemological problems that are beyond the scope of the store laboratory.

Tay Thye Sun, of the Far East Gemological Laboratory (Singapore), reported on jade treatments, especially jadeite that has been bleached (to remove iron oxide staining or dark inclusions with, e.g., hydrochloric acid) and impregnated with a polymer or other substance (to fill the voids left by the bleach). Mr. Tay noted many developments since the Fall 1992 *Gems & Gemology* article by E. Fritsch et al. (pp. 176–187) on the identification of this "B-jade." Chief among these is the use of different polymers with specific gravities and UV fluorescence reactions that more closely match those of untreated jadeite. Also, some treaters are using wax to impregnate the bleached jadeite, because a light surface "waxing" traditionally has been accepted in the jadeite industry. However, such a wax filler typically is not stable over time. It may be detected by suspiciously large "wax" peaks in the infrared spectrum. Mr. Tay also reported that gemologists could gain important information by examining the jadeite surface with a loupe or microscope: Unbleached jadeite has a compact interlocking grain texture (evident as a smooth surface with only minor pitting), whereas bleached jadeite may have a loose interlocking grain structure (evident in the presence of polishing marks and numerous pits).

Finally, **Dr. Jim Shigley**, director of research at GIA, reviewed the current status of high pressure/high temperature (HPHT) treated diamonds. GIA has now examined more than 2,000 GE POL "colorless" diamonds, including several both before and after treatment. He described a number of the distinctive internal features seen (as reported in the article by T. Moses et al. in the Fall 1999 *Gems & Gemology*, pp. 14–22) as well as the importance of spectroscopic indicators. Dr. Shigley also mentioned the yellow-to-green HPHT-treated diamonds currently being produced by various groups (and described by I. Reinitz et al. in the Summer 2000 *Gems & Gemology*, pp. 128–137).

Alice Keller

Editor, *Gems & Gemology*

De Beers's newly stated direction. Reporting from the World Diamond Congress in Antwerp, held July 17–19, GIA President William Boyajian supplied the following information.

As a result of a highly publicized strategic review by the consulting firm Bain & Company, of Boston, De Beers announced to its sightholders on July 12 that it would end its efforts to control world diamond supply and instead focus its energies on building global diamond demand. De Beers's key strategy is to be the "supplier of choice" in the industry. Although it will not abandon the market to its own self-interest, it will end its former broad-brush "custodial" role of matching worldwide supply to demand. Instead, the company will work to become "a more finely calibrated instrument designed primarily to serve the interests of De Beers and its main clients," as announced by Nicholas Oppenheimer in his recent Chairman's Message.

In addition, De Beers will be discontinuing the use of "Central Selling Organisation" (CSO) in favor of a new identity as the "Diamond Trading Company" (DTC), and will allow its clients to leverage this name along with their own individual branded names. DTC will appear with the famous slogan "A diamond is forever" in new diamond ads, and a new "Forevermark" logo has been introduced (figure 1). However, De Beers will reserve its super-brand "De Beers" name for the De Beers Group of Companies alone. A set of "best practice" principles is being established for sightholders, to ensure continued consumer confidence in the allure and mystique of untreated natural diamonds through their commitment to the highest professional and ethical standards. Another important component of the new strategy, a special policy statement, involves the introduction of objective criteria that sightholders must meet by demonstrating efficient distribution and marketing abilities.

Figure 1. Diamonds to be sold through De Beers's Diamond Trading Company may be branded with the "Forevermark," which will also be an important advertising tool.



A key goal for De Beers is to increase shareholder value, and one way to do this is to reduce its diamond stockpile. With the emergence of new diamond producers in recent years, the supply aspect of the diamond industry has become much more competitive. Too often we use the cliché "competition is good." Yet De Beers's new strategy may very well propel the world's leading diamond organization into an even stronger leadership position. Clearly, De Beers's stated new direction is one of the most monumental decisions ever cast by the group, and it will no doubt have a huge impact on every level of the diamond pipeline for years to come.

William E. Boyajian

President, Gemological Institute of America

Adapted with permission from the GIA Insider, Vol. 2, No. 15, July 20, 2000.

COLORED STONES AND ORGANIC MATERIALS ■

Mosaic ammonite. In almost every gem mining operation, most of the material recovered is either not of gem quality or too small for most jewelry purposes. Although the occasional recovery of large and fine-quality stones makes mining exciting, it is the commercial value of the overall production that commonly determines if a mine is economical. Among "mine-run" material, nongem rough with good crystal form may be marketed as mineral specimens. Finding a market for small fragments and pebbles, however, is another matter entirely.

Recently, at the suggestion of GIA Education vice president Brook Ellis, Rene M. Vandervelde, chairman of Korite International in Calgary, Alberta, Canada, provided the Gem News editors with two samples of some new mosaic triplets of fossilized ammonite derived from their mine in Alberta. Instead of the layer of fossilized ammonite typically seen in "Ammolite" doublets and triplets, the central layer in these assembled stones was fashioned from tiny angular flakes of iridescent ammonite shell that were bound in hard plastic.

The two assembled cabochons examined weighed 1.89 and 0.97 ct (figure 2). Note how well the appearance of these ammonite assemblages resembles the natural crackled pattern commonly seen in Ammolite. Even though the unaided eye can identify these assembled stones as triplets when viewing them from the side, the fact that they are assembled from tiny flakes of iridescent ammonite shell becomes apparent only with magnification, when the jagged edges of the individual ammonite shell fragments are readily apparent (figure 3). We also noted a few flattened gas bubbles trapped along the contact planes between the glass dome and the plastic central layer, and between the ammonite fragments and the surrounding plastic. In the round cabochon, a spherical gas bubble was observed suspended in the plastic central layer near the edge of the cabochon (again, see figure 3).

Each assemblage consisted of a transparent glass cap with an R.I. of 1.52, a central layer of hard transparent



Figure 2. Composed of tiny angular flakes of iridescent ammonite shell encased in a plastic that is sandwiched between a glass cap and a black opaque backing material, these two assembled cabochons make attractive use of otherwise unusable fragments. The oval measures $9.90 \times 7.58 \times 3.59$ mm, and the round piece measures $7.01\text{--}7.09 \times 3.08$ mm. Photo by John I. Koivula.

plastic that encased small angular fragments of fossilized iridescent ammonite shell, and a backing layer of opaque black material. The central plastic layer and the black backing melted when a thermal reaction tester was applied.

The assemblages showed no fluorescence to long-wave UV radiation, but they did fluoresce a strong, chalky, slightly bluish white to short-wave UV. When we examined the samples without magnification, as well as with a microscope set up for UV examination, it was our general impression that the fluorescence came from the

Figure 3. With magnification, the jagged edges of the individual ammonite shell fragments are clearly visible. Notice the small gas bubble trapped in the plastic layer at the left edge of the assembled cabochon. Photomicrograph by John I. Koivula; magnified 15 \times .



glass dome, and its glow caused the center layer to appear fluorescent as well. Disassembly of one of the cabochons would be required, however, to confirm which components were actually responsible for the reaction.

On a Gem Trade Laboratory identification report, this material would be identified as: "Triplet, consisting of a glass top and mosaic inlay of natural fossilized ammonite shell fragments with a thick black backing."

Gemmy anhydrite from Iran. Faceted anhydrite is a very rare collector's stone, with only a few known localities in the world. It is difficult to cut, as it has a low hardness (3.5) and perfect cleavage in one direction. A new find of facetable anhydrite (figure 4) comes from Iran's Hormoz and Qeshum Islands in the Persian Gulf. A few dozen stones were recovered on the surface of a typical salt dome by a Czech speleological expedition that was exploring very unusual large caves formed from massive halite.

The anhydrites occurred as loose crystals up to about 8 cm in length, but usually only small portions were transparent. One specimen with anhydrite growing on quartz crystals was found. The surfaces of some anhydrite crystals were "parqueted" (similar to heliodor crystals from Ukraine) due to natural etching. Twinned crystals were rare. The anhydrite crystals examined were colorless, light violet, or (very rarely) pink (see, e.g., figure 4 inset). Refractive indices measured on a polished oriented crystal were $n_{\alpha} = 1.570$, $n_{\beta} = 1.576$, and $n_{\gamma} = 1.616$, with a high birefringence of 0.046. Specific gravity (measured hydrostatically) was 2.95-2.96. The crystals showed no lines in the visible spectrum with a hand spectroscope, and no fluorescence to UV radiation.

Typical inclusions seen with a microscope were multiphase negative crystals as well as at least three types of colorless crystals. One type was identified as quartz on the basis of its shape (figure 5) and bright interference colors (seen even in plane-polarized light). Groups of unidentified rounded anisotropic crystals were found in another cut stone. Isotropic included cubes were probably halite. Some stones also contained small black crystals that are probably hematite. Almost all the cut anhydrites contained parallel mirror-like cleavage planes. The approximately 20 faceted anhydrites examined ranged from 1 to 5 ct, although one 22.74 ct stone has already been faceted (again, see figure 4) and even larger rough exists.

The area also has produced facetable colorless and purple fluorite, yellow apatite (very similar to the material from Durango, Mexico), and colorless danburite (although this last material would produce only small cut stones). Other minerals include bipyramidal hematite crystals, dolomite twins, halite, pyrite, and augite. The quartz crystals occasionally found were milky due to abundant, very fine curved fibers (which were not identified).

Jaroslav Hyrsl (Hyrsl@kuryr.cz)
Kolin, Czech Republic

Aquamarine from southeast India. Fine aquamarines have been mined from the eastern Indian state of Orissa and occasionally from the southeastern state of Madras (see Fall 1989 Gem News, p. 179). This contributor reports that during the past few years another source in southeast India has produced some significant aquamarines (including some large crystals, as in figure 6), from which several stones have been faceted (figure 7). According to K. C. Pandey, managing director of Superb Minerals in Maharashtra, India, the source is a pegmatite in the Karur district of Tamil Nadu State. Irv Brown, of I. Brown Fine Minerals in Fallbrook, California, stated that a single pocket produced two large greenish blue crystals with moderate to strong saturation, and approximately 7–10 kg of smaller greenish blue crystals with weak to moderate saturation. The unheated 30.30 ct cushion-shaped stone in figure 7 represents the finest blue seen from this locality.

The gemological properties of this material are consistent with those published for aquamarine. A slight color shift was observed, from a strong greenish blue in incandescent light to a slightly greenish blue in daylight.

Edward Boehm (joebgem@aol.com)

Joeb Enterprises, Solana Beach, California

Coral exploration resumes in Hawaii. The deep-water “precious” coral-fishing industry fishery in the Hawaiian islands has been nearly dormant for the past 20 years. However, several recent developments suggest that the coral-fishing industry in Hawaii could revive in the near future.

Jewelry-quality coral is known from seven beds in Hawaii, although it has been commercially harvested from only one of these (Makapu’u, off Oahu). The most economically important coral varieties in this area are black (*Antipathes spp.*), pink (*Corallium spp.*), gold (*Gerardia spp.*), and bamboo (*Lepidisis olapa*). Black coral

Figure 5. Inclusions of euhedral quartz were seen in some of the Iranian anhydrites. Photomicrograph by Jaroslav Hyrsl; magnified 9×.



Figure 4. These colorless to light pink anhydrites (4.00, 5.89, and 22.74 ct) were cut from crystals as large as 8 cm (see inset) that were recently found on Iran’s Hormoz and Qeshum Islands in the Persian Gulf. Photos by Jaroslav Hyrsl.

Figure 6. This gem-quality aquamarine crystal from Tamil Nadu State in southeastern India measures 31 cm long and weighs 10 kg. Photo courtesy of K. C. Pandey.





Figure 7. Some large stones have been faceted from the Tamil Nadu aquamarine; the trilliant shown here weighs 179 ct. The 30.30 ct cushion-cut aquamarine represents the finest color seen to date from this locality; both stones are reportedly unheated. Courtesy of I. Brown and S. Wilensky; photo by Maha Tannous.

generally occurs at depths less than 100 m, whereas the others are found in deep water (350–1,500 m; R. W. Grigg, "History of precious coral fishery in Hawaii," *Precious Corals and Octocoral Research*, Vol. 3, 1994, pp. 1–18).

In December 1999, the Western Pacific Regional Fishery Management Council adopted regulatory changes to the 1979 document "Fishery Management Plan for the Precious Coral Fisheries of the Western Pacific Region." The Council is the policy-making organization for the management of fisheries in the Exclusive Economic Zone (from 3 to 200 nautical miles offshore) around Hawaii and other U.S. possessions in the Pacific. These changes include a ban on nonselective harvest, a minimum size for harvest, and submission of videotapes for stock assessments. A second set of regulatory changes—adopted by the Council this past summer and based in part on 1999–2000 surveys of coral resources around the main Hawaiian Islands—are designed to create an environmentally responsible incentive for encouraging the exploration and discovery of new coral beds. Both of these measures are currently awaiting Secretary of Commerce approval. The first may be ratified as early as Fall 2000, and the second may be ratified by early 2001. Many environmental concerns are still related to the harvest of corals, some of which are considered endangered species, so harvesting and export will be affected by political decisions in the U.S. and elsewhere in the world.

Renewed interest in the coral fishery and technological advances in harvesting capabilities have spurred these recent regulatory changes. One company, American Deepwater Engineering, obtained an exploratory permit (a permit to harvest in areas where the presence or size of the "precious" coral resource is unknown) and is selectively harvesting deep-water corals with two one-man submersibles. Senior editor Brendan Laurs visited with

president and COO Scott Vuillemot last May, and saw attractive pink coral that had been harvested recently (figure 8). Selective extraction allowed for the collection of relatively large, undamaged pieces that will have a high yield of jewelry-quality material. The firm is marketing some of the pink and gold coral it has harvested through Maui Divers in Honolulu.

Brendan Laurs
Senior Editor, Gems & Gemology

Fresnoite: A first examination. Having been in the business of gem identification for more than half a century, we at GIA seldom come across a gem mineral that we have never encountered before in faceted form. Such was the case when we recently had the opportunity to study a 0.69 ct fresnoite, a transparent to translucent yellow tetragonal barium titanium silicate named for its initial discovery near Fresno, California. The stone was a freeform pentagonal step cut that measured $7.22 \times 4.63 \times 2.80$ mm (figure 9). It was loaned for examination by C. D. (Dee) Parsons, a gemologist and lapidary from Santa Paula, California.

Figure 8. This attractive pink coral was recently harvested by a manned submersible from waters about 1,300 m deep off Makapu'u, Oahu. Photo by Brendan Laurs.





Figure 9. This 0.69 ct fresnoite was our first encounter with this mineral as a fashioned gem. Courtesy of C. D. (Dee) Parsons; photo by Maha Tannous.

We first sought to confirm that the stone was fresnoite. We recorded refractive indices of 1.765–1.773, yielding a birefringence of 0.008. A uniaxial optic figure, as would be expected from a tetragonal mineral, was clearly visible in cross-polarized light through the table facet. The two dichroic colors observed were yellow and near-colorless. The stone was inert to long-wave UV radiation, but it fluoresced a strong, slightly chalky whitish yellow to short-wave UV. Examination with a Beck prism spectroscope revealed a weak 447 nm absorption line. The specific gravity, an average of three sets of hydrostatic weighings, was 4.60. Since all of the above properties matched, within acceptable tolerance, those previously recorded in the mineralogical literature for fresnoite (see, e.g., Gaines et al., *Dana's New Mineralogy*, 1997, p. 1145), we concluded that this faceted gem was in fact fresnoite.

To characterize the material in detail, we performed advanced testing. Energy-dispersive X-ray fluorescence (EDXRF) qualitative chemical analysis by GIA Gem Trade Lab research associate Sam Muhlmeister revealed abundant barium and silicon, as expected. However, it was difficult to determine the presence of titanium by this technique, because of interference from the strong barium peaks.

With the permission of Mr. Parsons, an X-ray powder diffraction pattern was obtained by Gem News editor Dino DeGhionno. Comparison of the powder pattern with a standard materials database confirmed the earlier gemological identification as fresnoite. Shane Elen, of GIA Research, recorded a Raman spectrum so that it could be added to our Raman database.

Only a few weeks after this initial examination, and entirely independent of the earlier study, we received more fresnoite for examination, a 0.20 ct shield-shaped mixed cut and an 8.24-mm-long crystal that weighed 1.86 ct (figures 10 and 11). These examples were provided by Michael Gray of Graystone Enterprises in Missoula,



Figure 10. This 0.20 ct faceted fresnoite and 1.86 ct crystal are reportedly from the Junnila mine in San Benito County, California. Courtesy of Michael Gray; photo by Maha Tannous.

Montana, who stated that they came from the Junnila mine in San Benito County, California, just a few miles from the famous Benitoite Gem mine (see S. Kleine, "The great fresnoite discovery of 1998," *Rock and Gem*, Vol. 29, No. 3, 1999, pp. 52–59).

With the data obtained from the earlier stone, it was relatively easy to identify both of these samples as fresnoite. The only discrepancy was the 4.51 S.G. of the cut stone, compared to the 4.60 previously obtained. However, specific gravity determination is less certain for such a small stone.

Because fresnoite also has a synthetic counterpart grown by the Czochralski pulling process (see, e.g.,

Figure 11. The faceted fresnoites contained numerous partially healed fractures, which are useful in separating them from nearly flawless Czochralski-pulled synthetics. Photomicrograph by John I. Koivula; magnified 15 \times .



U. Henn, "Synthetischer Fresnoit," *Gemmologie: Zeitschrift der Deutschen Gemmologischen Gesellschaft*, Vol. 48, No. 4, 1999, pp. 232–233, it is important to be able to separate this rare natural collector's gem from its synthetic equivalent. By design, Czochralski pulling tends to result in nearly flawless crystals. During his examination of a faceted 6.11 ct Czochralski-grown synthetic fresnoite, the only inclusion noted by Henn (1999) was a small spherical gas bubble visible at 40× magnification. This is in sharp contrast to the numerous "fingerprint" fluid inclusions along partially healed fractures (figure 11) that we observed in the faceted natural fresnoites. The other gemological properties were essentially identical. Therefore, observation of inclusions serves as an important means to separate natural fresnoite from its synthetic counterpart.

Figure 12. Some superb gem tourmaline crystals have been recovered from pegmatites in Brazil. This specimen (10 cm tall) of tourmaline on quartz and cleavelandite is from the Santa Rosa area in Minas Gerais. Courtesy of Wayne Thompson; photo by Jeff Scovil.



Gemological Presentations at the 31st International Geological Congress. From August 6 to 17, more than 4,000 participants from 103 countries convened in Rio de Janeiro for the 31st International Geological Congress, which featured three sessions on gems. Abstracts of all 6,179 presentations were supplied to Congress participants in searchable format on CD-ROM (some of these were submitted and accepted, but were not actually presented at the meeting). A searchable database containing many of the abstracts is also available on the Congress Web site (www.31igc.org) until 2002. Presentations relating to gemstones encompassed geology, localities, treatments, and gem identification; the following were attended by this contributor.

Brazilian gemstones were highlighted in several talks. **C. P. Pinto** (CPRM-Serviço Geológico do Brasil, Belo Horizonte) and **A. C. Pedrosa-Soares** (Federal University of Minas Gerais, Belo Horizonte) provided a useful compilation of the geology of Brazilian gem deposits. Most are related to granitic pegmatites, hydrothermal veins, or geodes in basaltic lava flows. Emerald, aquamarine, tourmaline, topaz, chrysoberyl, alexandrite, amethyst, citrine, agate, opal, and morganite are the main gem materials being produced. **R. Wegner** (Federal University of Paraíba, Campina Grande) and co-authors provided updates on recent gem and mineral discoveries in the states of Paraíba and Rio Grande do Norte. These include gem-quality crystals of "golden" beryl (up to 7 cm long) and herderite (up to 12 cm long) from the Alto das Flechas pegmatite, color-zoned yellow-green-blue apatite (nearly 20 cm long) from the Alto Feio pegmatite, and cat's-eye triplite from the Alto Serra Branca pegmatite. Wegner et al. also reviewed important Brazilian tourmaline and aquamarine deposits. Significant gem deposits are found in numerous pegmatites within two provinces: *Oriental* (or *Eastern*) in the states of Minas Gerais, Bahia, and Espírito Santo, and *Northeastern* in Ceará, Paraíba, and Rio Grande do Norte. In both provinces, gem tourmaline (figure 12) is found in highly evolved granitic pegmatites, whereas aquamarine typically forms in less-differentiated granitic pegmatites.

M. V. B. Pinheiro (Federal University of Minas Gerais, Belo Horizonte) and co-authors used electron paramagnetic resonance, Mössbauer spectroscopy, and optical absorption to study natural and treated (irradiated and/or heated) Brazilian gem tourmalines. In pink elbaite, they confirmed the presence of Mn^{2+} and noted that irradiation intensified the pink color, while heating to about 450°C decolorized pink and blue crystals and lightened green ones. **N. L. E. Haralyi** (IGCE-UNESP, Rio Claro) noted that white (not colorless) diamonds may show brownish red, orange, yellow, and greenish yellow "opalescent" colors; they also may have rather low specific gravities (e.g., 3.46 for one from Juina in northwest Mato Grosso State).

Geologic investigations of numerous gem materials were presented. **G. Harlow** (American Museum of

Natural History, New York) and **S. S. Sorensen** (Smithsonian Institution, Washington, DC) examined the geology of jade deposits and key localities. Jadeite, found in only eight major deposits worldwide, is associated with blueschist metamorphism at plate boundaries. Nephrite generally forms by metasomatism of dolomite or serpentinite. **J. Townsend** (Geological Survey of South Australia) presented remote-sensing images and suggested that opal deposits in Queensland and South Australia formed adjacent to ancient stream channels (paleochannels). Data for the Coober Pedy area have been released in CD-ROM format, and enterprising opal miners are already using the information to prospect for more deposits.

W. B. Simmons (University of New Orleans, Louisiana) and co-authors illustrated the chemical evolution of gem tourmalines from North America (San Diego County, California, and Newry, Maine), Russia, Madagascar, and northeastern Brazil. The chemistry of the tourmaline Y-site strongly correlates to color, with Fe, Mn, Ti, and Cu being important chromophores. **C. Ionescu** (Babes-Bolyai University of Cluj-Napoca, Romania) et al. described several quartz-family gem materials from the Baia Mare area in northwestern Romania. These materials formed in a variety of geologic environments, including geysers and hydrothermal veins cutting andesitic volcanic rocks. **F. L. Sutherland** (Australian Museum, Sydney) and **D. Schwarz** (Gübelin Gem Lab, Lucerne, Switzerland) reviewed the distribution and genetic origin of basalt-hosted corundum (including “magmatic,” “metamorphic,” and mixed magmatic/metamorphic suites). Such corundum has been recorded in 15 countries and associated with more than 40 basalt fields. Dr. Schwarz also presented a summary of emerald formation; most deposits formed in continental collision zones due to fluid-rock interactions.

In presentations on gem identification, **D. Schwarz** and co-authors described trace-element fingerprinting of rubies and sapphires to separate natural from synthetic stones using Ga, Ti, and V, and to differentiate between deposits—even within a single country, such as Madagascar—using V, Cr, Ga, Fe, and Ti. According to Schwarz et al., synthetic emeralds have relatively low Na and Mg contents, and may contain elements such as Ni and Cu that are not found in natural emeralds; synthetic alexandrite generally contains low Ga and Sn contents, although certain Russian synthetics may have high Ge, Ga, and Sn. **W. B. Stern** (Basel University, Switzerland) and D. Schwarz explained the benefits of using EDXRF analysis to measure trace-element data nondestructively. This method provides rapid measurement of elements ranging from Na to U (atomic weights of 11 to 92), at detection limits typically ranging from 20 to 200 ppm. In a study of untreated and heated natural and synthetic sapphires, **T. Häger** (Johannes Gutenberg University, Mainz, Germany) demonstrated that traces of Fe (~50 ppm) are needed in addition to abundant Mg to develop defect centers that produce yellow color. **W. B. Size**



Figure 13. Lapidaries at the Madagascar Treasures warehouse in Antananarivo cut and polish a variety of local materials. The owner of the facility, Gilles Mannequin (in the blue shirt), examines a piece in progress. Photo by Brendan Laurs.

(Fernbank Museum of Natural History, Atlanta, Georgia) and co-authors performed nondestructive chemical analyses to aid in the identification of Pre-Columbian artifacts from Costa Rica and Guatemala: They found jadeite, nephrite, serpentinite, and silica minerals.

J. E. Shigley (GIA Research, Carlsbad, California) and co-authors reviewed the characteristics of natural versus synthetic diamonds, with particular emphasis on their inclusions and the growth features seen with UV fluorescence and cathodoluminescence. **E. Fritsch** (University of Nantes, France) predicted that in the future more-sensitive techniques (such as laser ablation ICP-MS and luminescence spectroscopy) will likely be necessary to detect the increasingly subtle differences between natural stones and their treated or synthetic counterparts. Digital imaging is already useful in the collection and archiving of scientific and commercial images (such as gem photos in lab reports), and is likely to become even more useful.

Brendan Laurs
Senior Editor, Gems & Gemology

Visit to a Malagasy lapidary facility. Although Madagascar is becoming an increasingly important source of gem rough, most of this material is cut elsewhere, such as in Bangkok and Sri Lanka. Nevertheless, large quantities of massive gem materials are fashioned locally into a variety of ornamental objects, which are exported to Europe and the United States.

While in Madagascar last November, this contributor visited one such lapidary facility, Madagascar Treasures, in the capital city of Antananarivo. The clean and efficient facility, owned and designed by Gilles Mannequin, employs 20 Malagasy lapidaries (see, e.g., figure 13). The workers use saws, polishing wheels, and sphere-making machines to form decorative objects such as cubes, eggs, obelisks, spheres, bookends, paperweights, and game



Figure 14. These three purplish red rubies (0.26 to 0.38 ct) come from the Mercaderes–Río Mayo area of Cauca, Colombia. Courtesy of Jaime Rotlewicz; photo by Maha Tannous.

pieces. A wide variety of Malagasy gem materials are used, such as rock crystal, smoky and rose quartz, labradorite, blue calcite marble, petrified wood, septarian nodules, and jasper.

The facility also processes celestite geodes and fossil nautiloids and ammonites, as well as quartz, black tourmaline, and opaque blue corundum crystals. The crystals are trimmed and cleaned at the warehouse, in preparation for sale as mineral specimens. Iron stains are removed from the tourmaline and corundum crystals using heated oxalic acid. The nautiloids and ammonites typically range from 12 to 16 cm in diameter, with larger specimens reaching 30 cm; they are recovered at two new localities, in west-central Madagascar and in the south near Ilakaka. The fossilized shells are sliced in half and then polished to reveal attractive patterns formed by the internal chambers, which commonly contain recrystallized calcite. In rare cases, the ammonites show iridescent areas. Mr. Mannequin noted that in order to comply with government regulations, all fossils exported from Madagascar must show evidence of polishing.

Brendan Laurs

Senior Editor, Gems & Gemology

Rubies (and sapphires) from Colombia. Although Colombia is famous for its emeralds, it also produces other gem materials. While Gem News editors MLJ and SFM were in Colombia in spring 1998, they were shown several examples of rough and cut gem corundum from alluvial deposits in the Mercaderes–Río Mayo area of Colombia's Cauca Department by Jaime Rotlewicz of C. I. Gemtec Ltda., Bogotá. Sometime later, Mr. Rotlewicz sent us a parcel of three fashioned rubies (figure 14), one water-worn sapphire crystal, and 12 fashioned sapphires (see, e.g., figure 15) from this locality. Sapphires from Colombia were previously described by P. C. Keller et al. ("Sapphire from the Mercaderes–Río Mayo area,

Cauca, Colombia," Spring 1985 *Gems & Gemology*, pp. 20–25), so we concentrated our efforts on characterizing the rubies.

Gemological properties were consistent among the three rubies (a 0.26 ct marquis, a 0.30 ct pear, and a 0.38 ct oval). All were transparent and purplish red, with pleochroic colors of purple-red and orange-red; none showed any reaction to the Chelsea (color) filter. The largest stone had R.I. values of 1.761–1.770 (birefringence of 0.009); the other two had R.I. values of 1.761–1.769 (birefringence of 0.008). The specific gravity, measured hydrostatically, was 4.05–4.12 (the largest ruby had the lowest value); these rather high values are probably due to measurement errors associated with the small size of the stones. All three rubies fluoresced weak red to long-wave UV radiation and very weak red to short-wave UV. All three had typical ruby spectra when viewed with a handheld spectroscope.

Among the inclusions seen with magnification were: clouds (in two samples; in one of these, the cloud showed a hexagonal growth pattern), "fingerprints" (in two samples), stringers (in one sample), an unidentified tube-shaped crystal (in one sample), a white crystal with a stress fracture (in another sample), needles resembling boehmite (in two samples), and crystals resembling apatite (in one sample). Boehmite and apatite inclusions, as well as clouds, also were noted by Keller et al. (1985) in sapphires from this region.

Semi-quantitative EDXRF chemical analyses were performed by Sam Muhlmeister in the same manner as described in the article by Muhlmeister et al. ("Separating natural and synthetic rubies on the basis of trace-element chemistry," Summer 1998 *Gems & Gemology*, pp. 80–101). The three rubies had trace-element contents of 0.14–0.19 wt.% Cr_2O_3 , 0.31–0.50 wt.% iron (as FeO), 0.02–0.05 wt.% TiO_2 , 0.01–0.02 wt.% Ga_2O_3 , and 0.09–0.13 wt.% CaO. Vanadium and manganese were below detection limits; however, traces of silicon, phosphorus, potassium, and chlorine also were present. (Many of these elements might reside in mineral inclusions, such as Ca and P in apatite.) The iron and titanium contents, as well as the relative amounts of iron, vanadium, and gallium, were typical for rubies from basaltic environments (again, see Muhlmeister et al., 1998).

Mr. Rotlewicz reports that rubies and pink sapphires represent only 1% of the gem corundum that has been found in this area. He added that there is no organized mining at the present time and that the area is not considered safe for visitors.

Lavender sugilite with green spots. Sugilite (occasionally known by the trade name "Lavulite") is familiar to gemologists as an ornamental material from the Kalahari manganese field in the Republic of South Africa, notably from the Wessels and N'Chwaning mines near Hotazel (see, e.g., J. E. Shigley et al., "The occurrence and gemological properties of Wessels mine sugilite," Summer 1987 *Gems*

ew Gemology, pp. 78–89). The massive gem material is a complex metamorphic rock that consists mainly of the mineral sugilite, $\text{KNa}_2(\text{Fe}^{2+}, \text{Mn}^{2+}, \text{Al})_2\text{Li}_3\text{Si}_{12}\text{O}_{30}$. Gem sugilite normally ranges from purple to violet, although its formula does not require this color, should other chromophores be present.

Recently a client submitted a “lavender”-colored (i.e., light violet) rock with some brown and bright green inclusions to the SSEF laboratory (figure 16). He was interested in having the green specks identified. We obtained Raman spectra from the green material in a polished slab. The peak identification led to the mineral sugilite, and we were surprised to see full agreement with our reference spectrum from a piece of violet sugilite. A bulk chemical analysis with EDXRF determined the presence of all the detectable elements expected in the sugilite formula, with the exception of Al (which is nonessential). Notably, the green spots also showed a chromium signal, a novelty at least for sugilite from the Wessels mine. Also, we noted that the paler lavender areas contained less manganese than the typical violet sugilite. A small amount of Ca was registered in the EDXRF spectrum of our violet reference sample as well as in the green area of the client’s stone. The main difference between the violet material and the green spots was the presence of Cr.

The (optional) aluminum in the above-listed general chemical formula replaces the elements Fe and Mn. Chromium is another valid candidate for this replacement, as noted in the green spots. We have thus another silicate mineral where chromium admixtures provide a lovely green color, as is the case for emerald (beryl), fuchsite (muscovite mica), and so on. The isolated nature of the spots suggests that the chromium may be derived from earlier Cr-minerals (perhaps chromite) that were altered during the metamorphism of the parent rocks. The Cr then was locally introduced into the growing sugilite crystals, coloring portions of the material green.

HAH

Paraíba tourmaline update. On August 9–11, these contributors visited northeastern Brazil to gather firsthand information on the mining, production, and geology of the popular, brightly colored Paraíba (cuprian) tourmaline (see, e.g., E. Fritsch et al., “Gem-quality cuprian-elbaite tourmalines from São José da Batalha, Paraíba, Brazil,” Fall 1990 *Gems & Gemology*, pp. 189–205). They accompanied Brian Cook (Nature’s Geometry, Graton, California) and Marcelo Bernardes (Manoel Bernardes Ltd., New York), and were hosted by Heitor Barbosa at the São José da Batalha mine in Paraíba State. Mr. Barbosa first discovered gem crystals of the copper-bearing tourmaline at this pegmatite deposit in 1987. After nearly a decade of disorganized activity by various groups, Mr. Barbosa reclaimed ownership of the deposit in the spring of 2000. With debris cleared from the underground workings and fluorescent lighting recently installed, two teams



Figure 15. These eight sapphires (0.49–2.08 ct) show the range of colors available from the Mercaderes–Rio Mayo deposit. Courtesy of Jaime Rotlewicz; photo by Maha Tannous.

of miners have now begun working new areas of the pegmatites with pneumatic hammers (figure 17).

The rapid price escalation of Paraíba tourmaline has also made it economically feasible to rework the mine tailings, the discarded material that was previously removed from the mine. Mr. Barbosa is building two processing plants to wet-sieve the tailings. Processing facilities are also under construction or in operation by two other groups that had stockpiled tailings and alluvial and colluvial material from areas adjacent to the mine (figure 18). These operations were the only source of production during our visit, and occasionally produce small pieces of gem rough.

Facetable cuprian tourmaline has also been found at two other pegmatite mines in the area, located 45–60

Figure 16. The green spots in these two pieces of lavender sugilite are not a different mineral, but rather sugilite colored by chromium. Each sample is 4 cm wide; photo by H. A. Hänni.





Figure 17. Underground mining has resumed at the historic São José da Batalha tourmaline mine in Paraíba State, Brazil. Here, miners use pneumatic hammers to excavate the 40-cm-wide pegmatite dike. Photo by Brendan Laurs.

km northeast in adjacent Rio Grande do Norte State. The more distant one of these lies just east of the town of Parelhas; it has been called the Capoeira or Boqueirãozinho pegmatite (J. Karfunkel and R. R. Wegner, "Paraíba tourmalines: Distribution, mode of occurrence and geologic environment," *Canadian Gemmologist*, Vol. 27, No. 4, 1996, pp. 99–106). Last December, however, a new venture (Mineração Terra Branca Ltda.) began working the deposit, which has been renamed "Mulungu." At the time of our visit to Mulungu with host Ronaldo Miranda, the miners were drilling and blasting in two of three shafts, which were accessed using electric winches and reached depths of 33 m (figure 19). A processing plant was being tested for wet-sieving and hand-sorting the tourmaline from both the mined material and colluvium derived from downslope of the pegmatites. Although we saw no tourmaline production during our visit, a small pocket of gem-quality blue-to-green crystals was reportedly discovered last April (R. Miranda, pers. comm., 2000). Melee-size gemstones have also been cut from clear fragments within larger translucent to semitransparent crystals that are "frozen" within the pegmatite. Similar crystals occasionally yield facetable cuprian tourmaline at the other mine in the area, the Alto dos Quintos pegmatite (again, see Karfunkel and Wegner, 1996); however, we did not visit that deposit.



Figure 18. Fragments of gem-quality Paraíba tourmaline are occasionally recovered from stockpiled tailings, as well as from alluvial and colluvial material, at the São José da Batalha mine. This newly constructed processing plant will separate gravel-sized material from colluvium; the gravel will undergo further concentration at another nearby plant. Photo by Brendan Laurs.

An article updating the mining, production, and geology of the São José da Batalha mine is being prepared.

Brendan Laurs

Senior Editor, Gems & Gemology

James E. Shigley

Director, GIA Research

Tourmaline with an apparent change-of-color in one pleochroic direction. Earlier this year, gem dealer Jay Boyle of Fairfield, Iowa, called our attention to an unusual tourmaline that he had purchased in Sri Lanka in January 2000. The 2.33 ct cushion mixed cut, which measured $8.88 \times 8.39 \times 4.72$ mm, appeared strongly pleochroic in reddish brown and green (similar to andalusite) in incandescent light, but looked uniformly green in fluorescent light.

When viewed table-up in daylight-equivalent fluorescent light, this gemstone was brownish yellowish green, with even color distribution (pleochroism is not considered in assessing color distribution). The overall color shifted only slightly between daylight-equivalent fluorescent light and incandescent light; however, the evident pleochroism changed markedly. Normally, we determine pleochroic colors using a polariscope in daylight-equivalent

fluorescent light; for this sample, these colors were dark yellowish green and brown-orange. In this case, we also looked at the pleochroism in incandescent light, and were surprised to find that the stone still showed the same brown-orange pleochroic color, but the yellow-green was much brighter (lighter and more saturated). The overall effect was an oenophile's delight: In incandescent light, this tourmaline resembled red Burgundy wine in its typical green bottle; however, in daylight-equivalent fluorescent light, the bottle looked empty (figure 20)!

Other gemological properties were as follows: optic character—uniaxial negative; (Chelsea) color filter reaction—orange to red; refractive indices—1.620–1.640; birefringence—0.020; specific gravity (measured hydrostatically)—3.06; inert to long-wave UV radiation, and very chalky weak greenish yellow fluorescence to short-wave UV. A spectrum taken with a handheld spectroscope in the brown-orange direction revealed a 400–500 nm cutoff, a weak band at 610–630 nm, and weak lines at 650 and 670 nm. Magnification revealed stringers and growth tubes, which are typical inclusions in green tourmaline. At our request, Sam Muhlmeister collected EDXRF spectra, and found major Mg, Al, Si, and Ca, and trace Ti, V, Cr, Fe, Zn, Ga, and Sr. Both the chemistry and the gemological properties are consistent with uvite, the calcium magnesium tourmaline. Perhaps the vanadium and chromium contents are responsible for the shifts in the green pleochroic color that cause this unusual visual effect.

Although Mr. Boyle purchased this tourmaline in Sri Lanka, he cautioned us that Sri Lankan dealers now get their materials from many areas and this stone might have come from somewhere else. The chemistry and gemological properties of this stone are in good agreement with the tourmalines from Umbasara, Tanzania, which were described in two reports in the *Journal of Gemmology* (A. Halvorsen and B. B. Jensen, "A new colour-change effect," Vol. 25, No. 5, 1997, pp. 325–330; and Y. Liu et al., "Colour hue change of a gem tourmaline from Umba Valley, Tanzania," Vol. 26, No. 6, 1999, pp. 386–396). In those tourmalines, one pleochroic color is green and the other shifts from



Figure 19. Gem-quality cuprian elbaite was reportedly recovered from this shaft at the Mulungu mine in Rio Grande do Norte State, Brazil. An electric winch and steel bucket are used to transport both miners and rock material. Photo by Brendan Laurs.

orange to "wine red" as the sample thickness increases. Thus, in the stone we examined, the transmitted pleochroic brown-orange color would appear as red reflections (with about twice the optic path length) when the stone was viewed table-up.

One final caution: According to the literature, tourmalines can be treated to appear to have an "alexandrite-like" change of color, by painting some facets with red ink (G. L. Wycoff, "What's happening in gemcutting," *American Gemcutter*, No. 122, 1997, pp. 3, 26–28). We checked this stone for inked facets but saw no evidence of this treatment.

Figure 20. This 2.33 ct tourmaline seems to shift colors in the brown pleochroic direction, but in fact it is the green direction that shifts in color, as shown here in incandescent light (left) and daylight-equivalent fluorescent light (right). Courtesy of Jay Boyle; photos by Maha Tannous.

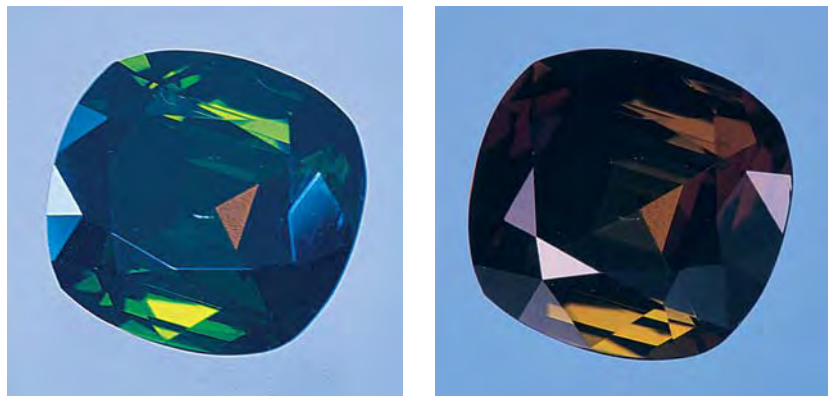




Figure 21. Represented as hematite, these strongly magnetic beads proved to be manufactured barium iron oxide. The beads measure approximately 8 mm in diameter; photo by Maha Tannous.

SYNTHETICS AND SIMULANTS

Magnetic hematite imitation in jewelry. A Parisian commercial gift dealer submitted to the French Gemological Laboratory in Paris two necklaces and two bracelets of purported hematite bead jewelry from China. The beads in the necklaces were indeed hematite (as indicated by the reddish brown streak and chemical composition as determined with EDXRF); they were weakly attracted to a magnet, as is commonly the case with the Brazilian hematite that is found in abundance on the market today.

However, the beads forming the bracelets caught the attention of the laboratory's assistant director, Heja Garcia-Guillermine: They were so strongly magnetic that they stuck to one another even when they were not strung (figure 21). Such strong magnetic behavior clearly is not typical of hematite. Also, the streak was black, and EDXRF analysis performed on an EDAX machine showed the presence of barium (Ba) in addition to iron. Consequently, the beads were sent to the University of Nantes for further testing.

X-ray diffraction analysis performed on a Siemens 5000 diffractometer proved the material to be barium iron oxide, $\text{BaFe}_{12}\text{O}_{19}$. Although this formula resembles that of hematite, Fe_2O_3 , the material is clearly manufactured, as there is no known natural equivalent. It belongs to the well-studied family of hexagonal ferrites, which are industrially important and are the basis of many permanent magnets, such as those that decorate refrigerators. Prof. Olivier Chauvet, of the Institut des Matériaux Jean Rouxel at the University of Nantes, estimated (using simple tests) that the magnetic field created by these beads is of the order of 10 Gauss. Such a field is dangerous for some magnetic storage media (computer diskettes), and is potentially dangerous to some computer screens.

We also noted that when the beads were allowed to arrange themselves in a line without constraint, their drill holes were far from parallel to the line created by the beads (again, see figure 21). Oddly, these holes were

sometimes almost perpendicular to the line; so when these beads are strung, they are not in their most stable position relative to one another.

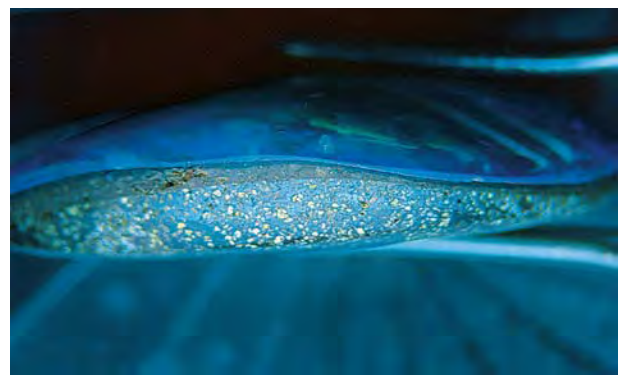
When the dealer informed his original provider that some of the beads were not hematite, the supplier was shocked. He stated that these magnetic beads have been sold all over Europe as hematite with no problem, and that this dealer was the first one to complain. *EF*

Curved quadruplet boulder opal imitations. A parcel of material represented as boulder opal was purchased at the February 2000 Tucson show by Parisian lapidary Alexandre Wolkonsky. The free-form, flat cabochons ranged from 1.26 to 10.67 ct. Because of the unusual stated locality (China), and the low price of the parcel compared to equivalent pieces from Australia, the gemological properties of these samples were carefully studied. Under magnification, it was clear that the material was not natural boulder opal, but rather an assembled quadruplet with the following four layers (from top to bottom):

- Natural opal top, with a typical appearance and refractive index (1.44)
- A very thin, black layer of apparently even thickness
- A brown layer of homogeneous color but irregular thickness
- An ironstone base typical of that seen on boulder opal, with limonite, clay, and an occasional opal veinlet

The homogeneous brown and black layers did not melt on contact with a hot point, but rather they softened and flaked off. In some of the samples examined, the brown layers contained gas bubbles, which identified the material as a plastic. This was confirmed with a Bruker RFS 100 FT-Raman microspectrometer, which revealed a broad signal around 3000 cm^{-1} that is typical of C-H

Figure 22. This boulder opal simulant is a quadruplet that consists of natural opal, layers of black and brown materials, and natural ironstone. Most remarkably, the bottom surface of the opal layer, and the top surface of the ironstone layer, are curved rather than planar. Photomicrograph by E. Fritsch; magnified 2.5 \times .



groups found in organic matter such as plastic (see B. Schrader, *Raman/Infrared Atlas of Organic Compounds*, VCH, Weinheim, Germany, 1989, pp. N-01–N-11). The black layer was probably added to enhance color contrast, as does the thin layer of black patch that is sometimes seen backing “black” boulder opal (see, e.g., R. W. Wise, “Queensland boulder opal,” Spring 1993 *Gems & Gemology*, pp. 4–15).

Most remarkably, the bottom surface of the natural opal layer and the top surface of the ironstone layer were not always flat and planar. In some stones, these layers were clearly curved (figure 22), in contrast to other assembled stones, which generally contain planar contact surfaces. The non-coincidence of these two surfaces was compensated by the variable thickness of the brown plastic layer. EF

MISCELLANEOUS

Concave faceting technique developed for sapphires. After more than 10 years of research, faceter Richard Homer of Gems by Design, Kent, Ohio, has made a significant development in the concave faceting of corundum. According to Mr. Homer, “In order to perfect this technique, I had to understand exactly how combinations of flat and curved facets would interact with the light entering the sapphire. My concave cutting system allows me to manipulate concave facets to one tenth of a degree. This process allows for much greater accuracy and control of the faceting material than does concave *carving* of sapphires.” Because sapphire has a high refractive index and subadamantine luster, concave faceting makes the fashioned sapphires appear dramatically brighter (see, e.g., figure 23), especially for medium- to lighter-toned material; this is partially due to the diminished extinction brought about by the specialized faceting on the pavilion. Concave facets also help minimize the impact of color zoning and veils on the appearance of the stone.

One of the challenges that had to be overcome was working with the directional hardness of corundum. Undercutting and polishing grooves in the pavilion (figure 24) that produce the characteristic brilliance of concave-cut gems proved especially problematic. A series of special diamond-impregnated polishing spindles had to be constructed to make it possible to concave-facet this challenging gem material.

Lila Taylor (gem3@att.net)
Schorr Marketing and Sales
Santa Barbara, California

ANNOUNCEMENTS

Visit *Gems & Gemology* staff in Tucson. *Gems & Gemology* editors Alice Keller, Brendan Laurs, and Stuart Overlin will join Subscriptions manager Debbie Ortiz at the *Gems & Gemology* booth in the Galleria section (middle floor) at the Tucson Convention Center for the

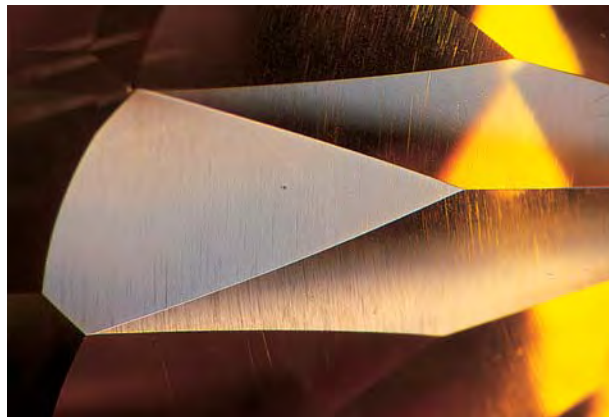


Figure 23. New faceting technology developed by Ohio faceter Richard Homer is being used to intensify the brilliance of sapphires (here, 3.69 to 6.95 ct) by placing concave facets on their pavilions. Courtesy of Schorr Marketing and Sales; photo by Maha Tannous.

AGTA show, January 31 to February 5. Stop by to ask questions, share information for Gem News, or just say hello. And take advantage of the many back issues—and special prices—we’ll be offering.

GANA exhibit at the Carnegie Museum. “Lapidary Art,” a selection of contemporary works by the Gem Artists of North America (GANA), will be on display through January 8, 2001, at the Carnegie Museum of Natural History in Pittsburgh, Pennsylvania. The exhibit will showcase works by lapidary artists Susan Allen,

Figure 24. Seen with the microscope and reflected light, the concave nature of the pavilion facets are evident on this sapphire. Photomicrograph by John I. Koivula; magnified 5x.



Elizabeth Lyons Beunaiche, Michael Christie, Thomas McPhee, Nicolai Medvedev, Gil Roberts, Sherris Cottier-Shank, Lee Allen Speights, and Lawrence Stoller. For more information, call 412-622-3131, or visit www.CarnegieMuseums.org/cmnh.

GAGTL Conference 2000. The Gemmological Association and Gem Testing Laboratory of Great Britain will host its annual conference on October 29, 2000, at London's Barbican Conference Centre, with presentations on diamonds, colored gems, and pearls. In conjunction with the conference, one-day GAGTL workshops will cover gemstone inclusions (Oct. 25), diamonds (Oct. 31), and counter sketching (Nov. 1). Additional attractions include a visit to De Beers (Oct. 27) and a tour of the Gilbert Collection at Somerset House (Oct. 30). For further information, visit www.gagtl.ac.uk/gnews.htm; contact Mary Burland at 44-20-7404-3334 (phone), 44-20-7404-8843 (fax); or e-mail gagtl@btinternet.com.

1st Brazilian Symposium on the Treatment and Characterization of Gems. This conference will take place November 5–8, 2000, at the Federal University of Ouro Preto, Minas Gerais, Brazil. Topics include types of gem treatments and their status in Brazil, techniques for growing and identifying synthetics, analytical techniques and characterization methods, cause of color in gems, and origin determination. Excursions to gem and mineral deposits in the Ouro Preto region will occur on November 9. For details, e-mail gemas2000@cpd.ufop.br or visit www.ufop.br/eventos/gemas.htm (in Portuguese).

Fabergé exhibit in Tucson. More than 60 Fabergé pieces, including some of the Czar's Imperial Easter Eggs, will be on display February 8–11 at the 2001 Tucson Gem and Mineral Society (TGMS) Show, held in the Tucson Convention Center.

Hong Kong International Jewellery Show. The 18th annual show will take place March 5–8, 2001 at the Hong Kong Convention & Exhibition Centre. In addition to hundreds of gem and jewelry exhibitors, the show will feature a series of seminars conducted by international jewelry associations. For details, call Jessica Chan at 852-2240-4354, or visit <http://hkjewellery.com>.

Diamond exposition in Paris. From March 10 to July 15, 2001, this exposition at the Muséum National d'Histoire Naturelle in Paris will focus on the geologic origin, properties, and mining history of diamonds. On display will be several important historical diamond jewelry pieces,

as well as contemporary creations, from numerous museums and private collections. For more information, contact Hubert Bari at 33-40-793856 (phone), 33-40-793524 (fax), or e-mail bari@mnhn.fr.

Opal Symposium 2001. The 2nd National Opal Symposium will be held in Coober Pedy, Australia, April 10–12, 2001. The conference will feature two days of presentations and workshops covering prospecting, mining techniques, operational health and safety, and native title in relation to opal mining. For details, call 61-88-672-5298, fax 61-88-672-5699, or e-mail info@opalsymposium.com, or visit www.opalsymposium.com.

ICA Congress. The International Colored Gemstone Association (ICA) will hold its next Congress in Sydney, Australia, from April 29 to May 4, 2001. The Congress will take place at Sydney's new Convention and Exhibition Centre, "Star City." In addition to speaker presentations, workshops, and panel discussions about colored gemstones, participants will have the opportunity to visit an opal mine. For more information, visit www.gemstone.org or contact the ICA in New York at 212-688-8452 (phone), 212-688-9006 (fax), or e-mail gembureau@gemstone.org.

Geochemistry and Mineralogy of Gemstones Symposium. Hosted by Virginia Polytechnic Institute and State University, this symposium will take place as part of the Eleventh Annual V. M. Goldschmidt Conference, May 20–24, 2001, in Roanoke, Virginia. For more information, e-mail gold2001@vt.edu or visit www.lpi.usra.edu/meetings/gold2001.

ERRATA

1. In the Summer 2000 article by I. M. Reinitz et al. on HPHT-treated yellow to green diamonds, both photos in figure 10 (p. 135) were taken by Maha Tannous.

2. The Summer 2000 abstract (pp. 186–187) of the article by A. T. Collins et al., "Colour changes produced in natural brown diamonds by high-pressure, high-temperature treatment," was attributed to the wrong abstracter; it was actually written by Ilene Reinitz. The abstract was edited to imply a causal relationship between the mutual destruction of vacancies and interstitial carbon atoms, and the reduction of brown color in type IIa diamonds. Although both changes result from HPHT treatment, in fact the causes of the brown color and its reduction are still unknown.

GEMS & GEMOLOGY

Challenge

Winners 2000



This year, over 250 dedicated readers participated in the 2000 *Gems & Gemology* Challenge. Entries arrived from all corners of the world, as readers tested their knowledge on the questions in the Spring 2000 issue. Those who earned a score of 75% or better received a GIA Continuing Education Certificate recognizing their achievement. The participants who scored a perfect 100% are listed below.

AUSTRALIA Cranebrook, New South Wales: George Newman. *Dodges Ferry, Tasmania*: Robin Hawker. *Logan, Queensland*: Ken Hunter ♦ **BELGIUM** *Diegem*: Guy Lalous. *Diksmuide*: Honore Loeters. *Hemiksem*: Daniel De Maeght. *Ruiselede*: Lucette Nols ♦ **BRAZIL** *São Paulo*: Daniel Berringer, Ana Flavia Pantalena ♦ **CANADA** *Bissett, Manitoba*: Paul Gertzbein. *Bobcaygeon, Ontario*: David R. Lindsay. *Calgary, Alberta*: Diane Koke. *Cowansville, Québec*: Alain Deschamps. *St. Catharines, Ontario*: Alice J. Christianson. *Toronto, Ontario*: Ken Miller. *Vancouver, British Columbia*: Michael Cavanagh ♦ **CROATIA** *Zagreb*: Sandra Crkvenac ♦ **CZECH REPUBLIC** *Praha, Kamyk*: Karel Marik ♦ **FRANCE** *Paris*: Marie-France Chateau ♦ **GREECE** *Thessaloniki*: Ioannis Xylas ♦ **INDONESIA** *Jakarta*: Warli Latumena ♦ **ITALY** *Bordighera*: Beviacqua Lorenza. *Caltanissetta, Sicilia*: Francesco Natale. *Lucca*: Roberto Filippi. *Porto Azzurro, Livorno*: Giuseppe Diego Trainini. *Valenza*: Rossella Conti. *Vicenza*: Francesca Zen ♦ **JAPAN** *Kyoto*: Takuma Koyanagi ♦ **MALAYSIA** *Georgetown, Penang*: Lee-Khoon Ng ♦ **NETHERLANDS** *Amsterdam*: P.A.G. Horninge. *Rotterdam*: E. van Velzen. *Voorburg*: W. van der Giessen. *Wassenaar*: Jane M. Orsak ♦ **PHILIPPINES** *Mandaluyong City, Metro Manila*: Mark Alexander B. Velayo ♦ **PORTUGAL** *Figueira, V. du Bispo, Algarve*: Johanne Jack. *Viseu*: Rui P. Branco ♦ **SCOTLAND** *Edinburgh*: James W.M. Heatlie ♦ **SPAIN** *Playa P. Farnals, Valencia*: Monika Bergel-Becker. *Port de Sóller, Baleares*: J. Maurici Revilla Bonnin ♦ **SWITZERLAND** *Rodersdorf*: Heinz Kniess. *Zollikon*: Adrian Meister. *Zürich*: Eva Mettler ♦ **UNITED STATES** ♦ **Alabama** *Gadsden*: Jerome D. Thomas. *Hoover*: Ronald C. Redding ♦ **Arizona** *Chandler*: LaVerne M. Larson. *Tucson*: Molly K. Knox ♦ **California** *Burlingame*: Sandra MacKenzie-Graham. *Carlsbad*: Michael T. Evans, Brian I. Genstel, William J. Herberts, Mark S. Johnson, Jan Lombardi, Diane H. Saito, Abba R. Steinfeld. *Escondido*: Martin Harmon. *Fremont*: Ying Ying Chow. *Morgan Hill*: Douglas Mays. *Pacifica*: Diana L. Gamez. *Rancho Cucamonga*: Sandy Mac Leane. *Redwood City*: Starla Turner. *San Rafael*: Robert A. Seltzer. *Ukiah*: Charles "Mike" Morgan ♦ **Colorado** *Colorado Springs*: Deborah Doty. *Denver*: Mary Shore, Alan J. Winterscheidt. *Ft. Collins*: Frank Sullivan. *Longmont*: William Lacert. *Pueblo*: Naoma Ingo ♦ **Connecticut** *Simsbury*: Jeffrey A. Adams ♦ **Florida** *Clearwater*: Tim Schuler. *Sunny Isles Beach*: Fabio S. Pinto ♦ **Georgia** *Hampton*: Ella Golden ♦ **Illinois** *Mokena*: Marianne Vander Zanden. *Northbrook*: Frank E. Pintz. *Oaklawn*: Eileen Barone. *Peoria*: John Fitzgerald. *Troy*: Bruce Upperman ♦ **Iowa** *Iowa City*: Gary R. Dutton. *West Des Moines*: Franklin Herman ♦ **Louisiana** *Baton Rouge*: Harold Dupuy ♦ **Maine** *South Freeport*: Arthur E. Spellissy Jr. ♦ **Massachusetts** *Braintree*: Alan R. Howarth. *Brookline*: Martin Haske. *Chatham*: William Parks. *Lynnfield*: John A. Caruso. *Uxbridge*: Bernard M. Stachura ♦ **Maryland** *Darnestown*: Ron Suddendorf. *Potomac*: Alfred L. Hirschman ♦ **Missouri** *Perry*: Bruce L. Elmer ♦ **Montana** *Helena*: Werner Weber ♦ **Nebraska** *Omaha*: Ann Coderko ♦ **Nevada** *Las Vegas*: Deborah A. Helbling. *Reno*: Terence E. Terras ♦ **New Jersey** *Hawthorne*: Donna Beaton ♦ **New Mexico** *Santa Fe*: Leon Weiner ♦ **North Carolina** *Creedmoor*: Jennifer Jeffreys-Chen. *Durham*: Kyle D. Hain. *Hendersonville*: Robert C. Fisher. *Kernersville*: Dr. Jean A. Marr. *Manteo*: Eileen Alexanian ♦ **Ohio** *Athens*: Colette Harrington. *Toronto*: Vincent Restifo ♦ **Oregon** *Beaverton*: Robert H. Burns. *Clackamas*: Evelyn A. Elder. *Salem*: Donald Lee Toney. *Scappoose*: Cinda V. di Raimondo ♦ **Pennsylvania** *Schuylkill Haven*: Janet L. Steinmetz. *Wernersville*: Lori Perchansky. *Yardley*: Peter R. Stadelmeier ♦ **South Carolina** *Sumter*: James S. Markides ♦ **Tennessee** *Altamont*: Clayton L. Shirlen ♦ **Texas** *Corpus Christi*: Warren A. Rees. *El Paso*: Richard A. Laspada. *Houston*: Frieder H. Lauer ♦ **Virginia** *Hampton*: Edward A. Goodman. *Sterling*: Donna B. Rios ♦ **Washington** *Lakebay*: Karen Lynn Geiger ♦ **Wisconsin** *Beaver Dam*: Thomas G. Wendt. *Milwaukee*: William Bailey



Answers (See pp. 81-82 of the Spring 2000 issue for the questions):

(1) d, (2) a, (3) b, (4) c, (5) c, (6) d, (7) b, (8) b, (9) a, (10) a, (11) c, (12) b, (13) b, (14) d, (15) a, (16) c, (17) b, (18) d, (19) b, (20) c, (21) b, (22) d, (23) d, (24) d, (25) d

Book Reviews

Susan B. Johnson & Jana E. Miyahira-Smith, Editors

THE MICROWORLD OF DIAMONDS

By John I. Koivula, 157 pp., illus., publ. by Gemworld International, Northbrook, IL, 2000. US\$95.00*

John Koivula has very successfully created a text that should excite all gemologists, especially lovers of diamonds. In addition, for those interested in gemstone photomicrography, there are more than 400 beautiful and fascinating color photographs.

The opening chapters discuss the virtues of diamonds and the 4 Cs, followed by a brief glossary of diamond properties. Chapter 4 starts with the origins of diamonds, and then proceeds to a detailed discussion of diamonds in ancient times, chemical formulas, crystal structure, and optical and physical properties; it ends with geologic and geographic locations. Chapter 5 covers inclusion identification, breaking the topic down into a number of levels. The author begins by discussing the importance of the microscope to gemology. He then delves into the laboratory use of such sophisticated techniques as X-ray diffraction, laser Raman microspectrometry, and structural and chemical analysis for research and identification.

Chapter 6 begins with the evolution of the microscope from simple lenses to the modern instruments we have at our disposal today. Also discussed are the various lighting techniques used in photomicrography. Later chapters are devoted to micro-features of natural diamonds, diamond enhancements, gem-quality synthetic diamonds, and diamond simulants. The book ends with a comprehensive list of diamond-related definitions. One somewhat unusual feature is that a bibliography is

found at the end of each chapter rather than at the back.

It is difficult to find fault with this book: It is very readable, and the author's marvelous photomicrographs are a feast for the eyes. Readers of *Gems & Gemology* will, I am sure, appreciate the time and effort that have gone into the production of *The MicroWorld of Diamonds*.

ANTHONY DE GOUTIÈRE

Victoria, British Columbia, Canada

GEMSTONES: QUALITY AND VALUE, Volume 1

By Yasukazu Suwa, 143 pp., illus., publ. by Sekai Bunka Publishing, Tokyo (2nd ed., English translation), 1999. US\$84.00*

So you've determined that the stone you're looking at is a natural alexandrite. Now the question is, "Where does it fit in the world of gemstones?" Is it the finest quality? If not, what does a finer quality look like? How rare is it in the marketplace? Comparing two alexandrites, which one is more valuable? How much more valuable?

The answers to these questions usually emerge from years of experience in the colored stone industry. But even with experience, there are often gaps in our knowledge. Unless we are constantly working with a large range of sizes and qualities of gemstones, it can be difficult to know this information and even more difficult to communicate it to others. For 24 of the more popular gemstones, this book does an amazing job of drawing us into their marketplace. Included are four-page sections on aquamarine, amethyst, alexandrite, round brilliant diamond,

melee diamond, Colombian emerald, Zambian emerald, Sandawana emerald, jadeite, lapis lazuli, moonstone, "light" opal, black opal, peridot, Mogok ruby, Thai ruby, rhodolite, Sri Lankan sapphire, Kashmir sapphire, pink topaz, tanzanite, green tourmaline, Paraíba tourmaline, and turquoise. Additional sources also are mentioned in some of the sections (e.g., turquoise has descriptions for material from Arizona, Iran, and China). Some additional varieties or species are briefly mentioned as well (e.g., almandite and grossularite in the rhodolite section).

Highlighting the book are color photographs of more than 500 different loose stones or pieces of stone-set jewelry, with more than a quarter of these listing carat or gram weight and value in U.S. dollars. For each stone except Kashmir sapphire, Mr. Suwa has provided a Quality Scale grid with five beauty grades across the top and seven levels of tone along the side, for a total of 35 possible combinations. Many of these combinations—from three (for melee diamond) to 28 (for jadeite)—are illustrated by color photos of individual stones. For most of these gems, these are the best visual representations of quality ranges this reviewer has ever seen. An additional chart shows which of these examples would fall within one of three grades of gem quality, jewelry quality, or accessory quality. These three grades also are used in two other charts: One shows what percentage of each grade in a

*This book is available for purchase through the GIA Bookstore, 5345 Armada Drive, Carlsbad, CA 92008. Telephone: (800) 421-7250, ext. 4200; outside the U.S. (760) 603-4200. Fax: (760) 603-4266.

particular carat weight would be found in the fashioned stone market, and the other gives a value index for three different carat weights and the three different quality grades, to illustrate the relative values of different weights or grades.

The color printing in *Gemstones: Quality and Value* is excellent, with the possible exception of the aquamarine chapter, where the stones shown in the "country of origin" section appear very different in color and saturation from those reproduced on the quality scale.

I was first introduced to this book by a student who was taking one of our Colored Stone Grading extension classes. She is a consumer who has the time, money, and passion to learn as much as she can about gemstone quality and value. She said that she constantly uses this book as a reference for making her buying decisions. Anyone in the trade who could not answer the questions posed in the first paragraph of this review when looking at any of these stones would also find this book invaluable.

DOUGLAS KENNEDY
Gemological Institute of America
Carlsbad, California

THE DIAMOND FORMULA— DIAMOND SYNTHESIS: A GEMMOLOGICAL PERSPECTIVE

By Amanda S. Barnard, 166 pp.,
illus., publ. by Butterworth-
Heinemann, Oxford, England, 2000.
US\$39.95*

This book provides the gemologist with a convenient summary of the important concepts related to the synthesis of diamond, the identification of gem-quality synthetic diamonds, and the potential impact of synthetic diamonds on the jewelry industry. The author has surveyed the scientific and gemological literature to organize the relevant information into a convenient and readable format.

The book is divided into three

sections. The first deals with the history of diamond synthesis, which culminated with the successful growth of diamond in the early 1950s. The second section discusses the gemological aspects. Here a summary of the physical properties of diamond is followed by a discussion of the means to identify synthetic diamonds using both standard gem-testing equipment and the more advanced scientific instruments that are found today in many gemological laboratories. The information for much of this discussion was taken from articles published over the past two decades in the gemological literature. The third section briefly discusses the synthesis of thin films of diamond by chemical vapor deposition. (The products of this method have so far had little or no impact on the jewelry trade.)

The information presented in all three sections is complete and well organized. The text is illustrated by black-and-white photographs, line drawings, and several tables. There are no color photos. The one major drawback of the book is the lack of photos of some of the visual features that are key to the identification of synthetic diamonds, such as color zoning, grain-ing, metallic inclusions, and patterns of ultraviolet fluorescence. A number of such photos have been published in the gemological literature, however, and the book does contain a reference list of articles taken from the literature through 1997.

This book is a valuable resource for gemologists interested in a summary of information on synthetic diamonds. Since gem-quality synthetic diamonds continue to be grown from metallic catalysts in high temperature/high pressure equipment, the information on synthetic diamond identification presented here is valid and will likely continue to be so until other synthesis techniques are developed.

JAMES E. SHIGLEY
Gemological Institute of America
Carlsbad, California

GEMS AND GEM INDUSTRY IN INDIA

By R. V. Karanth, 406 pp., illus., publ.
by the Geological Society of India,
Bangalore, India, 2000. US\$75.00
(hardbound), US\$60.00 (paperback).
E-mail: gsocind@bgl.vsnl.net.in

In dedicating this book to Peter Read, John Sinkankas, Basil Anderson, and L. A. N. Iyer (of Mogok gem-tract memoir fame), the author reveals that he was able to "pick up the threads of Gemmology" from their works. With this volume, Karanth has created a very readable general textbook of his own, for Indian gemologists in particular, while opening up the country's gem scene to non-Indian readers.

A short introduction is followed by an interesting historical account of the Indian gem industry, from pre-history to the present. Tables showing the imports and exports of gem and jewelry items between 1963 and 1996 illustrate the phenomenal growth in the country's diamond trade, by a factor of over 6,000 in terms of value within three decades! Subsequent chapters deal with the properties of gemstones, analytical methods, gem cutting—including a very good discussion of India's artisanal operations—and gemstone synthesis. The final chapters describe gem materials and their occurrences, with special reference to India (one of the book's strong points).

There are 119 black-and-white figures and eight full-color pages, each with six separate pictures. The black-and-white figures probably started out as reasonable photographs, but the printed reproductions leave a great deal to be desired. The color plates are better, but the objects often are too small within the frame. Typographical errors abound, but they are seldom serious and usually do not detract from the meaning of the text. There is a thorough international bibliography and a detailed appendix of Indian gemstone localities.

Gems and Gem Industry in India succeeds in producing a reasonably comprehensive gemology text for Indian students, and also in describing the modern Indian scene with localities and geological data for others. Readers will be alerted to India's potential in gemstone resources, and to the very rapid growth of its cutting and jewelry industries.

E. ALAN JOBBINS
Caterham, Surrey, England

BLACK OPAL

By Greg Pardey, hardcover, 204 pp., illus., publ. by GP Creations, Urungan, Queensland, Australia, 1999. With video (running time 1 hour 52 min.). US\$99.95. www.gpcreations.senet.com.au

With almost 30 years of experience as a commercial cutter of the famous black opal of Lightning Ridge, New South Wales, Greg Pardey explains "everything you need to learn about opal cutting," including tricks of the trade and step-by-step instructions. The instructions in the text are matched by the steps shown in the video—with the notable exception of a sanding step, which is described in the text only.

Background information on the occurrences of precious opal in the Great Artesian Basin is given, along with brief but useful remarks on the unique mining methods that have been developed in the Lightning Ridge area. These techniques allow much faster prospecting and development of opal deposits than was possible before. Inasmuch as the basin covers an enormous region in the eastern half of the continent, Mr. Pardey predicts that precious opal

will be produced for many years to come. These topics are treated in the first 23 minutes of the video, which is exceptionally clear and easy to follow.

Next comes the all-important art of examining black opal masses, which often occur in rough, nodular shapes that are coated with clay, and require careful delineation of the parts that may contain "precious" material. Beginning with an unprepossessing nodule, Mr. Pardey shows how touches of the grinding wheel open up the interior and give clues to the position of precious opal layers within the nodule. In this example, he eventually produces two fine cabochons, nicely shaped, with generous layers of precious opal on top of natural backings of dark gray potch. Because the layers of black opal usually are very thin, the opal typically is salvaged by cementing it to backings of black potch or to obsidian (the potch being preferred) to form doublets. Ultra-thin layers of precious material often are cemented both to a backing and to a lens-shaped cap of rock crystal quartz to form triplets. All of these steps—along with types of machinery and accessories, polishing agents, and more—are described in the book and the video.

On the whole, Mr. Pardey's combination book/video succeeds in teaching his method of cutting Lightning Ridge opal. However, his text could have been edited more closely. There are redundancies, misspellings, and other grammatical faults, and the content is sufficiently complex that it needs an index, which is lacking. Nevertheless, it is all understandable and interesting, especially the video. Lapidary and gemology clubs may find the video useful in two showings, the first on

current mining practices and machinery in the Lightning Ridge region, and the second on the lapidary processes.

JOHN SINKANKAS
*Peri Lithon Books
San Diego, California*

OTHER BOOKS RECEIVED

Diamonds and Mantle Source Rocks in the Wyoming Craton with a Discussion of Other U.S. Occurrences, by W. Dan Hausel, *Report of Investigations No. 53, 93 pp., illus., publ. by the Wyoming State Geological Survey, Laramie, WY, 1998, US\$10.00.* This volume is concerned primarily with descriptions of the diamond-bearing kimberlites and related rocks in the Wyoming craton, which underlies Wyoming and encompasses parts of Colorado, Montana, Idaho, Nevada, and Utah. More than 100 kimberlites and a large lamproite field are known in this region, and more than 130,000 diamonds have been produced so far. Yet diamonds in both primary—kimberlite or lamproite pipes—and secondary occurrences have been reported in about two dozen other states in the U.S. Each of these occurrences is described, which makes this the most complete compilation of its kind. The location maps, photos of occurrences, and original references also make this a truly valuable acquisition (at a nominal price)—not only for those interested in the history and future potential of diamonds in the United States, but also for those who wish to visit these localities.

A. A. LEVINSON
*University of Calgary
Calgary, Alberta, Canada*

Gemological



ABSTRACTS

EDITOR

A. A. Levinson
*University of Calgary
Calgary, Alberta, Canada*

REVIEW BOARD

Troy Blodgett
GIA Gem Trade Laboratory, Carlsbad

Anne M. Blumer
Bloomington, Illinois

Peter R. Buerki
GIA Research, Carlsbad

Jo Ellen Cole
GIA Museum Services, Carlsbad

R. A. Howie
Royal Holloway, University of London

Mary L. Johnson
GIA Gem Trade Laboratory, Carlsbad

Jeff Lewis
New Orleans, Louisiana

Taijin Lu,
GIA Research, Carlsbad

Wendi M. Mayerson
GIA Gem Trade Laboratory, New York

James E. Shigley
GIA Research, Carlsbad

Jana E. Miyahira-Smith
GIA Education, Carlsbad

Kyaw Soe Moe
GIA Gem Trade Laboratory, Carlsbad

Maha Tannous
GIA Gem Trade Laboratory, Carlsbad

Rolf Tatje
Duisburg University, Germany

Sharon Wakefield
Northwest Gem Lab, Boise, Idaho

June York
GIA Gem Trade Laboratory, Carlsbad

Philip G. York
GIA Education, Carlsbad

COLORED STONES AND ORGANIC MATERIALS

Colloidal and polymeric nature of fossil amber. D. Gold, B. Hazen, and W. G. Miller, *Organic Geochemistry*, Vol. 30, No. 8B, 1999, pp. 971–983.

A prevailing view among organic geochemists is that amber consists of an insoluble, continuously cross-linked, integral polymer network. In this study, four samples of amber (from the Baltic, Dominican Republic, South Carolina, and North Dakota) ranging from ~70 to ~30 million years old, as well as two samples of modern copal (New Zealand) and one of fresh resin (Minnesota), were used to test these assumptions about amber's molecular structure and composition. Pieces of each sample were heated and examined with a microscope. Portions were dissolved in an organic solvent (N,N-dimethyl-formamide [DMF]), and the liquid was examined with dynamic light scattering, scanning electron microscopy, gel permeation chromatography, infrared spectroscopy, and viscometry. The insoluble solid fraction was examined using dynamic rheology measurements.

The authors' interpretation of the data suggests that a large portion of amber does not consist of a tightly linked polymer network. Rather, tight polymers exist in discrete "packets" of insoluble, though solvent-swella-ble, colloidal particles. These are linked to one another, but can be dispersed when exposed to certain organic solvents (e.g., DMF). Analysis of the recent resins suggests that their structure results from reactions with air that modify the

This section is designed to provide as complete a record as practical of the recent literature on gems and gemology. Articles are selected for abstracting solely at the discretion of the section editor and his reviewers, and space limitations may require that we include only those articles that we feel will be of greatest interest to our readership.

Requests for reprints of articles abstracted must be addressed to the author or publisher of the original material.

The reviewer of each article is identified by his or her initials at the end of each abstract. Guest reviewers are identified by their full names. Opinions expressed in an abstract belong to the abstractor and in no way reflect the position of Gems & Gemology or GIA.

© 2000 Gemological Institute of America

surfaces of tiny packets of resin as they are exuded from a tree. Subsequent fossilization results in polymerization within, and cross-linking between, the preexisting packets and the eventual formation of amber. Volatile organic material of low molecular weight becomes trapped between these packets, and is released as they disperse under the influence of solvents. JL

DSC-measurements of amber and resin samples. P. Jablonski, A. Golloch, and W. Borchard, *Thermo-chimica Acta*, Vol. 333, 1999, pp. 87–93.

An amber sample is not necessarily the same age as the geologic formation in which it is found, because amber can be cycled by sedimentary processes before reaching the site of its final deposition. Except for the relatively few samples that contain insect fossils, age determination of amber has proved problematic due to its variable chemical composition, which produces only approximate radiometric ages. The analyses undertaken in this study seek a correlation between thermal behavior and age.

Differential scanning calorimetry (DSC) was used to measure exothermal characteristics (i.e., the evolution of heat) during the transformation of amber from a solid polymer to a liquid as a result of the annealing of three amber samples spanning a wide age range (10–25, 40–60, and 70–135 million years old). These measurements were compared to those of a recent (25-year-old) resin sample. The size of the exothermal peaks recorded correlates to the amount of volatile or reactive components, and is therefore a function of age. Because they recorded little difference in the thermal behavior of the oldest two samples, the authors suggest that the transformation of resin into amber is essentially complete after 60 million years. Given the small sample population, the results of this study are considered preliminary. JL

Grafting of cryopreserved mantle tissues onto cultured pearl oyster. C. Horita, H. Mega, and H. Kurokura, *Cryo-Letters*, Vol. 20, 1999, pp. 311–314.

Because the color of a cultured pearl is thought to be controlled mainly by the genetics of the donor mantle, white oysters are the preferred source of the mantle tissue grafted into Japanese oysters for pearl nucleation. However, white oysters are rare in both wild and cultivated populations. Thus, when white oysters are found, the mantle tissue must be preserved until it is used. This article describes experiments with cryopreservation (i.e., freezing) of such materials and compares the results with those obtained using “control” samples of fresh mantle tissue.

After careful preparation, strips of mantle tissue from a white pearl oyster (*Pinctada fucata martensii*) were cryopreserved for 14 months in liquid nitrogen. After thawing, the pieces were cut into 2 mm squares, and two squares were inserted into each pearl oyster (together with shell-bead nuclei, the standard procedure for saltwater cultured pearls); harvesting occurred 15 months later. An approximately equal percentage (~56%) of oysters in both

groups survived. However, the harvest rate (i.e., the number of cultured pearls per oyster) was significantly lower in the cryopreserved group compared to the control group (1.22 versus 1.86). Also, 77.2% of the samples obtained from oysters with cryopreserved mantles were nacreous cultured pearls of commercial value, compared to 96.2% for the control group.

It is the epithelial cells in the piece of mantle tissue that secrete the nacreous layer on the accompanying shell bead. Cryopreservation is thought to damage those cells, thereby decreasing their ability to form nacreous layers. However, no difference in quality was noted between nacreous pearls from cryopreserved mantle tissue and those from fresh mantle tissue. Thus, the main problem with this cryogenic technique is its low harvest rate.

MT

The opal bug—The role of bacteria. *Minfo*[®], *New South Wales Mining and Exploration Quarterly*, No. 65, November 1999, pp. 26–29.

The generally accepted explanation for the origin of the Australian opal deposits is that they formed very slowly in cracks and other voids, and as replacements in fossils, from aqueous silica gels. In this *weathering model*, these gels are thought to be derived from the intense chemical weathering of sedimentary rocks (mostly feldspathic sandstones) under the action of percolating groundwater. Conditions of low (i.e., atmospheric) pressure and quiescence are required. However, two alternate models were presented at the 1st National Opal Mining Symposium held in Lightning Ridge, Australia, in March 1999.

The *syntectonic model* advocates that faults formed by tectonic events provided the pathways for movement of silica-laden fluids from which opal precipitated. This model requires that the opal be precipitated rapidly from pressurized fluids with temperatures (i.e., >100°C) that are well above those usually associated with surface processes, and that the tectonic features (i.e., faults) and opal precipitation are coincident. The *bacteria model* stems from the recognition, by high-resolution electron microscopy, of layers of bacteria within “nobbies”—mostly rounded, irregular masses of potch opal from Lightning Ridge—and evidence of fungi lining the cavity walls that surround nobbies. The presence of these organisms, which are believed to be derived from the overlying soil and rock material, suggests that the nobbies formed at temperatures of 20°C or less by slow and partial filling events that supplied siliceous solutions into open cavities. The bacteria may have played a part in the precipitation of the opal, by acidifying their environment and promoting the growth of the tiny silica spheres that constitute opal. AAL

Raman spectroscopic study of 15 gem minerals. E. Huang, *Journal of the Geological Society of China* [Taiwan], Vol. 42, No. 2, 1999, pp. 301–318.

The Raman active modes of each of 15 gem minerals have been collected in the low-wavenumber (~1500–150 cm⁻¹)

and high-wavenumber (~3800–2800 cm⁻¹) regions. Typical Raman spectra are presented for beryl, chrysoberyl, corundum, diamond, grossular, jadeite, kyanite, nephrite, olivine, quartz, spinel, topaz, tourmaline, zircon, and tanzanite. A flow chart is presented to assist in the identification of these minerals from their characteristic Raman modes. RAH

Spectres Raman des opales: Aspect diagnostique et aide à la classification [Raman spectra of opals: Diagnostic features and an aid to classification]. M. Ostrooumov, E. Fritsch, B. Lasnier, and S. Lefrant, *European Journal of Mineralogy*, Vol. 11, No. 5, 1999, pp. 899–908 [in French with English abstract].

Because Raman spectroscopy is sensitive to short-range order and water content, this nondestructive method is more useful than X-ray diffraction for classifying opals. The position of the apparent maximum of the main Raman band at low wavenumbers can be used to classify opals according to their degree of crystallinity. The most amorphous opals are those from Australia, which have a maximum beyond 400 cm⁻¹, whereas the maximum for better-crystallized Mexican opals is at ~325 cm⁻¹; Brazilian opals are intermediate between the two. The position of the various bands in the Raman spectra of the samples appears to be characteristic of their geographic origin and geologic origin (volcanic versus sedimentary). RAH

Texture formation and element partitioning in trapiche ruby. I. Sunagawa, H.-J. Bernhardt, and K. Schmetzer, *Journal of Crystal Growth*, Vol. 206, 1999, pp. 322–330.

Trapiche rubies have six red growth sectors separated by six opaque yellow to white dendritic (i.e., branching) “arms” that run from the central core to the six corners of the hexagonal crystal (see Summer 2000 Gem News, pp. 168–169). This article explores the trace-element chemistry and origin of these unusual textural features, which are found in some specimens from Mong Hsu, Myanmar.

X-ray microfluorescence and electron microprobe analyses, as well as microscopic examinations, on polished slabs cut perpendicular to the c-axis showed both chemical and growth zoning. The opaque arms consist of ruby with heterogeneous concentrations of solid (e.g., calcite and dolomite), liquid, or two-phase inclusions. Zoning of trace elements (particularly chromium) revealed differential rates of crystal growth. The authors conclude that the opaque arms formed first during a period of rapid growth; the red growth sectors formed during a subsequent period of slower, layer-by-layer growth. The rapid growth implied by trace-element partitioning in the arms was controlled by temperature. The growth of the interstitial ruby phases was governed by the kinetic factors dictated by the dendritic branches. JL

Trace-element fingerprinting of jewellery rubies by external beam PIXE. T. Calligaro, J.-P. Poirot, and G. Querré, *Nuclear Instruments and Methods in Physics Research B*, No. 150, 1999, pp. 628–634.

PIXE (proton-induced X-ray emission) is a powerful analytical technique that enables the determination of chemical elements with great accuracy and precision (even in trace amounts). With such a “chemical fingerprint,” it is sometimes possible to determine the geographic origin of a gemstone. In this case, 64 rubies mounted in a prestigious necklace were analyzed by PIXE at the Louvre Museum in Paris. Their minor- and trace-element contents were compared to those in a database of 200 rubies from deposits in Afghanistan, Cambodia, India, Kenya, Madagascar, Myanmar, Sri Lanka, Thailand, and Vietnam. Multivariate statistical processing of the data for Ti, V, Cr, Fe, and Ca yielded a high probability that 63 rubies were from Myanmar. The remaining ruby came from either Thailand or Cambodia.

Although PIXE requires sophisticated equipment, the technique offers high sensitivity and accuracy, is nondestructive, and can be performed on objects of any size without sample preparation. WMM

DIAMONDS

Color cathodoluminescence of natural diamond with a curvilinear zonality and orbicular core. E. P. Smirnova, R. B. Zezin, G. V. Saparin, and S. K. Obyden, *Doklady Earth Sciences*, Vol. 366, No. 4, 1999, pp. 522–525.

Rough diamonds from several localities in Yakutia and the Ural Mountains were studied by cathodoluminescence of plates cut parallel to selected planes [e.g., (100)], to determine the origin of their unusual structure. These diamonds have orbicular cores surrounded by flat faces, which results in a “curvilinear” structure. The diamonds are believed to have formed in two stages. The orbicular core formed first from an immiscible drop of superdense, carbon-bearing fluid within a silicate melt. As indicated by certain textures, particularly “dendritic arrows” that point inward from the core’s surface, diamond crystallization proceeded from the periphery to the center of the core; certain metals crystallize in an analogous manner. The diamonds acquired their external octahedral shape during the second growth stage, in which the cores were overgrown by diamond in a linear manner. AAL

Diamonds from Wellington, NSW: Insights into the origin of eastern Australian diamonds. R. M. Davis, S. Y. O’Reilly, and W. L. Griffin, *Mineralogical Magazine*, Vol. 63, No. 4, 1999, pp. 447–471.

Rough diamonds (~0.17 ct) from alluvial deposits near Wellington, New South Wales (NSW), are characterized on the basis of their morphology, mineral inclusions, δ¹³C values, N content and aggregation state, and internal structure. The diamonds represent two types of formation.

The larger group is indistinguishable from diamonds found worldwide in kimberlitic and lamproitic host rocks; this group is inferred to have formed in a peridotitic mantle source in Precambrian subcratonic lithosphere. The smaller group has unique internal structures (which show evidence of growth in a stress field), unusually heavy $\delta^{13}\text{C}$ values, and Ca-rich eclogitic inclusions. This group is inferred to have formed in a subducting plate. Diamonds of both groups have external features (corrosion structures and polish) that indicate transport to the surface by lamproite-like magmas. The diamonds show evidence of long residence at the Earth's surface and significant reworking; they are not accompanied by typical diamond indicator minerals.

Alluvial diamonds from the Wellington area were discovered in 1851, but the largest known accumulation of diamonds (approximately 500,000 carats) in New South Wales was discovered 600 km to the northeast at Copeton and Bingara. Diamonds from the latter two localities have received the most scientific study over the years. Only ~4,000 carats of diamonds have been reported from the Wellington area. RAH

Fluvial characteristics of the diamondiferous Droogeveldt gravels, Vaal Valley, South Africa. R. I. Spaggiari, J. D. Ward, and M. C. J. de Witt, *Economic Geology*, Vol. 94, No. 5, 1999, pp. 741–748.

The Droogeveldt gravels, one of the more famous alluvial diamond diggings in South Africa's Vaal River basin, were mostly exploited before 1917. Nearly 500,000 carats of diamonds, with an average stone size of >1 ct, were recovered. This includes 18 diamonds that weighed more than 100 ct each. The richest deposits were linear, gravel-filled depressions in the bedrock, known as "sluits" to the 19th century prospectors and miners. Three hypotheses have been proposed to explain the origin of these deposits. The first suggested that because the sluits are linear, they represent eroded kimberlite dikes. Another proposed that the gravels occupying the sluits were derived from local erosion of older but topographically higher deposits and were deposited via slumps and landslides into the depressions. The third hypothesis characterized the sluits as remnants of a paleo-Vaal River channel system.

Although the trend of the sluits parallels that of regional dikes and rock lineaments, the lack of kimberlite in the gravels suggests that they were not derived from the weathering of kimberlite dikes. Also, although some of the sediments were surely derived from local erosional processes, the source of the diamondiferous gravels was a fluvial system. Well-rounded and smooth rock fragments—as well as scoured, pot-holed, and polished bedrock—all point to a fluvial origin for the gravels. Ancient rivers of the paleo-Vaal drainage basin exploited preexisting weaknesses in the bedrock to cut their courses; this explains why the sluits are parallel to regional rock fabrics. The bulk of the diamonds probably came from kimberlites in the greater Kimberley area. JL

Growth of high purity large synthetic diamond crystals.

R. C. Burns, J. O. Hansen, R. A. Spits, M. Sibanda, C. M. Welbourn, and D. L. Welch, *Diamond and Related Minerals*, Vol. 8, No. 8–9, 1999, pp. 1433–1437.

Researchers at De Beers's Diamond Research Laboratory have succeeded in growing relatively large (up to 4.6 ct) type IIa near-colorless synthetic diamonds. This research builds on previous methods of growing large (up to 25 ct), nitrogen-rich, yellowish type Ib synthetic diamonds using a cobalt/iron solvent/catalyst. This and other solvent/catalyst combinations are discussed, as well as the use of "nitrogen getters"—elements such as titanium and aluminum that remove nitrogen from the melt by forming stable nitrides—to grow type IIa near-colorless synthetic diamonds with very low nitrogen contents (0.01–0.4 ppm).

Cobalt/titanium and iron/aluminum solvent/catalyst combinations are used. One significant drawback to the "nitrogen getters" is that their products (e.g., titanium nitride) contribute to the development of large amounts of inclusions. The concentration of inclusions increases proportionally to the amount of "getters" in the melt. Adding boron to the iron/aluminum solvent/catalyst produced synthetic blue diamonds (type IIb) up to 5.1 ct. The presence of long-lived phosphorescence, following exposure to short-wave UV radiation, helps distinguish these synthetics from natural diamonds. PGY

The impact of new diamond marketing strategies on the diamond pipeline. C. Even-Zohar, *Mazal U'Bracha*, Vol. 15, No. 115, November 1999, pp. 35–38, 40, 41, 44–46.

For the first time since the 1930s, De Beers is experiencing competition from rough diamond producers either entering the business (e.g., Canada's Ekati mine) or no longer selling through the CSO (e.g., Australia's Argyle mine). This insightful article analyzes the profound ramifications throughout the diamond pipeline.

The most dramatic change stems from the fact that the equilibrium between supply and demand—and the price stability that De Beers has historically maintained through the single-channel marketing system—is no longer guaranteed by De Beers. This will result in De Beers-CSO being transformed from essentially a cartel structure to that of "Dominant Player in a Competitive Environment." Three major ramifications are that: (1) each rough diamond producer will fight for market share; (2) De Beers will stop supporting the price of rough, which will fluctuate; and (3) De Beers will no longer hold "buffer stocks," thus enabling its rough diamond competitors to sell more.

Meaningful competition currently exists only at the rough diamond production level. Ultimately, competitive dominance, or even survival, will require building a "diamond pipeline" from the mine to the consumer. Different supply chains will emerge by means of such financial mechanisms as consolidations, mergers, vertical integration, and joint alliances. Evidence for an emerging supply

chain is found in the highly publicized relationship between Tiffany & Co. (a retailer) and Canada's Aber Diamond Corp. (a likely rough diamond producer in 2003). Less visibly, De Beers itself has expanded downstream as a diamond manufacturer; it is also a seller of polished diamonds, although only through sightholders at present.

In the future, the success of a diamond jewelry retailer may depend on forming a strategic alliance with a polished diamond manufacturer whose affiliation with a rough producer will ensure the appropriate quality and quantity of rough. AAL

Magnetic mapping of Majhgawan diamond pipe of central India. B. S. P. Sarma, B. K. Verma, and S. V. Satyanarayana, *Geophysics*, Vol. 64, No. 6, 1999, pp. 1735–1739.

Geophysical surveys that use minute differences in the magnetic properties of rocks are well established in various aspects of kimberlite exploration, particularly for locating a pipe and determining its aerial extent. This article illustrates how such surveys can be used to interpret vertical features within a single kimberlite pipe.

For this study, a three-dimensional magnetic model of the Majhgawan kimberlite pipe (currently the only producing diamond mine in India) was constructed by making reasonable assumptions about the responses of the different rock types that make up the pipe within the regional geomagnetic field. The computed results compare favorably with field data obtained by an older magnetic survey of the same pipe. Both reveal the complexity of the pipe at depth, and support the hypothesis that the pipe is made up of three concentric vertical intrusive bodies, and that the central and most diamondiferous portion might be the result of a later intrusion. JL

Manufacture of gem quality diamonds: A review. D. Choudhary and J. Bellare, *Ceramics International*, Vol. 26, 2000, pp. 73–85.

This article presents a technical review of current technology to grow synthetic diamond. Two methods—the *solvent catalyst* and the *temperature gradient* (or *reconstitution*) technique—have been used to produce single-crystal synthetic diamond at high temperatures and pressures. The article focuses on describing the thermodynamics and kinetics of the diamond growth process, and the kinds of apparatus used for this purpose. [Abstracter's note: The solvent catalyst technique uses a solvent (usually a molten metal) to promote the direct conversion of graphite into diamond at high temperature and pressure; this method was first developed by researchers at General Electric to grow gem-quality synthetic diamonds in a "belt" apparatus. In the reconstitution technique, synthetic diamond is grown from a source of carbon (typically diamond powder), also at high temperature and pressure. Here, the driving force for the reaction is a temperature gradient within the apparatus. The carbon dissolves in a solvent at the hotter end of the apparatus, and the car-

bon atoms crystallize on a diamond seed crystal at the cooler end of the apparatus. This technique is used by Sumitomo, De Beers, General Electric, and Russian researchers to grow gem-quality diamonds.]

The vast majority of the synthetic diamonds produced are smaller-size crystals used for various industrial applications (usually as abrasives or in cutting tools). A brief mention is made of the growth of polycrystalline diamond by the chemical vapor deposition (CVD) technique. The reference list includes citations for many of the important published articles on diamond synthesis. Little mention is made of the use of synthetic diamonds for jewelry applications. Nonetheless, the article is a good summary of the present state of diamond synthesis technology. JES

Namibia's diamond riches. *Mining Journal*, London, Vol. 333, No. 8555, October 29, 1999, pp. 344–345.

Following a chronology of the history of diamonds in Namibia since their discovery in 1908 to the establishment of the Namibian Diamond Corp. (or Namdeb, equally owned by the Namibian Government and De Beers) in 1994, the current status of Namibian diamond-mining operations is presented. Particular emphasis is placed on the "forbidden territory," a diamond-rich area along the Atlantic coast of Namibia that extends from the Orange River north about 310 km to Hottentot Bay. Namibia's traditional onshore diamond-mining operations are concentrated in this region, particularly in beach or shelf gravels that sit on deeply gullied bedrock. Namdeb's most extensive operations are along a thin coastal strip extending about 100 km north of the Orange River, with a width of 3 km in the southern end that narrows to just 200 m in the north. The average ore thickness is about 2 m. The depth of overburden, while generally less than 7 m, can reach 20 m. Large-capacity industrial vacuum machines were introduced in 1993 for collecting the diamond-bearing sediments.

As an extension of onshore operations, diamondiferous gravels are recovered up to 20 m below sea level (~200 m seaward of the high water mark) by constructing protective sand walls along the shoreline. Although onshore production is steady at about 700,000 carats annually, the ore grade is decreasing; proven onshore reserves are sufficient to last another 10 years. The vast majority of Namibia's diamonds are gem quality with values of about \$290/ct, among the highest in the world.

Namibia's future as a major diamond producer lies with offshore marine mining, which began in the early 1960s. Although mining initially was restricted to shallow waters, recent technological advances have enabled the mining of these huge, low-grade (but high-value) offshore diamond reserves up to the edge of the continental shelf (or 200 m water depth). The fleet now consists of eight vessels owned by De Beers Marine. Geophysics is used to produce high-resolution images of the ocean floor, and sampling locations are pinpointed with the global positioning system (GPS). Seabed crawlers agitate the sediment with blasts of water,

and use suction to draw gravel onboard the mining vessels, where the diamonds are extracted. Annual offshore production is currently about 500,000 carats, although this figure is expected to increase steadily. MT

Rough rewards. L. Rombouts, *Basel Magazine*, August 2000, pp. 39, 41–43.

Highlights of 1999 world rough diamond production in 20 countries are presented. For the more important mines, these highlights include tonnes of ore mined, carats recovered, average value of production, and the operator (e.g., Debswana). The total world supply of rough in 1999 was valued at \$8.1 billion, of which \$7.25 billion came from mine production (up 8% over 1998) and the remainder from De Beers's stockpile. Botswana was the largest producer by value, with the Jwaneng mine alone producing \$1.14 billion of rough.

World production by volume (weight), however, declined from 120 million carats (Mct) in 1998 to 111 Mct in 1999. This was due to a sharp decrease in production from the Argyle mine as the pit is being expanded. Argyle's production will decrease even further in the next few years, but it should rebound to 1999 levels in 2003 (when mining is scheduled to start in the expanded pit). By volume, Australia is the largest producer, with almost all of its diamonds coming from the Argyle mine. Social, political, and economic effects of diamond mining on selected countries (e.g., South Africa, Angola, and Russia) are discussed briefly.

The article also discusses new mine developments and exploration worldwide, with particular emphasis on Canada. In 1999, during its first year of full production, Canada's Ekati mine produced 2.51 Mct valued at \$421 million (2.2% of the world's rough diamonds by weight and 5.8% by value) for an average value of \$168/ct. By 2003, with production expected from the Diavik and Snap Lake kimberlite bodies, Canada's annual contribution to world supply should increase by an additional 6–8 Mct. PGY

Spectroscopy of defects and transition metals in diamond.

A. T. Collins, *Diamond and Related Materials*, Vol. 9, 2000, pp. 417–423.

Spectroscopic and electron paramagnetic resonance (EPR) studies of nickel in diamond have been conducted for almost two decades. Recently, optical centers attributed to cobalt have also been documented. Significant progress has been made in understanding the nature of the defects and the interrelationships between the optical and EPR phenomena.

Following a brief summary of the properties of some fundamental defects that affect the optical, electronic, and EPR characteristics of diamond, Dr. Collins critically reviews the various studies of diamonds with nickel- or cobalt-related defect centers. Concluding paragraphs note that extensive experimental and theoretical studies of nickel in natural and HPHT-grown synthetic diamond

have begun to yield plausible models for the defects involved. The work on cobalt, although at an earlier stage, indicates important analogies between nickel-related and cobalt-related centers. However, there are many nickel-related defects for which no models have been devised. The challenge for future work in this area is to expand the understanding of nickel-related centers and to explain the differences in behavior between nickel and the other transition metals. SW

Study on inclusion in synthetic diamond. B. Lin, H. Wan, and M. Peng, *Kuangwu Yanshi (Bulletin of Mineralogy, Petrology and Geochemistry)*, Vol. 18, No. 4, 1999, pp. 308–309 [in Chinese with English abstract].

An inclusion in a synthetic diamond was shown by electron microprobe and X-ray diffraction analyses to be a "melnikovite" [greigite, $\text{Fe}^{2+}\text{Fe}_2^{3+}\text{S}_4$]. It is suggested that the oxidation-reduction environment during the growth of this crystal allowed the coexistence of Fe^{2+} and Fe^{3+} . RAH

Synthetic blue diamonds hit the market. C. P. Smith and G. Bosshart, *Rapaport Diamond Report*, June 4, 1999, Vol. 22, No. 20, pp. 114–116.

Until recently, most gem-quality synthetic diamonds have been deep yellow to brownish orange (type Ib), but now a blue (type IIb, containing boron) synthetic diamond has entered the market. Manufactured since 1998 by Ultimate Created Diamond Co., Golden, Colorado, this synthetic was first seen at the Tucson Gem and Mineral Show in February 1999, in stones ranging from 0.03 to 0.45 ct. Production at the end of 1999 was anticipated to be 200 carats per month. The largest rough reported was slightly over 1 ct, and the largest polished was 0.62 ct. All of the stones examined by the authors had excellent colors, ranging from "fancy light blue" to "fancy dark blue." They are grown by a thermal gradient method (called TOROID), which is more expensive than the better-known "belt apparatus" and "BARS" (split sphere) techniques.

These synthetic blue diamonds can be identified by careful observation with either a loupe or a microscope. They have characteristic and readily apparent metallic inclusions that most frequently form thick tablets oriented along growth zones. The metallic inclusions also give rise to magnetism, the strength of which is directly related to the size and number of inclusions. Color zones in these synthetics have sharp borders, in contrast to the more even coloration of natural blue diamonds. The synthetic blue diamonds are also readily identified by their distinctive chalky yellow fluorescence to short-wave UV radiation and long-lasting phosphorescence; natural type IIb blue diamonds generally are inert to both short- and long-wave UV. Because of the growing demand for fancy-color blue diamonds, the industry may well see more such synthetics in the market. PGY

Tertiary-age diamondiferous fluvial deposits of the lower Orange River Valley, southwestern Africa. R. J. Jacob, B. J. Bluck, and J. D. Ward, *Economic Geology*, Vol. 94, No. 5, 1999, pp. 749–758.

Two terraces (19–17 and ~5–2 million years old, respectively) in the lower reaches of the modern Orange River were the focus of this study, to determine the mechanism by which these alluvial diamond deposits formed. Although low grade, the terraces yield diamonds that average 1–2 ct and are predominantly (>95%) gem quality. Fieldwork was complemented by satellite-image processing and seismic data interpretation, to confirm that such deposits can be located and their boundaries delineated.

The data support the conclusion that diamonds concentrated in common sedimentological trapsites (e.g., scour pools, holes, and gravel bars) on the surface of the bedrock in the ancient river system. Diamond concentrations are higher in the older terrace deposits (10–40 carats per hundred tons) than in the younger ones (~0.3 ct per hundred tons). However, the older deposits are more difficult to locate than the extensive younger deposits. Given the usefulness of remote-sensing exploration techniques and the conclusions about fluvial controls on diamond deposition derived from this study, the authors suggest that these low-grade but high-value basal diamondiferous deposits make worthy exploration targets. JL

GEM LOCALITIES

Amethyst aus Brasilien [Amethyst from Brazil]. R. Balzer, *Lapis*, Vol. 24, No. 10, 1999, pp. 13–18 [in German].

This article briefly sketches the discovery and history of amethyst and agates in Brazil's Rio Grande do Sul State, especially the role of immigrants from Idar-Oberstein, and then describes the deposits. Amethyst occurs in vugs in the Paraná basalts, which cover about 1,200,000 km² and are 119–149 million years old. Both open-pit and underground mining are used to recover the amethyst vugs. The recovery of intact vugs is difficult and requires considerable manual labor. In most cases, the vugs are broken into pieces and the gem-quality amethyst is preformed, sorted, and exported as cutting rough. Idar-Oberstein continues to be the primary destination because of existing family ties. Consequently, only recently was a gem-cutting school established in Lageado, Rio Grande do Sul. The article is illustrated with a map and 13 excellent photos that show the landscape, mining activities, and amethyst specimens. RT

Exotic origin of the ruby deposits of the Mangari area in SE Kenya. A. Mercier, P. Debat, and J. M. Saul, *Ore Geology Reviews*, Vol. 14, 1999, pp. 83–104.

Ruby deposits in the Mangari area of southeastern Kenya occur in the Proterozoic geologic province known as the Mozambique Belt. The deposits are associated with ultrabasic bodies that were emplaced into metasedimentary rocks. The ruby-bearing ore forms local concentrations,

or less frequently pegmatitic veins, at the contact between these rocks, and it also forms veins within the ultrabasic bodies.

Petrographic studies suggest that the ruby deposits were formed at temperatures around 700°–750°C, at pressures of 8–10.5 kbar. The metasedimentary host rocks experienced a lower peak metamorphism at 620°–670°C, at pressures of 5.4 to 6.7 kbar. These data and field observations suggest that the ruby deposits were not formed by contact metamorphism of the ultrabasic intrusives with the metasedimentary rocks; rather, they were formed deeper within the earth and subsequently uplifted to their present-day exposure level when the ultramafic bodies were emplaced as thrust sheets. Elsewhere in the Mozambique Belt, ruby deposits in Tanzania (at Longido and Lossogonoi) and southwestern Madagascar (at Fotadrevo-Ejeda) occur in association with ultrabasic rocks, but both the intrusives and the country rocks were subjected to the same pressure/temperature conditions (i.e., granulite facies), which also match those of the Mangari deposits. The authors surmise that granulite-facies metamorphic conditions were required for ruby formation throughout the Mozambique Belt. JL

Mineralogical characteristics of chatoyant quartz in Luodian County, Guizhou. M. Deng, *Kuangwu Yanshi (Bulletin of Mineralogy, Petrology and Geochemistry)*, Vol. 18, No. 4, 1999, pp. 416–417 [in Chinese with English abstract].

Chatoyant quartz from the Luodian deposit may have originated in quartz veins within blue asbestos. Brown-green, light green, and bluish green in color, this quartz contains parallel fibers of tremolite. In bright sunshine or incandescent light, it shows dazzling chatoyancy. RAH

Mineralogical and geochemical investigation of emerald and beryl mineralisation, Pan-African Belt of Egypt: Genetic and exploration aspects. H. M. Abdalla and F. H. Mohamed, *Journal of African Earth Sciences*, Vol. 28, No. 3, 1999, pp. 581–598.

Precambrian (more than 570 million years old) emerald and beryl deposits in southern Egypt are associated with two different geologic features. The Nugrus Thrust, a regional ductile shear zone, hosts emerald deposits in biotite schists. Beryl associated with granitoids is found either in greisen bodies or in pegmatitic lenses and veins. Thirteen samples of beryl (color[s] unspecified) and emerald from the region were analyzed petrographically and geochemically to aid in exploration for additional deposits and to examine the generally held assumption that all Egyptian emeralds are of metamorphic origin.

Fluid flow processes associated with the emerald deposits were contemporaneous with the tectonic development of the Nugrus Thrust and the emplacement of the granitic bodies, which postdate regional metamorphic events. The chemical zoning of the emerald crystals reflects typical magmatic fractionation patterns. The data

suggest that the emerald mineralization depends on syn-tectonic intrusive events and the chemistry of magmatic fluids, rather than on host-rock chemistry or regional metamorphism. *JL*

Raspberry-red grossular from Sierra de Cruces Range, Coahuila, Mexico. C. A. Geiger, A. Stahl, and G. R. Rossman, *European Journal of Mineralogy*, Vol. 11, No. 6, 1999, pp. 1109–1113.

Hitherto unknown, grossular with a raspberry-red hue is the subject of this study, which examined one specimen to determine the cause of its unusual color. The grossular occurs as subhedral to euhedral crystals, up to ~1 cm in diameter, associated primarily with calcite and quartz in contact-metamorphic rocks. Electron microprobe analyses established the chemical composition, and both Mössbauer and UV-Vis data were gathered to examine the absorption spectra.

The primary chromophore detected was manganese (Mn). Total Mn (reported as 1.65 wt.% MnO) in the sample consisted of ~10% Mn³⁺ and probably ~90% Mn²⁺. Absorption bands indicated the presence of Mn²⁺ in the dodecahedral site. Mn³⁺ resided in the octahedral site of point symmetry $\bar{3}$, which in this grossular was slightly distorted relative to the normal garnet site. The color is related to the octahedral coordination of Mn³⁺ and the transitions it allows within the crystal structure. *JL*

Ruby from Tunduru-Songea, East Africa: Some basic observations. G. Hamid, S. M. B. Kelly, and G. Brown, *Australian Gemmologist*, Vol. 20, No. 8, pp. 326–330.

Gem corundum with a bright pink to purplish red hue is recovered from river gravels in the Tunduru-Songea area of southern Tanzania, and sold in Bangkok. Most, but not all, of these rubies appear to have been heat treated prior to sale. The rubies have refractive indices of $n_e=1.760-1.765$ and $n_o=1.768-1.773$ (yielding a birefringence of 0.008–0.009) and specific gravity values of 3.95–4.04. The characteristic inclusions found in both the obviously heat-treated and minimally heat-treated stones are described. *RAH*

JEWELRY HISTORY

The rise and fall of an enterprise cluster in Africa: The jewellery industry in South Africa. M. Da Silva, *South African Geographical Journal*, 1999, Vol. 18 No. 3, pp. 156–162.

An enterprise cluster is a spatially defined, highly specialized industrial district in which linkages and cooperation between small- and medium-size businesses provide economies of scale and scope. This article analyzes the jewelry-industry cluster of Johannesburg by tracing its development over time, and identifying patterns of change and the factors responsible for them.

The modern jewelry industry in Johannesburg dates from the late 1930s. Growth was stimulated by the coun-

try's isolation during World War II and the establishment of the South African Jewellers' Association, which frequently lobbied on behalf of the industry. During the immediate post-war period, the wholesale and retail sectors of the industry fared well compared to the manufacturing sector, which was unable to obtain protective tariffs. However, the entire jewelry industry was adversely affected in 1949 by the combined effects of import controls on jewelry and reduced gold supplies for manufacturing, both of which were motivated by government fiscal policies and the belief that jewelers were involved in smuggling. The absence of a common cultural or socioeconomic background resulted in a lack of effective political action on the part of the industry.

Conditions improved during the economic boom of the 1960s, and in 1972 the newly formed Jewellery Council of South Africa emerged to speak for an expanded trade that now included the mining and watch sectors. The industry reached its zenith in the late 1970s, but this era was short lived. By the mid-1980s, taxes on jewelry had reached 50%, effectively killing the industry.

Since the early 1990s, there has been a revival of the gem and jewelry industry in the Johannesburg Central Business District. The centerpiece is "Jewel City," a four-block complex under one roof that accommodates about 200 businesses ranging from manufacturers to diamond dealers, as well as related organizations such as the Diamond Bourse and the South African Diamond Board. At present, the industry is working together on several fronts, but only time will tell whether this commitment to collaboration will be sustained. *AMB*

The use of gemstones in antique jewellery. A. Miller, *ICA Gazette*, January/February 2000, pp. 16–17.

A brief history of antique jewelry (here defined as items older than 200 years) is presented, starting with jewelry created by primitive man. These pieces consisted of shell, seeds, and bones. Highlights of ancient Chinese, Egyptian, Greek, Etruscan, Roman, and pre-Columbian jewelry vividly demonstrate the skill and artistry of the earliest jewelers, and provide evidence of trade in gemstones. Later, Byzantine jewelers mastered the delicate art of enameling, while Medieval jewelers made magnificent ecclesiastical pieces featuring rubies, sapphires, garnets, and emeralds. For various reasons, the wearing of gems, and in some cases gold and silver, was prohibited in England and France between 1283 and the 1720s except for royalty and other privileged groups.

The jewelry arts were rejuvenated during the Renaissance, with intricate and imaginative jewels being produced. Much of what we know of Renaissance and subsequent jewelry is based on portraits. Their detail, especially since the 15th century, has enabled jewelry historians to determine not only who wore jewelry, but also to surmise which gems were used during specific time periods. A list of about 40 gemstones frequently found in antique jewelry is included. *AMB*

JEWELRY RETAILING

Mistakes jewelers make when they retire. *Jewelers' Circular Keystone*, Vol. 170, No. 10, 1999, pp. 142–144.

Wilkerson & Associates (Stuttgart, Arkansas) has assisted in more than 4,000 jewelry store closings across the U.S. over the past 30 years. The firm also helps jewelers plan for retirement well ahead of time, so that costly financial mistakes are avoided and the maximum potential of the business is realized.

Possibly the most common mistake retiring jewelers make is overestimating the value of their inventory. The typical retiring jeweler almost never recovers his or her inventory cost, sometimes losing up to 70% by selling to a bulk buyer. Another common mistake is personally financing the purchase to allow the new owner time to become profitable, when in fact the new owner may fail. Further, many jewelers mistakenly believe that their store is worth upwards of five times its annual volume.

Wilkerson & Associates recommends that, to prepare for retirement, jewelers convert as many assets as possible into cash and savings, increase their turnover, reduce receivables, and make their store as profitable as possible. The firm is currently launching a Trade Transition Association (TTA) to help jewelers properly plan for retirement. TTA will feature a retirement guidebook and a newsletter, offer a customized transition plan, and host educational seminars. *MT*

The return of the middleman. J. McDonald, *GemKey Magazine*, Vol. 1, No. 5, July–August 1999, p. 68.

Online auctions have generated more complaints of fraud than any other Internet business, creating a new niche for escrow services. Internet auction sites such as eBay are simply a venue for auction transactions, and they specifically state that they do not authenticate users, verify items offered for sale, or guarantee payments for items. The opportunities for fraud in this arena are both obvious and enormous.

Internet escrow services act as middlemen between the buyer and the seller in much the same way as escrow services in the real estate and financial securities fields. Once the parties make a deal, the buyer typically pays the escrow company the agreed price for the goods. The seller then ships the buyer the goods for inspection; usually up to three days are allowed. If the buyer is satisfied, then the escrow company is notified and immediately transmits payment to the vendor.

This article identifies four escrow firms and explains a few variations in their *modus operandi*, including fee schedules (e.g., flat or tiered sliding pricing). At least one of the firms takes responsibility for merchandise that is lost or damaged in transit in certain situations.

Internet escrow services clearly have utility in various segments of the gem and jewelry market. Ironically, one of the advantages of the Internet is that it generally eliminates the middleman, yet Internet escrow services are an outgrowth of this marketing medium. *AAL*

PRECIOUS METALS

Metallurgy of microalloyed 24 carat [sic] golds. C. W. Corti, *Gold Bulletin*, Vol. 32, No. 2, 1999, pp. 39–47.

The softness of pure gold (24K) has generally precluded its use in jewelry manufacturing in most Western societies. However, 99.0% minimum fineness is the standard in China and Taiwan, because such purchases are treated as investments. Accordingly, there is a need for hardened 24K gold that can be manufactured into jewelry. This article describes a number of alloys that have been developed with a fineness of 99.5–99.9%. The addition of 0.5 wt.% or less of an element in the finished product is called “microalloying”; gold with this fineness can still be called pure (fine) gold and sold as such (24K).

The theoretical basis for the hardening of gold is explained, and some potential alloying elements are discussed. For the small amount of alloyed material to contribute significantly to solution hardening, it must have a low density and a smaller atomic size than gold crystals. These impurities create distortions in the metallic crystal lattice structure that help prevent slipping along molecular planes. The elements that have the greatest potential for gold microalloys, on both a theoretical and experimental basis, are calcium, beryllium, and the rare-earth metals (e.g., cerium). Whereas conventional alloying with copper and silver changes the color of gold, microalloys do not produce a color change. The application of these microalloying techniques to improving the hardness of 21K or 22K gold is considered as well. *Paige Tullos*

PIXE in an external microbeam arrangement for the study of finely decorated Tartesian gold jewellery items. G. Demortier, F. Fernando-Gomez, M. A. Ontalba Salamanca, and P. Coquay, *Nuclear Instruments and Methods in Physics Research B*, No. 158, 1999, pp. 275–280.

Several ancient recipes for joining gold parts of jewelry items are known. Some include natural chrysocolla, glue, or amber, while others use alloys made from a mixture of copper, silver, and gold. Common soldering techniques were alloy brazing (the fusion of a metallic alloy at 800°–850°C, which produces a permanent joining after cooling of a liquid phase) and solid-state diffusion bonding (the diffusion at about 900°C of copper from a very fine powder of deoxidized copper ore to form an alloy). Brazing, diffusion bonding, local fusion without any additional alloy, and organic gluing are all present in one particular piece of jewelry from the Achemenide period (4th century BC).

The concentrations of copper and silver in narrow areas of finely decorated gold jewelry items of Tartesian (Spain, 5th–6th century BC) age were determined by the nondestructive PIXE (proton-induced X-ray emission) technique to identify the method of soldering. A fragment of a 5th century BC diadem (crown) recovered in the necropolis of “El Raso de Candeda” (Avila) was the main focus of this study; two pendants of similar age from a different site were also studied.

Two scans were performed on the diadem, one across the alignment of granules, the other along a parallel region where the granulations disappear. On the basis of the changes in concentrations of copper and silver along the traverses, the authors conclude that brazing was the soldering procedure used to fix the granules in the grooves. Brazing was also used to solder the pendants. *MT*

SYNTHETICS AND SIMULANTS

Controlled crystallization of emerald from the fluxed melt.

S. N. Barilo, G. L. Bychkov, L. A. Kurnevich, N. I. Leonuk, V. P. Mikhailov, S. V. Shiryaev, V. T. Koyava, and T. V. Smirnova, *Journal of Crystal Growth*, Vol. 198/199, Part 1, 1999, pp. 716–722.

Details are given of the carefully controlled procedures used to grow well-formed gem-quality synthetic emerald crystals as large as 150 ct from a flux. The starting material is a mixture of natural beryl dissolved in a low-viscosity $\text{PbO-V}_2\text{O}_5$ flux. Oriented seed crystals of synthetic emeralds cut parallel to the $(10\bar{1}0)$ and $(11\bar{2}0)$ faces are required. The growth temperature ranges from 900° to 1250°C . The best results are obtained with large-volume platinum crucibles that are rotated (dynamic mode), a cooling rate of 0.5°C per day, and a growth period of three to four months. Although chromium, and to a lesser extent vanadium, are the primary chromophores in emerald, color variations are reported in these synthetics with the addition of small amounts of cerium, molybdenum, iron, and nickel. Nickel, for example, tends to lighten the color, whereas extra iron oxide is added to obtain a yellowish green color similar to that of Ural emeralds. When properly grown, these crystals are uniform in color and exhibit no inclusions. Besides their obvious gemological use, the crystals have industrial applications in lasers and low-noise microwave amplifiers. *KSM*

Pulsation processes at hydrothermal crystal growth (beryl as example).

V. G. Thomas, S. P. Demin, D. A. Four-senko, and T. B. Bekker, *Journal of Crystal Growth*, Vol. 206, 1999, pp. 203–214.

Hydrothermally grown crystals such as synthetic quartz, ruby, sapphire, and emerald frequently show growth zoning parallel to the crystallization front (i.e., parallel to the seed plate), but there is no published explanation for this phenomenon. The sharp growth zone boundaries can be observed microscopically, or sometimes with the naked eye.

A series of experiments were carried out to determine if there is a correlation between temperature fluctuations and growth zoning. Synthetic beryl crystals were grown in an autoclave on oriented seed plates, using a temperature gradient of 70°C between the nutrient and the seed. Growth periods ranged from 15 to 25 days.

A correlation was established between temperature fluctuations (pulsations)—caused simply by switching the autoclave on and off—and growth zoning in the synthetic

beryl crystals. Periodic temperature fluctuations (e.g., 1.5°C within time intervals of 6 hours) correlated to zonality of the optical density within growth zones parallel to the seed plate. Extrapolating the results, the authors suggest that growth zoning in hydrothermal crystals can be explained by sporadic temperature variations within the autoclave, which cause pulsations in the mass transfer of the nutrients to the growth zone. *Karl Schmetzer*

TREATMENTS

Analysis of fissure-filled turquoise, emeralds, and rubies by near-infrared spectroscopy.

D. W. Armstrong, X. Wang, C. R. Beesley, and R. Rubinovitz, *American Laboratory*, Vol. 31, No. 20, October 1999, pp. 41–42, 44, 47.

One of the biggest challenges facing the gem trade is the detection of organic fillers used to improve the appearance of surface-reaching fissures in gemstones. This article focuses on the use of two nondestructive, cost-effective techniques that require little or no sample pre-treatment or preparation—near-infrared (NIR) spectroscopy and diffuse reflectance infrared Fourier transform spectroscopy (DRIFTS)—to detect and identify enhancement agents used in turquoise, emeralds, and rubies.

NIR spectra were obtained for over 30 organic resins and oils that reportedly are used to fill fractures in gemstones. The spectra of four common organic filler materials (epoxy, wax, cedarwood oil, and Thai “red oil”) are illustrated. These spectra were then compared with those for treated and untreated stones. The fillers were successfully identified in many of the samples. NIR is most effective for aggregates and opaque gems such as turquoise and, potentially, jade and chalcedony. The relatively low sensitivity of NIR was sometimes a problem for identifying fillers in treated emeralds and rubies. In those instances, the superior sensitivity of DRIFTS enabled the detection of small amounts of resins or oil in the treated samples. Thus, NIR and DRIFTS are complementary methods in gem-treatment detection technology. *MT*

The effect of the gamma-irradiation dose combined with heat on the colour enhancement of colourless quartz.

M. V. B. Pinheiro, F. S. Lameiras, K. Krambrock, J. Karfunkel, and J. B. da Silva, *Australian Gemmologist*, Vol. 20, No. 7, 1999, pp. 285–288.

The color of quartz family gemstones can be altered by heat treatment, high-energy irradiation (e.g., gamma rays), or a combination of both. This article reports the color changes observed in 19 specimens of colorless quartz that were subjected to variable doses of cobalt 60 gamma radiation followed by heating. All the specimens were obtained from the same vein deposit, near São João da Safira, Minas Gerais, Brazil. They contained significant concentrations (100–700 ppm) of Fe and Al, with Fe:Al ratios of 0.13–0.32. These elements, and particularly the Fe:Al ratio, are the main contributors to color in irradiated quartz.

Irradiation at doses of 7.6–187 kGy (exposure times not given) produced various shades of smoky gray; higher doses produced darker specimens. Following slow heating (5°/min to 250°C) in air, the resulting colors (according to increasing radiation dosage) were pale yellow, yellow, greenish yellow, “olive” green, greenish orange, orange, and reddish brown. All the colors were stable to natural light and to temperatures up to 250°C. Greenish yellow (“green-gold”) and reddish brown (“cognac”) are presently the two most marketable colors. Thus, with the right combination of irradiation and controlled heating (and favorable contents of Fe and Al), it is possible to obtain marketable quartz in many colors. *TL*

Radioactivity of neutron-irradiated cat’s-eye chrysoberyls.

S. M. Tang and T. S. Tay, *Nuclear Instruments and Methods in Physics Research B*, No. 150, 1999, pp. 491–495.

Highly radioactive cat’s-eye chrysoberyls have appeared in Southeast Asian markets (see Fall 1997 Gem News, pp. 221–222). The original material reportedly came from India and was irradiated with neutrons somewhere in Asia for color enhancement. This article is the first estimate of the potential health threat of such stones if they are worn close to the skin (within 0.5 cm). Because no irradiated stones were available to the authors for testing, they used an indirect approach to determine the potential radiation hazard. In this approach, the typical chemical impurities and their concentrations in three non-irradiated cat’s-eye chrysoberyls from India (two from Orissa, one from Kerala) were determined. Then the activities of all the radioactive nuclides that can be produced by neutron activation from these impurities, as well as from the constituent elements of chrysoberyl (O, Be, and Al), were calculated. On the basis of the activities so obtained, the radiation dose that would result from an irradiated cat’s-eye chrysoberyl with these chemical characteristics was estimated.

Of all the radioactive nuclides that could be created by neutron activation (based on a 1 ct stone with ~1% Fe), only four—⁴⁶Sc, ⁵¹Cr, ⁵⁴Mn, and ⁵⁹Fe—would not have “cooled down” to the internationally accepted level of specific residual radioactivity (2 nCi/g) within a month after irradiation. Three of these—⁴⁶Sc, ⁵¹Cr, and ⁵⁹Fe—would fall to the safe limit in about 15 months; ⁵⁴Mn would remain above the safe limit for seven years. Clearly, such a hypothetically neutron-irradiated stone presents a significant health hazard. Because of the compositional variability in chrysoberyls from different localities, others may be either more or less radioactive after neutron activation. *KSM*

Verneuil synthetic corundums with induced “fingerprints.”

J. Free, I. Free, G. Brown, and T. Linton, *Australian Gemmologist*, Vol. 20, No. 8, 1999, pp. 342–347.

Flux-healed, quench-crackled Verneuil synthetic ruby and sapphire are being produced in Chanthaburi, Thailand. First, the Verneuil boules are heated and then plunged into water to generate the quench-crackled effect. After the boules have been cobbled to yield small facetable fragments, these pieces are heat treated in an unspecified colorless flux for two days in a kerosene-fired kiln. The process is completed with a one-day heat treatment in an acetylene-fired kiln. The key identifying features are curved color banding or striae, a “checkerboard” pattern of flux-filled fractures, and increased transparency to short-wave UV radiation. *RAH*

MISCELLANEOUS

Carving out a future. *Basel Magazine*, No. 7, October 1999, pp. 33–34.

Although Idar-Oberstein has traditionally been the ultimate center for gem carvings, it recently has fallen on difficult times. The decline of the Asian and Middle East economies has weakened their markets for gem carvings. Another contributing factor is competition from Hong Kong and mainland China. Nevertheless, Idar-Oberstein is encouraged by emerging new markets in Europe, the U.S., and once again Asia. These markets, which appreciate Idar-Oberstein’s craftsmanship, are being created by a new generation of connoisseurs with different tastes.

Today, potential buyers include not only sheiks and the traditional wealthy, but also technology moguls. Recognizing that the newly rich from the technology sector may not be as appreciative of traditional carving styles, some Idar-Oberstein carvers are creating items that are entirely different from anything done before. Interviews with four successful carvers in this arena indicate the following preferences by current buyers: carvings with a matte instead of a highly polished finish; sweeping, soft styles characteristic of Art Nouveau; and classic-antique themes inspired by ancient Egyptian and Greek motifs to which a modern touch is added.

Idar-Oberstein still maintains its reputation as the world’s leader in fine carvings, and it also has access to unrivaled stocks of rough. Ultimately, though, it remains to be seen whether the region can succeed in attracting a new generation of carvers while maintaining its heritage of superior craftsmanship. *JY*